

**Alkylation of adenine: A synthetic and computational study of the
reaction mechanism**

By

Dominique Marie-Jeanne Solange Buyens

Supervisor: Dr Lynne A. Pilcher

Co-supervisor: Prof Ignacy Cukrowski

Submitted in partial fulfilment of the requirements for the degree

Master of Science

In the Faculty of Natural & Agricultural Sciences

University of Pretoria

Pretoria

(April, 2015)

Declaration

I, Dominique Marie-Jeanne Solange Buyens, declare that the thesis/dissertation, which I hereby submit for the degree Masters of Science at the University of Pretoria, is my own work and has not previously been submitted by me for a degree at this or any other tertiary institution.

The X-ray structure determinations reported in this thesis were performed by Mr D. C. Liles, and the NMR spectra reported in this thesis were performed by E. Palmer, at the University of Pretoria.

Signature:.....

Date:.....

Acknowledgements

The author wishes to thank Dr. Lynne Pilcher and Prof Ignacy Cukrowski for their guidance, support and extensive knowledge in the research completed in this dissertation. She also wishes to thank Eric Palmer for performing the NMR spectroscopy, Dave Lilies and Prof Van Rooyen for performing the X-ray crystallography, Dr. Darren Riley for his insight and suggestions throughout the research and the interlending team at the library of UP who retrieved unreachable articles in such short periods of time. To Marc Buyens, Dr. Vicki Tolmay, Dr. John Tolmay and Samuel Tolmay, who took the time to proof read this thesis, the author is extremely thankful. She extends her gratitude to her family and friends for all the support and long hours of company, especially Isabelle Buyens, during the undertaking of this research; the University of Pretoria, for being a second home and financially helping with the degree; the NRF for their financial support; and Coffee Buzz, for always being welcoming and staying open till late hours, in weekends and during holidays so that students can refuel themselves with coffee.

A special thank you goes to the late Prof Robert Vlegaar, for his kindness and sharing his knowledge in the field of Organic chemistry and NMR spectroscopy.

Table of Contents

List of figures	i
List of Tables	ix
List of abbreviations	xiii
Abbreviates for labelled compounds and atoms:	xv
Summary	xvi
Chapter 1	1
1.1. Shikimate kinase as a potential drug target for <i>Mycobacterium tuberculosis</i>	1
1.2. The KIE of Shikimate kinase	3
1.3. Mechanistic pathways for phosphoryl transfer	5
1.4. Studying the reactivity of Adenine - a possible inhibitor for shikimate kinase	9
Chapter 2	11
2.1. Characterisation of an N9-benzyladenine isomer: Confusion in the literature	11
2.1.1 Synthesis of N9-benzyladenine and its structural isomer	11
2.1.2 Characterisation of the major and minor structural isomer by NMR spectroscopy	13
2.1.2.1 Characterisation of major structural isomer by NMR spectroscopy	13
2.1.2.2 Characterisation of the minor structural isomer by NMR spectroscopy	16
2.1.3 Alternative synthesis of N-benzyladenine structural isomers	18

2.1.4 N3- and N9-substituted adenine as directing groups to yield N7- and N3-substituted adenines	23
2.2 Results and Discussion	28
2.2.1 Characterisation of N3- and N9-benzyladenine by 2D ^1H - ^{13}C NMR correlation spectroscopy	28
2.2.2 NMR analysis and structural assignments for N9-benzyladenine	29
2.2.3 NMR analysis and structural assignments for N3-benzyladenine	34
2.2.4 Solvent effects on the synthesis of N9-benzyladenine	40
2.2.5 $\text{S}_{\text{N}}2$ substitution reaction studied by ^1H NMR spectroscopy	43
2.2.6 Dimroth rearrangement: explanation for the conversion of N9- to N3-benzyladenine	47
2.2.7 Alkylation of adenine and 2,6-dichloropurine with other electrophiles	50
2.3 Conclusions from the synthetic study	52
Chapter 3	53
3.1 Introduction	53
3.1.1 The prototropic tautomers of adenine	53
3.1.2 Adenine tautomers in gas phase and solvent phase	59
3.2 Results and discussion	64
3.2.1 Stability trend of the prototropic tautomers of adenine	64
3.2.2 Stability of N-benzyladenine regio-isomers	65
3.3 The interaction between benzyl bromide and adenine	68
3.3.1 Exploring the sites of alkylation of adenine under a $\text{S}_{\text{N}}2$ mechanism	69

3.3.2 The stable form of the adenine anion	70
3.4 A closer look into the control of the reaction paths	79
3.4.1 Comparing the IQA defined energy terms of N1, N3, N7, and N9 atoms within each pathway	82
3.4.2 Interactions between fragments	84
3.4.2.1 Interaction between fragment $\mathcal{G} = \{N, C15\}$ and fragment \mathcal{H}	85
3.4.2.2 Interaction between polyatomic fragments $\mathcal{M} = \{AD^-\}$ and $\mathcal{N} = \{Bn\}$	88
3.4.2.3 The change in intra-fragment interaction energy for $M = \{AD^-\}$ and $N = \{Bn\}$ in each pathway	91
3.4.2.4 The change in $N \cdots \mathcal{M}$ and $N \cdots \mathcal{N}$ interaction energies along each reaction path	93
3.4.2.5 Comparing the diatomic interaction energies of specific interactions along each reaction path	96
3.5 Conclusions from the computational study	105
Chapter 4	106
4.1 The deuteration of adenine	106
4.2 Results and discussion	112
4.2.1 Investigation of the mechanism of adenine deuteration	113
4.2.2 The sp^3 mediated mechanism for deuteration	113
4.2.3 The carbene mediated mechanism for deuteration	115
4.2.3.1 Refinement of the “pull” mechanism proposed for Group 4 kinases	118
4.2.4 Deuterating N3- and N9-benzyladenine	119

4.3 Conclusions from the deuteration study	128
Chapter 5	130
5.1 Conclusion	130
5.2 Future work	135
Chapter 6	137
Experimental	137
General	137
Preparation of N-alkylated adenine derivative	138
Deuteration experimental:	141
General procedure for deuteration of purine derivatives:	141
Deuteration of N3- and N9-benzyladenine.	141
Deuteration of the N7- and N9-2,6-dichloropurine derivatives.	142
Deuteration of N9-allyl-2,6-dichloropurine	143
Deuteration of N7-allyl-2,6-dichloropurine	143
N9-benzyladenine NMR scaled reaction	143
Supporting Material	145
References	146

List of figures

Figure 1: Benzylation of adenine under basic conditions	xvii
Figure 1.1: Overview of the shikimate pathway.	1
Figure 1.2: Phosphorylation of shikimate by shikimate kinase.	2
Figure 1.3: Structure of ATP with a hydrogen atom at the C8 position.	3
Figure 1.4: The effect of low ATP and C8D-ATP concentration on the KIE_H and KIE_D for SK, Hexokinase, Acetate and GS_0 . ⁶	4
Figure 1.5: Effect of ATP (black squares) and C8D-ATP (black circles) on the specific activity of SK and Hexokinase. ⁶	5
Figure 1.6: The "push" mechanism demonstrated for shikimate kinase. ⁷	7
Figure 1.7: The "pull" mechanism demonstrated for Group 4 Kinases. ⁷	8
Figure 2.1: N9-substituted adenine indicating IUPAC numbering of atoms.	11
Figure 2.2: S_N2 substitution mechanism for synthesis of N9-benzyladenine. X: halide leaving group.	12
Figure 2.3: Structural isomers of benzyladenine: N1- (N1-Bn), N3- (N3-Bn), N7- (N7-Bn), N9- (N9-Bn) and N6-benzyladenine (N6-Bn).	13
Figure 2.4: 1H NMR spectrum chemical shifts (ppm) of aromatic protons of N9-benzyladenine in DMSO- d_6 . *assignment by Siah and Lambertucci **assignment by Nair, Sun, and Petrov....	14
Figure 2.5: HMBC and HSQC 1H - ^{13}C correlations of C2-H (A) and C8-H (B). Double bonds and alkyl groups are removed for simplicity of the demonstration.	15
Figure 2.6: Theoretical HMBC 1H - ^{13}C correlations of N1- (N1-R), N3- (N3-R), N7- (N7-R) and N9- (N9-R) alkylated adenines. Double bonds and hydrogens are removed for simplicity of the demonstration.	16

Figure 2.7: ^1H NMR spectrum chemical shift (ppm) assignments of C2-H and C8-H in DMSO- d_6 . * ²³ ** ³⁰ *** ²⁶	17
Figure 2.8: Synthesis of N3-benzyladenine- $^{15}\text{N}6$ (N3-Bn-$^{15}\text{N}6$). ³³	18
Figure 2.9: Neutral (2a) and anionic form (2a) of 6-methylthiopurine. ³⁵	19
Figure 2.10: Synthesis of N ⁶ -benzyladenine- $^{15}\text{N}6$ (N6-Bn-$^{15}\text{N}6$) and N9-benzyladenine- $^{15}\text{N}6$ (N9-Bn-$^{15}\text{N}6$). ³³	19
Figure 2.11: Synthesis of N9-benzyladenine $^{15}\text{N}9$ (N9-Bn-$^{15}\text{N}9$) and N6-benzyladenine- $^{15}\text{N}9$ (N6-Bn-$^{15}\text{N}9$). ³³	20
Figure 2.12: Synthesis of N6-benzyladenine- $^{15}\text{N}1$ (N6-Bn-$^{15}\text{N}1$). ³³	20
Figure 2.13: Resonance stability of pyrimidine (N1-Bn and N3-Bn) and imidazole (N7-Bn and N9-Bn) substitution.....	23
Figure 2.14: Pyrimidine ring substitution: 6 electron π system in the pyrimidine and imidazole ring by charge separation. ³⁶	23
Figure 2.15: Concentration of positive charge in pyrimidine ring at the transition state. ⁴⁶	24
Figure 2.16: N3-benzyladenine as a directing group for synthesis of N7-methyladenine. ⁴⁰	25
Figure 2.17: N9-substituted adenine 16 as a directing group for the synthesis of N1-benzyladenine N1-Bn . ⁴¹	26
Figure 2.18: Structural isomers of N-benzyladenine: N1- (N1-Bn), N3- (N3-Bn), N7- (N7-Bn), N9- (N9-Bn) and N6-benzyladenine (N6-Bn).....	28
Figure 2.19: Crystal structures of N3- and N9-benzyladenine (N3-Bn and N9-Bn , respectively).	28
Figure 2.20: ^1H NMR spectrum (ppm) for N9-benzyladenine in DMSO- d_6 (400 MHz).....	29
Figure 2.21: HSQC of N9-benzyladenine in DMSO- d_6 (400 MHz), y-axis: ^{13}C NMR (ppm), x-axis: ^1H NMR (ppm). Solid line: carbon correlation with directly bonded proton.....	30
Figure 2.22: Predicted HMBC ^1H - ^{13}C correlations for N9-benzyladenine.....	31

Figure 2.23: HMBC of N9-benzyladenine in DMSO-d₆ (400 MHz), y-axis: ¹³C NMR (ppm), x-axis: ¹H NMR (ppm). Dotted line: hovering correlation with the directly bonded proton. Solid line: carbon correlation with protons 2 or more bonds away. 32

Figure 2.24: HMBC of N9-benzyladenine in CDCl₃ (400 MHz), y-axis: ¹³C NMR (ppm), x-axis: ¹H NMR (ppm). Dotted line: hovering correlation with the directly bonded proton. Solid line: carbon correlation with protons 2 or more bonds away. 33

Figure 2.25: ¹H NMR spectrum (ppm) of N9-benzyladenine in MeOD-d₄ (400 MHz). 33

Figure 2.26: HMBC of N9-benzyladenine in MeOD-d₄ (400 MHz), y-axis: ¹³C NMR (ppm), x-axis: ¹H NMR (ppm). Dotted line: hovering correlation with the directly bonded proton. Solid line: carbon correlation with protons 2 or more bonds away. 34

Figure 2.27: ¹H NMR spectrum (ppm) for N3-benzyladenine in DMSO-d₆ (400 MHz). 35

Figure 2.28: Predicted HMBC ¹H-¹³C correlations for N3-benzyladenine. 35

Figure 2.29: HMBC of N3-benzyladenine in DMSO-d₆ (400 MHz), y-axis: ¹³C NMR (ppm), x-axis: ¹H NMR (ppm). Dotted line: hovering correlation with the directly bonded proton. Solid line: carbon correlation with protons 2 or more bonds away. 36

Figure 2.30: HMBC of N3-benzyladenine in CDCl₃ (400 MHz), y-axis: ¹³C NMR (ppm), x-axis: ¹H NMR (ppm). Dotted line: hovering correlation with the directly bonded proton. Solid line: carbon correlation with protons 2 or more bonds away. 37

Figure 2.31: ¹H NMR spectrum (ppm) of N3-benzyladenine in CDCl₃ (A) vs. N9-benzyladenine in DMSO-d₆ (B) (400 MHz). 37

Figure 2.32: ¹H NMR spectrum (ppm) of N3-benzyladenine in DMSO-d₆ (A) vs. N9-benzyladenine in CDCl₃ (B), (400 MHz). 38

Figure 2.33: ¹H NMR spectrum (ppm) of N3-benzyladenine in MeOD-d₄ (400 MHz). 38

Figure 2.34: HMBC of N3-benzyladenine in MeOD-d ₄ (400 MHz), y-axis: ¹³ C NMR (ppm), x-axis: ¹ H NMR (ppm). Dotted line: hovering correlation with the directly bonded proton. Solid line: carbon correlation with protons 2 or more bonds away.....	39
Figure 2.35: ¹ H NMR spectra (ppm) of NMR scaled reaction of deprotonated adenine A , and at 0 to 12 hours (0hr , 1hr , 2hr , 3hr , 4hr , 5hr and 12 hr) after addition of benzyl bromide, in DMSO-d ₆ (400 MHz).....	44
Figure 2.36: Dimroth rearrangement for conversion of N1- to N6-benzyladenine.	47
Figure 2.37: Dimroth rearrangement mechanisms for the conversion of N3- to N9-benzyladenine.....	48
Figure 2.38: Water catalysed Dimroth rearrangement of 1-(Δ ² -isopentenyl)adenine 18 to 6-(Δ ² -isopentenyl)adenine 19	49
Figure 2.39: Water catalysed Dimroth rearrangement for N9- to N3-benzyladenine.....	49
Figure 2.40: Synthesised adenine and 2,6-dichloropurine derivatives.	50
Figure 2.41: Migration of double bond between the allyl form (23 and 25) and the prop-1-enyl (23a and 25a) form of N9- and N3-allyl-adenine.	51
Figure 2.42: Migration of double bond between the allyl form (22 and 26) and the prop-1-enyl (22a and 26a) form of N9- and N7-allyl-2,6-dichloropurine.....	51
Figure 3.1: Structural isomers of N-benzyladenine.	53
Figure 3.2: Adenine tautomers.	54
Figure 3.3: Adenine-imine tautomers.	55
Figure 3.4: Adenine derivatives.	55
Figure 3.5: Ten π electrons of adenine.....	57
Figure 3.6: Purine tautomers.	58
Figure 3.7: "Pyrrole" like and "imine" like nitrogens in the purine system of N9-H.	62
Figure 3.8: Molecular graphs of adenine tautomers.....	65

Figure 3.9: Structural isomers of N-benzyladenine.	65
Figure 3.10: N6-Bn isomers.....	66
Figure 3.11: Molecular graphs of most stable endo-purine N-Bn isomers.....	67
Figure 3.12: Scheme of S _N 2 pathways leading to the N1, N3, N7 and N9 regio-isomers.....	70
Figure 3.13: Deprotonated form of adenine, AD⁻	71
Figure 3.14: Exocyclic deprotonated isomers of adenine.	71
Figure 3.15: Molecular graph of deprotonated adenine AD⁻	73
Figure 3.16: Gaussian numbering scheme of atoms for the N9-H and AD⁻	74
Figure 3.17: A graphic representation of the maximum gain (red) and maximum depletion (blue) of ρ _{BCP} (A), and the greatest to lowest change in N(A) (biggest to smallest circles, respectively) (B).	75
Figure 3.18: Fragments of molecular system: $\mathcal{M} = \{\text{AD}^-\}$, $\mathcal{N} = \{\text{Bn}\}$, $\mathcal{O} = \{\text{Br}\}$	88
Figure 3.19: Diatomic interactions between atoms of fragment \mathcal{M} with atoms of fragment \mathcal{N}	89
Figure 3.20: Intra-fragment interaction energy of molecular fragment $\mathcal{M} = \{\text{AD}^-\}$ and $\mathcal{N} = \{\text{Bn}\}$ composed of all diatomic interactions between of atoms of the fragment concerned.....	92
Figure 3.21: Interaction energy of the reactive nitrogen (N) of fragment \mathcal{M} with all other atoms (X) in fragment \mathcal{M} , $\sum_{\substack{X \neq N \\ X \in \mathcal{M}}} E_{\text{int}}^{\text{NX}}$, and the interaction energy of N of fragment \mathcal{M} with all other atoms (X) of fragment \mathcal{N} , $\sum_{\substack{N \in \mathcal{M} \\ X \in \mathcal{N}}} E_{\text{int}}^{\text{NX}}$	93
Figure 3.22: Potential energy profile of the N1-pathway leading to N1-benzyladenine with molecular graphs	98
Figure 3.23: Potential energy profile of the N7-pathway leading to N7-benzyladenine with molecular graphs	99

Figure 3.24: Potential energy profile of the N3-pathway leading to N3-benzyladenine with molecular graphs	103
Figure 3.25: Potential energy profile of the N9-pathway leading to N9-benzyladenine with molecular graphs	104
Figure 4.1: The p-orbital donating ability of heteroatoms attached to the carbene.	107
Figure 4.2: Conversion of bis-[1,3-diphenyl-2-imidazolidinyldene] 4.1 to 2-methoxy-1,3-diphenylimidazolidine 4.4 . ¹⁰⁵	107
Figure 4.3: Hydrogen-deuterium exchange at the C2 proton in thiamine 4.5 . ¹⁰⁵	108
Figure 4.4: Deprotonation of 3-substituted 1-methoxypyridinium ions 4.8 at the ortho or para position to R ₁ to form the corresponding ylides 4.9a or 4.10a followed by deuteration at the respective carbanion, 4.9b and 4.10b respectively. ⁹⁹	108
Figure 4.5: Delocalization of the positive charge in the aromatic substitution transition state of N9- and N3-benzyladenine (4 and 5 , respectively) for the deuteration of the C8 and C2 proton (a and b , respectively). ³⁶	109
Figure 4.6: Delocalization of the positive charge in the aromatic substitution transition state of N7-benzyladenine (6) for the deuteration of the C8 and C2 proton (a and b , respectively). ³⁶ ..	110
Figure 4.7: Protonated 1 and non-protonated 2 form of the carbene intermediate as demonstrated for N9-benzyladenine. ³⁶	110
Figure 4.8: Resonance form of N3-benzyladenine.....	110
Figure 4.9: Deuteration of the adenine moiety of ATP.....	112
Figure 4.10: Deuteration of the C2 proton on an imidazole ring.	113
Figure 4.11: The sp ³ mediated mechanism for the deuteration at C8 of N9-benzyladenine.	114
Figure 4.12: Failure of the sp ³ mediated mechanism for the deuteration at C2 of N9-benzyladenine.....	114
Figure 4.13: The sp ³ mediated mechanism for the deuteration at C8 of N3-benzyladenine.	115

Figure 4.14: Failure of the sp^3 mediated mechanism for the deuteration at C2 of N3-benzyladenine.....	115
Figure 4.15: Base catalysed carbene mechanism for deuteration at C8 of N9-benzyladenine..	116
Figure 4.16: Failure of the base catalysed carbene mechanism for deuteration at C2 of N9-benzyladenine.....	117
Figure 4.17: Failure of the base catalysed carbene mechanism for deuteration at C8 on N3-benzyladenine.....	117
Figure 4.18: The base catalysed carbene mechanism for deuteration at C2 of N3-benzyladenine.	118
Figure 4.19: Refined “pull” mechanism for proton transfer based on the movement of electrons for formation of a carbene.....	119
Figure 4.20: Deuteration of N3- and N9-benzyladenine. N3-benzyladenine C2-H and C8-H 1H NMR spectrum (ppm) in MeOD- d_4 (400 MHz): N3-C2 and N3-C8 , respectively. N9-benzyladenine C2-H and C8-H 1H NMR spectrum chemical shifts (ppm): N9-C2 and N9-C8 , respectively. A : initial 1H NMR spectrum of N3-/N9-benzyladenine, B : 1H NMR spectrum after addition of Na (0.5 eq) and heating at 60 °C, C : 1H NMR spectrum of reaction 24 hours after addition of Na, D : 1H NMR spectrum 48 hours after addition of Na, E : 1H NMR spectrum after heating at 60 °C for 20 minutes.....	120
Figure 4.21: Importance of amino group in the sp^3 mediated mechanism.....	122
Figure 4.22: N9-substituted 2,6-dichloropurine.....	123
Figure 4.23: Carbene mediated mechanism of deuteration at the C8 position of N9-allyl-2,6-dichloropurine 23	123
Figure 4.24: Carbene mediated mechanism of deuteration at the C8 position of N7-allyl-2,6-dichloropurine 26	124

Figure 4.25: ^1H NMR spectra (ppm) of the deuteration of N9-allyl-2,6-dichloropurine in MeOD- d_4 (400 MHz). **A:** immediately after addition of Na (0.5 eq) and heating at 60°C for 20 minutes, **B:** 1 hour after heating at 60°C , **C:** 3 hours after heating at 60°C with added Na (0.1eq), **D:** 5 hours after heating at 60°C with added Na (0.1eq)..... 125

Figure 4.26: ^1H NMR spectra (ppm) of the deuteration of N7-allyl-2,6-dichloropurine in MeOD- d_4 (400 MHz). **A:** immediately after addition of Na (0.5 eq) and heating at 60°C for 20 minutes, **B:** 40 minutes after heating at 60°C with added Na (0.1 eq). 126

Figure 4.27: Initial and final ^1H NMR spectra of the allyl-2,6-dichloropurine derivatives during deuteration in MeOD- d_4 (400 MHz). **A:** initial ^1H NMR spectrum of N9-allyl-2,6-dichloropurine after addition of Na (0.5 eq) and heating at 60°C , **B:** final ^1H NMR spectrum of deuterated N9-allyl-2,6-dichloropurine, **C:** initial ^1H NMR spectrum of N7-allyl-2,6-dichloropurine after addition of Na (0.5 eq) and heating at 60°C , **B:** final ^1H NMR spectrum of deuterated N7-allyl-2,6-dichloropurine..... 127

Figure 4.28: Inter-conversion between the N9-allyl-2,6-dichloropurine **23** and N7-allyl-2,6-dichloropurine **26** under deuteration conditions. 128

List of Tables

Table 2.1: Synthetic procedures for N9-benzyladenine from adenine and benzyl bromide.	12
Table 2.2: ¹ H NMR spectrum chemical shifts (ppm) of N9-benzyladenine.	13
Table 2.3: ¹³ C NMR spectrum chemical shifts (ppm) for N9- and N3-benzyladenine.	14
Table 2.4: ¹ H NMR spectrum chemical shifts (ppm) of the assigned structural isomer of N9-benzyladenine.	17
Table 2.5: C8-H and C2-H ¹ H NMR spectrum chemical shifts (ppm) in DMSO-d ₆ of unlabelled and ¹⁵ N-labelled N-benzyladenine regio-isomers. ³³	21
Table 2.6: N-benzyladenine regio-isomers ¹ H NMR spectrum chemical shifts (ppm) in DMSO-d ₆	21
Table 2.7: ¹ H NMR spectrum δ chemical shifts values between C2-H and C8-H of each N-benzyladenine isomer.	22
Table 2.8: ¹ H NMR spectrum chemical shifts (ppm) of N7-benzyladenine in DMSO-d ₆ . ⁴²	25
Table 2.9: ¹ H and ¹³ C NMR spectrum chemical shifts (ppm) reported for N3-, N7-, and N9-benzyladenine in DMSO-d ₆	26
Table 2.10: ¹ H NMR chemical shifts (ppm) for N9-benzyladenine.	29
Table 2.11: ¹³ C NMR chemical shifts (ppm) for N9-benzyladenine.	30
Table 2.12: ¹ H NMR chemical shifts (ppm) for N3-benzyladenine.	34
Table 2.13: ¹³ C NMR chemical shifts (ppm) for N3-benzyladenine.	35
Table 2.14: Reaction conditions for benzylation of adenine using benzyl bromide.	41
Table 2.15: Effect of water on the ratio of N9:N3.	42
Table 2.16: ¹ H NMR spectrum chemical shifts (ppm) of CH ₂ of reported by-products in DMSO-d ₆	45
Table 2.17: ¹ H NMR δ C2-H and C8-H chemical shift (ppm) of N3- and N9-adenine derivatives.	50

Table 3.1: Difference in relative free energy (ΔG) between adenine tautomers (ΔG_A) with their corresponding purine tautomers (ΔG_P). ⁷¹	58
Table 3.2: Relative to N9-H, electronic energies (ΔE , kcal/mol) and free energies (ΔG , kcal/mol) of adenine tautomers in the gas phase.	59
Table 3.3: Relative to N9-H, energy (ΔE , kcal/mol) and free energy (ΔG , kcal/mol) of adenine tautomers in liquid phase.	60
Table 3.4: Dipole moment (μ), in Debye, of adenine tautomers.	61
Table 3.5: Experimentally determined dipole moment (μ), in Debye, of N-benzyladenine derivatives in dioxane.	62
Table 3.6: Relative to N9-H , the difference in electronic energy (ΔE , kcal/mol) of adenine tautomers.	64
Table 3.7: Relative to N9-Bn-1 , difference in electronic energy (ΔE , kcal/mol) of the most stable conformer of each endo-purine N-Bn regio-isomer.	67
Table 3.8: Relative to N9-Bn-1 , difference energies (ΔE , kcal/mol) of the most stable exo-purine N6-Bn isomers.	68
Table 3.9: Relative to AD⁻ , differences in electronic energies (ΔE , kcal/mol) of deprotonated adenine isomers to assess effect of deprotonation at the exocyclic NH ₂ group.	72
Table 3.10: Change in electron density ($\Delta\rho(\mathbf{r})$ in a.u.) and electron population ($\Delta N(A)$ in e) resulting from deprotonation of N9-H to yield AD⁻	74
Table 3.11: Potential energy, E (a.u.), of ref state of each pathway with molecular graph indicating the Gaussian numbering scheme.	77
Table 3.12: Relative to relevant ref state, changes in energy (ΔE , kcal/mol) along the N1-, N3-, N7- and N9-pathway.	78
Table 3.13: Relative to relevant ref state, changes in IQA define energy terms (kcal/mol) of the reactive nitrogen along each pathway for selected $d(N,C15) = \sim 2.3(\text{TS}), 2.0$ and $\sim 1.5(\text{eq}) \text{ \AA}$. ..	83

Table 3.14: Relative to relevant ref state changes in inter-fragment interaction energy, $\Delta E_{\text{int}}^{\mathcal{G}\mathcal{H}}$ (kcal/mol), between fragment $\mathcal{G} = \{\text{N,C15}\}$ and fragment \mathcal{H} for each reaction path. 85

Table 3.15: Relative to relevant ref state, changes in intra-fragment diatomic interaction energy, $\Delta E_{\text{int}}^{\mathcal{G}}$ (kcal/mol) and self-energy, $\Delta E_{\text{self}}^{\mathcal{G}}$ (kcal/mol), of fragment $\mathcal{G} \{\text{N,C15}\}$ 87

Table 3.16: Relative to relevant ref state, changes in inter-fragment interaction energy, $\Delta E_{\text{int}}^{\mathcal{M}\mathcal{N}}$, $\Delta E_{\text{int}}^{\mathcal{M}\text{O}}$ and $\Delta E_{\text{int}}^{\mathcal{N}\text{O}}$ (kcal/mol) along each pathway for selected $d(\text{N,C15}) = \sim 2.3(\text{TS}), 2.0$ and $\sim 1.5(\text{eq}) \text{ \AA}$ 90

Table 3.17: Relative to relevant ref state, changes in intra-fragment interaction energy, $\Delta E_{\text{int}}^{\mathcal{M}}$ and $\Delta E_{\text{int}}^{\mathcal{N}}$ (kcal/mol) for fragment $\mathcal{M} = \{\text{AD}^{-}\}$ and $\mathcal{N} = \{\text{Bn}\}$, respectively, along each pathway for selected $d = \sim 2.3(\text{TS}), 2.0$ and $\sim 1.5(\text{eq}) \text{ \AA}$ 92

Table 3.18: Relative to the relevant ref state changes in the interaction energy between the reacting nitrogen N and atoms of the fragment $\mathcal{M} = \{\text{AD}^{-}\}$, $\Delta \sum_{\substack{X \neq \text{N} \\ X \in \mathcal{M}}} E_{\text{int}}^{\text{NX}}$ (kcal/mol), and the interaction energy between the reactive nitrogen and atoms of the fragment $\mathcal{N} = \{\text{Bn}\}$, $\Delta \sum_{\substack{N \in \mathcal{M} \\ X \in \mathcal{N}}} E_{\text{int}}^{\text{NX}}$ (kcal/mol) along each pathway for selected $d = \sim 2.3(\text{TS}), 2.0$ and $\sim 1.5(\text{eq}) \text{ \AA}$ 94

Table 3.19: Relative to the ref state, changes in diatomic interaction energy, $\Delta E_{\text{int}}^{\text{AB}}$ (kcal/mol), for additional interactions of the N1-pathway. 97

Table 3.20: Relative to the ref, changes in diatomic interaction energy, $\Delta E_{\text{int}}^{\text{AB}}$ (kcal/mol), for additional interactions of the N7-pathway. 97

Table 3.21: Relative to the initial ref state, changes in diatomic interaction energy, $\Delta E_{\text{int}}^{\text{AB}}$ (kcal/mol), for Br interactions of the N1-pathway. 100

Table 3.22: Relative to the initial ref state, changes in diatomic interaction energy, $\Delta E_{\text{int}}^{\text{AB}}$ (kcal/mol), for Br interactions of the N7-pathway.....	100
Table 3.23: Relative to the initial state, changes in diatomic interaction energy, $\Delta E_{\text{int}}^{\text{AB}}$ (kcal/mol), for additional interactions of the N3-pathway.....	101
Table 3.24: Relative to the initial state, changes in diatomic interaction energy, $\Delta E_{\text{int}}^{\text{AB}}$ (kcal/mol), for additional interactions of the N9-pathway.....	101
Table 3.25: Relative to the initial ref state, changes in diatomic interaction energy, $\Delta E_{\text{int}}^{\text{AB}}$ (kcal/mol), for Br interactions of the N3-pathway.....	102
Table 3.26: Relative to the initial ref state, changes in diatomic interaction energy, $\Delta E_{\text{int}}^{\text{AB}}$ (kcal/mol), for Br interactions of the N9-pathway.....	102
Table 4.1: Pd/C catalysed deuteration of adenine and adenosine. ¹¹⁰	111
Table 4.2: Integral ratio $\int x/i$ of the proton peaks in the ¹ H NMR spectra A to E	121
Table 4.3: ¹ H NMR spectrum chemical shifts (ppm) of N7 and N9-allyl-2,6-dichloropurine in MeOD-d ₄ with Na.	124

List of abbreviations

ADP: Adenosine diphosphate
AR: Adenosine receptors
Arg: Arginine
Asp: Aspartic acid
ATP: Adenosine triphosphate
BCP: Bond Critical Point
Bn: Benzyl
Br: Bromine
C8D-ATP: ATP deuterated at the C8 position
C₀: Quaternary carbon
CDCl₃: Chloroform-d
COSMO: CONductor-like Screening Model
Cs₂CO₃: Caesium carbonate
D₂O: Deuterium oxide/Heavy water
DFT: Density Functional Theory
DMF: Dimethylformamide
DMSO: Dimethyl sulfoxide
DMSO-d₆: Dimethyl sulfoxide-d₆
DO⁻: Deuterioxide
E: Electronic energy
eq: Equivalentents (Chapter 2,4 and 5)
eq: Equilibrium (Chapter 3)
Et₃N: Triethylamine
fin: Final state
G: Gibbs free energy
Glu: Glutamic acid
Gly: Glycine
GS₀: Deadenylylated glutamine synthetase
H₂O: Water
HMBC: Heteronuclear Multiple Bond Correlation
HOMA: Harmonic Oscillator Measure of Aromaticity

HOMED: Harmonic Oscillator Model of Electron Delocalization index

HSQC: Heteronuclear Single Quantum Coherence

IEFPCM: Integral equation formalism variant

IFN: Interferon

IQA: Interacting Quantum Atoms

K₂CO₃: Potassium carbonate

K^tOBu: Potassium tert-butoxide

KIE: Kinetic isotope effect

KOH: Potassium hydroxide

Lit: Literature

Lys: Lysine

MeOD-d₄: Methanol-d₄

Mtb: *Mycobacterium tuberculosis*

N(A): Electron population of atom A

Na: Sodium

NaH: Sodium hydride

NaOH: Sodium Hydroxide

NHC: N-heterocyclic carbene

NICS: Nucleus-Independent Chemical Shifts

NMR: Nuclear magnetic resonance

NOESY: Nuclear Overhauser Effect Spectroscopy

PCM: Polarizable Continuum Model

Pd/C: Palladium/carbon

PDE: Phosphodiesterase

Ph: Phenyl ring

PO₄: Phosphate

QTAIM: Quantum Theory of Atoms in Molecules

ref: Reference state

RT: Room temperature

SCRF-PB: Poisson-Boltzmann self-consistent reaction field

Ser: Serine

SCIPCM: Self-Consistent Isodensity PCM

SK: Shikimate kinase

Thr: Threonine

TS: Transition state

UV: Ultraviolet

1°: Primary

2°: Secondary

3°: Tertiary

$(\rho(r))$: Electron density

ρ_{BCP} : Electron density at each bond critical point between two bonded atoms A and B

Abbreviates for labelled compounds and atoms:

AD⁻: Deprotonation of adenine

N-Bn: N-benzyladenine

N1-Bn: N1-benzyladenine

N3-Bn: N3-benzyladenine

N7-Bn: N7-benzyladenine

N9-Bn: N9-benzyladenine

N6-Bn: N6-benzyladenine

N1-R: N1-alkylated adenine

N3-R: N3-alkylated adenine

N7-R: N7-alkylated adenine

N9-R: N9-alkylated adenine

C2-H: C2 proton

C8-H: C8 proton

Summary

This dissertation describes the benzylation of adenine under basic conditions, the unequivocal determination of the identity of the products of this reaction, an exploration of the effect of solvent on the reaction, a thorough computational study of the reaction mechanism and an investigation into the hydrogen-deuterium exchange reaction of the N-benzyladenine products and related compounds.

The preferential sites of alkylation of adenine under basic conditions in DMSO were proven to be the N9 and N3 positions. X-ray crystal structures were obtained for both compounds. Formation of the N9-benzyladenine product is the most favoured in polar aprotic solvents, such as DMSO, and as the proportion of polar protic solvents, such as water, increases, so does the formation of the N3-benzyladenine product. Characteristic ^1H NMR δ chemical shifts of the purine ring protons and HMBC ^1H - ^{13}C correlation NMR spectroscopy were useful tools to assign the ^1H and ^{13}C NMR spectra chemical shifts and confirm that the solution structures were the same as the isolated crystals.

Simulating the $\text{S}_{\text{N}}2$ mechanism for the N1-, N3-, N7- and N9-pathways computationally, employing DMSO as the simulated solvent, resulted in ambiguous results when considering the electronic energies of initial, TS and final products alone. However, a novel approach was developed (employing IQA-defined energy terms) to study fragment interactions along the reaction paths. It provided a full explanation of the reaction mechanism and yielded results which supported the N3/N9 positions of alkylation over the N1/N7 sites. The preference for the sites of alkylation occurs after the transition state, in which the N1/N7 reaction paths fail to proceed favourably to the end product, N1- and N7-benzyladenine, respectively. The N9-

pathway dominates the N3-pathway at the product formation step, which corresponds to the N9-benzyladenine being the major product, as shown in Figure 1, and the N3-benzyladenine being the minor product from the benzylation of adenine.

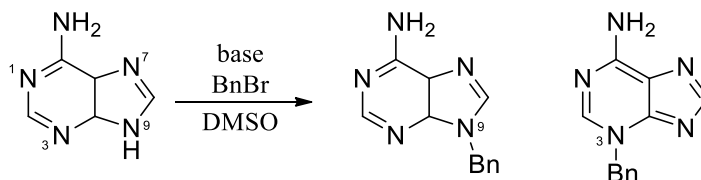


Figure 1: Benzylation of adenine under basic conditions

The faster rate of deuteration at the C8 position of N9-benzyladenine as compared to the deuteration rates at the C2 and the C8 of N3-benzyladenine, have shown support for a sp^3 mediated mechanism and a carbene mediated mechanism of deuteration based on the “push” and “pull” mechanisms proposed for the C8 proton transfer of ATP in kinase enzymes. The deuteration of the C8 proton of 2,6-dichloropurine derivatives supports the existence of the carbene mediated mechanism since these compounds lack the amine moiety necessary for the sp^3 mediated mechanism.

These results demonstrate how experimentation and computation have led to greater insights into the reactivity of adenine and its derivatives. This strategy provides a useful platform for future research into adenine reaction mechanisms and the role adenine plays in kinase catalysis.

Chapter 1

1.1. Shikimate kinase as a potential drug target for *Mycobacterium tuberculosis*

Mycobacterium tuberculosis (Mtb) is a major cause of human mortality, attacking immune-compromised individuals particularly in developing countries. The high incidence of drug resistant strains causing multidrug-resistant tuberculosis and extensively drug-resistant tuberculosis necessitates the development of novel drugs against the disease.¹ Current treatments are not satisfactory and are of excessive duration, such that there is often insufficient coverage which allows the bacteria to undergo its natural course of developing antibiotic resistance.² It is important that new drugs have a shorter treatment period, thus allowing for a reduced chance of the Mtb developing resistance to the drugs. This will also reduce the period and costs of medical treatment and hence is expected to result in increased patient compliance.² Most drug development for kinase enzymes is based on hit identification and relies on the affinity and selectivity of drug molecules.³ Simple screening initiatives against targets have not enhanced drug development fast enough. The strategy in this era must be on understanding the structure-function of targets and rational design of inhibitors.

The shikimate pathway is essential for the survival of *Mycobacterium tuberculosis*. The pathway (Figure 1.1) is responsible for the condensation of phosphoenol pyruvate and erythrose-4-phosphate via shikimate to chorismate which is the precursor molecule for aromatic amino acids and other secondary aromatic metabolites such as folic acid and ubiquinone.^{4,5}

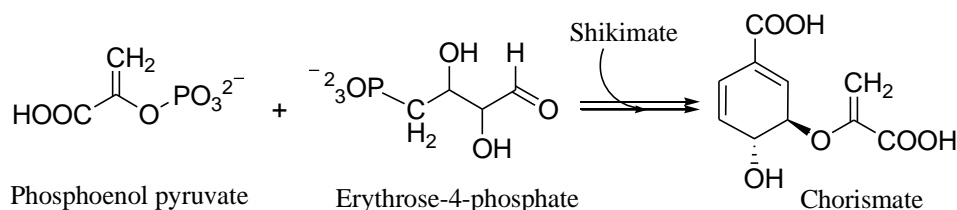


Figure 1.1: Overview of the shikimate pathway.

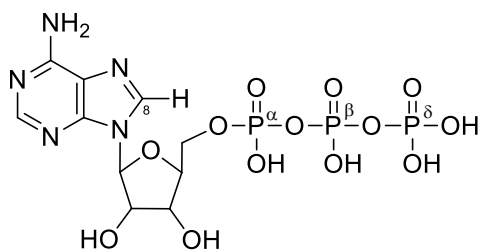


Figure 1.3: Structure of ATP with a hydrogen atom at the C8 position.

1.2. The KIE of Shikimate kinase

The adenylyl moiety was previously thought to do little except assist in holding the ATP in the enzyme active site. A comparative study of the concentration effect of ATP and ATP deuterated at the C8 position (C8D-ATP) of the ATP adenylyl moiety on six different kinases was performed (*Saccharomyces cerevisiae* hexokinase, *Escherichia coli* acetate kinase, *Escherichia coli* phosphofructokinase, *Escherichia coli* deadenylylated glutamine synthetase (GS₀), *Escherichia coli* adenylylated glutamine synthetase and *Mycobacterium tuberculosis* shikimate kinase).⁶ A concentration profile of ATP and C8D-ATP was generated for each enzyme (Figure 1.4, demonstrated for SK, Hexokinase, Acetate and GS₀). The hydrogen-deuterium kinetic isotope effect (KIE) was calculated using the rate constant of adenosine diphosphate (ADP) release, in which the KIE_H (Figure 1.4 black line),

$$\text{KIE}_H = \frac{v_H}{v_D},$$

was calculated along with its inverse, KIE_D (blue line),

$$\text{KIE}_D = \frac{v_D}{v_H},$$

where v_D is the specific activity of the enzyme in the presence of C8D-ATP and v_H is the specific activity in the presence of ATP.⁶ The concentration profiles obtained showed that all enzymes, except SK, demonstrated a KIE_D of > 5 fold at low ATP concentrations and decreased as the concentration of ATP increased. However, SK showed an increase in KIE_D as the concentration of ATP increased.⁶

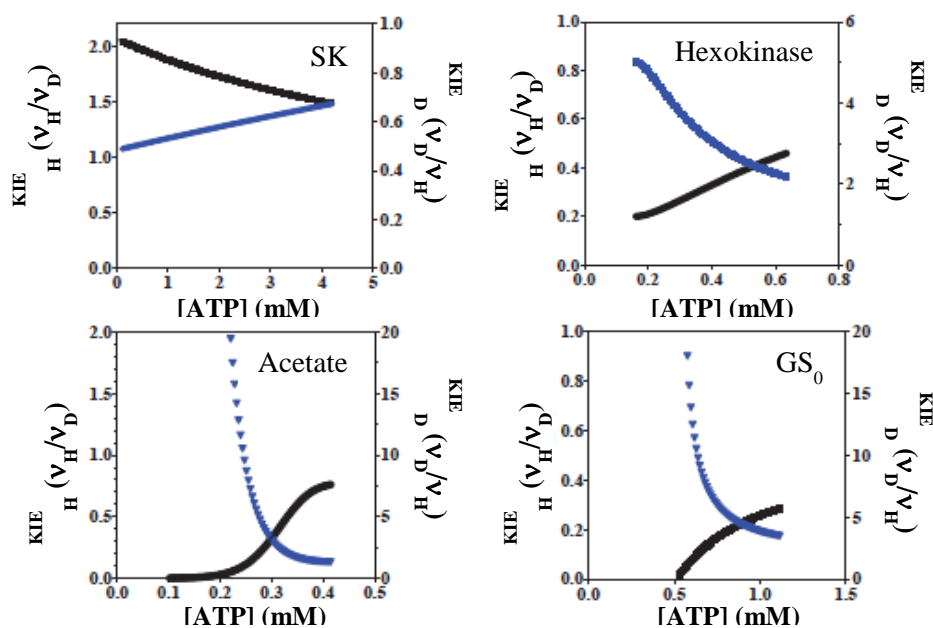


Figure 1.4: The effect of low ATP and C8D-ATP concentration on the KIE_H and KIE_D for SK, Hexokinase, Acetate and GS_0 .⁶

A primary KIE is based on the bond-breaking of the isotopically labelled hydrogen (deuterium) atom whereas a secondary KIE is based on the hybridization change of the atom α or β to the bonded deuterium. Therefore the KIE of ≥ 2 fold, observed for all six of the above enzymes, is strong evidence that the C8 proton (C8-H) plays a significant role in the regulation of kinase activity, such as in the binding of ATP and phosphoryl transfer.⁶⁻⁸

It was evident from the reaction of the 5 enzymes (excluding shikimate kinase) to the low concentration of ATP, that C8D-ATP increases the activity of the enzymes, whereas Mtb SK showed a decrease in activity.⁶ Figure 1.5 demonstrates this difference of C8D-ATP activity between Hexokinase and shikimate kinase. The specific activity of SK involving ATP (black squares) was higher in activity for lower ATP concentrations than for that of C8D-ATP (black circles) in which SK demonstrated a lower activity, indicating that the ATP binding and phosphoryl transfer is being inhibited by the presence of the C8 deuterium. The specific activity of Hexokinase resulting from ATP as a substrate (black squares) was lower than the specific

activity of C8D-ATP (black circles), therefore indicating that the activity of ATP binding and phosphoryl transfer has increased in the presence of the C8-deuterium.

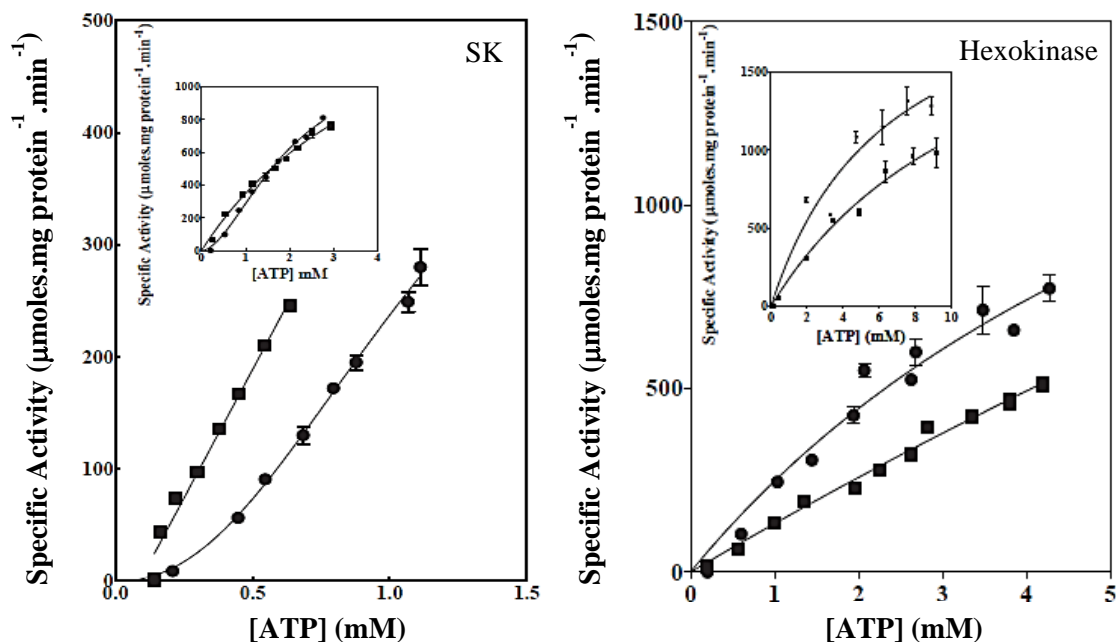


Figure 1.5: Effect of ATP (black squares) and C8D-ATP (black circles) on the specific activity of SK and Hexokinase.⁶

The enzymes were subjected to a 1:1 mixture of ATP and C8D-ATP in order to study the affinity of the enzymes for either ATP or C8D-ATP.⁶ In all six enzymes the specific activity obtained from the 1:1 mixture was higher than that of the specific activity when using ATP as a substrate, which indicated that the enzymes have higher affinity for the C8D-ATP over the ATP. However, it was shown via mass spectroscopy that SK prefers to bind to ATP, thus the appearance of SK preferring C8D-ATP could be due to a difference in binding equilibria.⁶

1.3. Mechanistic pathways for phosphoryl transfer

Two mechanisms, namely the “push” and “pull” mechanisms, were proposed by Kenyon and co-workers to explain the direct role of the C8 proton of the ATP adenyly moiety in the binding of ATP and phosphoryl transfer.^{7,8} The mechanisms were based on the conserved amino acids in

the active site of numerous crystallised kinases which are part of a certain mechanistic class depending on the similarity of the structural folds (fold-groups). The two mechanisms provide a means by which the C8 proton becomes labile in order to initiate a proton transfer cascade leading to the phosphoryl transfer. The necessity of the conserved amino acids in the active site of the 6 kinases was tested using the site-directed mutagenesis programme to generate mutated versions of the enzymes, which lack the conserved amino acids. This study indicated that the amino acids indeed play an important role in the functionality of the enzyme.^{7,8}

Group 2 kinases such as shikimate kinase and human adenylate kinase 1, have conserved amino acid residues in the ATP binding active site which allows for the “push” mechanism to occur.^{7,8} The “push” mechanism (Figure 1.6) involves:

- i. The deprotonation of the exo-amino group of the adenyl moiety by a carbonyl from a protein backbone (Figure 1.6 **1A**, green arrows), initiating the phosphoryl transfer.
- ii. The deprotonation of the exo-amino group triggers an electron cascade (part **1A**, red arrows) resulting in protonation of the adenyl C8 by a conserved arginine Arg110 group (part **1A**, blue arrows). The change in hybridization at the C8 position from sp^2 to sp^3 renders the C8-H more acidic.
- iii. The C8-H is transferred to the α - PO_4 via a threonine Thr17 group (part **1A**, black arrows), resulting in a proton transfer to the β - PO_4 via a conserved Arg117 (part **1A**, purple arrows).
- iv. There is subsequent deprotonation of the substrate hydroxyl group allowing for nucleophilic attack at the γ - PO_4 . The γ - PO_4 is consecutively protonated by a charge lysine amino acid Lys15 (part **1A**, orange arrows), resulting in a pentavalent γ - PO_4 intermediate with the substrate nucleophile.

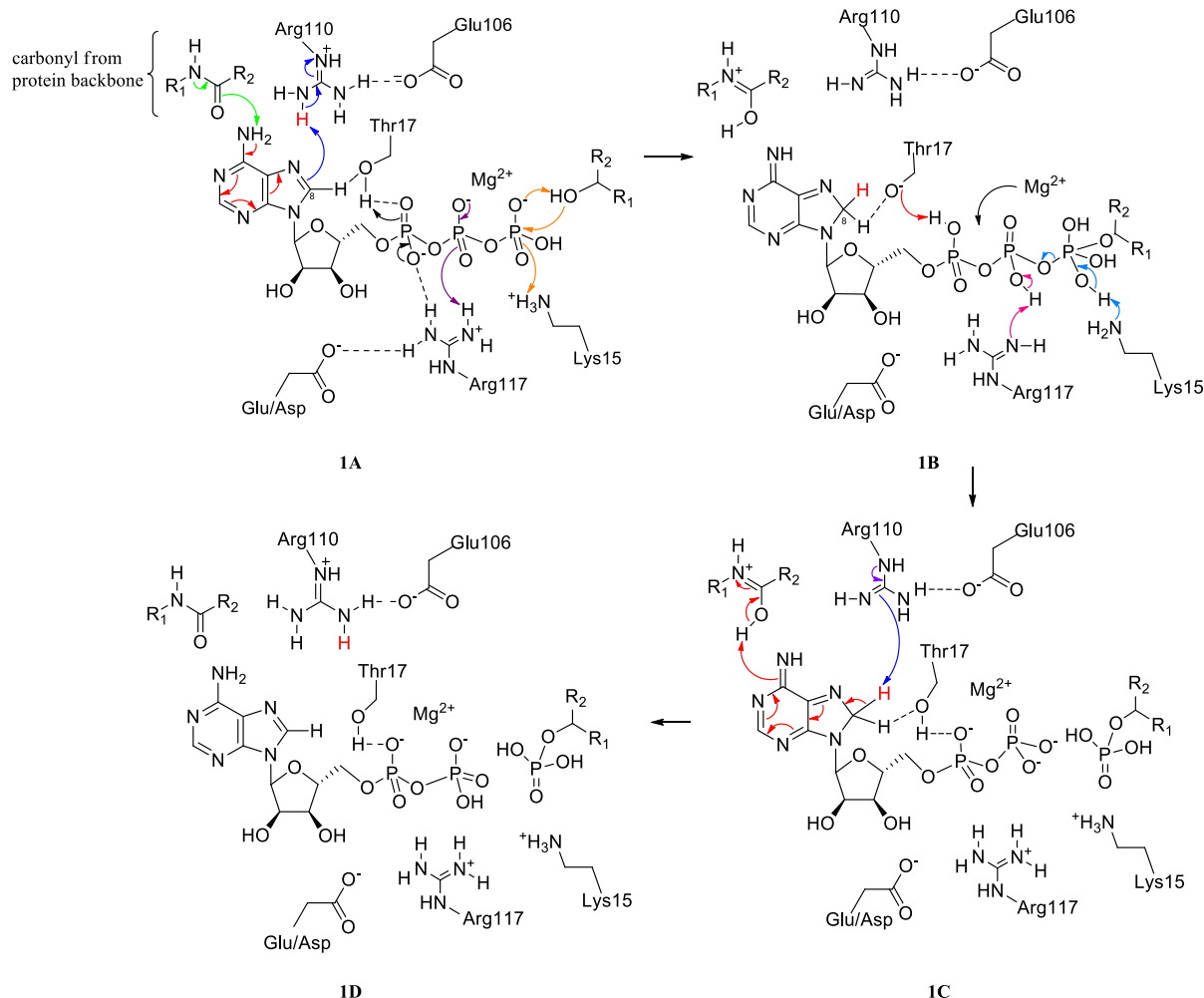


Figure 1.6: The "push" mechanism demonstrated for shikimate kinase.⁷

This set of electron and proton transfers regulates the breakage of the O—P bond between the β -PO₄ and γ -PO₄ groups (Figure 1.6, **1B**) via the γ -PO₄ pentavalent intermediate. The bond breakage is initiated by the Lys15 returning to its charged state, removing its donated proton from the γ -PO₄ resulting in an electron cascade to break the O—P bond (part **1B**, blue arrows), in which the Mg²⁺ moves from its β - γ PO₄ co-ordination to the α - β PO₄ co-ordination. The amino acids Arg117 and Thr17 return to their original ground states (part **1B**, pink and red arrows respectively), followed by the Arg110 removing the proton donated to C8 (part **1C**, blue arrows) which initially allowed for its change in hybridization from sp² to sp³. The removal of the C8 proton returns the carbon to its original sp² hybridized state triggering an electron cascade to move through the purine ring system, resulting in protonation of the exo-amino group

(part **1C** red arrows). The final state of the active site (part **1D**) leaves the shikimate in its phosphorylated form, shikimate-3-phosphate.^{7,8}

The “pull” mechanism (Figure 1.7) associated with Group 4 kinases,^{7,8} involves:

- i. The protonation of the adenyl N7 by the NH₂ of a Arg residue (Figure 1.7 **2A**, blue arrows) which triggers deprotonation of the C8 position by a serine/threonine (Ser/Thr) residue (part **2A**, red arrows), forming a carbene at the C8 position which is stabilized by an interaction with a carbonyl from a conserved glycine residue (part **2B**, dashed line from C8 to carbonyl carbon of Gly).
- ii. The Ser/Thr amino acid residue transfers the C8 proton to the α-PO₄ (part **2A**, red arrows). The proton from the α-PO₄ is transferred to the β-PO₄ via a conserved Arg residue (part **2A**, purple arrow).

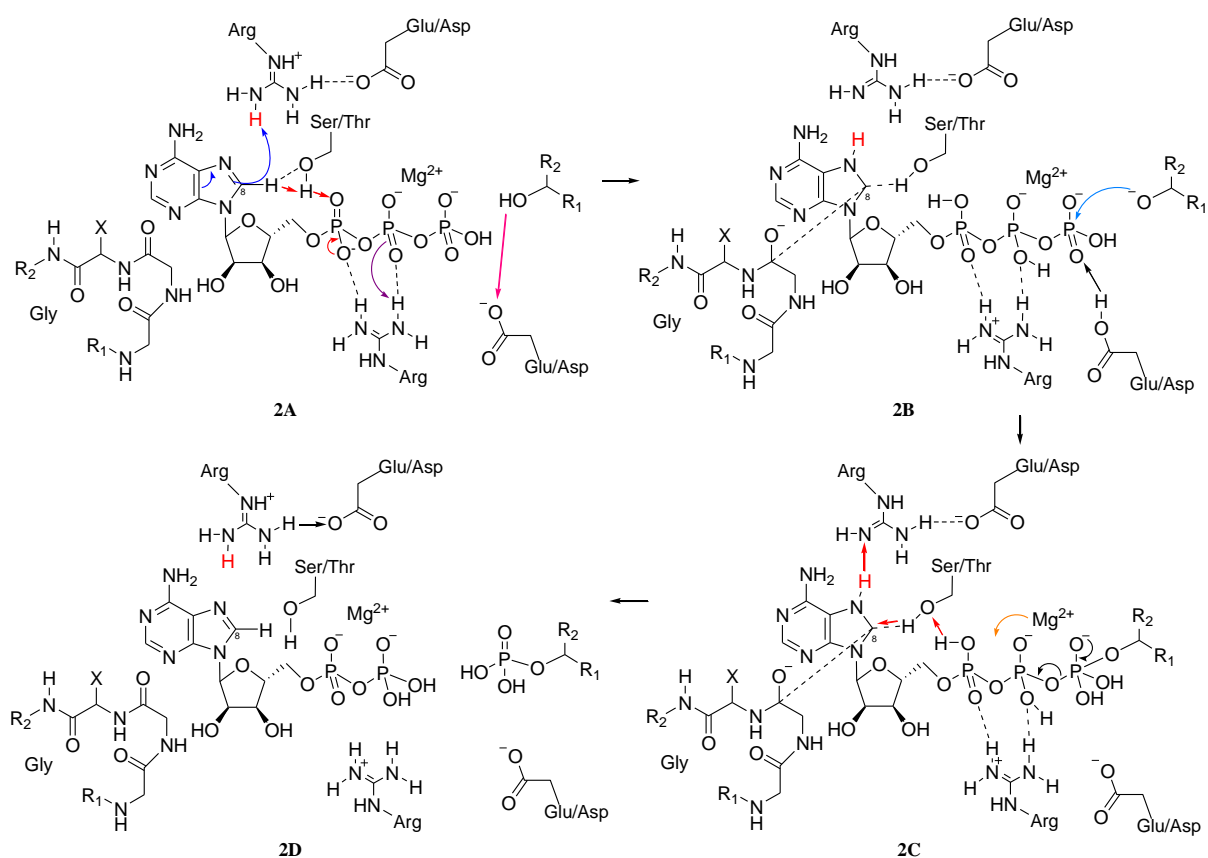


Figure 1.7: The “pull” mechanism demonstrated for Group 4 Kinases.⁷

- iii. Subsequently there is deprotonation of the hydroxyl group of the enzymes substrate by a glutamic acid/aspartic acid (Glu/Asp) residue (part **2A**, pink arrow), allowing for nucleophilic attack at the γ -PO₄ by the substrate (part **2A**, blue arrow). The protonated Glu/Asp residue transfers a proton to the γ -PO₄, resulting in a pentavalent γ -PO₄ intermediate, which in turn allows for the phosphoryl transfer (part **2C**, black arrows).
- iv. The co-ordination of Mg²⁺ changes from β - γ PO₄ to α - β PO₄ (part **2C**, orange arrow).
- v. The C8 regains its proton (part **2C**, red arrows), returning the electron density of adenylyl moiety back to its original state (part **2D**).

The mechanism demonstrated by Kenyon *et al.* (Figure 1.7) involves a series of electron movement as well as proton transfer. This mechanism is refined in Chapter 4 (section 4.2.3.1) indicating the electron movement based on the formation of a carbene.

1.4. Studying the reactivity of Adenine - a possible inhibitor for shikimate kinase

In kinases, the high energy phosphoryl transfer is mediated and regulated by the co-ordination of the C8-H of the ATP adenylyl moiety as well as the co-ordination of the adenylyl moiety in the active site.^{7,8} This is a new concept in the field of enzymology and could result in many breakthroughs in drug design, involving variation at the C8 position. The ATP adenylyl moiety, adenine, becomes an attractive scaffold for the design of inhibitors for Shikimate kinase due to it containing the regulative functionality. Using adenine as the main frame for possible drug derivatives against Mtb, deuteration of the C8 position could potentially allow for the KIE in kinase enzymes to be studied.

We wanted to explore the chemical reactivity of adenine and the deuteration of the C8 position to give a better foundation for the design of inhibitors. Therefore, the aims of this project were:

- i. To synthesise N9-adenine and purine derivatives, with main focus on N9-benzyl-adenine to investigate the regio-selectivity of adenine under basic S_N2 substitution conditions.
- ii. To simulate the S_N2 mechanism computationally and study the reactivity of adenine using classical and topological methods.
- iii. To explore the chemical reactivity of the C8-H in purines by exploring two possible mechanisms of hydrogen-deuterium exchange at the C8 position and studying the deuteration experimentally.

By studying these simpler systems, we believe we would be developing approaches that could be used to study reaction mechanisms, study the regio-selectivity of a compound, initiate synthesis of possible SK inhibitors, develop a frame work to study more complex systems and chemical reasons for the KIEs in future projects.

This thesis is therefore broken down into three main parts, Chapters 2, 3 and 4 each handling a specific concept on its own which contributes to a better understanding of adenine. Each chapter is treated as a mini-dissertation and consists of background information, results and discussion and a concluding section. The first section, Chapter 2, handles the experimental characterisation of adenines most reactive sites under S_N2 conditions. Chapter 3 discusses how computational methods were used to investigate the reasoning behind the preferred reactivity sites for the alkylation of adenine. The final section, Chapter 4, contains the mechanistic studies for the deuteration of adenine. An overall detailed conclusion is presented in Chapter 5.

Chapter 2

2.1. Characterisation of an N9-benzyladenine isomer: Confusion in the literature

2.1.1 Synthesis of N9-benzyladenine and its structural isomer

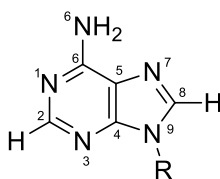


Figure 2.1: N9-substituted adenine indicating IUPAC numbering of atoms.

N9-substituted adenines (Figure 2.1) have been studied for many years because of their important biological roles. They have been synthesised as bioactive agents themselves or as precursors to active agents. N9-alkyladenine derivatives have highly potent cyclic nucleotide phosphodiesterase (PDE) inhibition, with high selectivity for PDE-4.¹² Specifically, N9-benzyladenine derivatives have the same PDE-4 inhibition profile which is improved immensely when a methyl group is added to the exocyclic nitrogen, N6.¹³ It is important to develop inhibitors for PDE as PDE can be targeted for anti-asthmatic,¹⁴ anti-inflammatory activity¹⁵⁻¹⁷ and activity against diseases such as multiple sclerosis and autoimmune disease.¹⁸ Other N9-substituted adenine derivatives have antiviral activity for DNA viruses and retroviruses¹⁹⁻²¹ (such as human immunodeficiency virus - HIV) and others are cytotoxic to tumour cell lines.^{20,22} N9-alkyladenine derivatives with bromine substituted at the C8-position are antagonists for the adenosine A_{2B} receptor (AA_{2B}R) and show interaction with all four adenosine receptors (ARs) (AA₁R, AA_{2A}R, AA_{2B}R, and AA₃R).²³ These AR targeting compounds show promise as potential therapeutic agents for cardiovascular and neurodegenerative diseases. N9-allyl-adenine

derivatives which have an alkyl group at the C8 position also behave as AR antagonists.²⁴ N9-substituted 8-oxoadenine derivatives have been shown to have interferon (IFN) inducing activity and have been synthesised from N9-substituted adenines, such as N9-benzyladenine.^{25,26} IFN inducers are being targeted as a new class of antiviral drugs.

The synthesis of N9-benzyladenine has been reported in many studies involving the synthesis of N9-substituted purines and is commonly synthesised by the alkylation of adenine through a S_N2 mechanism. The reaction involves deprotonation of the purine ring by a base (Figure 2.2), theoretically this occurs at the N9 position as the most common tautomeric form of adenine has the proton on N9 (discussed in Chapter 3),^{27,28} followed by a S_N2 substitution of the resulting adenine anion by an electrophile, which in this case is a benzyl halide.

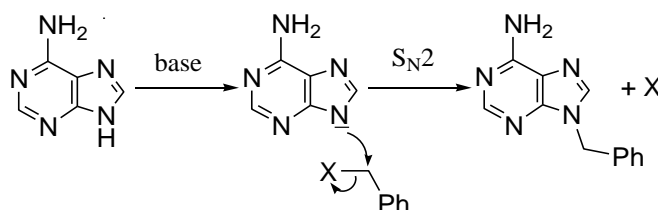


Figure 2.2: S_N2 substitution mechanism for synthesis of N9-benzyladenine. X: halide leaving group.

Various bases, solvents, temperatures and times have been employed for the synthesis of N9-benzyladenine (Table 2.1), each yielding a structural isomer as a minor product which is assigned as N3-benzyladenine or N7-benzyladenine. Possible structural isomers of N9-benzyladenine are N1-, N3, N7 or N6-benzyladenine (Figure 2.3).

Table 2.1: Synthetic procedures for N9-benzyladenine from adenine and benzyl bromide.

Base	Solvent	Time (hr)	Temperature (°C)	% Yield ratio
KOH	Aliquat 366	- ^b	Heated ^b	48: ^b (N9-Bn:N3-Bn) ²⁹
K ₂ CO ₃	DMF ^a	4	RT	53:23 (N9-Bn: N3-Bn) ²⁶
K ₂ CO ₃	DMF ^a	16	RT	60:21 (N9-Bn: N7-Bn) ²³
NaH	DMF ^a	24	60°	66:21 (N9-Bn: N7-Bn) ³⁰

^aDried solvent, ^b Yield % only given for N9-benzyladenine.

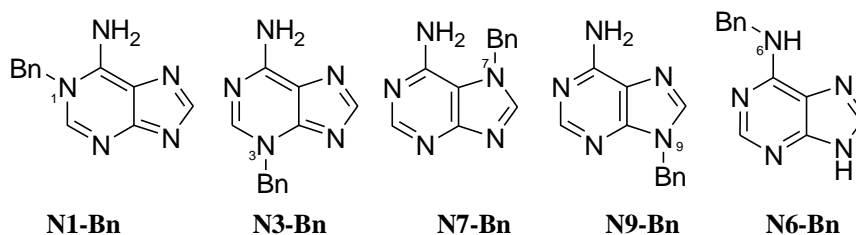


Figure 2.3: Structural isomers of benzyladenine: N1- (**N1-Bn**), N3- (**N3-Bn**), N7- (**N7-Bn**), N9- (**N9-Bn**) and N6-benzyladenine (**N6-Bn**).

2.1.2 Characterisation of the major and minor structural isomer by NMR spectroscopy

2.1.2.1 Characterisation of major structural isomer by NMR spectroscopy

The main characterisation of N9-benzyladenine and its structural isomer is based on the ^1H NMR spectrum chemical shift assignments of the C2-H and C8-H in the purine ring. The ^1H NMR chemical shifts in DMSO- d_6 and in CDCl_3 of N9-benzyladenine are given in Table 2.2.

Table 2.2: ^1H NMR spectrum chemical shifts (ppm) of N9-benzyladenine.

reference	C2-H	C8-H	NH ₂	Ph	CH ₂	Solvent
Siah <i>et al.</i> ²⁶	8.14	8.24	7.24	7.24–7.30	5.35	DMSO- d_6
Lambertucci <i>et al.</i> ²³	8.15	8.26	7.25	7.33	5.37	DMSO- d_6
Nair <i>et al.</i> ³⁰	8.28	8.17	7.29–7.33	7.29–7.33	5.38	DMSO- d_6
Sun <i>et al.</i> ³¹	8.26	8.15	-	7.26–7.34	5.37	DMSO- d_6
Petrov <i>et al.</i> ²¹	8.28	8.12	6.95–7.25	6.95–7.25	5.43	DMSO- d_6
Ranganathan <i>et al.</i> ³²	8.22, 8.22 ^a	-	-	7.30	5.41	DMSO- d_6
Platzer <i>et al.</i> ²⁹	8.32, 8.20 ^a	7.23	7.23	7.33	5.41	CDCl_3

^a Peaks were not assigned to C8-H or C2-H.

From Table 2.2, three points can be noted surrounding the ^1H NMR spectrum chemical shift assignments:

- The assignment of the C2-H and C8-H chemical shifts made by Siah *et al.*²⁶ and Lambertucci *et al.*²³ are in agreement with each other, having the C2-H in the 8.1 ppm region and the C8-H in the 8.2 ppm region.
- Studies by Nair *et al.*,³⁰ Sun *et al.*³¹ and Petrov *et al.*²¹ had interchanged the C2-H and C8-H assignment, having the C2-H in the 8.1 ppm region and the C8-H in the 8.2 ppm region (Figure 2.4).

- iii. Platzer *et al.*²⁹ had assigned the chemical shifts of the purine ring protons of N9-benzyladenine in CDCl₃ at 8.32 ppm and the other at 8.20 ppm. The shifts in CDCl₃ were similar to those in DMSO-d₆, but the peaks were not specifically assigned to the C2-H and C8-H.

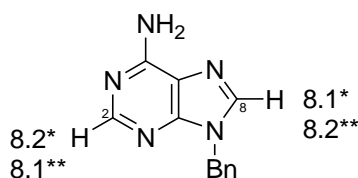


Figure 2.4: ¹H NMR spectrum chemical shifts (ppm) of aromatic protons of N9-benzyladenine in DMSO-d₆. *assignment by Siah and Lambertucci **assignment by Nair, Sun, and Petrov.

Siah *et al.*²⁶ and Platzer *et al.*²⁹ provided the assignments of the ¹³C NMR spectrum chemical shifts of N9- and N3-benzyladenine (Table 2.3). Considering that the two researchers recorded the ¹³C NMR spectra in different solvents, DMSO-d₆ and CDCl₃, the peaks that are assigned to the purine ring carbons match well. Interestingly, the C2 and C8 chemical shift assignments of the N3-benzyladenine, 143 ppm and 152 ppm, respectively, are reversed when compared to the N9-benzyladenine, 152 ppm and 140 ppm, respectively. The other carbon shifts vary only slightly between the two compounds.

Table 2.3: ¹³C NMR spectrum chemical shifts (ppm) for N9- and N3-benzyladenine.

Reference	C2	C4	C5	C6	C8	Ph	CH ₂	Solvent
N9-benzyladenine								
Siah <i>et al.</i> ²⁶	152.6	149.5	118.7	156.0	140.8	137.1 ^a , 128.6–127.5	46.1	DMSO-d ₆
Platzer <i>et al.</i> ²⁹	152.7	149.6	118.8	156.1	140.8	137.1 ^a , 127.7–127.5	46.2	CDCl ₃
N3-benzyladenine								
Siah <i>et al.</i> ²⁶	143.3	149.7	120.5	154.9	152.6	136.1 ^a , 128.6–127.9	52.1	DMSO-d ₆
Platzer <i>et al.</i> ²⁹	143.4	149.7	120.3	154.9	152.5	136.9 ^a , 128.6–128.0	52.0	CDCl ₃

^a Quaternary carbon in phenyl ring.

Platzer *et al.*²⁹ proposed how two-dimensional ¹H-¹³C correlated NMR spectroscopy, Heteronuclear Multiple Bond Correlation (HMBC) and Heteronuclear Single Quantum

Coherence (HSQC), can be used to assign the ^1H and ^{13}C NMR spectrum chemical shifts of adenine and its derivatives, irrespective of the solvent used and substituent effects. The acknowledgment of the upfield position of the C5 was an essential tool used to interpret the 2D ^1H - ^{13}C correlated NMR spectrum. The C5 resonates most upfield relative to the other purine carbons as it is the only carbon in the purine ring bonded to one nitrogen. The other carbons which are bonded to two nitrogens are more deshielded and therefore resonate more downfield.²⁹

Platzer *et al.*²⁹ proposed that the ^1H - ^{13}C correlations of protons either directly bonded to a carbon (HSQC) or 2 to 3 bonds away from a carbon (HMBC) are as follows:

- i. In an HMBC the C2-H shows strong correlations with C6 and C4 (Figure 2.5 **A**, blue arrows) and a weak correlation with C5 (part **A**, dotted arrow), and the C8-H has strong correlations with C5 and C4 (part **B**, blue arrows).

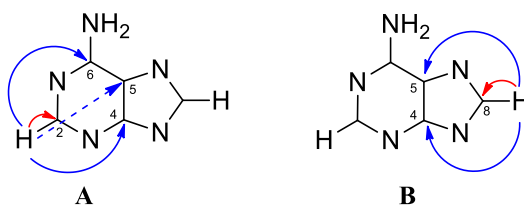


Figure 2.5: HMBC and HSQC ^1H - ^{13}C correlations of C2-H (**A**) and C8-H (**B**). Double bonds and alkyl groups are removed for simplicity of the demonstration.

- ii. In an HSQC the C2-H shows a correlation with its bonded C2 (part **A**, red arrow), while the C8-H shows a correlation with its bonded C8 (part **B**, red arrow).
- iii. In the HMBC C6 is differentiated from C4 by having its only correlation with the C2-H, while C5 is differentiated by having its only strong correlation with the C8-H and a very weak correlation with the C2-H. The C4 has strong correlations with both the C2-H and C8-H.

Platzer *et al.*²⁹ extended the use of the HMBC to identify the site of alkylation on purine rings. This is done by analysing the correlations of the protons from the alkyl carbon directly attached to N1, N3, N7 or N9 with the carbons in the purine ring.

In an HMBC Platzer *et al.*²⁹ proposed that:

- i. The N7-alkylated adenine would be differentiated from the N3- and N9-alkylated adenines as the protons from the N7-alkyl group would show correlations with C5 (Figure 2.6 **N7-R**, black arrows), while the protons from the N3- and N9-alkyl groups would show correlations with C4 (**N3-R** and **N9-R**, black arrows).

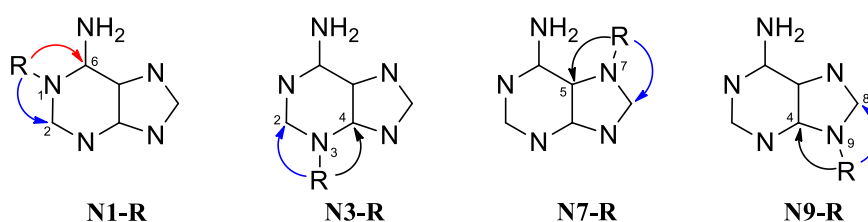


Figure 2.6: Theoretical HMBC ^1H - ^{13}C correlations of N1- (**N1-R**), N3- (**N3-R**), N7- (**N7-R**) and N9- (**N9-R**) alkylated adenines. Double bonds and hydrogens are removed for simplicity of the demonstration.

- ii. Alkylation at the pyrimidine ring, N1 and N3, can be differentiated from that of the imidazole ring, N7 and N9, as the protons on the N1- and N3-alkyl group would show correlations with C2 (Figure 2.6 **N1-R** and **N3-R**, blue arrows), whereas the protons on the N7- and N9-alkyl group would show correlations with C8 (Figure 2.6 **N3-R** and **N9-R**, blue arrows).
- iii. The N1-alkylated adenine would show correlations of the protons on the alkyl group with C6 (Figure 2.6 **N1-R**, red arrow).

2.1.2.2 Characterisation of the minor structural isomer by NMR spectroscopy

The ^1H NMR chemical shifts of the structural isomer, yielded as the minor product in the synthesis of N9-benzyladenine, are shown in Table 2.4. Siah *et al.*²⁶ and Platzer *et al.*²⁹ also

2.1.3 Alternative synthesis of *N*-benzyladenine structural isomers

Leonard and Henderson studied the mechanism in which N1- and N3-benzyladenine rearrange to N6-benzyladenine which exhibits cytokinin activity.^{33,34} Dimroth rearrangement is responsible for these inter-conversions, which involves an endocyclic heteroatom becoming an exocyclic heteroatom and vice versa, as well as the rearrangement of the endo-purine ring nitrogens (discussed in Section 2.2.6). In order to fully characterise the mechanism of these rearrangements, Leonard and Henderson synthesised ¹⁵N¹, ¹⁵N⁹ and ¹⁵N⁶ labelled N3-, N9- and N6-benzyladenines and characterised the products by ¹H NMR spectroscopy. To synthesize ¹⁵N⁶ labelled N3-benzyladenine (Figure 2.8, **N3-Bn-¹⁵N⁶**), Leonard made use of thiopurine chemistry developed by Neiman *et al.* whereby the neutral form of 6-methylthiopurine (**2**) alkylates specifically at the N3 position.³⁵

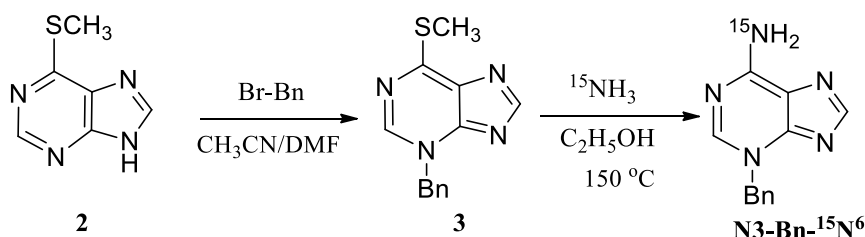


Figure 2.8: Synthesis of *N*3-benzyladenine-¹⁵N⁶ (**N3-Bn-¹⁵N⁶**).³³

The regio-selectivity of the alkylation is explained by the polarization, resulting from donation of electron density by the thioether group, concentrating at the N3 position (Figure 2.9, **2a**).³⁵ The thiopurine anion (**2b**) is said to undergo alkylation at the N9 and N7 positions as the negative charge is distributed equally on the N7 and N9. Leonard completed the synthesis of ¹⁵N⁶ labelled N3-benzyladenine (Figure 2.8) by treatment of N3-benzyl-6-methylthiopurine (**3**) with ¹⁵NH₃.

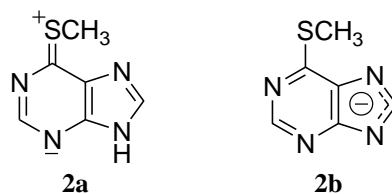


Figure 2.9: Neutral (**2a**) and anionic form (**2a**) of 6-methylthiopurine.³⁵

¹⁵N⁶ labelled N6-benzyladenine (Figure 2.10, **N6-Bn-¹⁵N⁶**) was synthesised by treating 6-chloropurine (**4**) with benzylamine-¹⁵N hydrochloride.³³

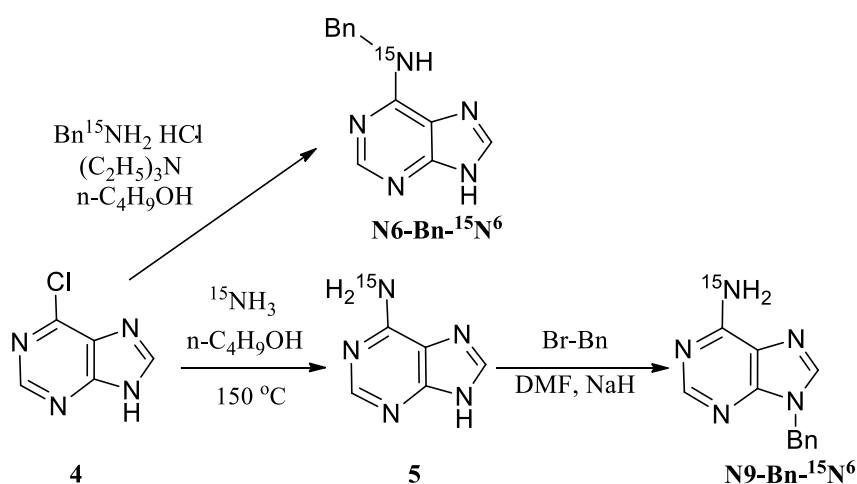


Figure 2.10: Synthesis of N⁶-benzyladenine-¹⁵N⁶ (**N6-Bn-¹⁵N⁶**) and N9-benzyladenine-¹⁵N⁶ (**N9-Bn-¹⁵N⁶**).³³

The synthesis of the labelled N9-benzyladenine derivatives, Figure 2.10 **N9-Bn-¹⁵N⁶** and Figure 2.11 **N9-Bn-¹⁵N⁹**, followed the same S_N2 substitution procedures provided by the articles described in section 2.1.1. The starting material adenine-¹⁵N⁶ (Figure 2.10, **5**) and adenine-¹⁵N⁹ (Figure 2.11, **7**) were reacted with benzyl bromide under basic conditions in DMF at room temperature for 16 hours to yield **N9-Bn-¹⁵N⁶** and **N9-Bn-¹⁵N⁹**, respectively.³³

¹⁵N⁹ labelled N6-benzyladenine (Figure 2.11, **N6-Bn-¹⁵N⁹**) was synthesised by treating 6-chloropurine-¹⁵N⁹ (**6**) with benzylamine hydrochloride.³³

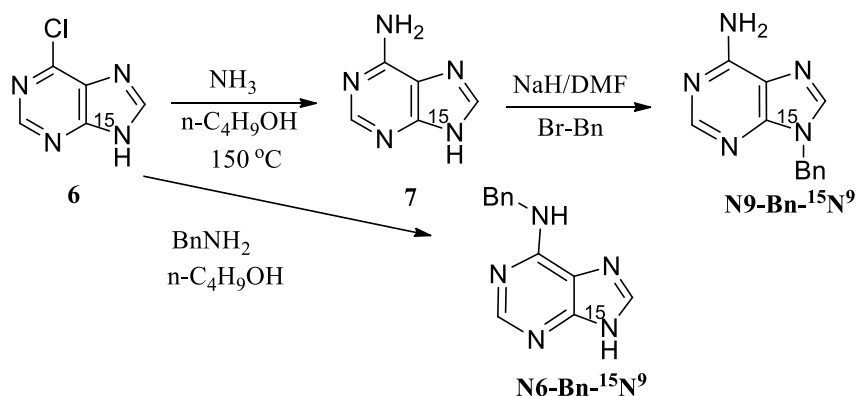


Figure 2.11: Synthesis of *N*9-benzyladenine- $^{15}\text{N}^9$ (**N9-Bn- $^{15}\text{N}^9$**) and *N*6-benzyladenine- $^{15}\text{N}^9$ (**N6-Bn- $^{15}\text{N}^9$**).³³

$^{15}\text{N}^1$ labelled *N*6-benzyladenine (Figure 2.12, **N6-Bn- $^{15}\text{N}^1$**) was synthesised by treating adenine- $^{15}\text{N}^6$ (**5**) with chloromethyl pivalate to yield 9-pivaloyloxymethyl adenine- $^{15}\text{N}^6$ (**8**), which then underwent a benzylation to yield 1-benzyl-9-pivaloyloxymethyl adenine- $^{15}\text{N}^6$ hydrobromide (**9**).

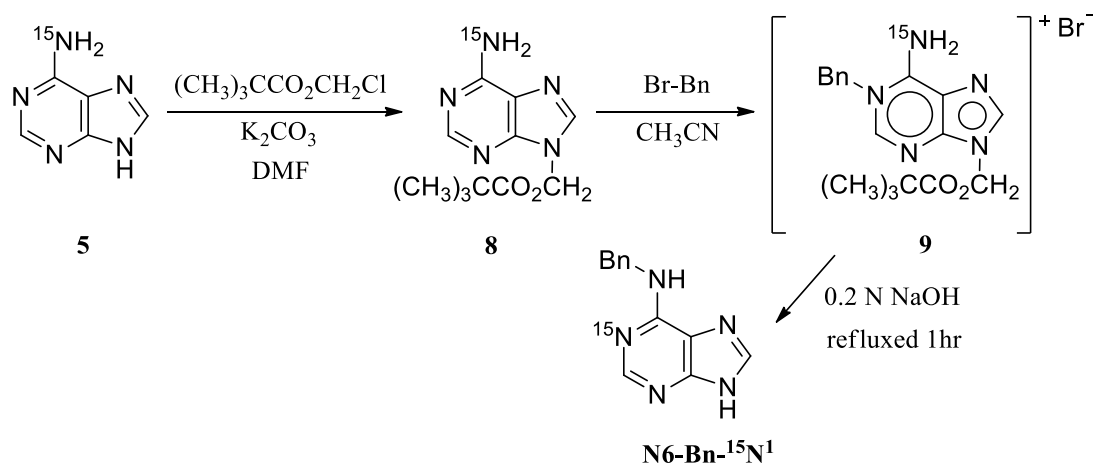


Figure 2.12: Synthesis of *N*6-benzyladenine- $^{15}\text{N}^1$ (**N6-Bn- $^{15}\text{N}^1$**).³³

The use of base (0.2 N NaOH) under reflux (1 hour) to remove the pivaloate protection from the *N*9 position resulted in a Dimroth rearrangement to yield *N*6-benzyladenine- $^{15}\text{N}^1$ (Figure 2.12, **N6-Bn- $^{15}\text{N}^1$**).³³

The positions of the ^{15}N labelled nitrogens were monitored by ^{15}N - ^1H spin-spin coupling of the aromatic protons, C2-H and C8-H. For *N*-benzyladenine- $^{15}\text{N}^1$ compounds, the C2-H is a doublet while the C8-H is a singlet, whereas the *N*-benzyladenine- $^{15}\text{N}^9$ compounds show a

doublet for the C8-H and a singlet for the C2-H. The *N*-benzyladenine-¹⁵N⁶ compounds show singlets for both the C2-H and the C8-H.³³

The ¹H NMR spectra of the unlabelled *N*-benzyladenine regio-isomers (Table 2.5) corresponded well with the labelled *N*-benzyladenine isomers.³³ The assignment of the ¹H NMR chemical shifts of N3- and N9-benzyladenine corresponds well to those made by Siah *et al.*²⁶ The assignment of the purine ring protons by Leonard and Henderson³³ in Table 2.5 can be compared with those of Fox³⁶ who took on the challenge of confirming the assignment of purine ring protons made by previous authors^{37,38} by replacing the C8-H of various *N*-benzyladenine regio-isomers (**N1-Bn**, **N3-Bn**, **N7-Bn**, **N9-Bn** and **N6-Bn**) with a deuterium (discussed in Chapter 4).

Table 2.5: C8-H and C2-H ¹H NMR spectrum chemical shifts (ppm) in DMSO-*d*₆ of unlabelled and ¹⁵N-labelled *N*-benzyladenine regio-isomers.³³

<i>N</i> -benzyladenine	N3-benzyladenine		N9-benzyladenine		N6-benzyladenine	
	C2-H	C8-H	C2-H	C8-H	C2-H	C8-H
unlabelled	8.53(s)	7.76(s)	8.17(s)	8.24(s)	8.18(s)	8.10(s)
¹⁵ N ⁶ labelled	8.54(s)	7.77(s)	8.18(s)	8.25(s)	8.18(s)	8.11(s)
¹⁵ N ⁹ labelled	-	-	8.17(s)	8.24(d, 9Hz)	8.18(s)	8.11(d, 8Hz)
¹⁵ N ¹ labelled	-	-	-	-	8.16(d, 16Hz)	8.09 (s)

Fox studied the effect of the position of the benzyl group on the ¹H NMR chemical shifts of the purine ring protons (Table 2.6).³⁶ As the benzyl group is electron withdrawing, it should pull electron density out of the purine ring, deshielding the C2-H and C8-H and thus causing them to move downfield compared to the chemical shifts in adenine.³⁶

Table 2.6: *N*-benzyladenine regio-isomers ¹H NMR spectrum chemical shifts (ppm) in DMSO-*d*₆.

Compound	C2-H	C8-H	Ph	CH ₂
Adenine	8.15	8.11	-	-
N1-benzyladenine	8.39	7.99	7.33	5.54
N3-benzyladenine	8.62	7.87	7.42	5.59
N7-benzyladenine	8.23	8.46	7.29	5.72
N9-benzyladenine	8.32	8.37	7.42	5.50
N6-benzyladenine	8.36	8.30	7.46	4.93

Fox's chemical shift values from the ^1H NMR spectrum might appear to be shifted compared to the reported values by Leonard,³³ however the trend in the relative positions of the chemical shifts between paired purine protons of each isomer (δ chemical shift) remains the same (Table 2.7). Fox hypothesised that substituting the group at the N6 position should have minimal effect on the chemical shift of the C2-H and C8-H as it is not directly bonded to the purine ring and hence shouldn't withdraw much electron density.³⁶ However, there was a dramatic change in the chemical shift of the protons. He postulated that this could be due to the benzyl group deactivating the ability of the N6 amino group to donate electron density into the ring.

Table 2.7: ^1H NMR spectrum δ chemical shifts values between C2-H and C8-H of each *N*-benzyladenine isomer.

<i>N</i> -benzyladenine	Leonard	Fox
N3-benzyladenine	0.77	0.75
N7-benzyladenine	0.20 ^a	0.23 ^a
N9-benzyladenine	0.07	0.05
N6-benzyladenine	0.08	0.06

^a ^1H NMR spectral data taken from reference.³⁹

The difference in the proton chemical shifts caused by substitution on the pyrimidine ring (N1 and N3) with that of substitution on the imidazole ring (N3 and N9) is linked to the resonance stability.³⁶ Although the bicyclic system remains aromatic with 10 π electrons ($4n + 2$), when each ring is considered individually, substitution on the pyrimidine ring allows it to have a 7 electron π system and the imidazole ring to have a 5 electron π system (Figure 2.13, **N1-Bn** and **N3-Bn**). This is less energetically favourable than the resonance achieved by substitution on the imidazole ring which has a 6 electron π system in both the pyrimidine and imidazole ring (Figure 2.13, **N7-Bn** and **N9-Bn**).³⁶

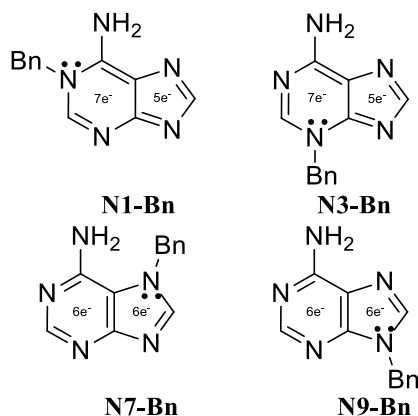


Figure 2.13: Resonance stability of pyrimidine (**N1-Bn** and **N3-Bn**) and imidazole (**N7-Bn** and **N9-Bn**) substitution.

The N1- and N3-benzyladenine can have a 6 electron π system in both the pyrimidine and imidazole rings (Figure 2.14). This, however, is achieved by charge separation, leaving the imidazole ring more negative than the pyrimidine ring, which could result in the C8-H being more upfield, due to shielding, than the C2-H.³⁶ The C2-H will experience less shielding due to the electron withdrawing effect from the positive charge on either N1 or N3, hence having its chemical shift more downfield than the C8-H.

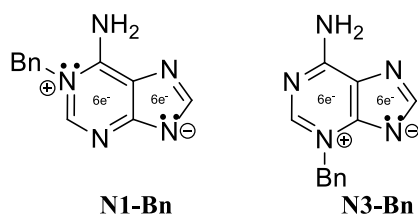


Figure 2.14: Pyrimidine ring substitution: 6 electron π system in the pyrimidine and imidazole ring by charge separation.³⁶

2.1.4 N3- and N9-substituted adenine as directing groups to yield N7- and N3-substituted adenines

The seminal work on the synthesis of adenine derivatives was carried out by Leonard and co-workers³⁹⁻⁴¹ and Montgomery *et al.*⁴²⁻⁴⁴ The ability to direct the alkylation to specific N-atoms by using removable blocking groups was reported by Leonard and Fujii in 1963,⁴⁰ in which N3-substituted adenine directed alkylation to the N7-position. The N3-substituted adenines were

prepared using the method reported by Montgomery *et al.*⁴³ in 1963 where by adenine and an alkyl halide in dimethylacetamide are refluxed without the presence of base.^{45,46} The result of the N3-position being alkylated under neutral conditions was explained by adenine being an ambient nucleophile allowing for alkylation on the N1- or N3-position,⁴⁶ where at the transition state a partial positive charge is distributed by resonance over the pyrimidine ring (Figure 2.15 **12**).

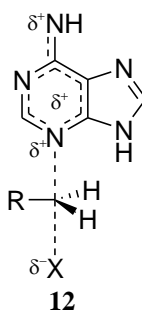


Figure 2.15: Concentration of positive charge in pyrimidine ring at the transition state.⁴⁶

However, the N3-position is less sterically hindered, rendering it more reactive. Polar aprotic solvents which can exhibit dipole character are most favourable for the reaction, as the solvent molecules could interact with the charged transition state, stabilising it.

Hence, Leonard *et al.*⁴⁰ synthesised N3-benzyladenine by heating adenine in dimethylacetamide with benzyl bromide and used the N3-substituent as a directing group for alkylation at the N7 position. N3-benzyladenine when heated in dimethylacetamide in the presence of methyl iodide [Figure 2.16, **N3-Bn**] undergoes methylation at the N7-position, yielding N3-benzyl-7-methyladenine iodide salt (**14**, where X = I), which results in the formation of N7-methyladenine (**15**) under hydrogenolysis. The N7-methyladenine (**15**) undergoes N3-alkylation and can be reverted back to the N3,7-disubstituted adenine (**14**, where X = Br) upon addition of benzyl bromide.

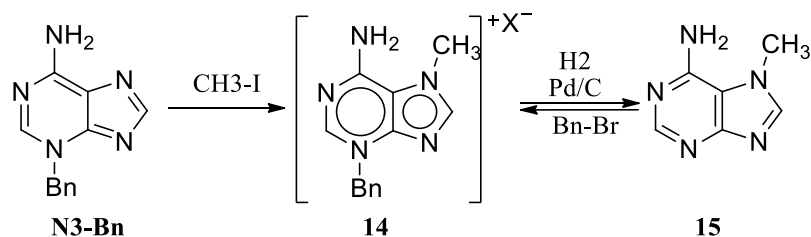


Figure 2.16: N3-benzyladenine as a directing group for synthesis of N7-methyladenine.⁴⁰

In 1986 Leonard *et al.*³⁹ reported an improved synthetic route for the synthesis of N7-alkyladenine via N3-alkylated adenine. N7-benzyladenine [Table 2.8] was synthesised by heating N3-benzyladenine in the presence of benzyl bromide to yield the N3,7-dibenzyladenine bromide salt, which was converted to N7-benzyladenine under hydrogenolysis.

Table 2.8: ¹H NMR spectrum chemical shifts (ppm) of N7-benzyladenine in DMSO-d₆.⁴²

Benzyladenine	C2-H, C8-H	NH ₂	Ph	CH ₂
N7-benzyladenine	8.35, 8.55	6.93	7.33	5.80

It was observed that the hydrogenolysis removes the benzyl group on the pyrimidine ring before the one on the imidazole ring. This method was similar to that reported by Montgomery to synthesise N7-benzyladenine.⁴²

The use of N3-substituted adenines to direct alkylation to the N7-position parallels that of N9-substituted adenines directing alkylation to the N1-position.⁴¹ The method used by Fox³⁶ to synthesise N1-benzyladenine was cross-referenced from Leonard and Fujii.⁴¹ The synthesis was accomplished by reacting N9-substituted adenine [Figure 2.17, **16**] with benzyl bromide which directed the alkylation to the N1-position, to form the N1,9-disubstituted bromide salt (**17**). The substituent at the N9-position acted as a directing and a blocking group which was removed in the last step of the synthesis by reaction of the disubstituted compound with hydrochloric acid to yield the desired N1-benzyladenine (**N1-Bn**). The N1-benzyladenine can undergo Dimroth rearrangement (See section 2.2.6) under refluxing basic conditions to yield N6-benzyladenine (**N6-Bn**) as shown in Figure 2.17.

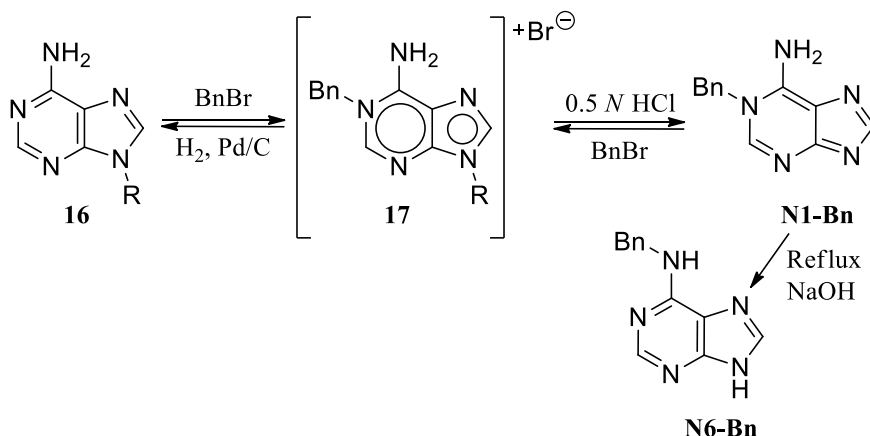


Figure 2.17: N9-substituted adenine **16** as a directing group for the synthesis of N1-benzyladenine **N1-Bn**.⁴¹

Synthetic methods reported by Montgomery *et al.*⁴²⁻⁴⁴ and Leonard *et al.*³⁹⁻⁴¹ have been used often in the current literature. Marek *et al.*⁴⁷ and Malinakova *et al.*⁴⁸ synthesised N3-, N7- and N9-benzyladenine via the methods described by Leonard *et al.*³⁹⁻⁴¹ and Montgomery *et al.*⁴²⁻⁴⁴ and provided their ¹H and ¹³C NMR spectral data of the synthesised compounds (Table 2.9).

Table 2.9: ¹H and ¹³C NMR spectrum chemical shifts (ppm) reported for N3-, N7-, and N9-benzyladenine in DMSO-*d*₆.

	N3-benzyladenine		N7-benzyladenine		N9-benzyladenine	
	Marek ⁴⁷	Malinkov ⁴⁸	Marek ⁴⁷	Malinkov ⁴⁸	Marek ⁴⁷	Malinkov ⁴⁸
C2-H ^a	8.29	-	8.18	-	8.16	-
C8-H ^a	7.76	-	8.43	-	8.25	-
C2 ^b	143.63	145.1	152.41	152.6	152.66	153.9
C4 ^b	150.31	148.8	160.14	159.3	149.49	149.9
C5 ^b	120.28	121.3	110.83	110.8	118.68	118.7
C6 ^b	154.88	156.4	151.48	151.8	155.99	156.0
C8 ^b	152.39	152.4	146.39	147.5	140.84	142.5

^a ¹H NMR, ^b ¹³C NMR

Thus to conclude from the above, in recent literature both N3- and N7-benzyladenine are reported as the minor product from the direct alkylation of adenine under basic conditions to synthesize N9-benzyladenine.^{23,30} This poses a problem surrounding the data obtained from research involving the use of N3 or N7-benzyladenine as the results are based on only one of the regio isomers. There is also contradiction in the assignment of the purine proton peaks for N3-

and N9-benzyladenine, which are also found in other purine derivatives, posing again a problem that the data surrounding deuteration of the purine protons could be misleading. As shown, extensive research surrounding the synthesis of adenine derivatives and motivation for ^1H NMR spectroscopy trends has been performed. In the 1960's, Leonard and Montgomery covered the synthesis of adenine derivatives using directing groups. However, much of the experimental data, such as the ^1H and ^{13}C NMR spectroscopy data are not reported, making it difficult to follow and confirm the *N*-benzyladenine regio-isomers. Alternative multistep synthetic methods have been developed to avoid the prevalence of the minor structural isomer; however for industry the synthetic procedure should be as short as possible.

In this research, the true identity of the minor product formed from direct alkylation of adenine under basic conditions will be confirmed. This will indicate the most reactive site of adenine under these conditions. The ^1H NMR spectrum chemical shift assignments of the purine ring protons in various solvents of the major and minor products will be analysed, which is essential for deuteration studies also carried out in this research (Chapter 4).

2.2 Results and Discussion

2.2.1 Characterisation of N3- and N9-benzyladenine by 2D ^1H - ^{13}C NMR correlation spectroscopy

N9-benzyladenine (Figure 2.18, **N9-Bn**) was the first compound to be synthesised to create a library of N9-alkylated adenine derivatives. The alkylation of adenine with benzyl bromide in DMSO as solvent was carried out under basic conditions, using potassium tert-butoxide (K^tOBU) as a base, at reflux temperature (110-120 °C) for 4 hours. This yielded the desired N9-benzyladenine as a major product. However, this synthesis led to the appearance of a minor product in a ratio of 9:1 (N9:N3).

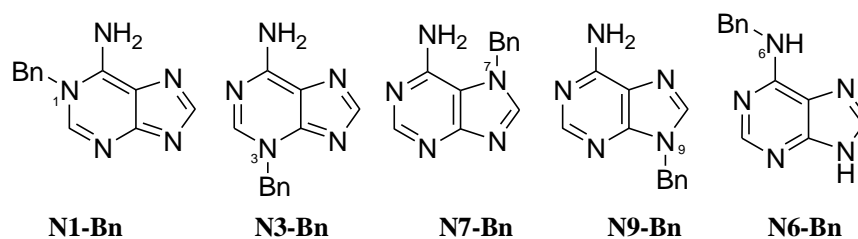


Figure 2.18: Structural isomers of N-benzyladenine: N1- (**N1-Bn**), N3- (**N3-Bn**), N7- (**N7-Bn**), N9- (**N9-Bn**) and N6-benzyladenine (**N6-Bn**).

The minor product was unambiguously assigned by X-ray crystallography (Supporting Material) as N3-benzyladenine (Figure 2.19) along with the confirmation of the N9-benzyladenine.

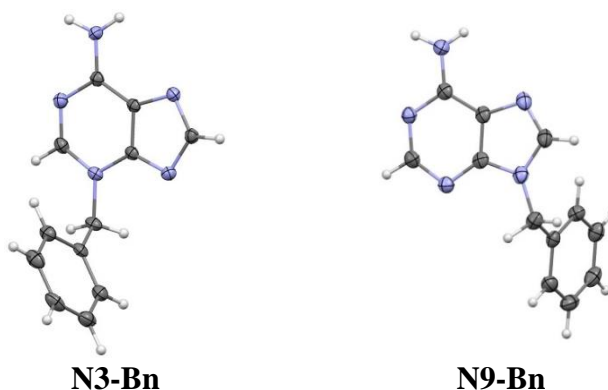


Figure 2.19: Crystal structures of N3- and N9-benzyladenine (**N3-Bn** and **N9-Bn**, respectively).

Careful analysis of NMR spectra and assignment of chemical shifts was carried out in order to confirm that the solution structures were indeed the same as the crystal structures and to unequivocally solve the confusion in the literature surrounding the assignment of the ^1H NMR spectrum chemical shifts.

2.2.2 NMR analysis and structural assignments for N9-benzyladenine

In DMSO- d_6 the ^1H NMR spectrum for N9-benzyladenine showed two singlet peaks at 8.26 ppm and 8.16 ppm (Figure 2.3), which corresponded to the C8-H and C2-H, respectively, in addition to the benzyl aromatic and CH_2 proton peaks. In this research, to solve the uncertainty in the literature as to which peak was the C2-H and which the C8-H, the assignment of all peaks was approached from a theoretical point of view.

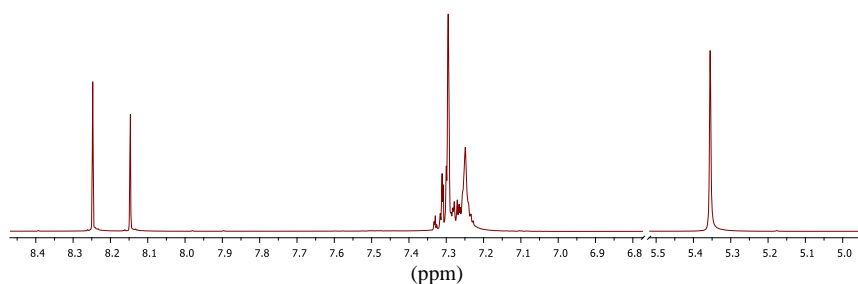


Figure 2.20: ^1H NMR spectrum (ppm) for N9-benzyladenine in DMSO- d_6 (400 MHz).

The ^1H and ^{13}C NMR spectra in DMSO- d_6 (Table 2.10 and Table 2.11, respectively), which were obtained from N9-benzyladenine corresponded well to the literature reported ^1H and ^{13}C NMR spectra in DMSO- d_6 .^{26,47}

Table 2.10: ^1H NMR chemical shifts (ppm) for N9-benzyladenine.

C2-H (1H, s)	C8-H (1H, s)	NH ₂ (2H, s)	Ph (5H, m)	CH ₂ (2H, s)	Solvent
8.16	8.26	7.23–7.33 (7H)		5.36	DMSO- d_6
8.38	7.78	6.02	7.25–7.38	5.36	CDCl_3
8.22	8.15	-	7.28–7.37	5.43	MeOD- d_4

Table 2.11: ^{13}C NMR chemical shifts (ppm) for N9-benzyladenine.

C2	C4	C5	C6	C8	CH ₂	Ph	Solvent
152.8	149.6	118.8	156.1	141.0	46.3	127.6–128.8 (C ₀ , 137.2)	DMSO-d ₆
152.2	150.1	119.3	154.8	141.0	47.6	128.1–129.4 (C ₀ , 135.5)	CDCl ₃
154.1	150.8	119.9	157.4	142.8	48.2	128.9–130.1 (C ₀ , 137.8)	MeOD-d ₄

The assignment of which protons are directly attached to a carbon was determined by HSQC (Supporting Material), which shows $^1J_{\text{H,C}}$ correlations between a carbon and its directly attached protons. The HSQC (Figure 2.21) showed a strong correlation between the carbon at 152.8 ppm with the proton at 8.16 ppm and a strong correlation between the carbon at 141.0 ppm and the proton at 8.26 ppm. Thus, the chemical shifts were assigned: the C2-H proton (8.16 ppm) with the C2 carbon (152.8 ppm) and the C8-H proton (8.26 ppm) with the C8 carbon (141.0 ppm).

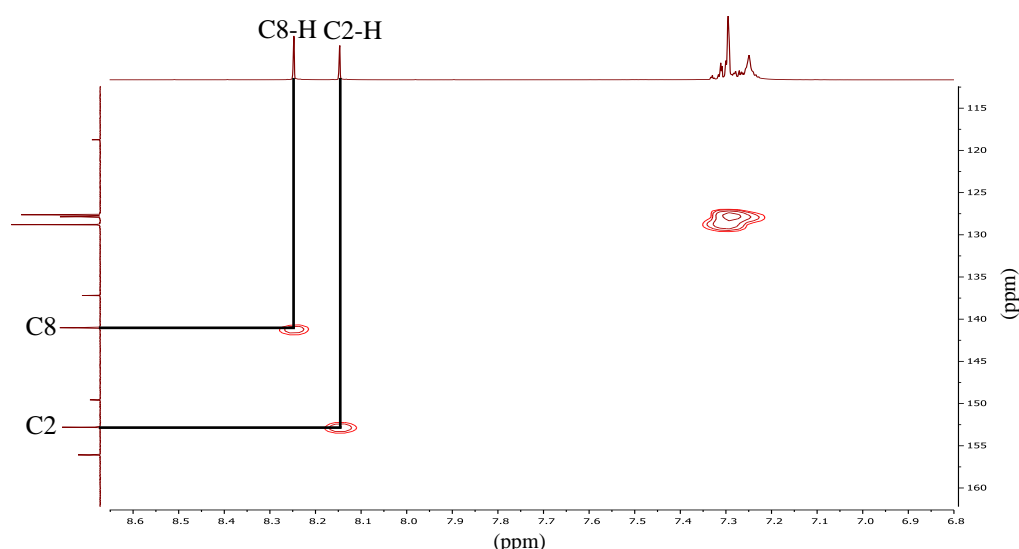


Figure 2.21: HSQC of N9-benzyladenine in DMSO-d₆ (400 MHz), y-axis: ^{13}C NMR (ppm), x-axis: ^1H NMR (ppm). Solid line: carbon correlation with directly bonded proton.

HMBC spectroscopy was an essential tool used in the assignment of carbon and hydrogens peaks in the ^{13}C and ^1H NMR spectra, respectively, in a compound with no $^3J_{\text{H,H}}$ correlations. Theoretically, as discussed by Platzer *et al.*,²⁹ it was possible to predict which carbons will correlate to which hydrogens, working with the analogy that a carbon correlates with hydrogens 2, 3 and possibly 4 bonds away from itself. Figure 2.22 demonstrates which carbon (start of

arrow from labelled carbon) is expected to correlate with which hydrogen (arrow head pointing to carbon to which the correlating hydrogen is attached) for N9-benzyladenine in the HMBC, making it possible to deduce how many correlations a carbon should have. It also shows the proton to which the carbon is directly attached by having two correlations “hovering” around the directly attached proton, which is found in the middle of the hovering correlation.

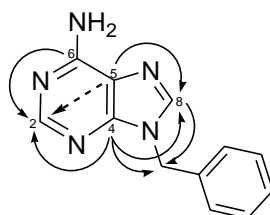


Figure 2.22: Predicted HMBC ^1H - ^{13}C correlations for N9-benzyladenine.

Thus, to distinguish C2 from C8, C2 has only one hovering correlation with its directly attached proton, whereas C8 has one hovering correlation with its directly attached proton and a correlation with the CH₂ protons of the benzyl group. C4 is differentiated from C5 and C6 by having 3 proton correlations, namely the C2-H, the C8-H, and the CH₂ protons. C6 and C5 are differentiated from each other by acknowledging that C6 will be further downfield than C5 because C5 is more shielded than C6 due to the electron donating resonance effect of the NH₂ group and having only one neighbouring nitrogen. C5 correlates with the C8-H and could potentially correlate with the C2-H (dotted arrow), however this is expected to be a weak correlation. The above trend was studied in various deuterated solvents, DMSO-d₆, CDCl₃ and MeOD-d₄.

From the HMBC of N9-benzyladenine (Figure 2.23), the predicted ^1H - ^{13}C correlations were observed: C6 having one correlation with the C2-H, C2 having one hovering correlation with the C2-H, C4 having three correlations (C8-H, C2-H and CH₂) and C8 having two correlations (one hovering with C8-H, and one direct correlation with CH₂). C5 showed the predicted correlation with the C8-H, however it also shows a weak correlation with the C2-H, and a strong correlation

with protons in the multiplet. The correlation in the multiplet is due to the NH₂ protons which are hidden among the benzene ring protons (integration is 7H). This was confirmed by D₂O exchange in which the correlation disappeared.

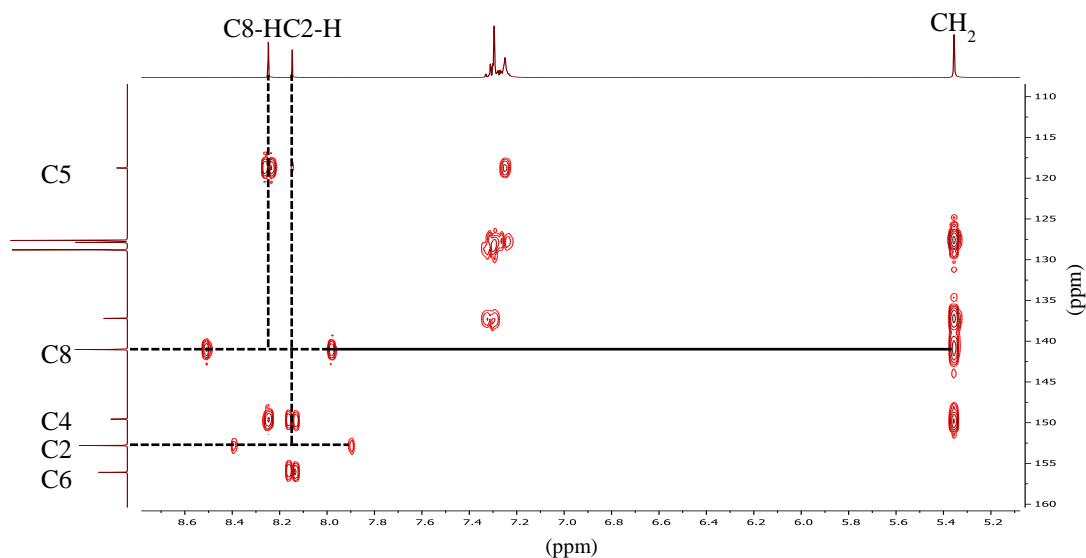


Figure 2.23: HMBC of N9-benzyladenine in DMSO-*d*₆ (400 MHz), y-axis: ¹³C NMR (ppm), x-axis: ¹H NMR (ppm). Dotted line: hovering correlation with the directly bonded proton. Solid line: carbon correlation with protons 2 or more bonds away.

This technique of predicting the HMBC ¹H-¹³C correlations was then used to analyse the chemical shifts in CDCl₃ and MeOD-*d*₄. Due to the low solubility of adenine derivatives in the two deuterated solvents, the quaternary carbons in the ¹³C NMR spectrum were not as dominant and in some cases absent compared to those that appeared when DMSO-*d*₆ was used. However their correlations with the hydrogens in the HMBC were still seen.

Performing the NMR spectroscopy series in CDCl₃ gave unexpected results. From the HMBC in CDCl₃ (Figure 2.24), the ¹H NMR spectrum chemical shifts of the C8-H and C2-H were reversed as compared to those in DMSO-*d*₆, having the C2-H at 8.38 ppm and the C8-H at 7.78 ppm. As will be discussed further on in section 2.2.3, it was also in contradiction with Platzers *et al.*²⁹ assignment of the N9-benzyladenine in CDCl₃, having the C8-H and C2-H at 8.20 ppm and 8.32 ppm region, which corresponds to the N3-benzyladenine in CDCl₃. The carbon chemical shifts in the ¹³C NMR spectrum were kept constant with those in DMSO-*d*₆. C5

does not have a correlation with any other proton in the HMBC except with the expected the C8-H and C2-H correlations, unlike in DMSO-d₆ where C5 correlates with the NH₂ protons.

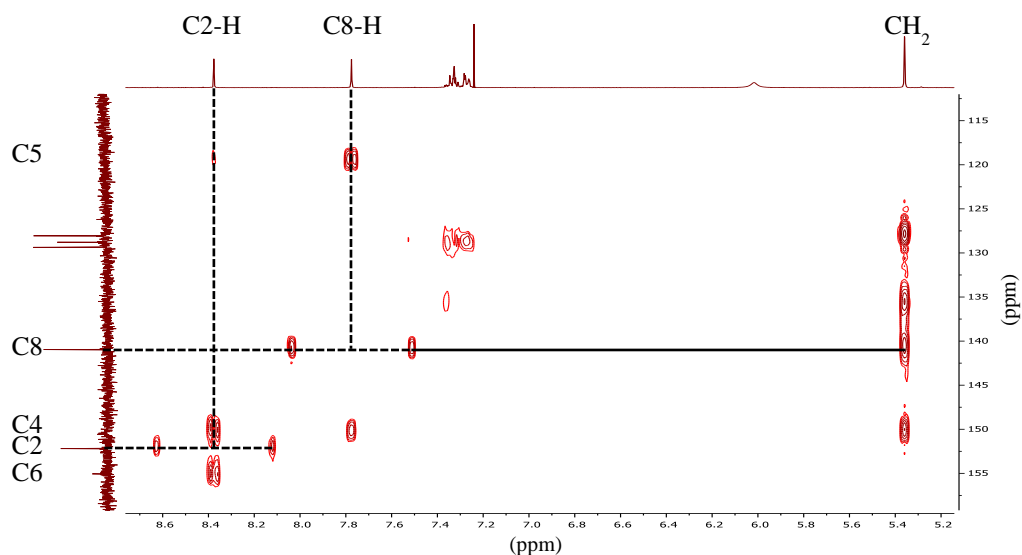


Figure 2.24: HMBC of *N*9-benzyladenine in CDCl₃ (400 MHz), y-axis: ¹³C NMR (ppm), x-axis: ¹H NMR (ppm). Dotted line: hovering correlation with the directly bonded proton. Solid line: carbon correlation with protons 2 or more bonds away.

The ¹H NMR spectrum of *N*9-benzyladenine in MeOD-d₄ (Figure 2.25) has the C2-H and C8-H purine ring proton singlets at 8.22 ppm and 8.15 ppm, respectively, the same region as they occur in DMSO-d₆. This similarity between the ¹H NMR spectrum in DMSO-d₆ and MeOD-d₄ could be misleading and one would assign the same position of the C2-H and C8-H in both solvents.

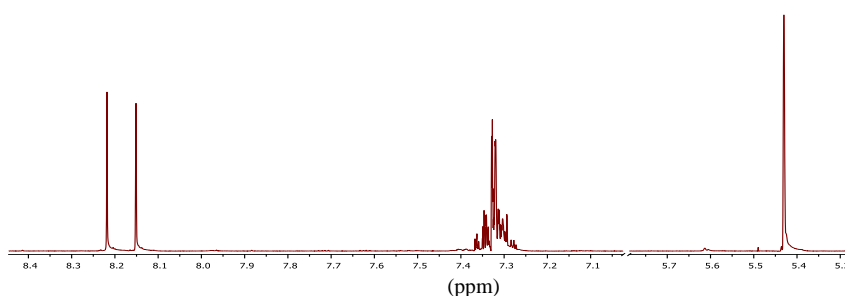


Figure 2.25: ¹H NMR spectrum (ppm) of *N*9-benzyladenine in MeOD-d₄ (400 MHz).

However, analysis of the HMBC in MeOD-d₄ (Figure 2.26) proved that the ¹H NMR spectral peaks were reversed compared to the assignment in DMSO-d₆, having the C2-H at 8.22 ppm and

C8-H at 8.15 ppm. The assignment of the ^1H NMR spectral peaks in MeOD-d_4 was essential as it is used to identify which proton in the purine ring system undergoes hydrogen-deuterium exchange (Chapter 4).

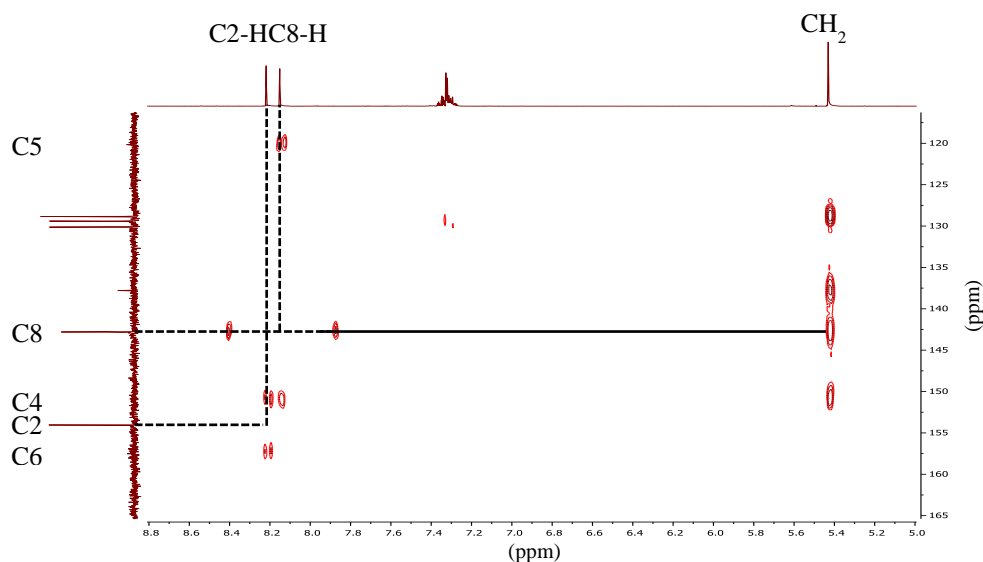


Figure 2.26: HMBC of *N9*-benzyladenine in MeOD-d_4 (400 MHz), y-axis: ^{13}C NMR (ppm), x-axis: ^1H NMR (ppm). Dotted line: hovering correlation with the directly bonded proton. Solid line: carbon correlation with protons 2 or more bonds away.

The hovering correlation of C2 with its directly attached proton (C2-H) was absent in the HMBC, along with the hovering correlation of the CH_2 with its directly attached protons. The reason for this was unclear, however due to the fact that the correlation had appeared in the HMBC with DMSO-d_6 and CDCl_3 , the absence could be due to solvent effects.

2.2.3 NMR analysis and structural assignments for *N3*-benzyladenine

The ^1H and ^{13}C NMR spectrum of the minor product *N3*-benzyladenine (Table 2.12 and Table 2.13 respectively) corresponded to the literature reported *N3*-/*N7*-benzyladenine ^1H and ^{13}C NMR spectrum.

Table 2.12: ^1H NMR chemical shifts (ppm) for *N3*-benzyladenine.

C2-H (1H, s)	C8-H (1H, s)	NH_2 (2H, s)	Ph (5H, m)	CH_2 (2H, s)	Solvent
8.57	7.78	7.94	7.27–7.47	5.51	DMSO-d_6
8.26	8.18	10.34, 6.70	7.39	5.58	CDCl_3
8.60	8.21	-	7.46–7.33	5.63	MeOD-d_4

Table 2.13: ^{13}C NMR chemical shifts (ppm) for N3-benzyladenine.

C2	C4	C5	C6	C8	CH ₂	Ph	Solvent
143.5	149.6	120.1	154.9	152.3	52.1	128.0–128.6 (C ₀ , 136.1)	DMSO-d ₆
146.2	148.4	115.0	153.8	144.5	53.7	128.8–130.0 (C ₀ , 132.9)	CDCl ₃
147.5	150.3	117.1	156.2	150.0	54.3	129.3–130.3 (C ₀ , 136.2)	MeOD-d ₄

The ^1H NMR spectrum of N3-benzyladenine in DMSO-d₆ (Figure 2.27) shows two singlet peaks at 8.57 ppm and 7.78 ppm, corresponding to the purine ring protons, and the NH₂ protons as a broad peak at 7.95 ppm, separated from the multiplet, unlike N9-benzyladenine in which the peaks overlapped in the same region.

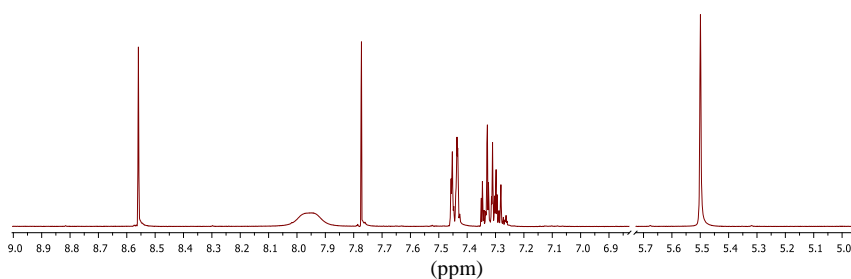


Figure 2.27: ^1H NMR spectrum (ppm) for N3-benzyladenine in DMSO-d₆ (400 MHz).

To determine the assignment of the peaks for N3-benzyladenine in the different solvents, the same theoretical prediction that was made for the N9-benzyladenine was applied (Figure 2.28). In this instance, C2 will have a hovering correlation with its directly attached proton and a correlation with the CH₂ protons from the benzene group, whereas C8 will have only one hovering correlation with its directly attached proton. C5, C4 and C6 will have the same ^1H - ^{13}C correlations as those predicted for N9-benzyladenine.

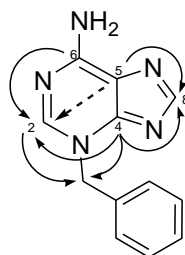


Figure 2.28: Predicted HMBC ^1H - ^{13}C correlations for N3-benzyladenine.

In the HMBC (Figure 2.29) the most upfield of the purine carbon shift, C5 (120.1 ppm), correlated with the C8-H but did not show an additional correlation with the C2-H or with the NH₂ protons.

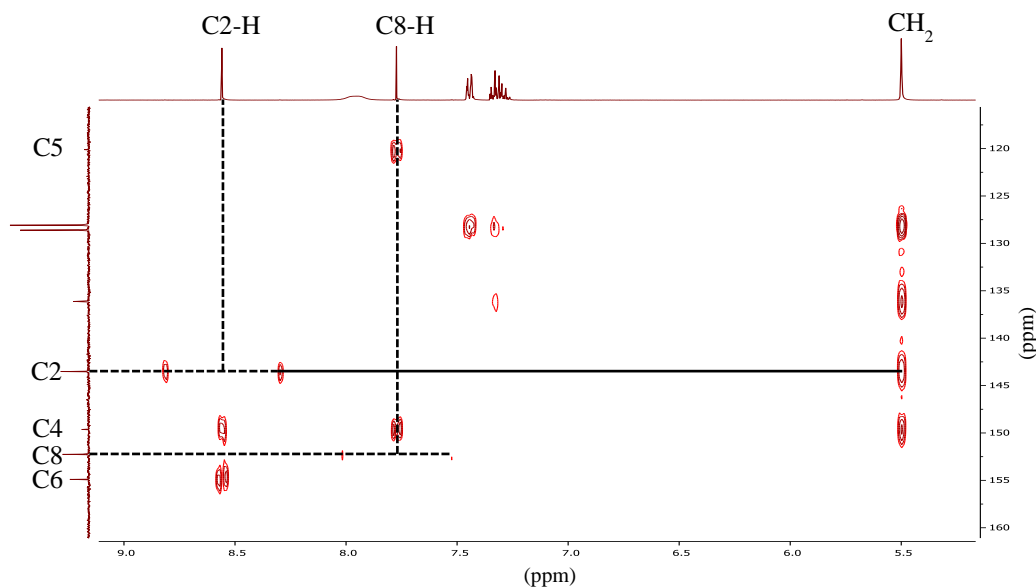


Figure 2.29: HMBC of N3-benzyladenine in DMSO-*d*₆ (400 MHz), y-axis: ¹³C NMR (ppm), x-axis: ¹H NMR (ppm). Dotted line: hovering correlation with the directly bonded proton. Solid line: carbon correlation with protons 2 or more bonds away.

C2 showed a hovering correlation with its attached proton (8.56 ppm) and a strong correlation with the CH₂ protons from the benzene group. However, C8 had a very weak correlation with its directly attached proton (7.77 ppm). The assignment of the C2-H and C8-H is the reverse of the literature reported values by Lambertucci *et al.*,²³ which reported the C2-H at 7.75 ppm and the C8-H at 8.55 ppm.

In the ¹H NMR in CDCl₃ of N3-benzyladenine the C2-H and C8-H peaks retained their relative positions as in DMSO-*d*₆ but occurred much closer together, having the C2-H at 8.26 ppm and C8-H at 8.18 as determined by the HMBC (Figure 2.30). The multiplet occurred as a single large peak that integrates to 5H. Conversely, in the ¹³C NMR spectrum, the C8 moves ±8 ppm downfield from 152.2 ppm to 144.3 ppm.

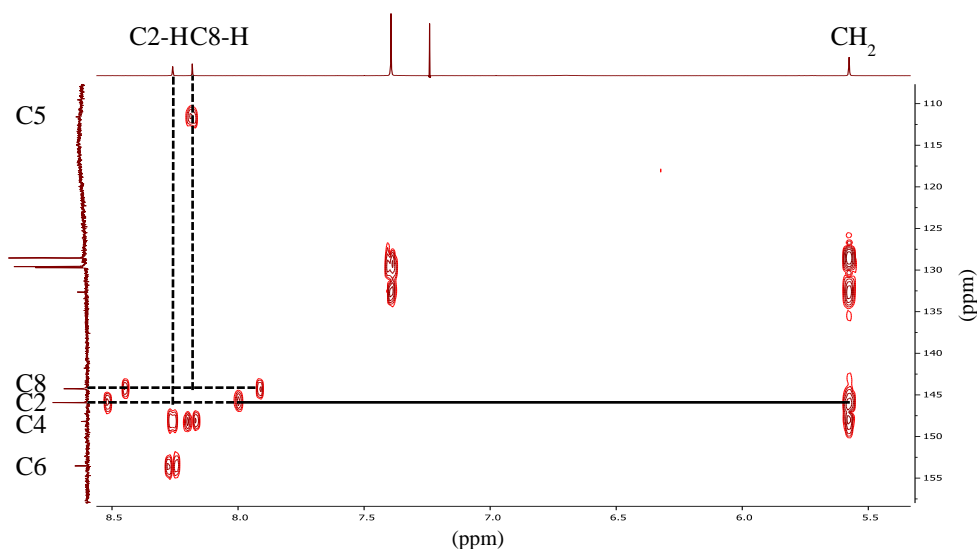


Figure 2.30: HMBC of N3-benzyladenine in CDCl_3 (400 MHz), y-axis: ^{13}C NMR (ppm), x-axis: ^1H NMR (ppm). Dotted line: hovering correlation with the directly bonded proton. Solid line: carbon correlation with protons 2 or more bonds away.

The assignment of the C2-H and C8-H ^1H NMR spectrum chemical shifts is in contradiction with the assignment of N3-benzyladenine by Platzer *et al.*,²⁹ who reported the C2-H and C8-H chemical shift assignments at 8.56 and 7.84 ppm, respectively, in CDCl_3 . It was shown earlier that these chemical shifts correspond to that of the N9-benzyladenine in CDCl_3 . A comparison of the ^1H NMR spectrum of N3-benzyladenine in CDCl_3 and N9-benzyladenine in DMSO-d_6 is shown in Figure 2.31 **A** and **B**, respectively.

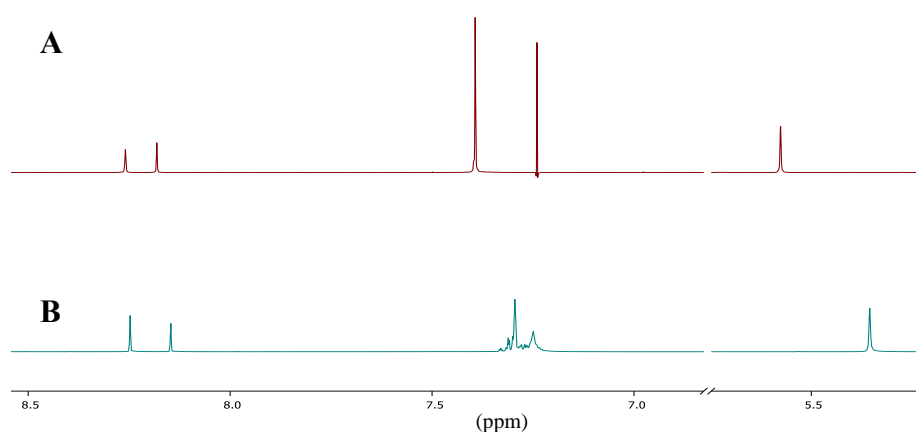


Figure 2.31: ^1H NMR spectrum (ppm) of N3-benzyladenine in CDCl_3 (A) vs. N9-benzyladenine in DMSO-d_6 (B) (400 MHz).

Comparing N3-benzyladenine in CDCl_3 (C2-H 8.26 ppm and C8-H 8.18 ppm) and N9-benzyladenine in DMSO-d_6 (C2-H 8.16 ppm and C8-H 8.26 ppm), the C2-H and C8-H peaks

occur in the same region with a very similar δ chemical shift between the two protons, δ 0.08 ppm and δ 0.10 ppm, respectively.

The same confusion can be seen with N3-benzyladenine in DMSO- d_6 (C2-H 8.57 and C8-H 7.78) and N9-benzyladenine in $CDCl_3$ (C2-H at 8.38 ppm and C8-H at 7.78 ppm), as shown in Figure 2.32 **A** and **B**, respectively. The N9-benzyladenine exhibited the characteristic far spread between the chemical shifts of the C2-H and C8-H (δ 0.60 ppm) that N3-benzyladenine possessed in DMSO- d_6 (δ 0.79 ppm).

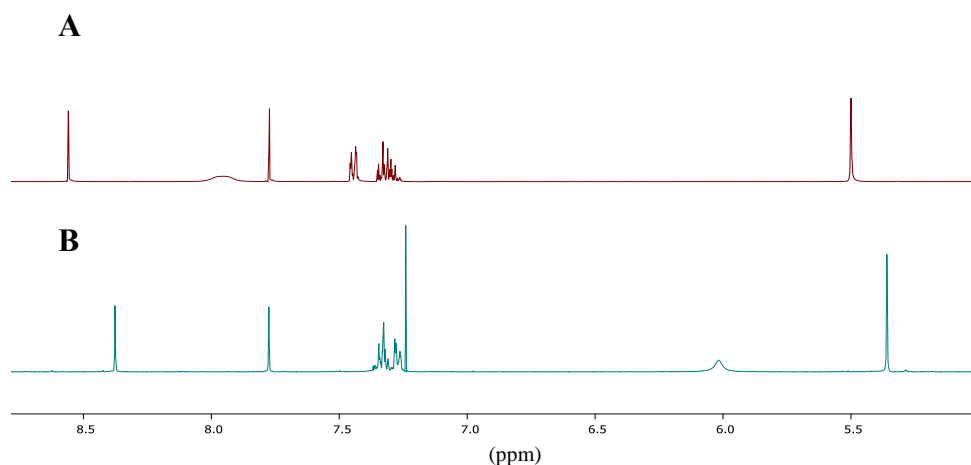


Figure 2.32: 1H NMR spectrum (ppm) of N3-benzyladenine in DMSO- d_6 (**A**) vs. N9-benzyladenine in $CDCl_3$ (**B**), (400 MHz).

In the N3-benzyladenine 1H NMR spectrum in MeOD- d_4 , an unusual occurrence of splitting of the C8-H and C2-H peaks occurred (Figure 2.33).

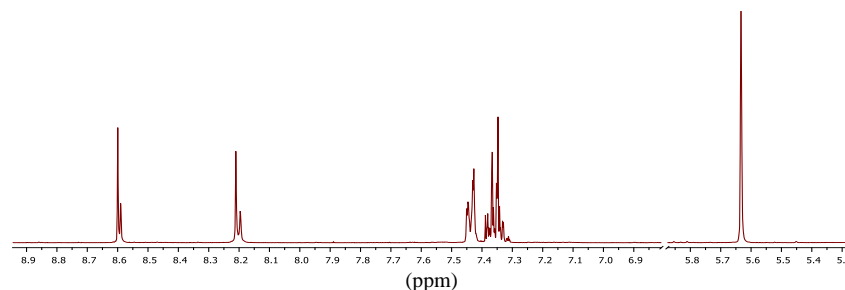


Figure 2.33: 1H NMR spectrum (ppm) of N3-benzyladenine in MeOD- d_4 (400 MHz).

The C2-H has its dominant singlet at 8.60 ppm and a minor singlet at 8.59 ppm, and the C8-H has its main singlet at 8.21 ppm and a minor singlet at 8.20 ppm.

The reason for this is unclear and solvent effect is expected to be the cause. The splitting of the peaks makes it seem as if a minor product occurs in solution, however integration of the CH₂ confirms that only one is present.

The HMBC (Figure 2.34) confirmed that the assignment of the C2-H and C8-H ¹H NMR chemical shifts kept their relative positions compared with those of N3-benzyladenine in DMSO-d₆ and CDCl₃, having the C2-H downfield to the C8-H. This assignment of the ¹H NMR spectral peaks was used to determine which proton undergoes deuterium exchange (Chapter 4).

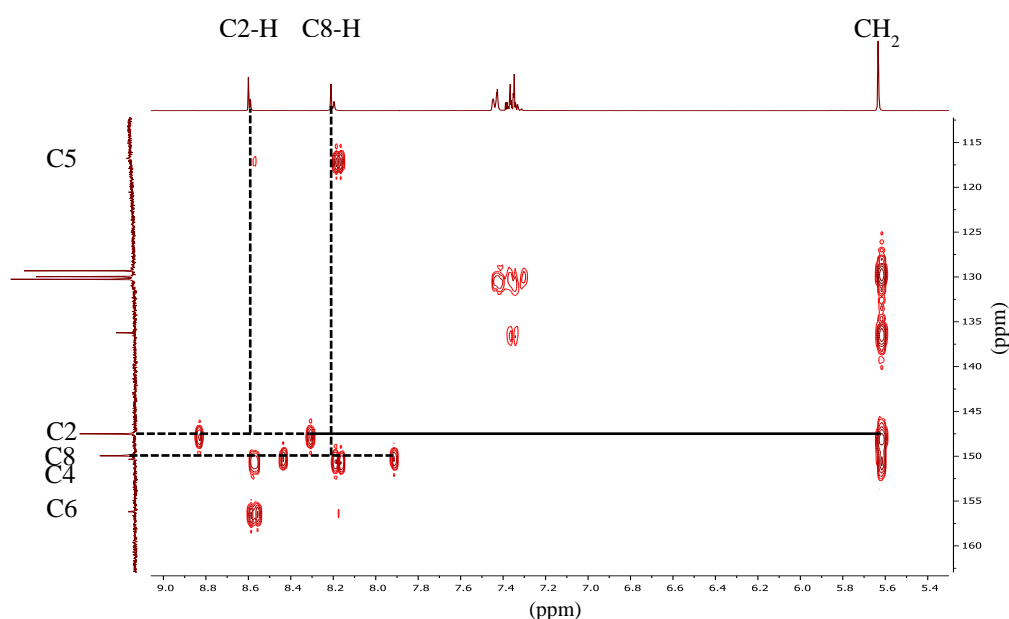


Figure 2.34: HMBC of N3-benzyladenine in MeOD-d₄ (400 MHz), y-axis: ¹³C NMR (ppm), x-axis: ¹H NMR (ppm). Dotted line: hovering correlation with the directly bonded proton. Solid line: carbon correlation with protons 2 or more bonds away.

The use of NMR techniques is often overlooked and from the purpose of this chapter it was seen how the chemical shifts of structures can be incorrectly assigned or incorrect structural isomers can be elucidated from the NMR spectra if NMR analysis is not done with caution. In literature, there is hardly any confusion with the ¹H NMR and ¹³C NMR spectra peak assignments of N9-benzyladenine apart from the reverse assignment of the C8-H and C2-H proton peaks in different solvents. Here it was shown how the correct proton and carbon peaks in the ¹H and ¹³C NMR spectra can be assigned by predicting the expected HMBC ¹H-¹³C

correlations. The NMR solvent can significantly shift the positions or reverse the assignment of the peaks of the N3- and N9-benzyladenine. However, with the techniques used, the effect of solvent does not influence the assignments.

2.2.4 Solvent effects on the synthesis of N9-benzyladenine

It has been reported that during the synthesis of N9-alkyladenine, increased amounts of N3-alkylated adenine forms as a result of heating the reaction in DMSO as a solvent with added base.⁴⁹ It has also been stated that heating the reaction of adenine with an alkyl halide in the absence of base yields N3-alkylated adenine,^{42,50} whereas heating the reaction in the presence of base allows for N9/N7 regio-isomers to form during the direct alkylation/benzylation.^{31,51-55} Sun and Hosmane investigated the synthesis of N9-benzyladenine and developed a new multistep synthetic route leading to the condensation of 1-benzyl-4-cyano-5-methoxymethyleneimino-imidazole with guanidine to yield the desired compound in a significant 70% yield without any regio-isomers as minor products.³¹ The use of a Mitsunobu reaction does yield N9- and N3-alkylated adenine as an alternative to S_N2 type reactions.⁵³ Regio-specific N9-adenine alkylation by 6-(heteroaryl)purines^{56,57} and bis-Boc protection⁵⁸ of adenine have been growing areas to eliminate the formation of minor regio-isomers.

It was shown that by direct alkylation of adenine it is not the N9/N7 regio-isomers that form but rather the N9/N3. It was considered how the ratio of N9:N3 be controlled using solvent during the benzylation of adenine by S_N2 substitution. In this section we show that the influence of solvent does not stop at the shifting of peaks in the ¹H NMR and ¹³C NMR spectra, but also plays a major role during the synthesis of N9-benzyladenine. Various solvent (Table 2.14) were used to study whether solvent itself could improve the N9:N3 ratio during synthesis, meaning lowering the N3-benzyladenine formation as much as possible. The best N9:N3 ratio was obtained when polar aprotic solvents, such as DMSO, DMF and Acetonitrile, were used (Table

2.14 No. 1–4). The ratio took a turning point when ethanol, a polar protic solvent, was used, increasing the yield of N3-benzyladenine such that the two products were formed in a 1:1 ratio (Table 2.14, No. 5). The N9:N3 ratio could be shifted until N3-benzyladenine became the major product when *tert*-butanol was employed as a solvent (Table 2.14, No. 6 and 7). However, the reaction in polar protic solvents required longer reaction times as starting material, adenine, was still present after 4 hours.

Table 2.14: Reaction conditions for benzylation of adenine using benzyl bromide.

No.	Solvent	Base	N9:N3
1	DMSO (dried)	K ^t OBu	9.5:0.5
2	DMSO (wet)	K ^t OBu	9:1–7:3 ^a
3	DMF (dried)	K ^t OBu	8:2
4	Acetonitrile	K ^t OBu	6:1 ^b
5	Ethanol	K ^t OBu	1:1
6	<i>tert</i> -butanol	K ^t OBu	1:3 ^b
7	<i>tert</i> -butanol	KOH	1:9 ^b

All reactions were stirred for 4 hours at refluxing temperature.

^a N9:N3 ratio varied depending on the dryness of the DMSO.

^b Starting material, adenine, was present.

All reactions in Table 2.14 were repeated numerous times, each producing consistent N9:N3 ratios, except reactions repeated in No. 2, where the series of reactions were performed over a time period in which the same batch of DMSO was used for the solvent. It was to note that the DMSO was not purposefully dried and hence became contaminated with water over time. The reactions performed in which the DMSO contained larger amounts of water, yielded increased amounts of N3-benzyladenine, indicating that the water could play a role in the formation of the N3 regio-isomer. Therefore, a set of reactions were run in which DMSO was spiked with various amounts of water to see whether the water caused the variation in the N9:N3 ratio (Table 2.15).

As the percentage of water increased in the DMSO-water mixture, the more N3-benzyladenine formed along with more starting material remaining in solution due to adenine having low

solubility in water. As water is a polar protic solvent, this followed the trend that N3-benzyladenine increases with polar protic solvents.

Table 2.15: Effect of water on the ratio of N9:N3.

water %	N9:N3
10	2:1
33	1:1
50	4:6

The relationship between polar aprotic solvents favouring N9-benzyladenine and polar protic solvents favouring the N3-benzyladenine could be the relation of S_N2 vs. S_N1 respectively.⁵⁹ S_N1 reactions are favoured in polar protic solvents and require an alkyl halide with a tertiary or secondary carbon ($3^\circ > 2^\circ \gg 1^\circ$). The nature of the electrophile benzyl bromide is not a true 1° alkyl halide and thus could favour an S_N1 type mechanism when the conditions are optimal, such as when performing the reaction in polar protic solvents.

When Rasmussen and Hope reported the solvent dependent variation in the N9:N3 ratio of alkylated products, they postulated that polar protic solvents (methanol and ethanol) led to increased amounts of the N3-alkylated product due to (i) weaker transition states in alcoholic solvents, (ii) the preference for the imidazole ring nitrogens, N7 and N9, to be involved in hydrogen bonding with the solvent or (iii) the adenine anion could accept a proton from the polar protic solvent, yielding neutral adenine which undergoes N3-alkylation.⁶⁰ They also reasoned that using dipolar aprotic solvents, the amounts of N3-alkylated products increased with increasing polarity of the solvents ($(\text{Me}_2\text{N})_3\text{PO} < \text{DMF} < \text{DMSO}$) as a result of the polar solvents weakening the S_N2 transition states or could potentially be S_N1 controlled due to the high polarity of some solvents.

The solvent dependent change in the N9:N3-benzyladenine ratio observed in our study could therefore be a result of S_N1 vs. S_N2 , where the N3-benzyladenine is more favoured under S_N1 conditions and the N9-benzyladenine is favoured under S_N2 conditions. The polar aprotic solvents used contained trace amounts of water, even when precautions were taken to dry the

solvents, which could have resulted in the formation of N3-benzyladenine. The use of bases which could form alcohols and water, such as K^tOBu and NaOH, respectively, could have provided an S_N1 microsolvation environment, which enabled the formation of N3-benzyladenine.

2.2.5 S_N2 substitution reaction studied by 1H NMR spectroscopy

The variation in the ratio of N9-:N3-benzyladenine in different solvents prompted us to perform the reaction in deuterated solvent to allow us to follow the reaction progress by 1H NMR analysis. The benzylation of adenine under basic conditions was performed on NMR scale, using DMSO- d_6 as solvent and K^tOBu as base, and analysed by 1H NMR spectroscopy for 12 hours to generate a “reaction profile” and understand at what stages and how the N9- and the N3-benzyladenine are formed.

The following information was deduced from the 1H NMR study:

- i. The addition of base, K^tOBu , to the solution of adenine and DMSO- d_6 formed the adenine anion, having the two purine ring protons at 7.93 ppm and 7.72 ppm and the broad NH_2 peak at 6.32 ppm (Figure 2.35, **A**).
- ii. Benzyl bromide was added and immediately analysed by 1H NMR spectroscopy (**0hr**). Based on the purine ring protons, the anion quantitatively converted to N9-benzyladenine as indicated by the strong singlets at 8.28 ppm and 8.16 ppm. No other significant purine proton peaks were present to support the formation of N3-benzyladenine as peaks at 8.57 ppm and 7.78 ppm were not visible. However, analysing the CH_2 proton peaks at the 5.0 ppm region, N9-benzyladenine had an intense CH_2 peak at 5.38 ppm alongside an unexpected CH_2 peak present at 5.54 ppm where the N3-benzyladenine CH_2 typically resonates.
- iii. Of most importance, there was first formation of N9-benzyladenine and other unidentified proton peaks before the formation of N3-benzyladenine. At the third

hour after the addition of benzyl bromide (**3hr**), proton peaks that resembled N3-benzyladenine C8-H and C2-H purine ring protons appeared at 7.77 ppm and 8.65 ppm, respectively. However the C2-H chemical shift occurred more downfield than expected from the pure N3-benzyladenine which has the C2-H chemical shift at 8.57 ppm. These peaks were relatively intense compared to those of the C2-H and C8-H of N9-benzyladenine.

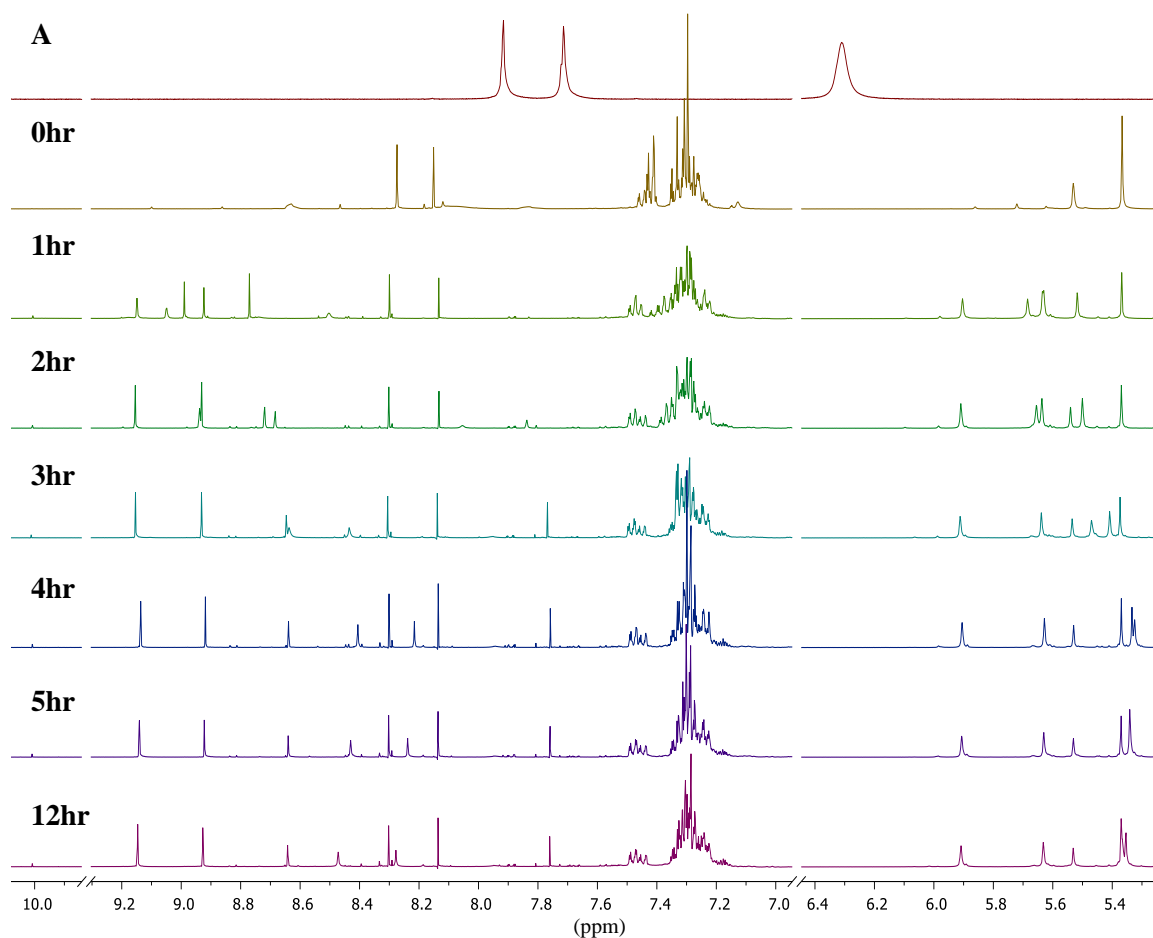


Figure 2.35: ^1H NMR spectra (ppm) of NMR scaled reaction of deprotonated adenine **A**, and at 0 to 12 hours (**0hr**, **1hr**, **2hr**, **3hr**, **4hr**, **5hr** and **12 hr**) after addition of benzyl bromide, in $\text{DMSO-}d_6$ (400 MHz).

- iv. The ^1H NMR spectra from **0hr** to **12hr** after the addition of benzyl bromide showed unidentified peaks present throughout the spectra, starting at trace amounts in the **0hr** ^1H NMR spectrum and becoming more dominant as time continued. The shifting in position or disappearance of the peaks overtime gave an indication that there was

either formation of unstable by-products or possible intermediates which lead to the formation of the *N*-benzyladenine regio-isomers. Certain proton peaks in the 5.0 ppm region of the ¹H NMR spectrum showed shifting in their relative positions which seemed to parallel that of the unidentified proton peaks further downfield at the 7.83 – 9.11 ppm region. The unidentified proton peaks that remained unchanged indicated stable by-products.

Beasley and Rasmussen studied the effect of the alkylating agent on the N1:N3:N7:N9 products ratio from the alkylation of neutral adenine.⁶¹ The synthesis of N3-benzyladenine was achieved by adding benzyl chloride to a solution of adenine in DMF at 100 °C. The benzylation of adenine under neutral conditions to yield N3-benzyladenine as a major product and N9-benzyladenine as a minor product, also lead to trace amounts of N1-, N7- and di-benzyladenine by-products. Rasmussen and Hope reported the effect of bases, solvents and concentration of adenine salt on the alkylation of adenine under basic conditions with benzyl chloride.⁶⁰

The products and by-products formed during both benzylation techniques were identified according to the ¹H NMR spectrum peaks of the CH₂ groups in both papers (Table 2.16).

Table 2.16: ¹H NMR spectrum chemical shifts (ppm) of CH₂ of reported by-products in DMSO-d₆.

Compound	δ CH ₂ (ppm)	
	Beasley ⁶¹	Rasmussen ⁶⁰
N3,7-dibenzyladenine	6.05, 5.64	6.00, 5.60
N7-benzyladenine	5.71	5.72
N3-benzyladenine	5.55	5.53
N1-benzyladenine	5.45	5.49
N9-benzyladenine	5.39	5.39
N1,9-benzyladenine	-	5.25
Unidentified	-	5.89

This is a valid method as the chemical shifts of the purine proton peaks in the ¹H NMR spectrum are sensitive to concentration, temperature and the presence of water.²⁷ Slight shifting of purine peaks have been observed in our ¹H NMR spectra.

Comparing the above reported ^1H NMR spectral data of the CH_2 proton chemical shifts to our NMR scaled reaction ^1H NMR spectrum obtained at **0hr** recorded, three similarities are seen:

- i. The first is the expected N3- and N9-benzyladenine CH_2 proton peaks at 5.54 ppm and 5.38 ppm, respectively, relating to the literature reported N3-benzyladenine CH_2 peak at 5.55/5.53 ppm and the N9-benzyladenine CH_2 peak at 5.39 ppm.
- ii. The second similarity is the chemical shift at 5.73 ppm (in trace amounts) which appears as it could be the recorded N7-benzyladenine which has the CH_2 proton chemical shift at 5.71/5.72 ppm.
- iii. The third similarity is the proton peaks (in trace amounts) at 5.87 ppm and 5.63 ppm that occur in a similar region as the reported N3,7-dibenzyladenine CH_2 proton peaks at 6.05/6.00 ppm and 5.64/5.60 ppm, or the peak at 5.87 ppm could relate to the recorded unidentified peak at 5.89 ppm, in which the peak at 5.63 ppm would also be unidentified.

Comparing the literature values above to the ^1H NMR spectrum obtained at **12hr** showed the presence of N3,7-dibenzyladenine, N3- and N9-benzyladenine CH_2 proton peaks with the an unidentified proton peak at 5.36 ppm. The appearance of N3,7-dibenzyladenine could be expected due to directed alkylation of N3-benzyladenine to the N7 position.³⁹ The formation of N1,9-dibenzyladenine could be expected along with the previously mentioned by-products as N9-benzyladenine directs alkylation to the N1 position.⁴¹

As there is shifting of unidentified proton peaks in the 7.83 – 9.11 ppm range of the ^1H NMR spectra and the N3-benzyladenine only forms after the N9-benzyladenine, the possibility of Dimroth rearrangement was considered.

2.2.6 Dimroth rearrangement: explanation for the conversion of N9- to N3-benzyladenine

The cytokinin activity of the compounds N1-benzyladenine and N1-(Δ^2 -isopentenyl)adenine was found to be due to their converted forms, N6-benzyladenine and N6-(Δ^2 -isopentenyl)adenine, respectively.³⁴ The conversion of N1-alkyladenine derivatives to N6-alkyladenine derivatives occurs via Dimroth rearrangement under autoclaving conditions (pH < 7) or under reflux in aqueous medium (pH > 7).^{33,34,62} The rearrangement involves ring opening and ring closing of certain N—C bonds in the purine ring system. Conversion of N1- to N6-benzyladenine involves ring opening and ring closing of the N1—C2 and N6—C2 bonds, respectively, as shown in Figure 2.36.

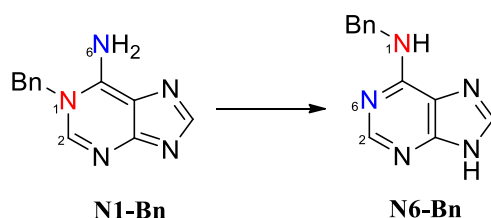


Figure 2.36: Dimroth rearrangement for conversion of N1- to N6-benzyladenine.

The Dimroth rearrangement suggested for the conversion of N1-(Δ^2 -isopentenyl)adenine to N6-(Δ^2 -isopentenyl)adenine followed the same ring opening and closing analogy.³⁴ Leonard and Henderson investigated the conversion of N3- to N6-benzyladenine, in which a range of possible Dimroth ring opening and closing mechanisms were proposed, including mechanisms that lead to the formation of N1-benzyladenine which in turn can be converted to N6-benzyladenine.³³ In the ¹⁵N labelling of specific nitrogens of N3-benzyladenine and comparing their products after autoclaving with ¹⁵N labelled N6-benzyladenine and known labelled N-benzyladenine regio-isomers (synthesis previously discussed in section 2.1.3), it was possible to trace the movements of the ¹⁵N labelled nitrogens from the labelled N3-benzyladenines. The isolated products after autoclaving of labelled N3-benzyladenine-¹⁵N6 were the N6-benzyladenine-¹⁵N, with the ¹⁵N labelled nitrogen equally distributed at positions N3 and N9,

and the N9-benzyladenine-¹⁵N, with the labelled nitrogen equally distributed at N1 and N6. It was proposed that both the imidazole and pyrimidine rings open, where the pyrimidine ring opens faster than the imidazole one.⁴¹

Two Dimroth rearrangement mechanisms for the conversion of N3-benzyladenine to N9-benzyladenine were postulated by Leonard and Henderson:³³

- i. The first mechanism involves ring opening of the N1—C2 and the N7—C8 bonds (Figure 2.37 **path a** leading the **N9-Bn-a**), followed by rotation along the C4—C5 bond and ring closure of the N1—C8 and the N7—C2 bonds.
- ii. Ring opening of the C2—N3 and C8—N9 bonds (Figure 2.37 **path b** leading the **N9-Bn-b**) followed by rotation along the C4—C5 bond and closure of the C2—N3 and C8—N9 bonds.

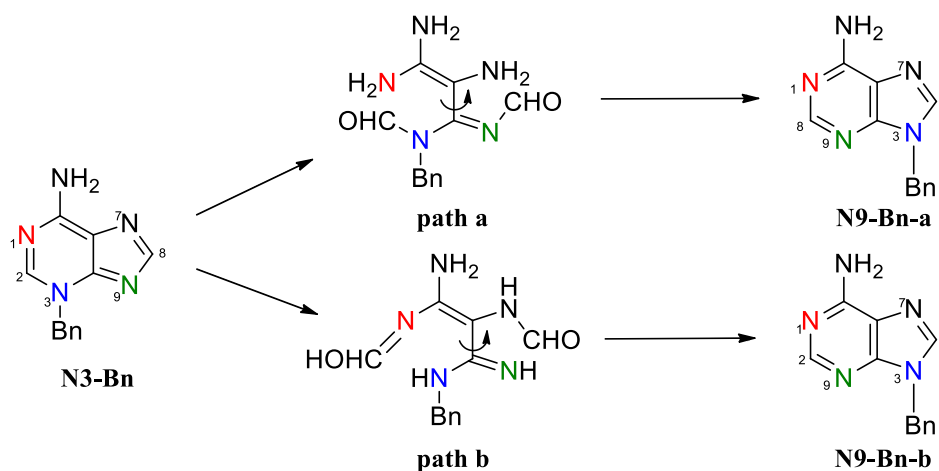


Figure 2.37: Dimroth rearrangement mechanisms for the conversion of N3- to N9-benzyladenine.

Since N3-benzyladenine can be converted to N9-benzyladenine,³³ it was considered that N9-benzyladenine could potentially be converted to N3-benzyladenine under reflux in basic conditions, leading to the formation of ring-open intermediates which could explain the unidentified proton peaks that occurred in the ¹H NMR spectra of the NMR scaled reaction and the formation of N3-benzyladenine which occurs after the formation of N9-benzyladenine. Leonard *et al.* postulated a mechanism for the conversion of 1-(Δ^2 -isopentenyl)adenine (Figure

2.38, **18**) to 6-(Δ^2 -isopentenyl)adenine (**19**) utilizing water as a base in which the hydroxide acts as a nucleophile which attacks at the C2 position of the purine ring.³⁴

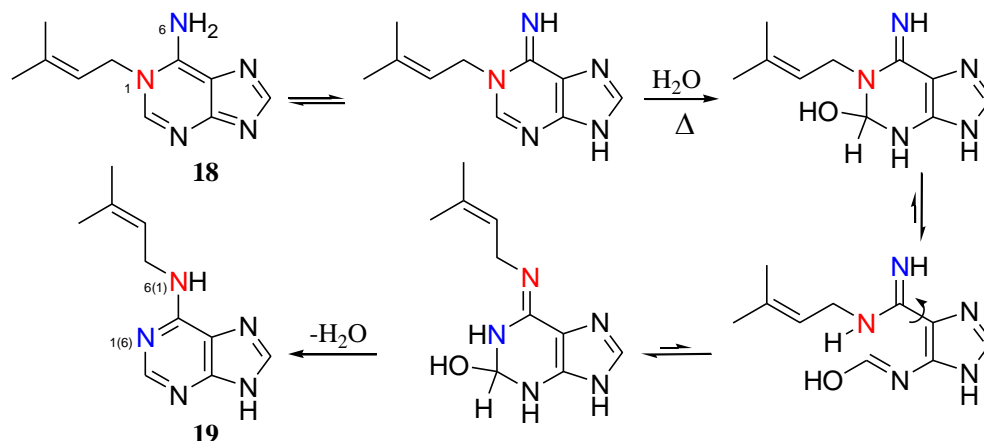


Figure 2.38: Water catalysed Dimroth rearrangement of 1-(Δ^2 -isopentenyl)adenine **18** to 6-(Δ^2 -isopentenyl)adenine **19**.

From the above works by Leonard *et al.*^{33,34} it could be reasoned that a similar water catalysed Dimroth rearrangement allows for the conversion of N9- to N3-benzyladenine by the hydroxyl nucleophile attacking the C2 and the C8 positions (Figure 2.39) as trace amounts of water was present in solution during the synthesis of N9-benzyladenine.

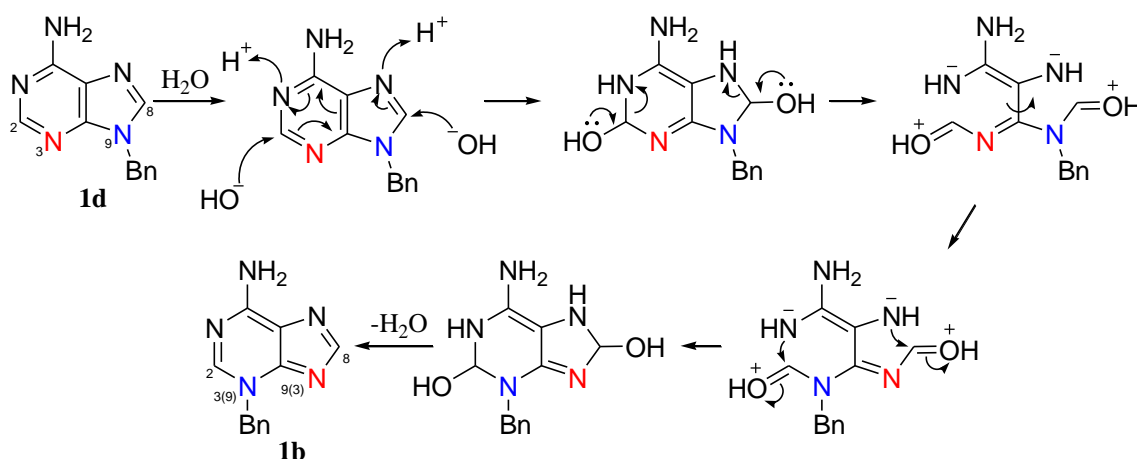


Figure 2.39: Water catalysed Dimroth rearrangement for N9- to N3-benzyladenine.

It could also be reasoned that when performing the reaction in polar protic solvents, such as ethanol and *tert*-butanol, the alcohols could take on the role of the nucleophile (water), attacking the C2 and the C8 positions. The addition of the nucleophilic at the C2 and C8 could occur simultaneously or not.

2.2.7 Alkylation of adenine and 2,6-dichloropurine with other electrophiles

A small library of possible Shikimate kinase inhibitors was synthesised by reacting adenine and 2,6-dichloropurine with various alkylating agents such as ethylene carbonate, propylene carbonate and allyl bromide to obtain the series of derivatives below (Figure 2.40).

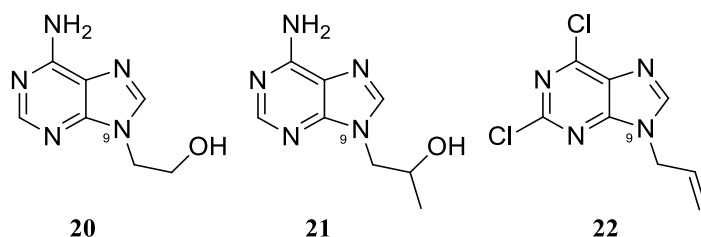


Figure 2.40: Synthesised adenine and 2,6-dichloropurine derivatives.

The adenine derivatives **20** and **21** were synthesised along with a minor structural isomer which was presumed to be the N3 regio-isomer due to the isomers demonstrating a similar trend in the ^1H NMR δ chemical shift between C2-H and C8-H of the N3-benzyladenine (Table 2.17).

Table 2.17: ^1H NMR δ C2-H and C8-H chemical shift (ppm) of N3- and N9-adenine derivatives.

Compound	N9-adenine derivative			N3-adenine derivative		
	C8	C2	δ	C2	C8	δ
benzyladenine	8.26	8.16	0.1	8.57	7.78	0.8
2-(6-Amino-purinyloxy)-ethanol (20)	8.06	8.13	-0.1	8.23	7.76	0.5
2-(6-Amino-purinyloxy)-propan-2-ol (21)	8.05	8.14	-0.1	8.57	7.76	0.8

This was supported by the N9-isomers demonstrating the same δ chemical shift between C2-H and C8-H of the N9-benzyladenine.

Allyl derivatives undergo migration of the double bond between the allyl form and the prop-1-enyl form under basic conditions.^{44,63,64} Therefore, synthesis of N9-allyladenine (Figure 2.41 **23**) leads to four compounds present in solution, which include the N9- and N3-allyladenines (Figure 2.41, **25**) along with both isomers undergoing the double bond migration (**23a** and **25a** respectively).

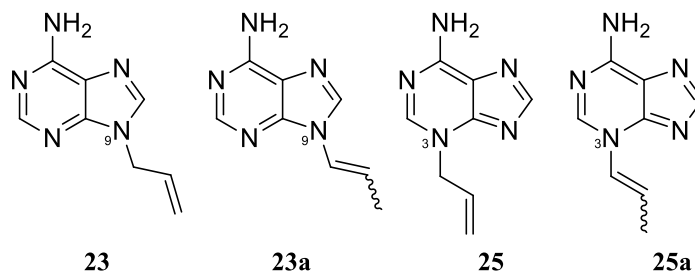


Figure 2.41: Migration of double bond between the allyl form (**23** and **25**) and the prop-1-enyl (**23a** and **25a**) form of N9- and N3-allyladenine.

The allylation of 2,6-dichloropurine under Mitsunobu conditions undergoes substitution at the N9 and N7 positions (Figure 2.42, **22** and **26** respectively), potentially due to the chlorines withdrawing electron density from the pyrimidine ring and as a result deactivating the ring and thus not allowing substitution at the N3 position.

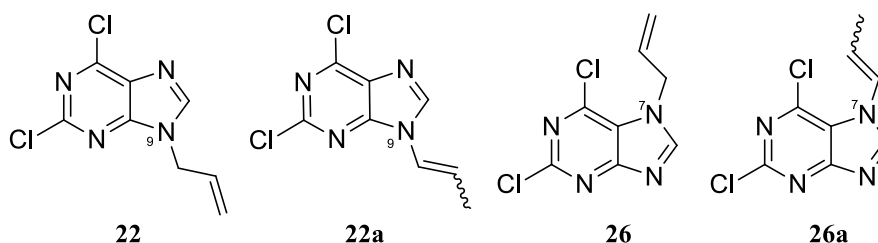


Figure 2.42: Migration of double bond between the allyl form (**22** and **26**) and the prop-1-enyl (**22a** and **26a**) form of N9- and N7-allyl-2,6-dichloropurine.

The N7 site of alkylation was confirmed by X-ray crystallography (Supporting Material). The resulting N9- and N7-allyl-2,6-dichloropurine from direct allylation also undergo the double bond migration, resulting in the N9- and N7-prop-1-enyl-2,6-dichloropurine derivatives (**22a** and **26a** respectively) therefore resulting in four products present in solution.

These reactions were not investigated further as the reactivity of adenine needed to be understood (Chapter 3) in order to understand how the molecule behaves under substitution conditions. The isolation of adenine and 2,6-dichloropurine derivatives proved to be a challenge, hence multistep ring closure synthesis techniques which eliminate the formation of by products are an optional route for synthesis.³¹

2.3 Conclusions from the synthetic study

To conclude from the results described above we can state that N9 is the major product and N3 the minor product when adenine is reacted with benzyl bromide in DMSO under basic conditions. The ^1H and ^{13}C NMR chemical shift assignments have been revised and questionable literature reports have been identified.

It is evident that solvent plays a major role in the synthesis of N9-benzyladenine. Polar aprotic solvents allowed for N9-benzyladenine to be the major regio-isomer and N3-benzyladenine to be the minor regio-isomer, whereas polar protic solvents reversed this occurrence, having N3-benzyladenine as the major regio-isomer. However, the reason as to why solvent plays such a selective role is not yet fully understood, it has been suggested that N3-benzyladenine is $\text{S}_{\text{N}}1$ controlled and therefore is more dominant in polar protic solvents.^{59,60} The NMR scaled reaction showed that the N9-benzyladenine forms first in solution (DMSO-d_6) within minutes of the addition of benzyl bromide with only trace amounts of by-products. As time continued there was first formation of unidentified proton peaks before the formation of N3-benzyladenine. Whether these unidentified proton peaks were related to unstable or stable by-products or Dimroth rearrangement intermediates is still unclear at this point and further research is needed on the matter.

Chapter 3

3.1 Introduction

3.1.1 The prototropic tautomers of adenine

As previously shown (Chapter 2), the benzylation of adenine under S_N2 substitution conditions leads to N9-benzyladenine (Figure 3.1, **N9-Bn**) as a major product and N3-benzyladenine **N3-Bn** as a minor product and not the N7-benzyladenine isomer **N7-Bn** as is often reported. To our knowledge, there is thus far no study surrounding the topic of why adenine undergoes alkylation at the N9 and N3 positions under basic conditions, as compared to the N9 and N7 positions. No previous research on the S_N2 mechanism involving adenine could be found and therefore, in order to have a sense of direction, we turned to what has been studied about adenine tautomers, the computational techniques used to evaluate the system and the differences observed at different levels of theory employed.

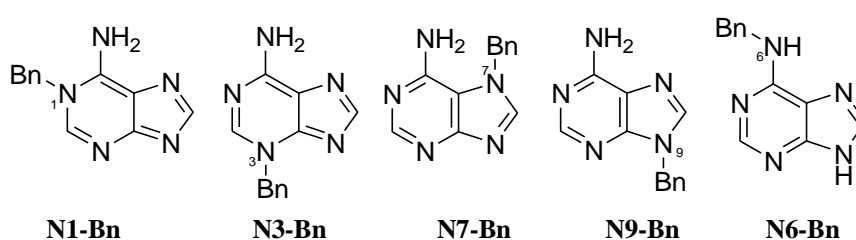


Figure 3.1: Structural isomers of *N*-benzyladenine.

The confusion of N3- vs. N7-alkylated adenine has not only occurred for *N*-benzyladenine, but for other adenine derivatives as well.⁶⁵ Kania and Gundersen⁶³ synthesised *N*-allyl adenine derivatives and stated that the synthesis of N9-allyl adenine yielded N3-allyl adenine as the minor isomer in contrast to their reference article Thibon *et al.*,⁵¹ which identified the minor compound as N7-allyl adenine. A major rationale for assigning the spectral data for the minor product to the

N7-structural isomer is presented in two articles, Sečkářová *et al.*⁶⁶ and Bartl *et al.*,⁶⁷ where it is stated that it is important to study the tautomeric equilibria of purines as this dictates the regioselectivity of alkylation. Similarly it was stated by Marek *et al.*,⁴⁷ that the N7-H and N9-H are the major purine tautomers (Figure 3.2), and therefore, the N9- and N7-alkylated purines are the major products from purine alkylation. Here, the relationship of the major substitution products of purine ring alkylation is being related to the dominance of purine tautomers.

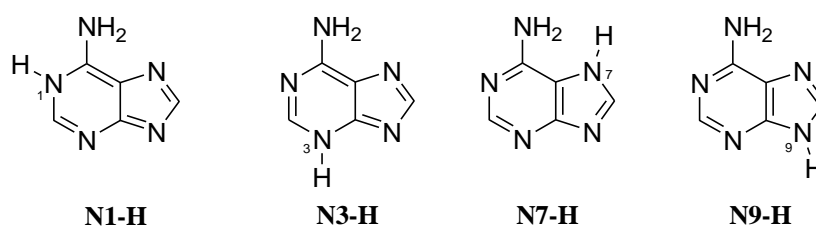


Figure 3.2: Adenine tautomers.

The prototropic tautomerism of adenine has been studied for decades, dating back to the 1950's, and is still being investigated due to the important biological role that adenine plays. Adenine is the most common component of nucleic acids to be studied due to its tautomeric form playing an important role in molecular recognition,²⁷ complex hydrogen bond interactions which modulate DNA or RNA recognition,⁶⁸ and DNA mutations due to rare tautomeric forms.^{28,47,69}

The parent molecule, adenine, has a prototropic proton that can move from nitrogen to nitrogen in the purine system, denoted as NH-NH tautomers, or from nitrogen to carbon, denoted as NH-CH tautomers. The NH-NH tautomers involve (i) a labile endo-purine proton, where the proton moves between the four purine ring nitrogens N1, N3, N7 and N9 as illustrated in Figure 3.2 and (ii) a labile proton on the *exo* NH₂ group, which allows for the rare NH-NH amine-imine tautomer series, shown in Figure 3.3.^{28,70} The NH-CH tautomers are considered as extremely rare tautomers and involve (i) the labile proton being situated on the carbons of the purine ring, with the (ii) amine-imine forms thereof.^{71,72}

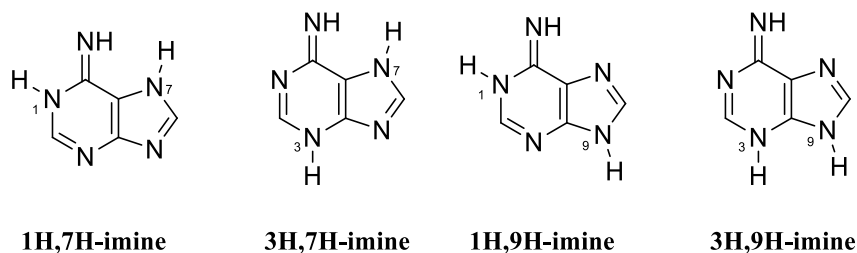


Figure 3.3: Adenine-imine tautomers.

In order to study the electron distribution⁴⁸ and the population^{70,73} of the tautomeric forms of adenine in solution, adenine derivatives are synthesised, in which an alkyl group is placed on the site of the prototropic hydrogen, thus creating **N1-R**, **N3-R**, **N7-R** and **N9-R** adenine derivatives (Figure 3.4) to mimic the N1-H, N3-H, N7-H and N9-H adenine tautomers, respectively.

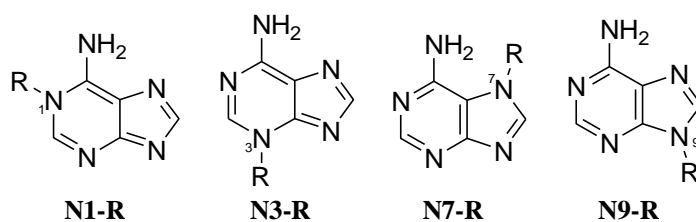


Figure 3.4: Adenine derivatives.

Dreyfus *et al.*⁷⁴ showed, by UV spectroscopy, that the amplitude-to-concentration ratio for a given temperature or temperature range, is proportional to the difference of the molar extinction coefficients of two equilibrium species. There was close similarity between the wavelength dependence of the amplitude-to-concentration and the differential spectrum (difference in molar extinction coefficient) of the N7/N9-methyladenines and the N7/N9-H adenine tautomers, which allowed the adenine tautomers to be studied via the alkylated adenine derivatives.

Raczyńska *et al.*^{71,72,75} considered all forms of adenine tautomers in order to study the change in the tautomeric mixture when moving from the neutral form of adenine to its oxidized and reduced forms in gas and solvent phase. The Harmonic Oscillator Model of Electron Delocalization (HOMED) index, reformulated from the resonance co-ordinate Harmonic

Oscillator Measure of Aromaticity (HOMA), was used to study the electron delocalization of the tautomers. HOMA is one of many techniques used to quantitatively describe the π -electron delocalization (aromaticity) of mono and polycyclic π -electron systems.⁷⁶⁻⁷⁸ It is a geometry based technique, compared to others which are energetic and magnetic based indices, and relies on equalization of bond lengths (due to σ -electron bonds which retain equal bond lengths) and symmetry in aromatic systems,

$$HOMA = 1 - \frac{\alpha}{n} \sum_{i=1}^n (R_{opt} - R_i)^2,$$

where n is the number of bonds considered, α is an empirical constant derived to allow HOMA = 0 for nonaromatic systems and HOMA = 1 for aromatic systems with all bonds lengths equal to optimal value (R_{opt}), and R_i is the actual bond length. In order to use HOMA the geometric properties, such as bond lengths R_i and R_{opt} , and the α constant must be known for the molecular system being studied. The HOMA was re-evaluated in 1993 to take into consideration the Jug and Koester resonance co-ordinate,⁷⁸ however this technique failed to consistently measure hetero-aromatic systems. Raczyńska *et al.*⁷⁷ reformulated the HOMA index in 2010 to the Harmonic Oscillator Model of Electron Delocalization (HOMED) index, which describes the π -electron delocalization of non-aromatic ($0.4 < \text{HOMED} < 0.8$) and aromatic systems ($\text{HOMED} \approx 1$). The HOMED measures the resonance effect of a π -electron system consisting of π - π conjugation, n - π conjugation and σ - π hyper conjugation ($\text{HOMED} < 0.4$) and aromaticity.

Thus, Raczyńska *et al.*⁷⁵ employed the HOMED index to study the electron delocalization in adenine tautomers and showed that the variations in the HOMED indices paralleled that of the variations of the relative Gibbs free energy for the neutral adenine tautomeric forms, having the NH-NH tautomers as the most favourable forms. Thus, due to the linear relationship between the HOMED and relative Gibbs free energy, it is concluded that the electron delocalization plays a role in the stability of adenine tautomers. The NH-NH tautomers contain various types of π - π

and n- π resonance conjugations per tautomer leading to differences in electron delocalization. Adenine has ten π electrons ($4n+2$) to participate in electron delocalization during tautomerization (Figure 3.5), eight π electrons contributed from the four π bonds (π - π conjugation) and two electrons in the p-orbital of the “pyrrole” like nitrogen (NHR₂) in the purine system (n- π conjugation).

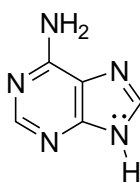


Figure 3.5: Ten π electrons of adenine.

In general, the NH-NH tautomers have stronger electron delocalization (HOMED > 0.7) than the NH-CH forms of adenine tautomers which require σ - π resonance conjugation (HOMED < 0.7).⁷¹ The number of resonance forms for each tautomer resulting from the difference in electron delocalization, determines the stability of a tautomer and hence its contribution to the tautomeric mixture. This was also supported by Maliňáková *et al.*,⁴⁸ employing Nucleus-Independent Chemical Shifts (NICS). NICS is a computational tool developed by Schleyer *et al.*⁷⁹ used to study aromaticity, non-aromaticity and anti-aromaticity by using the absolute magnetic shielding computed at ring centres for mono-cyclic systems and individual rings of poly-cyclic systems and is dependent on the number of π -electrons.⁷⁹⁻⁸¹ In relation to the standard NMR chemical shifts, the NICS ppm values are reversed, in which negative NICS values are indicative of aromaticity and positive NICS values are indicative of anti-aromaticity. NICS is in good agreement with other indices which are used to study aromaticity.⁸⁰ Maliňáková *et al.*⁴⁸ used N3-, N7- and N9-benzyl and methyl substituted adenines to model adenine tautomers in order to study the change in electron distribution of the purine ring based on isomerism, suggesting that the large difference in π -electron delocalization for N3-substituted

adenine, compared to N7- and N9-substituted adenines, could be the reason for the instability of the pyrimidine ring tautomers in purine compounds.

As a point of interest, the HOMED values calculated by Raczyńska *et al.*⁷⁵ increased slightly for the adenine tautomer N9-H as compared to that of its purine tautomer with a hydrogen at the C6 position instead of the exo-amino group (Figure 3.6, **P9-H**). This indicated that the amino group had an electron-donating effect on the aromatic purine system of adenine.

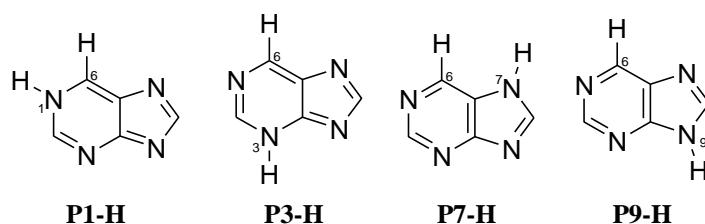


Figure 3.6: Purine tautomers.

The electron-donating ability of the NH₂ group was seen for the four adenine tautomers when compared to their purine tautomer forms, in which the effect was energetically favourable for the N9-H and N3-H tautomers (Table 3.1), with the difference in relative free energy, $\delta G = (\Delta G_A - \Delta G_P)$, between the adenine tautomer (ΔG_A , relative to N9-H) and its purine tautomer (ΔG_P , relative to P9-H) being 0.0 and -1.2 kcal/mol, respectively, and less favourable for the N1-H and N7-H tautomers, having δG being 6.2 and 5.1 kcal/mol, respectively.

Table 3.1: Difference in relative free energy (δG) between adenine tautomers (ΔG_A) with their corresponding purine tautomers (ΔG_P).⁷¹

Purine	ΔG_P^a	Adenine	ΔG_A^a	δG^a
P1-H	13.1	N1-H	19.3	6.2
P3-H	9.9	N3-H	8.7	-1.2
P7-H	3.8	N7-H	8.9	5.1
P9-H	0.0	N9-H	0.0	0.0

^a Calculated at B3LYP/6-311+G(d,p), in kcal/mol.

The energetic effect of the exo-NH₂ group is unfavourable for the N1-H and N7-H tautomers due to the repulsive intramolecular interaction between the hydrogen on the NH₂ group and the

hydrogen on the N1 and N7 positions, respectively. This effect is large in the gas phase, but it is dramatically reduced in the solution phase, with water as the simulated solvent, by energetically favourable interactions with the polar water molecules. The unfavourable interaction for the N1-H and N7-H does not greatly influence the electron delocalization for the pyrimidine ring and the imidazole ring, respectively.

3.1.2 Adenine tautomers in gas phase and solvent phase

Theoretical calculations of adenine tautomers in gas phase have been performed for many years, supporting the most stable tautomers as N1-H, N3-H, N7-H and N9-H. The N9-H adenine tautomer, being the most stable form, is dominant (Table 3.2) in the gas phase, having its electronic energy (E) and free energy (G) more negative by about 7.0 kcal/mol than the N3-H and N7-H tautomers and by more than 17.0 kcal/mol than the N1-H tautomer. The N9-H tautomer therefore constitutes the entire tautomer population (100%) in the gas phase.

Table 3.2: Relative to N9-H, electronic energies (ΔE , kcal/mol) and free energies (ΔG , kcal/mol) of adenine tautomers in the gas phase.

reference	N9-H	N3-H	N7-H	N1-H
ΔE				
Close <i>et al.</i> ^{82a}	0.0	8.1	8.3	18.8
Raczyńska <i>et al.</i> ^{71b}	0.0	8.3	8.4	18.7
Kim <i>et al.</i> ^{83c}	0.0	7.6	7.7	-
Fonseca Guerra <i>et al.</i> ^{84d}	0.0	7.7	8.3	17.7
Hanus <i>et al.</i> ^{28e}	0.0	8.0	7.6	17.7
Gu <i>et al.</i> ^{85h}	0.0	-	8.6	-
ΔG				
Laxer <i>et al.</i> ^{27f}	0.0	7.4	7.8	-
Raczyńska ^{71b}	0.0	8.7	8.9	19.3
Hanus <i>et al.</i> ^{28g}	0.0	7.4	7.5	17.4

^a B3LYP/6-31++G(d,p), ^b B3LYP/6-31+G(d,p) ^c MP2/6-311+G(d,p), ^d BP86/TZ2P, ^e RI-MP2/TZVPP//RI-MP2/TZVPP(5s3p2d1f, 3s2p1d), ^f B3LYP/6-311+G(2df,2p), ^g MP2/6-31G(d,p), ^h B3LYP/6-311G(d,p).

The trend from the lowest to the highest energy tautomer corresponds to the stability trend from the most stable to the least stable form, N9-H > N3-H \geq N7-H \gg N1H. This trend is

independent on the level of theory (B3LYP, MP2 or BP86) and basis sets used to perform the theoretical calculations.

Solvent effects on adenine have been studied due to their effect on stabilising rare tautomeric forms of adenine, effect on the reactivity of biomolecules, and ability to participate in dynamic processes themselves, such as tautomerization.^{28,68,69,83} Many papers state that only the N7-H and N9-H adenine tautomers exists in solution,^{82,86} in various N7-H:N9-H ratios depending on the experimental method used: 17:83 using ¹⁵N NMR in aqueous phase⁸⁷ or 13.5:86.5 in DMSO⁷³, 22:78 using femtosecond transient absorption and temperature jump relaxation in aqueous phase,^{70,74} 15:85 using ¹³C NMR in DMSO,⁸⁸ and 6:94 in isobutanol at 103 °C using fluorescence experiments.⁸⁹

Theoretical calculations, which showed that the N9-H adenine tautomer is dominant in gas phase, gave different results when solution phase is considered.^{27,28,48,83,84,90} The relative difference in electronic and free energies in solution phase decreased for all tautomers by more than half of that in the gas phase (Table 3.3).

Table 3.3: Relative to N9-H, energy (ΔE , kcal/mol) and free energy (ΔG , kcal/mol) of adenine tautomers in liquid phase.

Reference	N9-H	N3-H	N7-H	N1-H
ΔE				
Raczyńska <i>et al.</i> ^{71a}	0	4.6	2.6	7.8
Gu <i>et al.</i> ^{85b}	0	-	4	-
ΔG				
Laxer <i>et al.</i> ^{27c}	0	3.5	2.2	-
Hanus <i>et al.</i> ^{28d}	0	2.5	2.8	5.9
Kim <i>et al.</i> ^{83e}	0	3.9	1.9	-

^a B3LYP/6-311+G(d,p)/PCM(water), ^b B3LYP/6-311G(d,p)/SCI-PCM(water), ^c B3LYP/6-31G(d,p)/SCRF-PB(DMSO), ^d B3LYP/6-31G(d)/COSMO-PCM(DMSO), ^e B3W91/6-311+G(d,p)/IEFPCM(water).

The N9-H tautomer is still the most favoured form being 2.0 kcal/mol more stable than the N3-H and N7-H tautomers (the N7-H being marginally more stable than the N3-H tautomer) and 5.0 kcal/mol more stable than the N1-H tautomer. The stability trend observed from ΔE and

ΔG follows that obtained in the gas phase, $N9-H > N7-H \geq N3-H > N1H$, regardless of whether DMSO or water was used as the simulated solvent when the Polarizable Continuum Model (PCM) was employed.

The dramatic decrease in relative E and G energy values implies that the tautomeric mixture is different in solvent than it is in the gas phase, having greater populations of N7-H and N3-H. Raczyńska *et al.* predicted that the tautomeric mixture exists as N9-H (97.51%), N7-H (2.46%) and N3-H (0.02%).⁷¹ However, using combined DFT and molecular mechanics, Aidas *et al.*⁸⁷ predicted, in good agreement with experimental results from the ^{15}N NMR spectrum of N3-H, N7-H and N9-H, the N7-H and N9-H tautomeric population to be 17% and 83%, respectively, not supporting the co-existence of the N3-H tautomer in solution, stating that it is unlikely. The N7-H tautomer increases in population with increases in temperature and solvent polarity.²⁷ The increase in the N7-H tautomer in polar solvents is due to solvent stabilization of its higher dipole moment (Table 3.4) as compared to the N9-H tautomer, which has a lower dipole moment. The trend between the tautomers from the lowest to the highest dipole moment is: $N9-H < N3-H < N7-H < N1-H$.^{27,28,69,70,87}

Table 3.4: Dipole moment (μ), in Debye, of adenine tautomers.

Adenine tautomer	μ (D)	
	<i>Laxer</i> ^a	<i>M. Hanus</i> ^b
N9-H	2.45	2.8
N3-H	4.09	4.7
N7-H	6.74	6.8
N1-H	-	8.8

^a B3LYP/6-31G(d), ^b RI-MP2/TZVPP.

Bergmann *et al.*⁹¹ used substituted adenine derivatives to study the adenine tautomers, and concluded, using UV spectroscopy and dipole moments, that the N3-H tautomer possibly exists as the amino and imine form while the N7-H and N9-H exist only in the amino form. It was of note that the trend of the experimentally determined dipole moments of the *N*-benzyladenine

derivatives in dioxane (Table 3.5), N9-benzyladenine < N3-benzyladenine < N7-benzyladenine, corresponded well with the trend observed for the dipole moments of the adenine tautomers, N9-H < N3-H < N7-H.

Table 3.5: Experimentally determined dipole moment (μ), in Debye, of N-benzyladenine derivatives in dioxane.

N-benzyladenine	μ (D) ^a
N9-benzyladenine	2.73 ± 0.2
N3-benzyladenine	4.92 ± 0.1
N7-benzyladenine	8.10 ± 0.1

Experimentally, Laxer *et al.*²⁷ was one of the first to provide evidence for the existence of the N3-H tautomer through ¹⁵N NMR spectroscopy (DMSO-d₆ as solvent), using various ¹⁵N₅-labelled adenine and adenine derivatives. The broadening of a nitrogen spectral peak in a ¹⁵N NMR spectrum indicates tautomerization involving that nitrogen. Indeed, the N6 and the N1 nitrogen appeared as sharp narrow peaks, indicating that they are not involved in the tautomerization, ruling out the N1-H and imine tautomers as the predominate tautomers. This is in agreement with their computational data having both tautomers 12 kcal/mol higher in energy than the N9-H tautomer (B3LYP/6-31G(d,p)). The N3, N7 and N9 peaks occurred as broad small peaks in the ¹⁵N NMR spectrum, indicating that the tautomerization involves these three nitrogens. The nitrogen containing the proton is “pyrrole” like as the lone pair is in the p-orbital which contributes to the 4n+2 electron aromatic system (Figure 3.7, as indicated by the N9 nitrogen in N9-H), while the other nitrogens in the ring are “imine” like as their lone pair is in a sp² orbital, which is planar to the purine ring and does not contribute to the aromatic system.²⁷

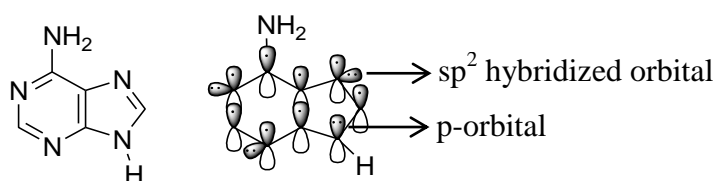


Figure 3.7: “Pyrrole” like and “imine” like nitrogens in the purine system of N9-H.

The “pyrrole” like nitrogen is thus more shielded and appears further upfield compared to the “imine” like nitrogens. In the case of adenine, the N9 nitrogen is the most shielded, at about –210 ppm in the ^{15}N NMR spectrum having the N1, N3 and N7 at –150 to –170 ppm, which indicates that the N9-H tautomer as being the most dominant in the tautomeric mixture in solution.²⁷ The smaller the difference in chemical shift values between the N7 and N9 peaks indicates enrichment in the N7-H tautomer. Gonnella *et al.*⁷³ also noted a decrease in the chemical shift difference between N9 and N7 when moving from DMSO to water, meaning that the N9-H is the most favoured tautomer in both solvents but N7-H more so in water than in DMSO. The N9-H tautomer dominates the N7-H tautomer as the lone pair of electrons of the N3 and the N9 in the N7-H tautomer experiences repulsion and the exo-amino group allows steric hindrance with the proton on the N7.^{27,73} The N9-H is stabilised by attractive interactions between the N3 lone pair of electrons with the N9 proton and the N7 lone pair of electrons with a proton on the NH_2 group. The N3-H has no repulsive interaction or steric hindrance such as the N7-H.

3.2 Results and discussion

3.2.1 Stability trend of the prototropic tautomers of adenine

Adenine has various tautomeric forms in solution and, as literature suggests, the N9-H tautomer is the dominant form followed by the N7-H tautomer.^{28,71,83} However, there was some uncertainty in the literature as to whether the N3-H tautomer existed in solution,⁸⁷ even though ¹⁵N NMR spectroscopy supported the existence of this tautomer.²⁷ The tautomeric mixture ratio in solution and the exact reasons for variation in population ratios upon temperature and solvent change is unknown; even after all the research which had been conducted surrounding the topic. This shows how complex the chemistry surrounding the adenine molecule is and how it can adapt to different environments.

Without making assumptions of the dominance of adenine tautomers, N1-H, N3-H, N7-H and N9-H were optimized without constraints in Gaussian 09 using the density functional theory (DFT), employing the B3LYP level of theory and 6-311G++(d,p) as a basis set. Structures were computed with the PCM simulating DMSO as a solvent (Table S1 in Supporting Material). Relative to the **N9-H** tautomer, differences in the electronic energy (ΔE) of the four adenine tautomers and their molecular graphs are shown in Table 3.6 and Figure 3.8, respectively.

Table 3.6: Relative to **N9-H**, the difference in electronic energy (ΔE , kcal/mol) of adenine tautomers.

Name	ΔE^a	Boltz %
N9-H	0.0	99.02
N7-H	2.7	0.97
N3-H	5.4	0.01
N1-H	8.6	0.00

^a B3LYP/6-311G++(d,p)/PCM(DMSO).

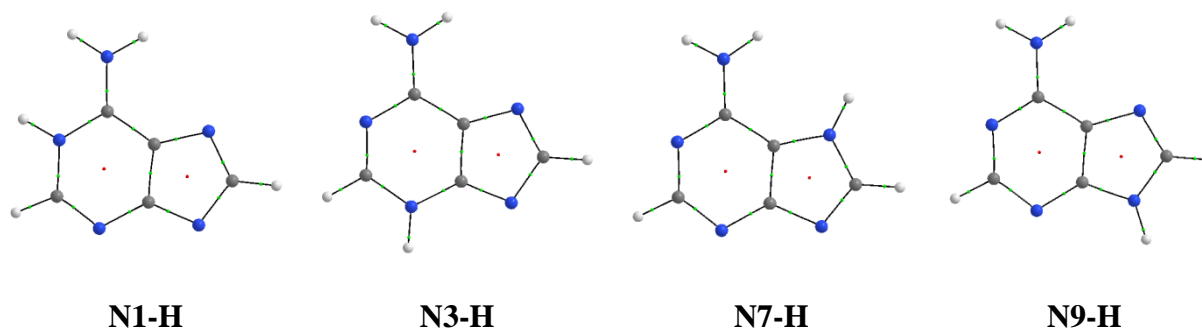


Figure 3.8: Molecular graphs of adenine tautomers.

Amongst the adenine tautomers, the **N9-H** tautomer was the most stable whereas the **N1-H** tautomer was the least stable with an energy difference of 8.6 kcal/mol. The stability trend seen in the ΔE of the adenine tautomers follows that from literature, being **N9-H** > **N7-H** > **N3-H** >> **N1-H** (denoted as N9 > N7 > N3 >> N1). It must be kept in mind that the energies calculated above are an approximation of the experimental relative energy of a molecular system in a solvent and are used only as a measure of the relative stabilities of the molecular systems in order to generate a trend which could be extended to the experimental energies.

3.2.2 Stability of *N*-benzyladenine regio-isomers

In literature it is stated that purine tautomers dictate the sites of alkylation. It was decided to explore the relationship between adenine tautomers and *N*-alkylated adenine derivatives. *N*-benzyladenine (N-Bn) regio-isomers (Figure 3.9) were chosen as the set of alkylated adenine derivatives.

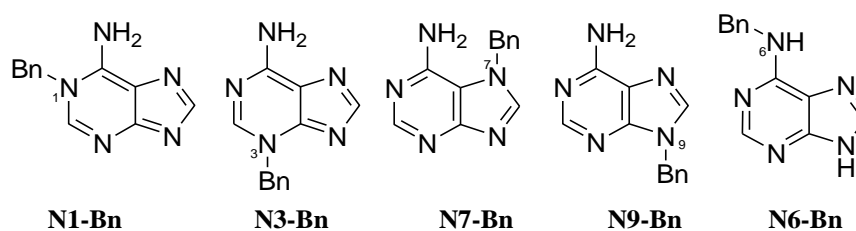


Figure 3.9: Structural isomers of *N*-benzyladenine.

The N-Bn regio-isomers involve four endo-purine regio-isomers (**N1-**, **N3-**, **N7-** and **N9-Bn**) and one exo-purine regio-isomer (**N6-Bn**).

A conformational search for all N-Bn isomers (Table S2 in Supporting Material) was carried out to generate a library of possible conformers to obtain the most likely form of each isomer. The **N6-Bn** regio-isomer had four possible pairs of isomers (Figure 3.10) due to the prototropic purine proton which could be situated on either four of the endo ring nitrogens (Figure 3.10, **N6-Bn-N1H/N3H/N7H** and **N9H**) generating four tautomers, in which each tautomer contained the conformer possibilities in which the benzyl group lies over the N7 (**1**) or over the N1 (**2**).

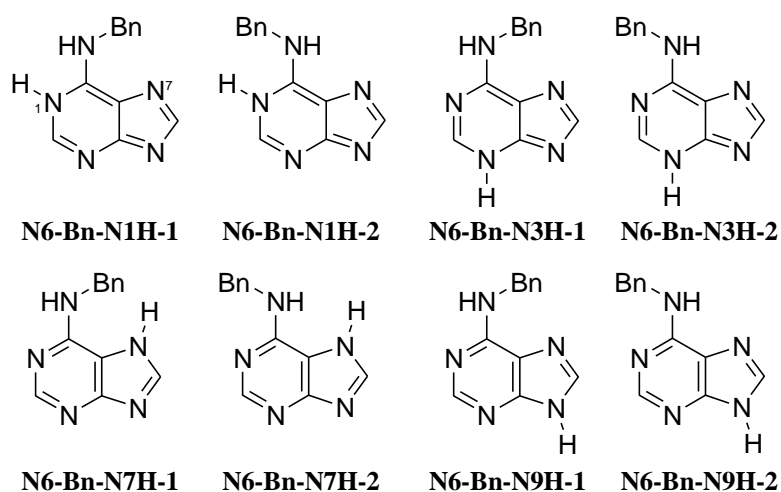


Figure 3.10: **N6-Bn** isomers.

All possible N-Bn conformers were optimized without constraints in Gaussian 09 (Table S3 in Supporting Material) employing B3LYP/6-311G++(d,p)/PCM(DMSO). The most stable conformer of each N-Bn regio-isomer was selected (N-Bn-X, where N = N1, N3, N6, N7, or N9 and X = conformer number). Relative to the most stable N-Bn conformer **N9-Bn-1**, the difference in *E* of the most stable conformer of each endo-purine N-Bn regio-isomer is shown in Table 3.7. At this stage all conformers of the exo-purine **N6-Bn** regio-isomer were omitted for simplicity when comparing the direct relationship between the tautomeric proton sites and the

site of alkylation, in which both occur on the endo-purine ring of adenine. The molecular graphs of the most stable endo-purine N-Bn conformers are presented in Figure 3.11.

Table 3.7: Relative to **N9-Bn-1**, difference in electronic energy (ΔE , kcal/mol) of the most stable conformer of each endo-purine N-Bn regio-isomer.

N-Bn	ΔE^a	Boltz %
N9-Bn-1	0.0	97.16
N7-Bn-2	3.7	0.18
N3-Bn-3	6.1	0.00
N1-Bn-3	11.4	0.00

^a DFT/B3LYP/6-311G++(d,p)/PCM(DMSO).

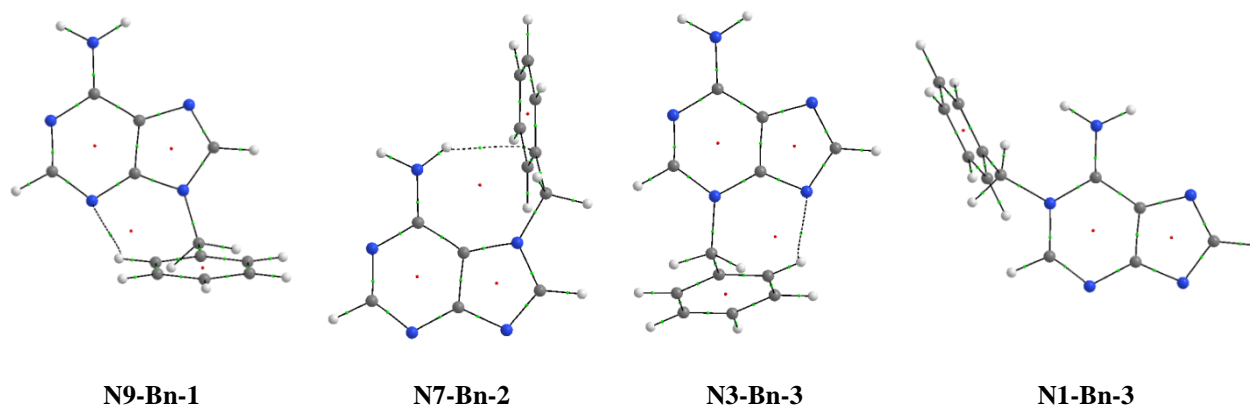


Figure 3.11: Molecular graphs of most stable endo-purine N-Bn isomers.

The ΔE between the most stable conformer of each endo-purine N-Bn regio-isomer follows the stability trend of the adenine tautomers: $N9 > N7 > N3 \gg N1$. This trend, which was more elaborate in the N-Bn isomers, could explain why many authors have synthesised adenine derivatives in order to study adenine tautomers^{47,48,70} and why some authors stated that the adenine tautomers dictate the regio-selectivity of alkylation.^{47,66,67}

It was apparent from the molecular graphs of **N9-Bn-1** and **N3-Bn-3** that there was an additional stabilising N...H intramolecular interaction and for **N7-Bn-2** there was an additional C...H intramolecular interaction (Figure 3.11, dotted lines). Both additional stabilising interactions were absent in the **N1-Bn-3** isomer which could be the reason for its lower stability ($\Delta E = 11.4$ kcal/mol) compared to the former mentioned isomers.

Turning our attention to the four pairs of the *exo*-purine **N6-Bn** regio-isomer, the tautomeric stability between them could be extracted by selecting the most stable conformer from each tautomeric pair. The difference in *E* relative to **N9-Bn-1** is shown in Table 3.8, in which the tautomeric stability trend $N9 > N7 > N3 > N1$, is observed. This stability trend was seen in adenine tautomers and in the most stable *endo*-purine N-Bn regio-isomers.

Table 3.8: Relative to **N9-Bn-1**, difference energies (ΔE , kcal/mol) of the most stable *exo*-purine N6-Bn isomers.

N-Bn	ΔE^a
N6_Bn_N9H_2	2.1
N6_Bn_N7H_3	5.0
N6_Bn_N3H_2	7.4
N6_Bn_N1H_2	11.0

^a DFT/B3LYP/6-311G++(d,p)/PCM(DMSO).

Combining the results, it was surprising to find the reoccurring stability trend of $N9 > N7 > N3 > N1$ regardless of the substituent, benzyl or proton, on the adenine frame, having **N9-Bn-1** and **N6-Bn-N9H-2** as the most stable forms, with ΔE of 2.1 kcal/mol. This indicated that the stability of adenine and its derivatives is dependent on the position of the substituent in the purine ring, having the substituent at the N9 position the most stabilising.

3.3 The interaction between benzyl bromide and adenine

It is commonly stated in literature that the site of alkylation of purines matches the position of the labile proton in the dominant tautomers N9-H and N7-H. It is therefore predicted that the dominant adenine alkylation products are the N9- and N7-substituted adenine isomers. However, this is not the case for adenine as N9- and N3-substituted adenine derivatives are the major products from direct alkylation, thus the preferred sites of alkylation under basic conditions are the N9 and N3 positions. The formation of these two substituted adenine derivatives does not follow the N-Bn isomer stability trend, $N9 > N7 > N3 > N1$, discussed above (section 3.2.2). This conflicting result indicates that the reaction is not thermodynamically

controlled, meaning that the reaction does not yield the most thermodynamically stable products. The regio-selectivity could be a result of kinetic control governed by transition state activation energies. To explore this possibility, we studied the reactivity of adenine towards S_N2 substitution by generating a potential energy profile for each *N*-alkylated adenine isomer, excluding the N6-alkylated possibility (exclusion is explained in section 3.2.2, which shows that the exo-amino group stays intact).

3.3.1 Exploring the sites of alkylation of adenine under a S_N2 mechanism

No literature precedent was found for the study of the S_N2 reaction pathway for the alkylation of purines, such as adenine. Therefore we undertook to determine which factors control the selectivity of N9 and N3 sites of alkylation of adenine over the N1 and N7 sites under S_N2 substitution conditions. We started by developing a scheme (Figure 3.12) showing the four pathways to be compared, N1-, N3-, N7-, and N9-pathway, leading to each regio-isomer, **N1-Bn**, **N3-Bn**, **N7-Bn** and **N9-Bn**, respectively. Each pathway was broken down into their individual steps, starting from the most stable tautomeric form of adenine (N9-H), then the generation of the nucleophile by deprotonation of adenine (**AD⁻**), followed by a S_N2 -type transition state for each pathway having two possible orientations (**N-Bn-TS1/2**, where N = site of alkylation N1, N3, N7 or N9). The **N-Bn-TS-1** transition states have no additional **N...H** interaction, whereas the **N-Bn-TS-2** transition states have an additional **N...H** interaction between a proton from the CH_2 of the benzene group and a nitrogen in the purine system. The **N-Bn-TS-2** transition states are expected to have additional stability due to the **N...H** interaction, rendering them more favourable than the transition states in which the **N...H** interaction is absent. The final structure of each reaction path is the resulting product of the S_N2 substitution (**N1-Bn**, **N3-Bn**, **N7-Bn** or **N9-Bn**).

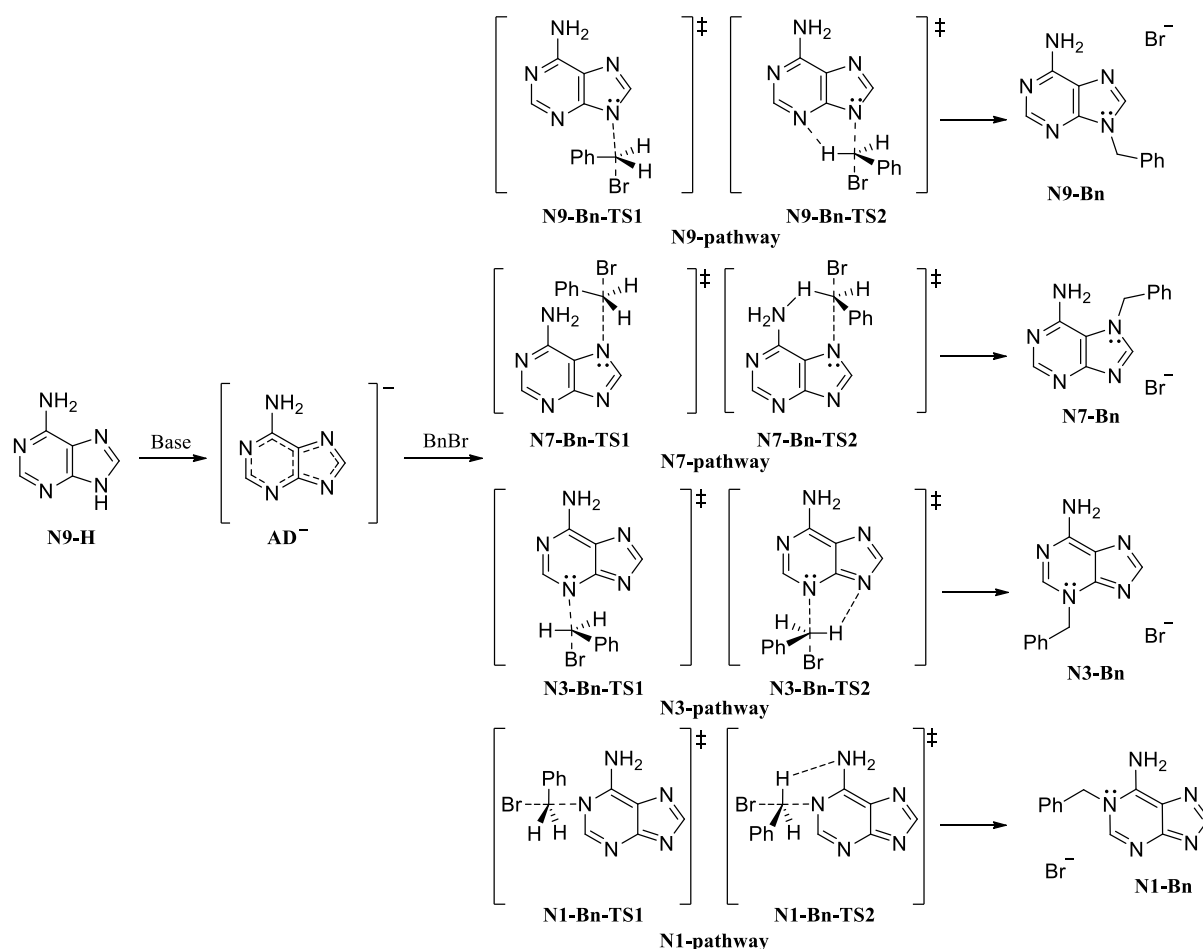


Figure 3.12: Scheme of S_N2 pathways leading to the N1, N3, N7 and N9 regio-isomers.

The possible S_N2 pathways (shown in Figure 3.12) were studied computationally with focus on the QTAIM and IQA-defined topological properties and energy terms which may govern the preferred sites of alkylation.

3.3.2 The stable form of the adenine anion

We have already demonstrated that the N9-H is the most stable adenine tautomer in solution (DMSO). Furthermore, in the synthesis of N9-alkyladenine, the main practise is subjecting adenine to highly basic conditions with an electrophile as the alkylating agent to promote S_N2 substitution reactions. Thus, we are dealing with deprotonated adenine which will in turn determine the site of alkylation. This already sets us apart from the authors who stated that it was adenine tautomers that control the regio-selectivity of alkylation. Adenine is expected to

undergo preferential deprotonation on the purine ring by removing the endocyclic proton, resulting in a resonance structure having the negative charge spread throughout the purine ring as seen in Figure 13. Note that this same anion is formed when the adenine tautomers N1-H, N3-H, N7-H and N9-H are deprotonated.

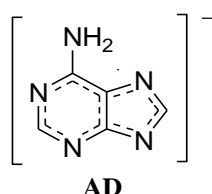


Figure 3.13: Deprotonated form of adenine, AD^- .

By contrast, deprotonation at the exocyclic amino group results in four pairs of possible isomers involving tautomers and conformers. Four tautomeric forms arise from the prototropic proton having four possible sites of attachment, N1, N3, N7 or N9 (Figure 3.14, $AD^-N1H/N3H/N7H/N9H$, respectively). Each tautomer has two low energy conformers resulting from the proton on the N6 either facing the N7 or the N1 (Figure 3.14, **1** and **2**, respectively).

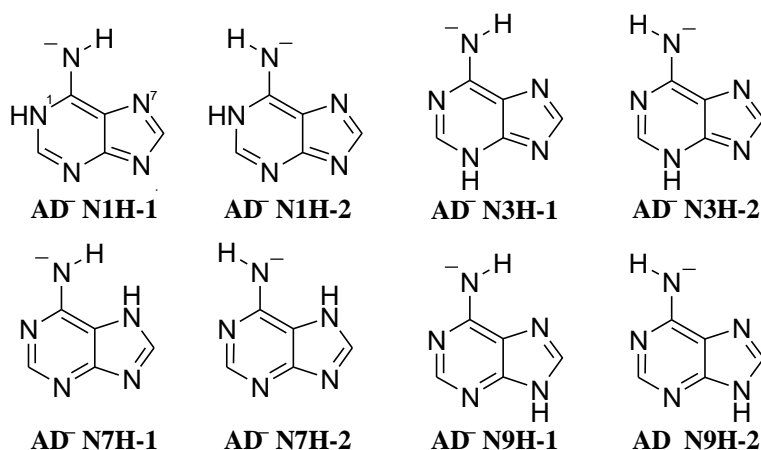


Figure 3.14: Exocyclic deprotonated isomers of adenine.

All possible isomers of deprotonated adenine were considered. The structures were optimized without constraint in Gaussian 09 employing B3LYP/6-311++(d,p)/PCM(DMSO) (Tables S4

and S5 in Supporting Material). Relative to AD^- , the difference in electronic energies (ΔE) of adenine isomers with the deprotonated exocyclic amino group are shown in Table 3.9.

Table 3.9: Relative to AD^- , differences in electronic energies (ΔE , kcal/mol) of deprotonated adenine isomers to assess effect of deprotonation at the exocyclic NH_2 group.

Name	ΔE^a	Boltz %
AD^-	0.00	100.00
$\text{AD}^- \text{N1H-1}$	8.77	0.00
$\text{AD}^- \text{N1H-2}$	11.48	0.00
$\text{AD}^- \text{N7H-2}$	12.51	0.00
$\text{AD}^- \text{N9H-2}$	13.22	0.00
$\text{AD}^- \text{N9H-1}$	13.47	0.00
$\text{AD}^- \text{N3H-1}$	14.21	0.00
$\text{AD}^- \text{N3H-2}$	14.45	0.00
$\text{AD}^- \text{N7H-1}$	14.81	0.00

^a DFT/B3LYP/6-311G++(d,p)/PCM(DMSO).

Deprotonation of the purine ring system, AD^- , is 8 kcal/mol more favourable than deprotonation of the exo-amino group. The effect of deprotonation at the NH_2 position was unfavourable regardless of the position of the endo-purine proton, which did not portray the stability trend of $\text{N9} > \text{N7} > \text{N3} > \text{N1}$ with regards to the substitution stability of adenine. However, within the deprotonated exo-amino group series, the stability trend of $\text{N1} > \text{N7} > \text{N9} > \text{N3}$ is observed and could be rationalised by studying the structures: the most stable forms, the N1 and N7 series, have the endo-purine ring proton in the nearby vicinity of the deprotonated amino group. The endo-purine ring proton has the potential to stabilize the resulting negative charge on the amino group, in which the N1 series has the proton three bonds away whereas the N7 series has the proton four bonds away. The two most stable forms from the N1 and N7 series, **$\text{AD}^- \text{N1H-1}$** and **$\text{AD}^- \text{N7H-2}$** , both have the N6 proton facing an un-substituted nitrogen, which could allow for an additional stabilising $\text{N} \cdots \text{H}$ interaction. The two less stable forms, **$\text{AD}^- \text{N1H-2}$** and **$\text{AD}^- \text{N7H-1}$** , have the N6 proton facing a protonated nitrogen, therefore having steric hindrance between the N6 proton and the $\text{N1}/\text{N7}$ proton, rendering them less stable. The

N9 and N3 series of exo-amino deprotonated adenine, have the N9 isomer more stable than the N3 isomer, which could be attributed to the N9 > N3 stability trend observed for the adenine tautomers.

From the above examination of the deprotonated forms of adenine, we can conclude that the deprotonation occurs on the purine ring leaving the exo-amino group protons intact, therefore excluding the N6-Bn regio-isomer as a possible product to form from the alkylation of adenine under basic conditions. The molecule which dictates the site of alkylation under basic conditions is therefore the deprotonated adenine structure \mathbf{AD}^- (Figure 3.15, molecular graph of \mathbf{AD}^-).

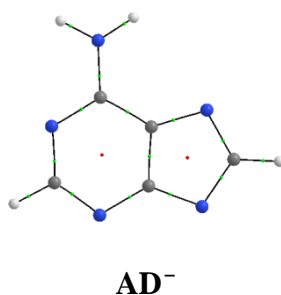


Figure 3.15: Molecular graph of deprotonated adenine \mathbf{AD}^- .

The next question we wished to investigate was whether the electron density distribution in the adenine anion was uneven and could be used to predict the site of alkylation. Due to the major site of alkylation being at the N9 position, it was expected that the N9 position had the highest electron density.

The electron population of atom A, $N(A)$, and electron density ($\rho(\mathbf{r})$) at each bond critical point (BCP) between two bonded atoms A and B, ρ_{BCP} , for N9-H and \mathbf{AD}^- are shown in Table 3.10 with the change in electron density, $\Delta\rho_{\text{BCP}}$, and electron population, $\Delta N(A)$, resulting from the deprotonation of **N9-H** to yield \mathbf{AD}^- . Note that the atom labels are reported as the Gaussian numbering scheme (shown in Figure 3.16) and not as the IUPAC nomenclature numbering system.

Table 3.10: Change in electron density ($\Delta\rho(\mathbf{r})$ in a.u.) and electron population ($\Delta N(A)$ in e) resulting from deprotonation of **N9-H** to yield **AD⁻**.

Electron density at BCP					$\Delta\rho_{\text{BCP}}$	Electron population $N(A)$			$\Delta N(A)$
atoms ^a		N9-H	AD⁻	AD⁻-N9H		atom A ^a	N9-H	AD⁻	
A	B								
C8	N9	0.3063	0.3326	0.0264	C8	5.028	5.119	0.090	
C4	N9	0.3069	0.3295	0.0226	H8	0.895	0.978	0.083	
C5	N7	0.3114	0.3171	0.0057	N7	8.103	8.162	0.060	
C2	N3	0.3424	0.3476	0.0052	N3	8.144	8.196	0.052	
C5	C6	0.3027	0.3049	0.0022	C6	5.023	5.075	0.052	
N6	H12	0.3394	0.3401	0.0006	C4	5.123	5.168	0.045	
N6	H11	0.3382	0.3388	0.0006	H2	0.946	0.978	0.032	
C6	N1	0.3400	0.3397	-0.0003	N1	8.148	8.177	0.029	
C2	H2	0.2894	0.2863	-0.0031	C2	4.979	5.007	0.028	
C8	H8	0.2898	0.2846	-0.0052	C5	5.624	5.649	0.026	
C2	N1	0.3362	0.3303	-0.0059	H11	0.573	0.589	0.016	
C6	N6	0.3274	0.3176	-0.0098	H12	0.572	0.586	0.014	
C5	C4	0.3162	0.3060	-0.0102	N6	8.138	8.148	0.010	
C4	N3	0.3441	0.3276	-0.0165	N9	8.163	8.169	0.006	
C8	N7	0.3632	0.3397	-0.0235	H10	0.543	-	-	
N9	H10	0.3358	-	-	-	-	-	-	

^a Gaussian numbering of atoms.

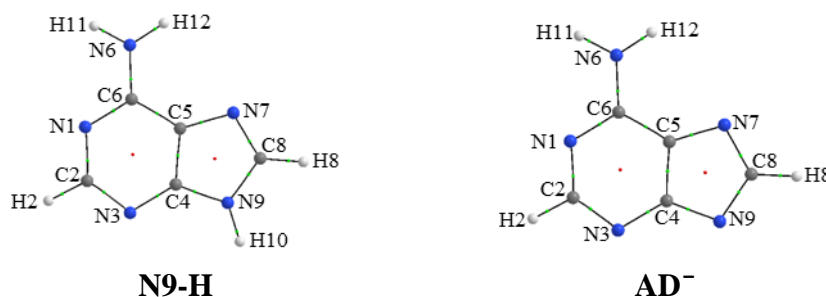


Figure 3.16: Gaussian numbering scheme of atoms for the **N9-H** and **AD⁻**.

The $N(A)$ at the five nitrogens of **AD⁻** portrays the trend of $N3 > N1 > N9 > N7 > N6$, indicating that N3 has the greatest electron population (8.196 e). This result might mean that theoretically the S_N2 substitution should preferentially occur at the N3 position.

It could be reasoned that if a molecule changes to a reacting state, such as adenine changing to the adenine anion, the molecule should return back to its initial state (substituted form of

adenine), therefore undergoing a reaction to achieve this. The area of reactivity of the reactive state should occur where the greatest change occurred relative to its initial state.

The analysis of $\Delta\rho_{\text{BCP}}$ shows that most of the electron density after deprotonation moved to the C8—N9 (+0.0264 a.u.) and the C4—N9 (+0.0226 a.u.) bonds (Figure 3.17 **A** red ovals) and was withdrawn from the C8—N7 (-0.0235 a.u.), C4—N3 (-0.0165 a.u.) and the C5—C4 (-0.0102 a.u.) bonds (part **A**, blue ovals).

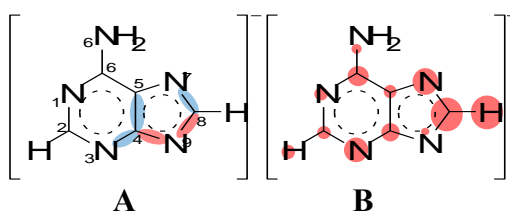


Figure 3.17: A graphic representation of the maximum gain (red) and maximum depletion (blue) of ρ_{BCP} (**A**), and the greatest to lowest change in $N(A)$ (biggest to smallest circles, respectively) (**B**).

The $\Delta N(A)$ shows that the electron population at the N9 position underwent minimal change (+0.006e), having the electron density move into its connecting bonds. All other atoms underwent significant change, having the greatest change at the C8 (+0.090e) and the H8 (+0.083e) atoms (Figure 3.17 **B**, large to small circles indicating large to minimal change in $N(A)$, respectively).

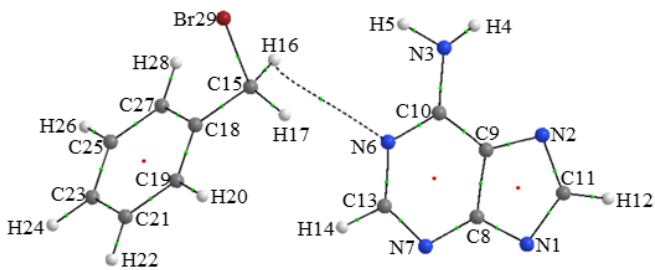
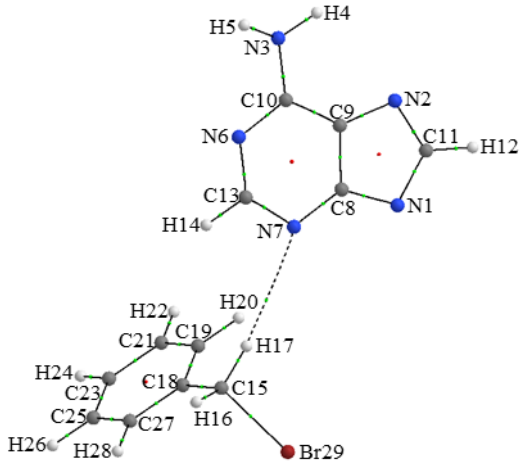
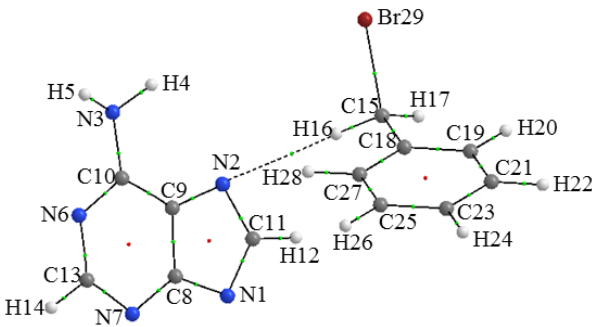
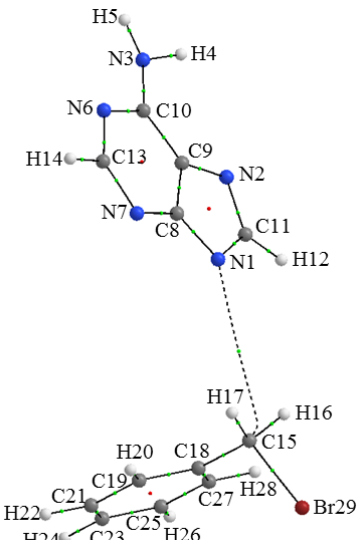
When moving from N9-H to AD^- , the greatest $\Delta N(A)$ and $\Delta\rho_{\text{BCP}}$ could be taken as an indication of the most reactive area. The imidazole ring underwent the greatest overall change, having the ρ_{BCP} at the C4—N9 and C8—N9 BCPs increase dramatically along with the C8, H8 and the N7 increasing the most in $N(A)$. Therefore, in order for the system (AD^-) to return to its initial state (N9-H/N9-substituted adenine), the imidazole ring would need to remove most of the additional electron density at BCPs and electron population at atoms, rendering it more reactive.

3.4.3 Generating S_N2 reaction paths for N1-, N3-, N7- and N9-benzyladenine

To study the kinetic control of the S_N2 mechanism upon the formation of N9- and N3-benzyladenine, the reaction paths were generated for the four pathways leading to N1-, N3-, N7- and N9-benzyladenine. The pathways were followed by simulating the S_N2 mechanism computationally, allowing deprotonated adenine AD^- and benzyl bromide to be brought closer together along a scanned co-ordinate which was created between the CH_2 of benzyl bromide and the relevant reacting N of the AD^- (where N = N1, N3, N7 or N9 for the N1-, N3-, N7- or N9-pathway, respectively). A distance of 4 Å between the C-atom (C15) of CH_2 of benzyl bromide and the corresponding reacting N of AD^- , $d(N,C15)$, was chosen as a starting point for each pathway and was decreased to 1.5 Å in 0.5 Å steps (Table S6 in Supporting Material). Four key positions from the above scan, $d(N,C15) = 4.0, 3.0, 2.0,$ and 1.5 Å, were chosen to perform the study in which each molecular system was fully optimized with a constrained $d(N,C15)$ distance. The molecular systems at the $d(N,C15) = 1.5$ Å were energy re-optimized without any constrain to obtain the lowest energy of each product at equilibrium, $d(N,C15) \sim 1.5(eq)$ Å (Table S7 in Supporting Material). The transition state of each pathway was calculated using the *Synchronous Transit-Guided Quasi-Newton* (STQN) Method, developed by H. B. Schlegel and co-workers^{92,93} (requesting the QST3 keyword in Gaussian 09) and occurred at varying distances, $d(N,C15) \sim 2.3(TS)$ Å, depending on the pathway (Table S7 in Supporting Material).

The potential energy profile of a reaction path was composed of the molecular systems at $d(N,C15)$ distances of 4.0, 3.0, $\sim 2.3(TS)$, 2.0, and $\sim 1.5(eq)$ Å (Table S8 in Supporting Material). The relevant energy-optimized molecular system at $d(N,C15) = 4.0$ Å for each pathway (Table 3.11) was chosen as the reference state (*ref*), against which every step along the potential energy profile was compared. The molecular systems at $d(N,C15) = 3.0, \sim 2.3(TS), 2.0$ and $\sim 1.5(eq)$ Å were chosen as final states (*fin*) along the reaction path. The change in a molecular system from the *ref* state to the *fin* state allowed us to study the (de)stabilising energy changes.

Table 3.11: Potential energy, E (a.u.), of ref state of each pathway with molecular graph indicating the Gaussian numbering scheme.

E (a.u.)	Initial state at $d(\text{N},\text{C}15) = 4.0 \text{ \AA}$
N1-pathway $E = -3312.1806$	
N3-pathway $E = -3312.1810$	
N7-pathway $E = -3312.1811$	
N9-pathway $E = -3312.1805$	

Relative to the relevant *ref* state, the changes in electronic energy (ΔE) for each step along the potential energy profile for each reaction path are shown in Table 3.12. The $d(\text{N,C15})$ that differed due to the unrestricted N—C15 bond distances for optimization of the transition state and final product are presented in brackets.

Table 3.12: Relative to relevant *ref* state, changes in energy (ΔE , kcal/mol) along the N1-, N3-, N7- and N9-pathway.

$d(\text{N,C15}) / \text{\AA}$	ΔE^a			
	N1-pathway	N3-pathway	N7-pathway	N9-pathway
4.0	0.0	0.0	0.0	0.0
3.0	1.4	1.9	1.4	1.5
~2.3(TS)	12.6 (2.29) ^b	9.9 (2.33) ^b	11.4 (2.33) ^b	9.4 (2.35) ^b
2.0	0.5	-6.7	-8.4	-9.5
~1.5(eq)	-24.1 (1.48) ^b	-26.5 (1.49) ^b	-29.6 (1.48) ^b	-32.9 (1.47) ^b

^a DFT/B3LYP/6-311++G(d,p)/PCM(DMSO) ^b actual $d(\text{N,C15})$ shown in brackets (\AA).

Comparing the ΔE at the $d(\text{N,C15})$ of 4.0 \AA and 3.0 \AA between each pathway gave insignificant differences between the molecular systems. The ΔE at the transition state (TS) $d(\text{N,C15}) \sim 2.3(\text{TS}) \text{\AA}$, is indicative of the activation energy. The N1-pathway displayed the largest activation energy (12.6 kcal/mol) at the TS compared to the other pathways, in which the ‘stability’ trend of $\text{N9} > \text{N3} > \text{N7} > \text{N1}$ was seen. The N7-pathway is 2.0 kcal/mol more unfavourable than the N9-pathway, which is not significant enough to rule it out, along with the N1-pathway, which is only 3.2 kcal/mol more unfavourable than the N9-pathway. After the TS, at $d(\text{N,C15}) = 2.0 \text{\AA}$, the stability trend of $\text{N9} > \text{N7} > \text{N3} \gg \text{N1}$ is seen, in which the N9-pathway is favoured the most by -9.5 kcal/mol. The N1-pathway at the distance of 2.0 \AA is still unflavoured by a further 0.5 kcal/mol, rendering this pathway the least likely pathway to be followed. The stability of the products at $d(\text{N,C15}) \sim 1.5(\text{eq}) \text{\AA}$ followed the trend of $\text{N9} > \text{N7} > \text{N3} > \text{N1}$, which corresponded to the trend of the most stable endo-purine N-Bn isomers (section 3.2.2).

The trends observed at $d(N,C15) \sim 2.3(\text{TS})$ and 2.0 \AA could indicate that it is at these two points along the reaction paths where the preference for the N3-/N9-benzyladenine is determined.

3.4 A closer look into the control of the reaction paths

As the kinetic control did not give clear indication for the preference of the N3 and N9 sites of alkylation over the N1 and N7 positions, the pathways were then studied in greater detail. Energy descriptors defined by IQA were used to develop a novel approach to analyse different energy contributions from the molecular system along a reaction path. To avoid confusion, the IQA-defined energy terms will first be explained in order to understand why we chose to study specific interactions.

The primary energy components from IQA are E_{add}^X , E_{self}^X , and E_{int}^{XY} , in which the overall energy of an atom in a molecule (atom A) is given by its additive energy E_{add}^A .⁹⁴⁻⁹⁶ The E_{add}^A energy term can be decomposed into two contributing energy terms, the self-atomic energy of atom A (E_{self}^A) and the diatomic interaction energy between atom A and any other atom (atom X) in the molecular system, E_{int}^{AX} . The E_{add}^A of atom A is defined as the sum of E_{self}^A and all halved E_{int}^{AX} contributions,

$$E_{\text{add}}^A = E_{\text{self}}^A + \sum_{X \neq A} 0.5 E_{\text{int}}^{AX} .$$

The overall energy of a molecule, E , is therefore composed of the sum of the additive energies of all the atoms:

$$E = \sum_X E_{\text{add}}^X .$$

Hence, the E of a molecule can also be written in terms of the self-atomic energies of all atoms and all unique diatomic interaction energies within a molecular system, $0.5 \sum_X \sum_{Y \neq X} E_{\text{int}}^{XY}$:

$$E = \sum_X E_{\text{self}}^X + 0.5 \sum_X \sum_{Y \neq X} E_{\text{int}}^{XY}.$$

The changes in the energy terms defined above can be monitored by relating the *fin* state to the *ref* state. Between two atoms, A and B, of a molecular system, the changes in IQA-defined energy terms are as follows:

$$\Delta E_{\text{self}}^A = {}^{\text{fin}} E_{\text{self}}^A - {}^{\text{ref}} E_{\text{self}}^A$$

$$\Delta E_{\text{int}}^{\text{AB}} = {}^{\text{fin}} E_{\text{int}}^{\text{AB}} - {}^{\text{ref}} E_{\text{int}}^{\text{AB}}$$

$$\Delta E_{\text{add}}^A = {}^{\text{fin}} E_{\text{add}}^A - {}^{\text{ref}} E_{\text{add}}^A = \Delta E_{\text{self}}^A + \Delta E_{\text{int}}^{\text{AX}},$$

where $\Delta E_{\text{int}}^{\text{AX}}$ is:

$$\Delta E_{\text{int}}^{\text{AX}} = \left(\sum_{X \neq A} {}^{\text{fin}} 0.5 E_{\text{int}}^{\text{AX}} \right) - \left(\sum_{X \neq A} {}^{\text{ref}} 0.5 E_{\text{int}}^{\text{AX}} \right).$$

With these IQA energy terms defined, the system can now be divided into particular interactions between fragments of the system as well as certain atoms interacting with fragments. A molecular system can be divided into (i) fragment $\mathfrak{F} = \{A, B\}$, composed of two selected atoms A and B of a molecular system, and fragment \mathfrak{H} , the remaining atoms in the molecular system, or into (ii) polyatomic fragments $\mathfrak{M}, \mathfrak{N}, \mathfrak{O} \dots$. Changes in these fragments' energy components can be monitored by relating the *fin* state of the concerned fragment to the *ref* state.

The intra-fragment diatomic interaction energy of fragment \mathfrak{F} , $E_{\text{int}}^{\mathfrak{F}}$, only consists of the interaction between the two selected atoms A and B:

$$E_{\text{int}}^{\mathfrak{F}} = E_{\text{int}}^{\text{AB}}.$$

In more general terms, the intra-fragment interaction energy of a polyatomic fragment \mathfrak{M} , $E_{\text{int}}^{\mathfrak{M}}$, is made of all unique diatomic interaction energies between the atoms constituting fragment \mathfrak{M} :

$$E_{\text{int}}^{\mathcal{M}} = 0.5 \sum_{X \in \mathcal{M}} \sum_{\substack{Y \neq X \\ Y \in \mathcal{M}}} E_{\text{int}}^{XY} .$$

Hence, the change in the intra-fragment interaction energy of polyatomic fragment \mathcal{M} , $\Delta E_{\text{int}}^{\mathcal{M}}$, when moving from the *ref* state to the *fin* state is calculated as

$$\Delta E_{\text{int}}^{\mathcal{M}} = {}^{\text{fin}} E_{\text{int}}^{\mathcal{M}} - {}^{\text{ref}} E_{\text{int}}^{\mathcal{M}} .$$

Focusing on the self-energy of the fragment \mathcal{G} , $E_{\text{self}}^{\mathcal{G}}$, it consists of the self-atomic energies of atoms A and B:

$$E_{\text{self}}^{\mathcal{G}} = E_{\text{self}}^{\text{A}} + E_{\text{self}}^{\text{B}} .$$

The change in self-energy for fragment \mathcal{G} , $\Delta E_{\text{self}}^{\mathcal{G}}$, when going from the *ref* state to the *fin* state can be calculated, giving an indication of the deformation energy of the fragment:

$$\Delta E_{\text{self}}^{\mathcal{G}} = \Delta E_{\text{self}}^{\text{A}} + \Delta E_{\text{self}}^{\text{B}} = ({}^{\text{fin}} E_{\text{self}}^{\text{A}} - {}^{\text{ref}} E_{\text{self}}^{\text{A}}) + ({}^{\text{fin}} E_{\text{self}}^{\text{B}} - {}^{\text{ref}} E_{\text{self}}^{\text{B}}) .$$

Considering a polyatomic fragment \mathcal{M} , its self-energy $E_{\text{self}}^{\mathcal{M}}$ is simply the sum of all self-atomic energies of the atoms which constitute fragment \mathcal{M} :

$$E_{\text{self}}^{\mathcal{M}} = \sum_{X \in \mathcal{M}} E_{\text{self}}^{\text{X}} .$$

The inter-fragment interaction energy between fragment \mathcal{G} and fragment \mathcal{H} , $E_{\text{int}}^{\mathcal{G}\mathcal{H}}$, is composed of all diatomic interaction energies between the atoms of fragment \mathcal{G} with the atoms of fragment \mathcal{H} , excluding the all intra-fragment diatomic interaction energies between atoms of fragment \mathcal{G}/\mathcal{H} :

$$E_{\text{int}}^{\mathcal{G}\mathcal{H}} = \sum_{X \in \mathcal{G}} \sum_{Y \in \mathcal{H}} E_{\text{int}}^{XY} .$$

The relative change in the inter-fragment interaction energy term involving diatomic fragment $\mathcal{G} = \{\text{A,B}\}$ and polyatomic fragment \mathcal{H} , $\Delta \sum_{X \in \mathcal{H}} E_{\text{int}}^{\mathcal{G}\text{X}}$, can be calculated from

$$\Delta \sum_{X \in \mathcal{H}f} E_{\text{int}}^{\mathcal{G}X} = \sum_{X \in \mathcal{H}f}^{\text{fin}} E_{\text{int}}^{\mathcal{G}X} - \sum_{X \in \mathcal{H}f}^{\text{ref}} E_{\text{int}}^{\mathcal{G}X} = \left(\sum_{\substack{A \in \mathcal{G} \\ X \in \mathcal{H}f}} E_{\text{int}}^{\text{AX}} + \sum_{\substack{B \in \mathcal{G} \\ X \in \mathcal{H}f}} E_{\text{int}}^{\text{BX}} \right)^{\text{fin}} - \left(\sum_{\substack{A \in \mathcal{G} \\ X \in \mathcal{H}f}} E_{\text{int}}^{\text{AX}} + \sum_{\substack{B \in \mathcal{G} \\ X \in \mathcal{H}f}} E_{\text{int}}^{\text{BX}} \right)^{\text{ref}}.$$

Finally, let us define the inter-fragment interaction energy between polyatomic fragment \mathcal{M} and polyatomic fragment \mathcal{N} , $E_{\text{int}}^{\mathcal{M}\mathcal{N}}$, as the sum of all diatomic interactions between atoms of fragment \mathcal{M} with the atoms of fragment \mathcal{N} ,

$$E_{\text{int}}^{\mathcal{M}\mathcal{N}} = \sum_{X \in \mathcal{M}} \sum_{Y \in \mathcal{N}} E_{\text{int}}^{\text{XY}}.$$

Hence, the change in the inter-fragment interaction energy between polyatomic fragments \mathcal{M} and \mathcal{N} from the *ref* state to the *fin* state can be obtained from

$$\Delta E_{\text{int}}^{\mathcal{M}\mathcal{N}} = \sum_{\text{fin}} E_{\text{int}}^{\mathcal{M}\mathcal{N}} - \sum_{\text{ref}} E_{\text{int}}^{\mathcal{M}\mathcal{N}}.$$

With all the IQA energy terms defined above, the tool to explain different contributions of energy in a molecular system is given. Energy contributions from specific atoms, interactions and fragments can now be investigated.

3.4.1 Comparing the IQA defined energy terms of N1, N3, N7, and N9 atoms within each pathway

For each reaction path, the IQA define energy terms, ΔE_{add}^X , ΔE_{self}^X , and $\Delta E_{\text{int}}^{\text{XY}}$, for all atoms in a molecular system were monitored relative to the relevant *ref* state (Tables S9–S20 in Supporting Material). The changes within these three energy terms showed that the greatest (de)stabilising changes occurred within the adenine anion frame, AD^- . In addition to these changes, the bromine atom (Br29) experienced strong stabilising changes in the self-atomic energy component, $\Delta E_{\text{self}}^{\text{A}}$, and strong destabilising changes in the diatomic interaction energy component, $\Delta E_{\text{int}}^{\text{AX}}$. This was reversed in the carbon atom (C15) from the CH_2 of the benzyl group, which experienced insignificant changes in the additive energy, but strong destabilising

$\Delta E_{\text{self}}^{\text{A}}$ and large stabilising $\Delta E_{\text{int}}^{\text{AX}}$ interaction energy changes were found as its 3D arrangement has changed due to the formation of the new N—C15 bond.

As there are 28 atoms in each molecular system, comparing the changes along each reaction path can become time consuming and complicated. We have therefore decided to turn our attention to the reacting nitrogen of each pathway: N1, N3, N7, and N9 in the N1-, N3-, N7- and N9-pathways, respectively. Selected data for the reactive nitrogen in each pathway is presented in Table 3.13. Significant changes in the IQA defined energy terms appeared from the transition state, $d(\text{N},\text{C15}) \sim 2.3(\text{TS}) \text{ \AA}$, onwards. At the transition state it was surprising to find that the change in atomic additive energy, $\Delta E_{\text{add}}^{\text{N}}$, of the reacting nitrogen was the smallest among all N-atoms of adenine (Tables S9, S12, S15 and 18 in Supporting Material). On the other hand, the values of the $\Delta E_{\text{self}}^{\text{N}}$ and $\Delta E_{\text{int}}^{\text{NX}}$ terms changed significantly but at the same time essentially cancelled each other out, hence the small overall change in $\Delta E_{\text{add}}^{\text{N}}$.

Table 3.13: Relative to relevant ref state, changes in IQA define energy terms (kcal/mol) of the reactive nitrogen along each pathway for selected $d(\text{N},\text{C15}) = \sim 2.3(\text{TS})$, 2.0 and $\sim 1.5(\text{eq}) \text{ \AA}$.

$d(\text{N},\text{C15}) / \text{ \AA}$		$\sim 2.3(\text{TS})$	2.0	$\sim 1.5(\text{eq})$
pathway	atom N	$\Delta E_{\text{add}}^{\text{N}}$		
N1	N1	-4.0	-10.6	-45.2
N3	N3	-4.8	-37.3	-56.2
N7	N7	-3.8	-14.9	-41.7
N9	N9	-4.7	-35.9	-57.3
		$\Delta E_{\text{self}}^{\text{N}}$		
N1	N1	34.7	54.6	104.1
N3	N3	39.8	72.8	118.5
N7	N7	30.0	73.2	129.5
N9	N9	36.4	77.6	136.9
		$\Delta E_{\text{int}}^{\text{NX}}$		
N1	N1	-38.7	-65.2	-149.3
N3	N3	-44.6	-110.1	-174.7
N7	N7	-33.8	-88.2	-171.2
N9	N9	-41.1	-113.6	-194.2

^a Common numbering nomenclature used, * reacting nitrogen in pathway.

The change in the IQA-defined energy terms for the reactive nitrogen of each pathway gave some useful insight into how the relevant nitrogen is being influenced by the changing molecular system:

- i. Initially, upon formation of the TS, $d(\text{N},\text{C}15) \sim 2.3(\text{TS}) \text{ \AA}$, all reaction paths have equal opportunity to form in regards to the changes at the relevant reactive nitrogen.
- ii. After the TS, $d(\text{N},\text{C}15)$ of 2.0 \AA , the changes in the IQA-defined energy terms $E_{\text{add}}^{\text{N}}$ and $E_{\text{int}}^{\text{NX}}$ suggest that the reaction is largely in favour of the N3-/N9-pathways, having significantly higher stabilising terms, and in least favour of the N1-/N7-pathways.
- iii. The N9-pathway is by far more favourable at $d(\text{N},\text{C}15)$ of $\sim 1.5 \text{ \AA}(\text{eq})$, suggesting that the competing N3-pathway that emerged from the previous step, $d(\text{N},\text{C}15) = 2.0 \text{ \AA}$, would be dominated by the N9-pathway.

The overall changes in the additive energy of the reacting nitrogen of each pathway lead to the N3-/N9-pathway as being the most favourable in that regard. The $\Delta E_{\text{add}}^{\text{N}}$ is the sum of $\Delta E_{\text{self}}^{\text{N}}$ and $\Delta E_{\text{int}}^{\text{NX}}$ terms, hence the dominance of the $\Delta E_{\text{int}}^{\text{NX}}$ term over the $\Delta E_{\text{self}}^{\text{N}}$ indicates that the preference for the N3-/N9- pathways to be followed could be a result from the influence of the interactions of the reactive nitrogen (of each pathway) with remaining atoms of both reacting molecules.

3.4.2 Interactions between fragments

It is important to realize that the product formation is a set of complex processes taking place when two molecules come from infinity and start to interact when the distance decreases along the reaction pathway. A simplifying approach taken here is based on a simple fact that when a reaction between two atoms is considered, then often their interaction leading to a final product (or the lack of) is explained in terms of their interaction energies, either highly attractive or

repulsive. Because two molecules are involved in product formation, it makes perfect sense to analyse interaction energies between them as well as interactions between leading atoms involved in the bond formation to rationalise the preferential reaction path. Considering just the final and initial states might be sometimes misleading, as it will be shown throughout this section, as the energy terms computed at different distances between molecules involved eliminate some potential reaction paths totally.

3.4.2.1 Interaction between fragment $\mathcal{G} = \{N, C15\}$ and fragment \mathcal{H}

The N—C15 bond formation was of particular interest as it might hold important information regarding the attachment to the different nitrogens on the purine ring. To study whether the bond was (de)stabilised along the pathways, a two atom fragment $\mathcal{G} = \{N, C15\}$, was selected with the remainder of the atoms in the molecular system being considered as fragment \mathcal{H} (see Tables S21–S24 in Supporting Material). The inter-fragment interaction energy between fragment \mathcal{G} and fragment \mathcal{H} of the *fin* states along a reaction path relative to the *ref* state, $\Delta E_{\text{int}}^{\mathcal{G}\mathcal{H}}$, for each pathway is shown in Table 3.14.

Table 3.14: Relative to relevant *ref* state changes in inter-fragment interaction energy, $\Delta E_{\text{int}}^{\mathcal{G}\mathcal{H}}$ (kcal/mol), between fragment $\mathcal{G} = \{N, C15\}$ and fragment \mathcal{H} for each reaction path.

Fragment \mathcal{G}	$\Delta E_{\text{int}}^{\mathcal{G}\mathcal{H}}$			
	{N6,C15}	{N7,C15}	{N2,C15}	{N1,C15}
d(N,C15) / Å	N1-pathway	N3-pathway	N7-pathway	N9-pathway
4.0	0.0	0.0	0.0	0.0
3.0	−38.5	−34.6	−37.6	−40.5
~2.3(TS)	65.4	37.5	62.4	42.9
2.0	114.9	64.2	102.1	61.0
~1.5(eq)	218.6	166.0	163.8	139.2

^a Gaussian numbering of atoms.

From the changes in the inter-fragment interaction energy presented above, some important interpretations can be made:

- i. An initial approach from $d(\text{N},\text{C15})$ of 4.0 to 3.0 Å of the two molecules is ‘promoted’ by equally high attractive inter-fragment energies for all reaction paths, again suggesting that all pathways start with an equal chance to form.
- ii. Interestingly, the moment a bond between N and C15 atoms starts to form, at the $d(\text{N},\text{C15})$ of $\sim 2.3(\text{TS})$ Å onwards, the $\Delta E_{\text{int}}^{\mathfrak{G}\mathfrak{H}}$ becomes repulsive for all reaction paths.
- iii. Importantly, a large difference in repulsive $\Delta E_{\text{int}}^{\mathfrak{G}\mathfrak{H}}$ values is observed between the N1-/N7-pathways and the N3-/N9-pathways when $d(\text{N},\text{C15})$ decreases from 3.0 Å, through the TS, to 2.0 Å where strengthening of the N—C15 bond takes place. This is a critical stage in the $S_{\text{N}}2$ mechanism and clearly, this inter-fragment interaction energy works against substitutions on N1 and N7 positions and is strongly in favour of substitution at the N3 and N9 positions.
- iv. Finally, on the product formation, $d(\text{N},\text{C15}) \sim 1.5$ Å, a large difference is observed between the N9- and N3-pathways making it by far more favourable for the former, corresponding very well with experimental data.
- v. The fact that $\Delta E_{\text{int}}^{\mathfrak{G}\mathfrak{H}}$ values for the N3- and N7-pathways at the equilibrium are comparable is irrelevant as already the N7-pathway was inhibited at the earlier stages where $\Delta E_{\text{int}}^{\mathfrak{G}\mathfrak{H}}$ for the N7-pathway was about 40 kcal/mol more repulsive.

The change in self-energy and the intra-fragment diatomic interaction energy of fragment \mathfrak{G} = {N,C15} along the reaction pathway (Table S25 and S26 in Supporting Material) is shown in Table 3.15.

Table 3.15: Relative to relevant ref state, changes in intra-fragment diatomic interaction energy, $\Delta E_{\text{int}}^{\mathcal{F}}$ (kcal/mol) and self-energy, $\Delta E_{\text{self}}^{\mathcal{F}}$ (kcal/mol), of fragment $\mathcal{F}\{N,C15\}$.

	N1-pathway	N3-pathway	N7-pathway	N9-pathway
Fragment \mathcal{F}^a	{N6,C15}	{N7,C15}	{N2,C15}	{N1,C15}
d(N,C15) / Å	$\Delta E_{\text{int}}^{\mathcal{F}}$			
~2.3(TS)	-53.0	-46.4	-47.1	-46.2
2.0	-109.6	-133.9	-132.0	-136.0
~1.5(eq)	-294.8	-292.3	-291.1	-303.0
	$\Delta E_{\text{self}}^{\mathcal{F}}$			
~2.3(TS)	27.9	33.6	24.4	29.7
2.0	46.7	69.7	69.1	73.1
~1.5(eq)	138.0	151.9	164.4	173.3
	$\Delta E_{\text{int}}^{\mathcal{F}} + \Delta E_{\text{int}}^{\mathcal{F}f}$			
~2.3(TS)	12.4	-8.9	15.3	-3.3
2.0	5.3	-69.7	-29.9	-75.0
~1.5(eq)	-76.2	-126.3	-127.3	-163.8

^a Gaussian numbering of atoms.

The $\Delta E_{\text{int}}^{\mathcal{F}} \gg \Delta E_{\text{self}}^{\mathcal{F}}$ indicates that the intra-fragment interaction energy is the dominating term, analysis of which allows for a number of observations:

- i. Firstly, in absolute terms, $\Delta E_{\text{int}}^{\mathcal{F}} \gg \Delta E_{\text{int}}^{\mathcal{F}f}$ for all reaction paths; this means that this intra-fragment interaction compensates for the destabilization coming from inter-fragment interactions, making it possible for the reaction to proceed towards products as the interaction between the two atoms is highly favourable.
- ii. Considering the N1-pathway at $d(\text{N,C15}) = 2 \text{ \AA}$, the destabilising $\Delta E_{\text{int}}^{\mathcal{F}f}$ term dominates the stabilising $\Delta E_{\text{int}}^{\mathcal{F}}$ term, which results in excluding this path as an option for further considerations.
- iii. Considering competition between the N3- and N7-pathways at $d(\text{N,C15}) = 2 \text{ \AA}$, the $\Delta E_{\text{int}}^{\mathcal{F}}$ terms are comparable but the sum of $\Delta E_{\text{int}}^{\mathcal{F}} + \Delta E_{\text{int}}^{\mathcal{F}f}$ is highly in favour of the N3-pathway (by about -40 kcal/mol) making the N7-pathway virtually impossible.

- iv. By far, the most stabilising contribution made by the $\Delta E_{\text{int}}^{\mathcal{G}}$ term is observed for the N9-pathway and when combined with the $\Delta E_{\text{int}}^{\mathcal{G},f}$ term, makes this path virtually the only one possible, which fully agrees with experimental data.

These results showed two aspects of the bond formation and it is important to understand which factors determine the preferential pathway. Even though the interaction between the two atoms composing the bond is stabilising, the effect the formation has on the rest of the molecular system plays a very important role, being highly destabilising for the N1-/N7-pathways and stabilising for the N3-/N9-pathways, which is comparable to experimental results.

3.4.2.2 Interaction between polyatomic fragments $\mathcal{M} = \{\text{AD}^- \}$ and $\mathcal{N} = \{\text{Bn}\}$

To study how the reagents are interacting with each other along each reaction path, the molecular system was divided into three fragments defined as \mathcal{M} , \mathcal{N} and \mathcal{O} (Figure 3.18): the deprotonated adenine AD^- - a polyatomic fragment \mathcal{M} , the benzyl Bn - a polyatomic fragment \mathcal{N} , and the bromide Br - a monoatomic fragment \mathcal{O} .

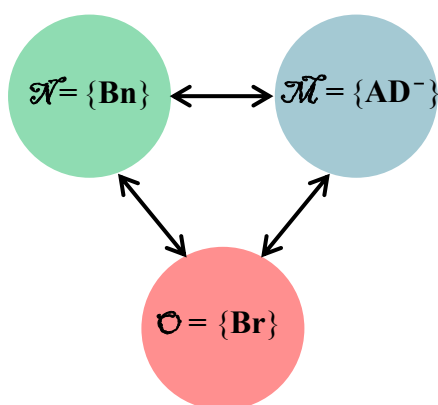


Figure 3.18: Fragments of molecular system: $\mathcal{M} = \{\text{AD}^- \}$, $\mathcal{N} = \{\text{Bn}\}$, $\mathcal{O} = \{\text{Br}\}$.

This was used to find out whether the three fragments interacted with each other in a (de)stabilising manner and to what extent. All possible interactions between fragments AD^- and Bn ($\mathcal{M} \cdots \mathcal{N}$), Bn and Br ($\mathcal{N} \cdots \mathcal{O}$), and AD^- and Br ($\mathcal{M} \cdots \mathcal{O}$) were considered.

When considering the interactions between any two fragments, such as fragments \mathcal{M} and \mathcal{N} , all diatomic interactions between atoms of fragment \mathcal{M} with all atoms of fragment \mathcal{N} (Figure 3.19) are summed up to give the inter-fragment interaction energy between \mathcal{M} and \mathcal{N} , $E_{\text{int}}^{\mathcal{M}\mathcal{N}}$. Note that the $E_{\text{int}}^{\mathcal{M}\mathcal{N}}$ does not include the diatomic interactions between atoms in the same fragment. This has been done for all inter-fragment interactions, $E_{\text{int}}^{\mathcal{M}\mathcal{N}}$, $E_{\text{int}}^{\mathcal{N}\mathcal{O}}$ and $E_{\text{int}}^{\mathcal{M}\mathcal{O}}$ (Tables S27–S34 in supplementary data).

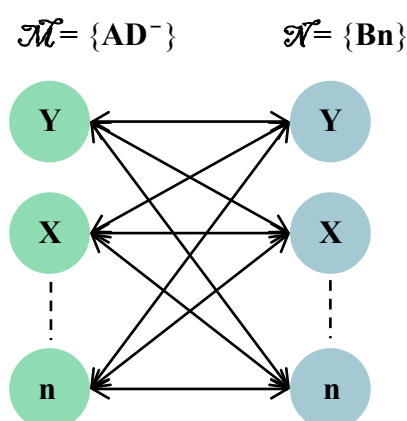


Figure 3.19: Diatomic interactions between atoms of fragment \mathcal{M} with atoms of fragment \mathcal{N} .

Relative to the relevant *ref* state, the changes in $E_{\text{int}}^{\mathcal{M}\mathcal{N}}$, $E_{\text{int}}^{\mathcal{N}\mathcal{O}}$ and $E_{\text{int}}^{\mathcal{M}\mathcal{O}}$ along each reaction path are presented in Table 3.16 for $d(\text{N},\text{C15})$ of $\sim 2.3(\text{TS})$, 2.0 and $\sim 1.5(\text{eq})$ Å.

The study of the inter-fragment interactions between the three fragments allowed us to compare how these interactions differed along the reaction paths, giving an indication of how the adenine anion preferred to interact and how strong the interactions were at the different nitrogen positions.

Table 3.16: Relative to relevant ref state, changes in inter-fragment interaction energy, $\Delta E_{\text{int}}^{\mathcal{M}\mathcal{N}}$, $\Delta E_{\text{int}}^{\mathcal{M}\mathcal{O}}$ and $\Delta E_{\text{int}}^{\mathcal{N}\mathcal{O}}$ (kcal/mol) along each pathway for selected $d(\text{N},\text{C15}) = \sim 2.3(\text{TS}), 2.0$ and $\sim 1.5(\text{eq})$ Å.

	N1-pathway	N3-pathway	N7-pathway	N9-pathway
$d(\text{N},\text{C15}) / \text{Å}$				
		$\Delta E_{\text{int}}^{\mathcal{M}\mathcal{N}}$		
$\sim 2.3(\text{TS})$	-82.7	-76.0	-70.2	-77.4
2.0	-122.9	-140.5	-136.1	-144.5
$\sim 1.5(\text{eq})$	-255.7	-251.1	-247.5	-262.2
		$\Delta E_{\text{int}}^{\mathcal{M}\mathcal{O}}$		
$\sim 2.3(\text{TS})$	14.1	17.3	14.2	19.3
2.0	-12.4	4.8	-9.7	8.2
$\sim 1.5(\text{eq})$	-14.6	7.9	-9.6	11.5
		$\Delta E_{\text{int}}^{\mathcal{N}\mathcal{O}}$		
$\sim 2.3(\text{TS})$	53.8	47.9	50.7	45.4
2.0	99.7	128.4	103.2	128.9
$\sim 1.5(\text{eq})$	102.3	122.6	105.7	122.8

The following is observed from the changes in the $E_{\text{int}}^{\mathcal{M}\mathcal{N}}$, $E_{\text{int}}^{\mathcal{N}\mathcal{O}}$ and $E_{\text{int}}^{\mathcal{M}\mathcal{O}}$ energy terms:

- i. At the TS, no large differences were observed in the energy terms. However, one must take note that $E_{\text{int}}^{\mathcal{M}\mathcal{N}}$ is most stabilising for the N1-pathway, which might be interpreted as unfavourable in the sense that if the transitional state is so stabilised, additional energy would be required to promote the reaction path towards the product.
- ii. The largest and most significant differences are observed after the TS, at $d(\text{N},\text{C15}) = 2.0$ Å, where three important observations can be made, namely (i) the $\Delta E_{\text{int}}^{\mathcal{M}\mathcal{N}}$ term promotes the N3-/N9-pathways as it is more negative by about 20 kcal/mol when compared with N1-pathway, (ii) the $\Delta E_{\text{int}}^{\mathcal{M}\mathcal{O}}$ is still attractive for the N1-/N7-pathways resulting in difficulty (demanding more energy) to remove the Br atom from the immediate reaction environment, and (iii) by far the largest repulsive $\Delta E_{\text{int}}^{\mathcal{N}\mathcal{O}}$ values are observed for the N3-/N9-pathways which facilitates the reaction by removing the Br atom from the immediate reaction environment. Clearly during this stage of the $S_{\text{N}}2$ mechanism, the N1-/N7-pathways are being eliminated.

- iii. The preferential formation of the N9-pathway is facilitated by the $\Delta E_{\text{int}}^{\mathcal{M}\mathcal{N}}$ term which becomes more negative, by about 11 kcal/mol, when compared with the N3-pathway. This is further supported by the $\Delta E_{\text{int}}^{\mathcal{M}\mathcal{O}}$ and $\Delta E_{\text{int}}^{\mathcal{N}\mathcal{O}}$ energy terms which are more repulsive in case of the N9-pathway (both fragments, \mathcal{M} and \mathcal{N} , remove the Br atom more effectively from the reaction environment).

The inter-fragment interactions between fragments \mathcal{M} , \mathcal{N} and \mathcal{O} need to be considered as a whole in order to understand how the entire molecular system is being influenced by changes in interactions between the fragments. The fragment interactions discussed above could potentially hold the reasoning for the N3-/N9-pathways being the preferred mechanistic routes, as there is no interference of the bromine atom.

3.4.2.3 The change in intra-fragment interaction energy for $M = \{\text{AD}^-\}$ and $N = \{\text{Bn}\}$ in each pathway

The reaction paths were further characterised by analysing the intra-fragment interaction energy of fragments $\mathcal{M} = \{\text{AD}^-\}$ and $\mathcal{N} = \{\text{Bn}\}$ (Figure 3.20) (Table S35–S38 in Supplementary Material) with main focus on $E_{\text{int}}^{\mathcal{M}}$ of $\mathcal{M} = \{\text{AD}^-\}$ as it should provide additional insight on how this fragment is being (de)stabilised due to its own interactions in a changing system.

Relative to the relevant *ref* state, the changes in the intra-fragment interaction energy, $\Delta E_{\text{int}}^{\mathcal{M}}$ and $\Delta E_{\text{int}}^{\mathcal{N}}$, of fragment $\mathcal{M} = \{\text{AD}^-\}$ and $\mathcal{N} = \{\text{Bn}\}$, respectively, along the reaction path are presented in Table 3.17 for each pathway at $d(\text{N},\text{C15}) = \sim 2.3(\text{TS})$, 2.0 and $\sim 1.5(\text{eq})$ Å.

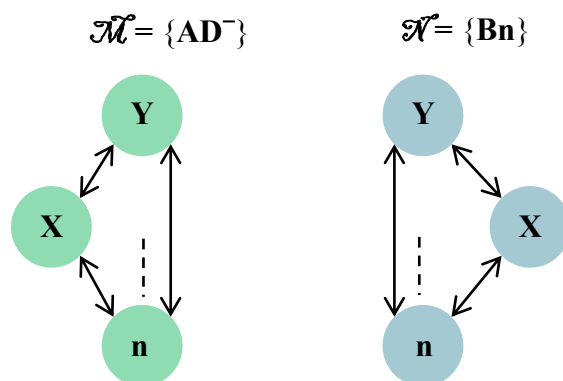


Figure 3.20: Intra-fragment interaction energy of molecular fragment $\mathcal{M} = \{\text{AD}^-\}$ and $\mathcal{N} = \{\text{Bn}\}$ composed of all diatomic interactions between of atoms of the fragment concerned.

Table 3.17: Relative to relevant ref state, changes in intra-fragment interaction energy, $\Delta E_{\text{int}}^{\mathcal{M}}$ and $\Delta E_{\text{int}}^{\mathcal{N}}$ (kcal/mol) for fragment $\mathcal{M} = \{\text{AD}^-\}$ and $\mathcal{N} = \{\text{Bn}\}$, respectively, along each pathway for selected $d = \sim 2.3(\text{TS})$, 2.0 and $\sim 1.5(\text{eq})$ Å.

d(N,C15) / Å	Fragment	N1-pathway	N3-pathway	N7-pathway	N9-pathway
	$\mathcal{M} = \{\text{AD}^-\}$			$\Delta E_{\text{int}}^{\mathcal{M}}$	
$\sim 2.3(\text{TS})$		-13.5	-22.0	1.6	-13.8
2.0		-41.0	-70.5	-44.6	-62.9
$\sim 1.5(\text{eq})$		-60.8	-94.4	-80.2	-104.7
	$\mathcal{N} = \{\text{Bn}\}$			$\Delta E_{\text{int}}^{\mathcal{N}}$	
$\sim 2.3(\text{TS})$		30.9	27.1	26.9	26.6
2.0		29.3	24.8	24.8	24.4
$\sim 1.5(\text{eq})$		33.5	29.1	27.4	28.5

The preferential formation of the N9-pathway is supported by the results shown in Table 3.17 in which a few factors play a role:

- i. The $\mathcal{N} = \{\text{Bn}\}$ fragment is destabilised for all pathways (for each reaction mechanism) having the $\Delta E_{\text{int}}^{\mathcal{N}}$ values most unfavourable for the N1-pathway.
- ii. The fragment $\mathcal{M} = \{\text{AD}^-\}$ on the other hand is highly stabilising for all pathways, having the $\Delta E_{\text{int}}^{\mathcal{M}} \gg \Delta E_{\text{int}}^{\mathcal{N}}$ from the d(N,C15) of 2.0 Å onwards, largely supporting the N3-/N9-pathways over the N1-/N7-pathways, eliminating the latter as a possibility.

- iii. At the product formation, $d(\text{N,C15}) \sim 1.5 \text{ \AA}$, the N9-pathway dominates the N3-pathway by about 20 kcal/mol in favour of the N9 reaction path.

3.4.2.4 The change in $\text{N}\cdots\mathcal{M}$ and $\text{N}\cdots\mathcal{X}$ interaction energies along each reaction path

Our last comparison involves the change in the overall interaction energy of the reactive nitrogen of fragment $\mathcal{M} = \{\text{AD}^-\}$ with all other atoms (X) in the fragment $\mathcal{M} = \{\text{AD}^-\}$,

$\sum_{\substack{X \neq \text{N} \\ X \in \mathcal{M}}} E_{\text{int}}^{\text{NX}}$, and the change in the overall interaction energy of the reacting nitrogen of fragment

$\mathcal{M} = \{\text{AD}^-\}$ with all other atoms (X) of fragment $\mathcal{X} = \{\text{Bn}\}$, $\sum_{\substack{N \in \mathcal{M} \\ X \in \mathcal{X}}} E_{\text{int}}^{\text{NX}}$, Figure 3.21 (Tables

S39–S42 in Supplementary Material).

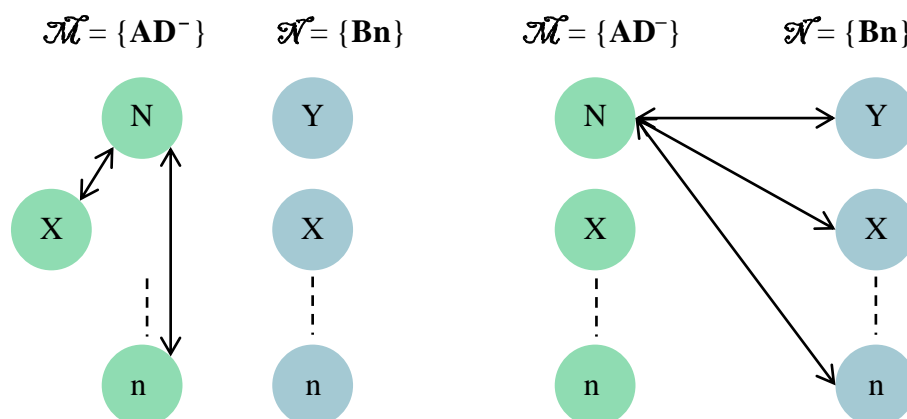


Figure 3.21: Interaction energy of the reactive nitrogen (N) of fragment \mathcal{M} with all other atoms (X) in fragment \mathcal{M} , $\sum_{\substack{X \neq \text{N} \\ X \in \mathcal{M}}} E_{\text{int}}^{\text{NX}}$, and the interaction energy of N of fragment

\mathcal{M} with all other atoms (X) of fragment \mathcal{X} , $\sum_{\substack{N \in \mathcal{M} \\ X \in \mathcal{X}}} E_{\text{int}}^{\text{NX}}$.

Relative to the relevant *ref* state, the sum of diatomic interaction energies between the reacting nitrogen N and atoms of fragment $\mathcal{M} = \{\text{AD}^-\}$, $\Delta \sum_{\substack{X \neq \text{N} \\ X \in \mathcal{M}}} E_{\text{int}}^{\text{NX}}$, and the sum of diatomic

interaction energy between the reacting nitrogen and atoms of fragment $\mathcal{A} = \{\mathbf{Bn}\}$, $\sum_{\substack{N \in \mathcal{M} \\ X \in \mathcal{A}}} E_{\text{int}}^{\text{NX}}$, of

each pathway is shown in Table 3.18 at $d(\text{N,C15}) = \sim 2.3(\text{TS})$, 2.0 and $\sim 1.5(\text{eq})$ Å.

Table 3.18: Relative to the relevant ref state changes in the interaction energy between the reacting nitrogen N and atoms of the fragment $\mathcal{M} = \{\mathbf{AD}^{-}\}$, $\Delta \sum_{\substack{X \neq N \\ X \in \mathcal{M}}} E_{\text{int}}^{\text{NX}}$ (kcal/mol), and the interaction energy between the reactive nitrogen and atoms of the fragment $\mathcal{A} = \{\mathbf{Bn}\}$, $\Delta \sum_{\substack{N \in \mathcal{M} \\ X \in \mathcal{A}}} E_{\text{int}}^{\text{NX}}$ (kcal/mol) along each pathway for selected $d = \sim 2.3(\text{TS})$, 2.0 and $\sim 1.5(\text{eq})$ Å.

	N1-pathway	N3-pathway	N7-pathway	N9-pathway
Atom A	N1	N3	N7	N9
$d(\text{N,C15}) / \text{Å}$			$\Delta \sum_{\substack{X \neq N \\ X \in \mathcal{M}}} E_{\text{int}}^{\text{NX}}$	
$\sim 2.3(\text{TS})$	-10.0	-28.8	-6.9	-18.8
2.0	-24.0	-67.2	-52.6	-68.2
$\sim 1.5(\text{eq})$	-16.4	-61.7	-70.4	-85.4
			$\Delta \sum_{\substack{N \in \mathcal{M} \\ X \in \mathcal{A}}} E_{\text{int}}^{\text{NX}}$	
$\sim 2.3(\text{TS})$	-104.6	-90.9	-89.8	-95.1
2.0	-164.6	-179.4	-175.6	-186.2
$\sim 1.5(\text{eq})$	-342.3	-331.1	-326.3	-346.2
			$\Delta \sum_{\substack{X \neq N \\ X \in \mathcal{M}}} E_{\text{int}}^{\text{NX}} + \Delta \sum_{\substack{N \in \mathcal{M} \\ X \in \mathcal{A}}} E_{\text{int}}^{\text{NX}}$	
$\sim 2.3(\text{TS})$	-114.6	-119.7	-96.7	-113.9
2.0	-188.6	-246.6	-228.2	-254.4
$\sim 1.5(\text{eq})$	-358.7	-392.8	-396.7	-431.6

The analysis of $\text{N} \cdots \mathcal{M}$ and $\text{N} \cdots \mathcal{A}$ interaction energies obtained for the reactive nitrogen leads to the following observations:

i) Most importantly, it is shown here that simple analysis of individual energy terms,

such as $\Delta \sum_{\substack{N \in \mathcal{M} \\ X \in \mathcal{A}}} E_{\text{int}}^{\text{NX}}$, can be misleading, as it would appear that the N1-pathway is the

most favoured at the TS. One must look at the combined effect on the molecular

system, $\Delta \sum_{\substack{X \neq N \\ X \in \mathcal{M}}} E_{\text{int}}^{\text{NX}} + \Delta \sum_{\substack{N \in \mathcal{M} \\ X \in \mathcal{N}}} E_{\text{int}}^{\text{NX}}$, in which all pathways have equal chance of forming

the transition state, the N7-pathway being the least favoured.

ii) The interaction of the reacting nitrogen with the benzyl fragment, $\Delta \sum_{\substack{N \in \mathcal{M} \\ X \in \mathcal{N}}} E_{\text{int}}^{\text{NX}}$, is

stabilising to a much higher extent than the stabilization of the AD^- , $\Delta \sum_{\substack{X \neq N \\ X \in \mathcal{M}}} E_{\text{int}}^{\text{NX}}$,

promoting the $\text{S}_{\text{N}}2$ reaction.

iii) The overall sum $\Delta \sum_{\substack{X \neq N \\ X \in \mathcal{M}}} E_{\text{int}}^{\text{NX}} + \Delta \sum_{\substack{N \in \mathcal{M} \\ X \in \mathcal{N}}} E_{\text{int}}^{\text{NX}}$ at $d(\text{N}, \text{C}15)$ of 2.0 Å highly supports the N3-

/N9-pathways over the N1-/N7-pathways, removing the latter for further consideration.

iv) The N9-pathway is the preferential pathway at the product equilibrium point, overruling the N3-pathway by 38 kcal/mol.

In conclusion of this section, it is important to highlight that the interaction between two atoms has a large influence not only between themselves but also on the entire molecular system. The critical stages of a reaction cannot always be determined by comparing the initial stage of a reaction with the final products or even at the transition state. As was shown above, the preferential N9-pathway with its competing N3-pathway emerge after the TS at $d(\text{N}, \text{C}15)$ of 2.0 Å, leaving the N1-/N7-pathways unable to proceed along the reaction path. The N3-pathway is largely eliminated as a possibility at the product formation stage, in which the N9-pathway dominated in all instances. This is in accordance with the experimental data, obtaining the N9-benzyladenine as a major product with the N3-benzyladenine as a minor one. It was also pointed out throughout the analysis of the energy terms that it is not feasible to consider the selected energy contributions individually but rather as a whole system, looking at the overall effect on the molecular system as it is undergoing attractive and repulsive changes when a reaction takes

place. From this aspect it was shown how the N1-/N7-pathways are unfavourable compared to the N3-/N9-pathways.

3.4.2.5 Comparing the diatomic interaction energies of specific interactions along each reaction path

To analyse every interaction occurring throughout a 28 atom molecular system is complicated and often confusing with so many atoms involved (Tables S43–S46 in Supplementary Material). Therefore we turned our attention to two aspects: (i) the N1-/N7-pathways displayed strong stabilising $E_{\text{int}}^{\text{N}^{\ominus}\text{C}^{\oplus}}$ and $E_{\text{int}}^{\text{N}^{\oplus}\text{C}^{\ominus}}$ interactions with the Br atom, preventing it from leaving the immediate reaction site, reducing its ability as a good leaving group required for $S_{\text{N}}2$ reactions, hence the diatomic interaction energies which involved the Br atom along the reaction path could hold some important information, and (ii) there are some additional interactions which could potentially influence the reacting system, often playing a stabilising role.

The potential energy profiles of the N1-/N7-pathways are demonstrated in Figure 3.22 and Figure 3.23 with the molecular graphs at each step along the reaction path showing the additional interactions which were investigated. A change in the diatomic interaction energy between selected atoms A and B relative to the *ref* state, $\Delta E_{\text{int}}^{\text{AB}}$, for the N1-/N7-pathways are presented in Table 3.19 and Table 3.20, respectively.

Four important observations can be noted for the diatomic interactions of the N1-/N7-pathways:

- i. The pathways are initially promoted by stabilising H17•••N6 and H16•••N2 interactions at $d(\text{N},\text{C}15) = 3.0 \text{ \AA}$, for the N1 and N7-pathways, respectively.
- ii. The N1-pathway displays an interaction between Br29•••H5 at $d(\text{N},\text{C}15) = 2.0 \text{ \AA}$ which is significantly stabilising.

- iii. The N7-pathway has C15•••N2 interaction about 20 kcal/mol more stabilising than the C15•••N6 interaction in the N1-pathway at d(N,C15) of 2.0 Å.
- iv. The N7-pathway at the product stage does not involve the additional C•••H interaction that was observed with the **N7-Bn-2** conformer studied earlier on in section 3.2.2. Instead all the additional interactions involved the Br atom.

Table 3.19: Relative to the ref state, changes in diatomic interaction energy, $\Delta E_{\text{int}}^{\text{AB}}$ (kcal/mol), for additional interactions of the N1-pathway.

d(N,C15) / Å		4.0	3.0	~2.3(TS)	2.0	~1.5(eq)
atoms ^a		$\Delta E_{\text{int}}^{\text{AB}}$				
A	B					
C15	N6	0.0	5.2	-53.0	-109.6	-294.8
H16	N6	0.0	0.9	-12.8	-11.6	-12.9
H17	N6	0.0	-45.9	-14.9	-14.8	-13.2
Br29	H5	0.0	-11.4	-11.3	-52.7	-29.0
C19	H5	0.0	-0.4	-6.7	-0.2	-0.7
Br29	H17	0.0	-1.3	-8.6	-14.4	-0.3
H20	N3	0.0	-0.4	-3.5	-4.2	-1.2
Br29	H20	0.0	-0.2	-2.5	-3.5	-1.0
Br29	C15	0.0	4.9	81.9	120.8	106.9

^a Gaussian numbering of atoms.

Table 3.20: Relative to the ref, changes in diatomic interaction energy, $\Delta E_{\text{int}}^{\text{AB}}$ (kcal/mol), for additional interactions of the N7-pathway.

d(N,C15) / Å		4.0	3.0	~2.3(TS)	2.0	~1.5(eq)
atoms ^a		$\Delta E_{\text{int}}^{\text{AB}}$				
A	B					
C15	N2	0.0	5.8	-47.1	-132.0	-291.1
Br29	H4	0.0	-10.2	-10.3	-45.1	-46.3
H16	N2	0.0	-42.7	-7.2	-9.9	-8.2
C19	H12	0.0	0.0	-1.4	-1.0	-1.2
H16	H4	0.0	5.5	1.6	2.4	-0.4
Br29	H16	0.0	-1.5	-7.3	-13.3	-7.2
Br29	C15	0.0	5.2	76.3	118.9	106.0

^a Gaussian numbering of atoms.

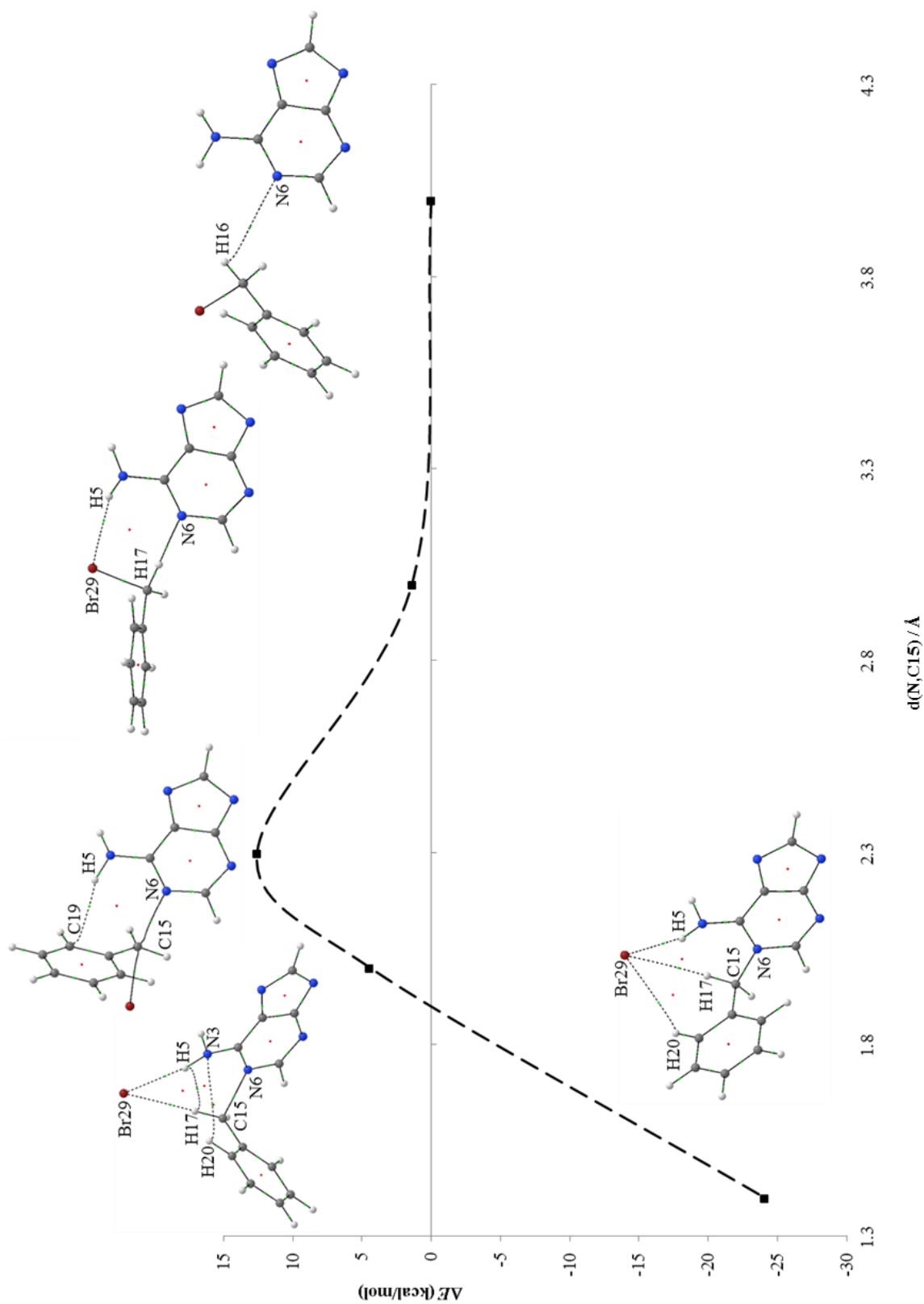


Figure 3.22: Potential energy profile of the N1-pathway leading to N1-benzyladenine with molecular graphs

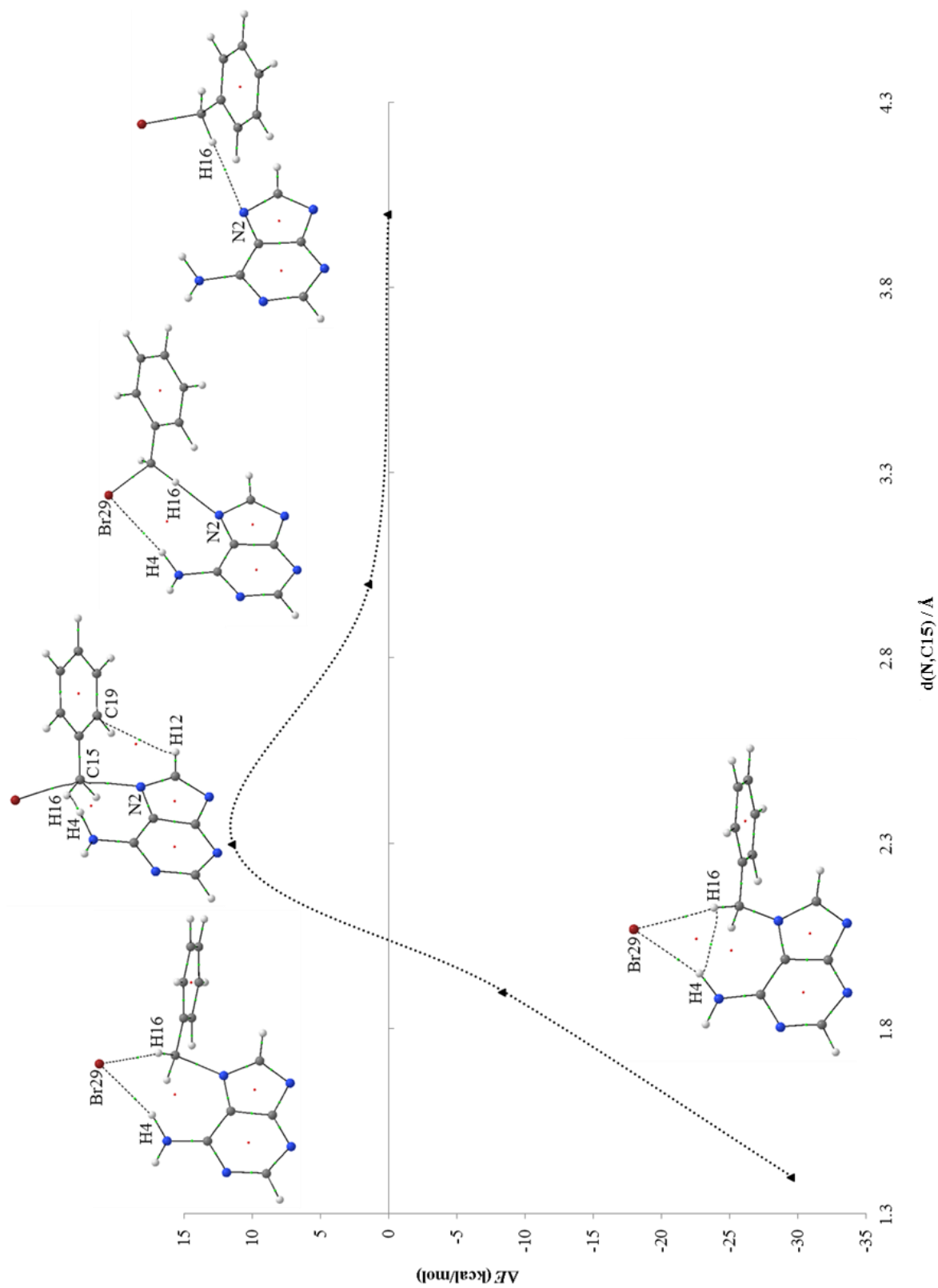


Figure 3.23: Potential energy profile of the N7-pathway leading to N7-benzyladenine with molecular graphs

The N1-/N7-pathways have additional large stabilising interactions involving the Br atom starting at the TS. It is evident from Table 3.21 and Table 3.22 that the N1-/N7-pathways involve many stabilising interactions along the reaction paths in which the Br atom interacts with the AD^- , especially at $d(\text{N},\text{C15}) = 2.0$ and ~ 1.5 Å. This implies that the Br atom is being kept within the immediate reaction site and strongly supports a previous comment about the large ‘stability’ of the N1-pathway hindering the reaction to continue due to additional energy required to promote the reaction further (section 3.4.2.2).

Table 3.21: Relative to the initial ref state, changes in diatomic interaction energy, $\Delta E_{\text{int}}^{\text{AB}}$ (kcal/mol), for Br interactions of the N1-pathway.

d(N,C15) / Å		4.0	3.0	$\sim 2.3(\text{TS})$	2.0	$\sim 1.5(\text{eq})$
atoms ^a						
A	B	$\Delta E_{\text{int}}^{\text{AB}}$				
Br29	C10	0.0	-8.6	-26.6	-57.3	-56.3
Br29	H4	0.0	-4.2	-9.4	-28.4	-55.1
Br29	C13	0.0	-5.2	-31.9	-43.8	-42.6
Br29	C8	0.0	-3.4	-19.0	-30.1	-30.9
Br29	C11	0.0	-3.4	-16.3	-30.2	-30.9
Br29	H5	0.0	-11.4	-11.3	-52.7	-29.0
Br29	C9	0.0	-2.0	-7.9	-17.4	-18.6

^a Gaussian numbering of atoms.

Table 3.22: Relative to the initial ref state, changes in diatomic interaction energy, $\Delta E_{\text{int}}^{\text{AB}}$ (kcal/mol), for Br interactions of the N7-pathway.

d(N,C15) / Å		4.0	3.0	$\sim 2.3(\text{TS})$	2.0	$\sim 1.5(\text{eq})$
atoms ^a						
A	B	$\Delta E_{\text{int}}^{\text{AB}}$				
Br29	C10	0.0	-5.8	-21.4	-51.8	-53.0
Br29	H4	0.0	-10.2	-10.3	-45.1	-46.3
Br29	C11	0.0	-2.6	-23.4	-39.5	-39.4
Br29	C13	0.0	-3.0	-18.9	-37.9	-38.4
Br29	C8	0.0	-2.3	-17.7	-32.3	-32.7
Br29	H5	0.0	-3.3	-9.3	-26.5	-27.2
Br29	C9	0.0	-1.7	-9.5	-17.7	-16.4

^a Gaussian numbering of atoms.

The N3-/N9-pathways are displayed in Figure 3.24 and Figure 3.25 respectively, with the relevant molecular systems along the reaction pathways indicating the additional interactions

that were investigated. A change in the diatomic interaction energies between selected atoms A and B relative to the *ref* state, $\Delta E_{\text{int}}^{\text{AB}}$, are presented in Table 3.23 and Table 3.24 for the N3-/N9-pathways, respectively.

Table 3.23: Relative to the initial state, changes in diatomic interaction energy, $\Delta E_{\text{int}}^{\text{AB}}$ (kcal/mol), for additional interactions of the N3-pathway.

d(N,C15) / Å		4.0	3.0	~2.3(TS)	2.0	~1.5(eq)
atoms ^a						
A	B	$\Delta E_{\text{int}}^{\text{AB}}$				
C15	N7	0.0	4.4	-46.4	-133.9	-292.3
H17	N7	0.0	-37.0	-8.5	-8.4	-6.9
Br29	H28	0.0	0.0	-1.8	-1.6	-1.3
H28	N1	0.0	-0.1	-1.4	-1.5	-6.9
Br29	H17	0.0	-1.1	-7.4	0.6	1.3
Br29	C15	0.0	3.8	73.1	124.1	112.6

^a Gaussian numbering of atoms

Table 3.24: Relative to the initial state, changes in diatomic interaction energy, $\Delta E_{\text{int}}^{\text{AB}}$ (kcal/mol), for additional interactions of the N9-pathway.

d(N,C15) / Å		4.0	3.0	~2.3(TS)	2.0	~1.5(eq)
atoms ^a						
A	B	$\Delta E_{\text{int}}^{\text{AB}}$				
C15	N1	0.0	6.1	-46.2	-136.0	-303.0
H17	N1	0.0	-48.0	-13.4	-12.7	-11.6
Br29	H17	0.0	-1.5	-7.3	0.1	1.5
Br29	H20	0.0	-0.2	-1.7	-1.2	-0.8
H28	N7	0.0	0.3	-0.4	-0.6	-3.2
Br29	C15	0.0	4.5	69.6	123.6	111.6

^a Gaussian numbering of atoms.

The N3-/N9-pathways are very similar regarding their additional stabilising interactions. However, the promoting interaction, H17•••N1 interaction, of the N9-pathway at $d(\text{N},\text{C15}) = 3.0$ Å, is 10 kcal/mol more favourable than the H17•••N7 interaction of the N3-pathway. There are two key differences between the N3-/N9-pathways and the N1-/N7-pathways:

- i. Firstly, the N3-/N9-pathways did not involve as many additional stabilising interactions as were found in the N1-/N7-pathways, potentially allowing the reaction

to continue without requiring additional energy to overcome the additional stabilising interactions.

- ii. Secondly, the N3-/N9-pathways did not have as many highly stabilising Br atom interactions compared to the N1-/N7-pathways, allowing the bromine atom to leave the immediate reaction site with much more ease, which is in favour for a S_N2 mechanism. This is supported by the diatomic interaction energies of the Br atom for the N3-/N9-pathways shown in Table 3.25 and Table 3.26, respectively.

Table 3.25: Relative to the initial ref state, changes in diatomic interaction energy, $\Delta E_{\text{int}}^{\text{AB}}$ (kcal/mol), for Br interactions of the N3-pathway.

d(N,C15) / Å		4.0	3.0	~2.3(TS)	2.0	~1.5(eq)
atoms ^a		$\Delta E_{\text{int}}^{\text{AB}}$				
A	B					
Br29	C13	0.0	-3.5	-24.8	-26.1	-42.9
Br29	C10	0.0	-2.2	-16.6	-21.2	-31.4
Br29	C8	0.0	-2.9	-23.5	-20.2	-27.0
Br29	C11	0.0	-2.2	-20.0	-19.0	-23.2
Br29	H5	0.0	-0.8	-6.2	-9.0	-13.1
Br29	H4	0.0	-0.8	-6.2	-8.8	-11.9

^a Gaussian numbering of atoms

Table 3.26: Relative to the initial ref state, changes in diatomic interaction energy, $\Delta E_{\text{int}}^{\text{AB}}$ (kcal/mol), for Br interactions of the N9-pathway.

d(N,C15) / Å		4.0	3.0	~2.3(TS)	2.0	~1.5(eq)
atoms ^a		$\Delta E_{\text{int}}^{\text{AB}}$				
A	B					
Br29	C11	0.0	-6.8	-22.5	-22.1	-35.5
Br29	C8	0.0	-4.9	-24.2	-22.3	-28.3
Br29	C13	0.0	-3.7	-23.0	-23.7	-26.6
Br29	C10	0.0	-3.1	-16.4	-19.1	-24.6
Br29	C9	0.0	-1.8	-7.5	-8.2	-12.1
Br29	H4	0.0	-1.3	-6.2	-7.4	-10.5
Br29	H5	0.0	-1.1	-6.0	-7.4	-9.6

^a Gaussian numbering of atoms.

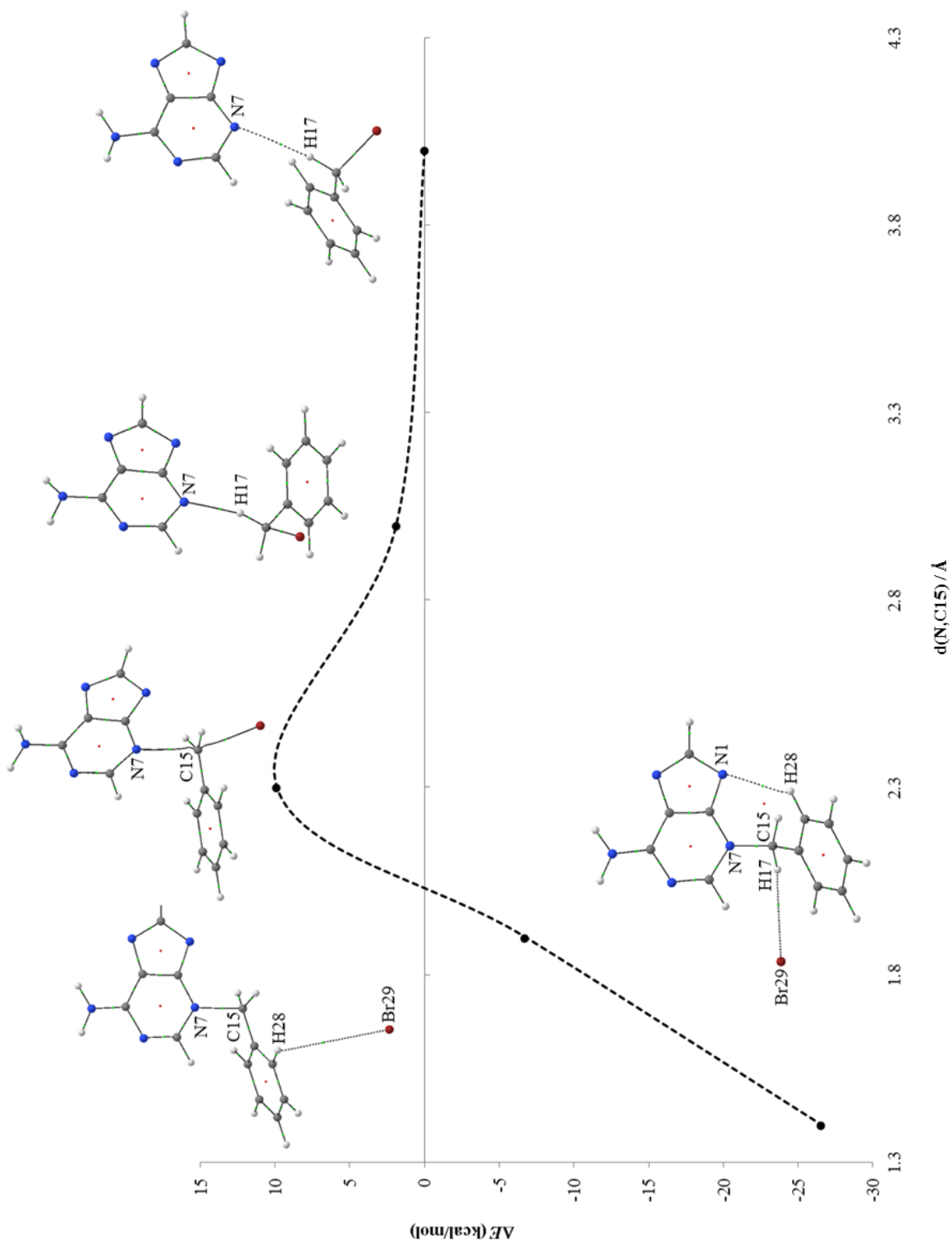


Figure 3.24: Potential energy profile of the N3-pathway leading to N3-benzyladenine with molecular graphs

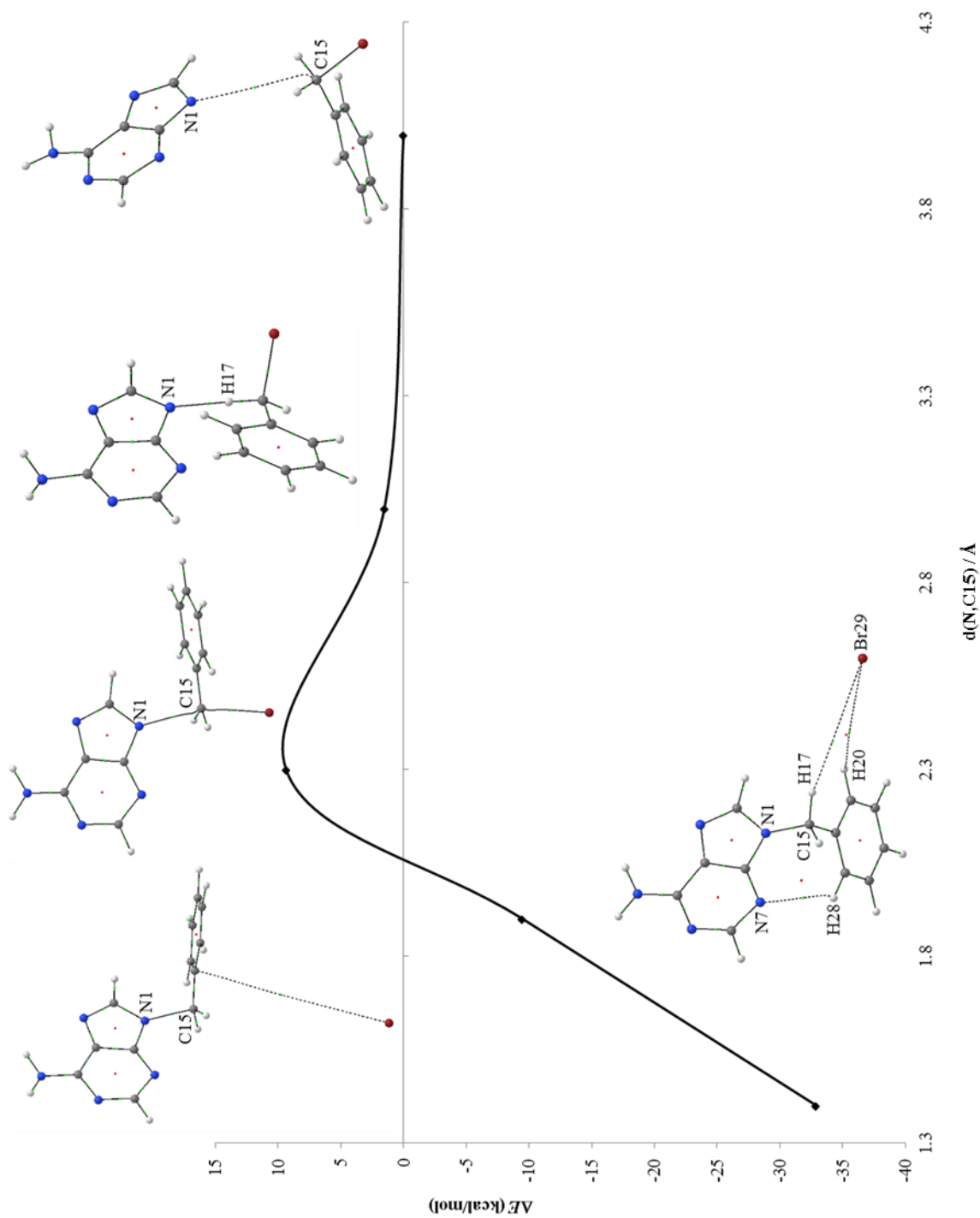


Figure 3.25: Potential energy profile of the N9-pathway leading to N9-benzyladenine with molecular graphs

In summary, the interactions observed above for all the pathways indicate that initially the pathways are promoted by a H•••N interaction before the C—N bond starts to form. The N1-/N7-pathways differed from the N3-/N9-pathways by having large stabilising interactions involving the Br atom. The N3-/N9-pathways therefore are in good agreement with the conditions required for a S_N2 mechanism, having the bromine atom as a good leaving group.

3.5 Conclusions from the computational study

The preference for the N3- and N9-pathway observed in the experimental section is supported by computational studies, having the N9-reaction path the most favoured in DMSO as a simulated solvent. The comparison of all reactions paths was not successful by simple comparison of the electronic energies, however, by comparing IQA defined terms for atoms and fragments along each reaction path, elimination of the N1-/N7-pathways was observed just after the transition state, $d(\text{N},\text{C15}) \sim 2.3 \text{ \AA}$, followed by the terms highly supporting the N9-pathway over the N3-pathway at the product formation step, $d(\text{N},\text{C15}) \sim 1.5 \text{ \AA}$.

Chapter 4

4.1 The deuteration of adenine

The exchange of an hydrogen atom for a deuterium atom, known as deuteration, has provided a variety of means to study chemical and biochemical problems. Deuteration can be used to (i) obtain structural information of DNA such as hydrogen bonding and stacking states of DNA,⁹⁷ (ii) simplifying ¹H NMR spectrum and Nuclear Overhauser Effect Spectroscopy (NOESY) as the proton peaks disappear when replaced with a deuterium allowing the spectrum to become less crowded,⁹⁸ (iii) studying substituents effects on rates of ylide formation,⁹⁹ and (iv) studying the inductive and coulombic effects on rates of deprotonation.¹⁰⁰ Drug metabolic pathways can be analysed using deuterium labelled forms of drugs. The advantage that some deuterated drugs follow different metabolic pathways, have different selectivity and resistance to metabolic change due to isotopic effects, allows the development of new sustained-release dosage as a result of isotopic effects.¹⁰¹ Methods of deuteration have been widely explored due to, amongst others, the above mentioned advantages, which is why methods of deuteration have been explored.

One such method of deuteration is that of base catalysed hydrogen-deuterium exchange on five and six membered heterocyclic cations through a carbene intermediate.¹⁰² A carbene is a divalent carbon with six electrons in its valence shell.¹⁰³ The most common occurring carbene is sp² hybridised and is bent in structure, as compared to the rare linear sp hybridised carbene. These carbenes have two non-bonding electrons in a sp² orbital and no formal charge on the carbene carbon.¹⁰⁴ The p-orbital of the carbene is vacant therefore making the carbene electron deficient. However, if heteroatoms such as nitrogen (N-heterocyclic carbene, NHC) are attached to the carbene, the lone pair of electrons in their p-orbital can be donated to the carbenes vacant p-orbital stabilising the carbene (Figure 4.1), decreasing the electrophilic nature of the carbene

and increasing its nucleophilic nature. The heteroatoms also have an inductive effect which stabilises the lone pair of electrons of the carbene.

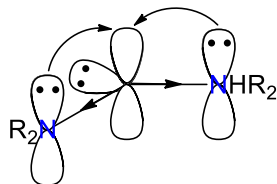


Figure 4.1: The p-orbital donating ability of heteroatoms attached to the carbene.

H. W. Wanzlick published a study on the nucleophilic nature of carbenes in 1962.¹⁰⁵ The conversion of bis-[1,3-diphenyl-2-imidazolidinyldene] (Figure 4.2, **4.1**) to 2-methoxy-1,3-diphenylimidazolidine **4.4** was expected to have occurred through a nucleophilic carbene. Compound **4.1** is spontaneously converted to its nucleophilic carbene form **4.2** which allows the protonation of the carbene carbon **4.3** followed by addition of a methoxy group to form the product **4.4**.

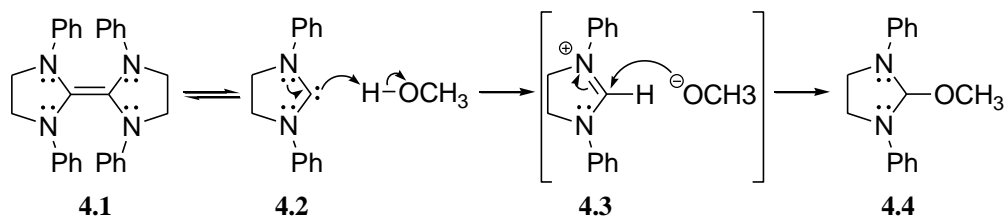


Figure 4.2: Conversion of bis-[1,3-diphenyl-2-imidazolidinyldene] **4.1** to 2-methoxy-1,3-diphenylimidazolidine **4.4**.¹⁰⁵

Wanzlick extended the concept of the nucleophilic carbene to the hydrogen-deuterium exchange at the C2 proton in thiamine (Figure 4.3, **4.5**). The proton is removed at the C2 position, to give the carbene intermediate **4.6c** which is stabilised by the resonance forms **4.6a** and **4.6b**. The intermediate **4.6c** exhibits nucleophilic nature and removes a deuterium from D₂O to form C2-deuterated thiamine **4.7**.¹⁰⁵

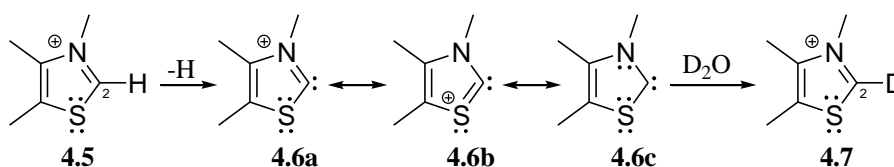


Figure 4.3: Hydrogen-deuterium exchange at the C2 proton in thiamine **4.5**.¹⁰⁵

Nowak-Wyndra and Szafran studied the R_1 and methoxy substituent effects on the formation of pyridinium ylides,⁹⁹ a positively charged heteroatom attached to a carbon with a lone pair of electrons, of 3-substituted 1-methoxypyridinium ions (Figure 4.4, **4.8**). Deprotonation by deuterioxide (DO^-) in D_2O at 75 °C at the ortho or para position to R_1 group led to the formation of an ortho **4.9a** or para **4.10a** ylide, respectively, which underwent addition of a deuterium at the carbanion, **4.9b** and **4.10b**, respectively. This is essentially a hydrogen-deuterium exchange via an ylide that is catalysed by DO^- .

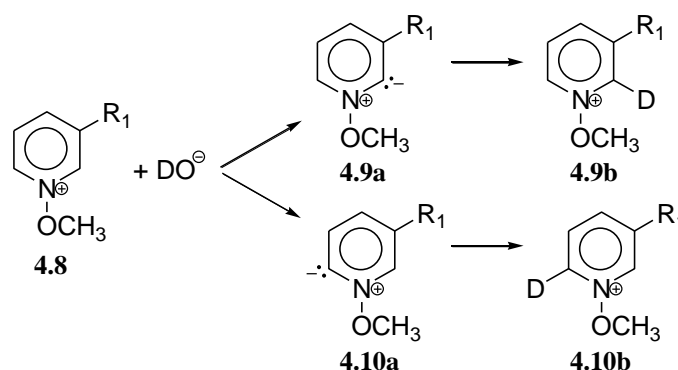


Figure 4.4: Deprotonation of 3-substituted 1-methoxypyridinium ions **4.8** at the ortho or para position to R_1 to form the corresponding ylides **4.9a** or **4.10a** followed by deuteration at the respective carbanion, **4.9b** and **4.10b** respectively.⁹⁹

In his PhD thesis, Fox³⁶ studied the deuteration of adenine, adenine derivatives (N1-, N3-, N7-, N9- and N6-benzyladenine), hypoxanthine, 6-chloropurine and adenosine. The non-deuterio analogues were heated in D_2O for a varied period of time, depending on whether the solution was homogenous (12 hours at 100 °C) or heterogeneous (> 12 hours at 100 °C). N7- and N9-benzyladenine both deuterated at the C8 position, with no exchange at the C2 position. N1-benzyladenine was unstable under the deuteration conditions, and N3-benzyladenine

underwent slight exchange at the C2 and C8 positions. The 6-chloropurine underwent 100% hydrogen-deuterium exchange at the C8 position while adenosine had 90% deuterium conversion at the C8 position. Fox concluded that the mechanism of deuteration must enable i) the C8 proton to undergo deuterium exchange much faster than that of the C2-H, ii) the electron donating substituent at the C6-position to have a minimal role in the deuterium exchange at the C8 position and iii) the C2-H and C8-H to exchange slowly in N3-benzyladenine.

Fox postulated two noteworthy mechanisms for the deuteration of the adenine derivatives (N1-, N3-, N6-, N7- and N9-benzyladenine). The first mechanism involved an electrophilic aromatic substitution at C8, in which the deuterium bonds to the C8 position, forming a sp^3 hybridized intermediate creating a resonance stabilised positive charge.³⁶ Fox reasoned that the electrophilic substitution by the deuterium in N9-benzyladenine has preference for C8 over C2 due to the increased delocalization of the positive charge in former [Figure 4.5, **4a**] as compared to the transition state of the C2 hydrogen-deuterium exchange **4b**. The proposed transition state intermediates for N3-benzyladenine, **5a** and **5b**, which showed less delocalization than **4a**, explained why the N3 product deuterated only slightly at both positions.

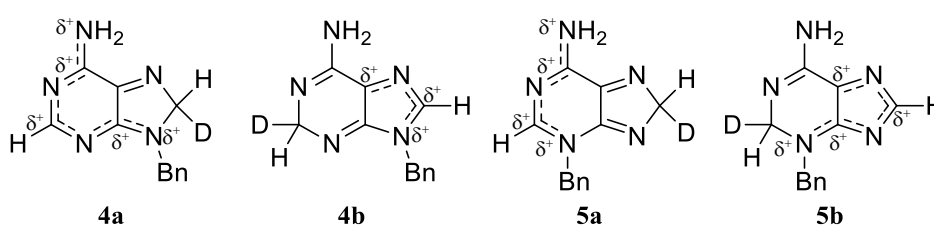


Figure 4.5: Delocalization of the positive charge in the aromatic substitution transition state of N9- and N3-benzyladenine (**4** and **5**, respectively) for the deuteration of the C8 and C2 proton (**a** and **b**, respectively).³⁶

The proposed transition state intermediates of N7-benzyladenine, **6a** and **6b** (Figure 4.6), did not explain the preference for the deuteration at C8 position.

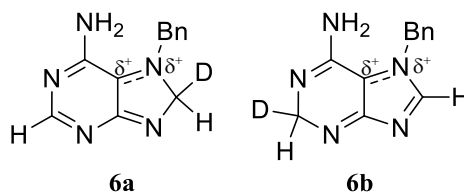


Figure 4.6: Delocalization of the positive charge in the aromatic substitution transition state of N7-benzyladenine (**6**) for the deuteration of the C8 and C2 proton (**a** and **b**, respectively).³⁶

The second mechanism Fox postulated was a carbene type mechanism, involving a protonated (Figure 4.7, **1**) and a non-protonated (Figure 4.7, **2**) form of N7 in the imidazole ring.³⁶ He reasoned, that change in ring strain energy due to the change in bond angles within the purine ring is less for a carbene in the imidazole ring (C8 carbene) than for one in the pyrimidine ring (C2 carbene), therefore deuteration of the C8 proton would occur more readily than that of the C2-H proton.

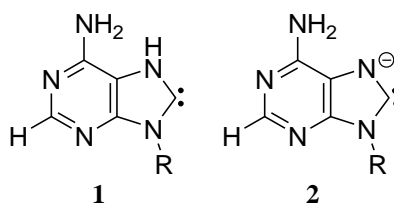


Figure 4.7: Protonated **1** and non-protonated **2** form of the carbene intermediate as demonstrated for N9-benzyladenine.³⁶

Fox argued that the lack of deuteration of the N3-benzyladenine was based on its resonance form (Figure 4.8), having the partial positive charge on the N3 and the partial negative charge on the imidazole ring which would prevent the loss of the C8-H proton. The slow exchange at the C2 position is due to increase in strain energy.³⁶

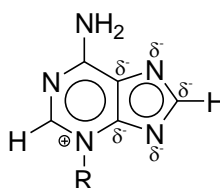


Figure 4.8: Resonance form of N3-benzyladenine.

Various other authors have succeeded in deuterating the C8 proton of adenine and in some cases the C2-H as well. Brush *et al.*⁹⁸ investigated the deuteration of an oligodeoxynucleotide at the purine C8 and cytosine C5 position using deuterioammonium bisulphate at pD 7.8 at 65 °C for 48 hours. The resulting ¹H NMR spectrum showed the adenine and guanine C8-H peaks had disappeared due to the hydrogen-deuterium exchange. Dhauoad *et al.*¹⁰⁶ deuterated adenine at the C8 position by heating adenine in D₂O at 80 °C for 2 hours. Iyer *et al.*¹⁰⁷ noted that when reacting aflatoxin B1 epoxide with poly(deoxyadenylic thymidylic acid) in deuterated buffer pH 7.2, the resulting adenine derivative is deuterated at the C8 position. Storr and co-workers^{108,109} deuterated the C8 proton in adenosine and 2-deoxyadenosine, respectively, in DMF with acetone-d₆ at 80 °C for 1 hour with Cs₂CO₃ as a catalyst, with no evidence for the deuteration at the C2 position. Ito *et al.*¹¹⁰ released a patent on the deuteration of heterocycles by refluxing in deuterated solvent in the presence of a palladium, nickel or cobalt catalyst. Adenine and adenosine were deuterated at the C8 and C2 positions, the ratio of the deuterated to the non-deuterated compound is presented in (Table 4.1). Esaki *et al.*¹⁰¹ deuterated various heterocycles by refluxing in D₂O at 104 °C using heterogeneous Pd/C as a catalyst.

*Table 4.1: Pd/C catalysed deuteration of adenine and adenosine.*¹¹⁰

Compound	Catalyst	Temperature (°C)	Time (hr)	Ratio
Adenine	10% Pd/C, D ₂ O, H ₂	110	24	48:52 ^a
		140	48	95:5 ^a
Adenosine	10% Pd/C, D ₂ O, H ₂	110	48	C8:94, C2:92
		140	48	C8:91, C2:91

^a The ratio of deuterated C8-H and C2-H to non-deuterated C8-H and C2-H.

4.2 Results and discussion

In order to create a library of possible inhibitors for the shikimate kinase enzyme in mycobacterium tuberculosis the deuteration of the adenine derivatives was essential as it was the deuterated form of ATP that allowed for inhibition of the enzyme.⁶⁻⁸ Kenyon *et al.* deuterated the adenine moiety of ATP (Figure 4.9, **4.13**) at the C8 position **4.14** by direct deuteration in deuterium oxide (D₂O) in the presence of the base triethylamine (Et₃N) at 60 °C for 144 hours.⁸ It was of interest however, to find a method of deuteration that required a shorter period of time and did not require a transition metal catalyst, and that would be more appropriate to compounds that weren't water soluble.

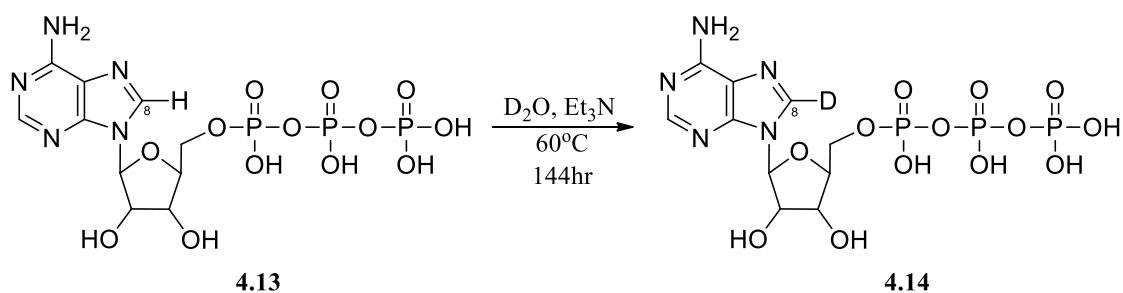


Figure 4.9: Deuteration of the adenine moiety of ATP.

The C2 proton on an imidazole ring (Figure 4.10, **4.15**) is deuterated in the presence of MeOD-d₄ and sodium metal (Na).¹¹¹ The combination of MeOD-d₄ and Na allows for the formation of sodium methoxide ion and hydrogen gas. The imidazole is protonated on the unsubstituted nitrogen creating a positive charge which is resonance-stabilised **4.16**. As discussed previously, both nitrogens need a lone pair of electrons in the p-orbital in order to stabilize the carbene by donating their electrons to its vacant p-orbital. Therefore the protonation of the unsubstituted nitrogen is needed as this would allow the nitrogen to have its p-orbital electrons free for donation. The methoxide ion deprotonates the C2 proton **4.16**, forming a carbene at the C2 position of the imidazole ring **4.17**. From Wanzlick,¹⁰⁵ it can be assumed that

the stable form of the carbene is the neutral form, **4.19**. The carbene **4.17**, which is nucleophilic, picks up a deuterium ion to form the deuterated imidazole compound **4.18**.

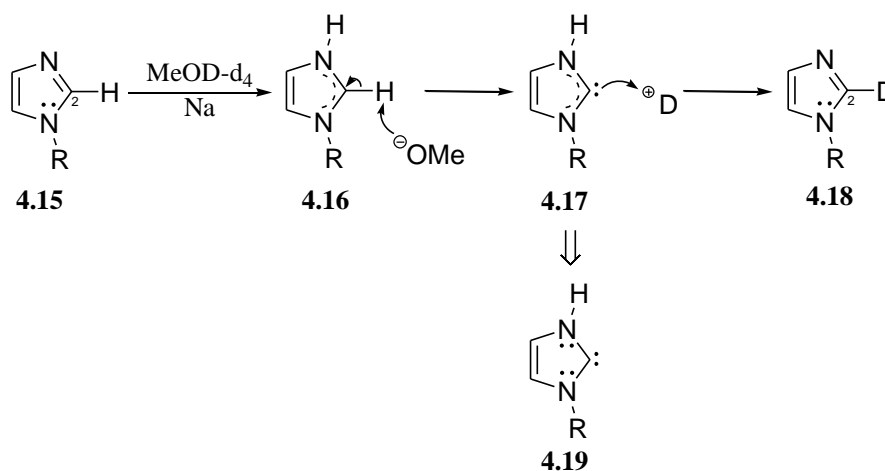


Figure 4.10: Deuteriation of the C2 proton on an imidazole ring.

4.2.1 Investigation of the mechanism of adenine deuteriation

Adenine and other heterocyclic rings have been deuterated previously. Fox proposed mechanisms for the deuteriation.³⁶ In particular, he favoured a mechanism involving a carbene intermediate over a tetrahedral sp^3 intermediate. Mechanisms of deuteriation involving the carbene mediated route seems the most plausible as it has been suggested more over than that of the sp^3 mediated electrophilic substitution.^{36,111} The mechanism for the deuteriation of N3- and N9-benzyladenine was studied in this research in order to analyse the reactivity of the C8 proton and to synthesis deuterated inhibitors. Two possible mechanisms are proposed and investigated based on the plausible “push” and “pull” mechanisms for the proton transfer in the shikimate kinase.^{7,8}

4.2.2 The sp^3 mediated mechanism for deuteriation

The first mechanism is a sp^3 mediated mechanism that mimics the “push” mechanism for the proton transfer in shikimate kinase⁷ in that it involves a base (methoxide ion) that removes a proton from the exo-amino group, as shown in Figure 4.11 a, generating a cascade of electron

movement that flows through the purine ring to pick up a deuterium at the C8, resulting in an intermediate with a sp^3 carbon at the C8 position (part **b**). A methoxide ion removes the proton at the C8 position, yielding the desired deuterated adenine derivative (part **c**). The deuterium is less likely to be removed and replaced with an hydrogen due to the kinetic isotope effect, in which the C—D bond requires more energy to break due to its lower zero-point energy, as compared to the C—H bond.¹¹²

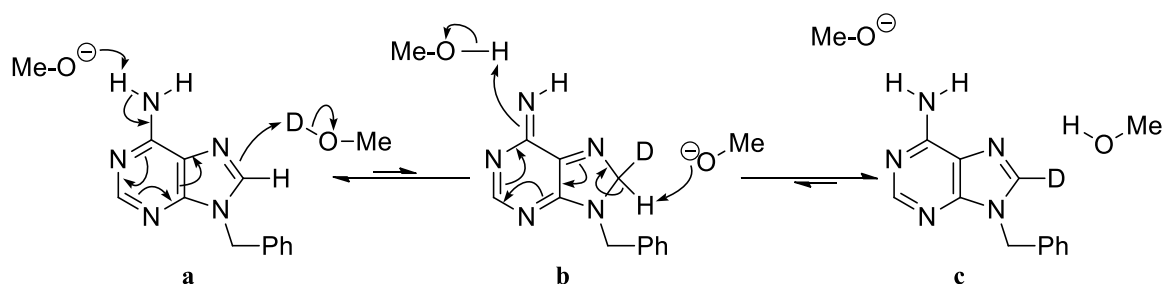


Figure 4.11: The sp^3 mediated mechanism for the deuteration at C8 of N9-benzyladenine.

Figure 4.11 shows the sp^3 mediated mechanism for the N9-benzyladenine and demonstrates that the hydrogen-deuterium exchange should be possible at the C8 position. However, when considering this mechanism for the deuteration at the C2 position of N9-benzyladenine (Figure 4.12) there is a failure to move the electrons (red arrows) to allow for the formation of a sp^3 carbon at the C2 position, thus not allowing deuteration at C2 of N9-benzyladenine.

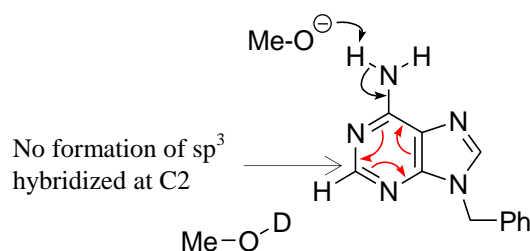


Figure 4.12: Failure of the sp^3 mediated mechanism for the deuteration at C2 of N9-benzyladenine.

The sp^3 mediated mechanism is applied to the deuteration of N3-benzyladenine. The same cascade of electron movement that occurs for the deuteration of the C8 proton of N9-

benzyladenine take place for the deuteration of the C8 proton of N3-benzyladenine (Figure 4.13 a–c), therefore indicating that this mechanism would allow deuteration to take place at the C8 position.

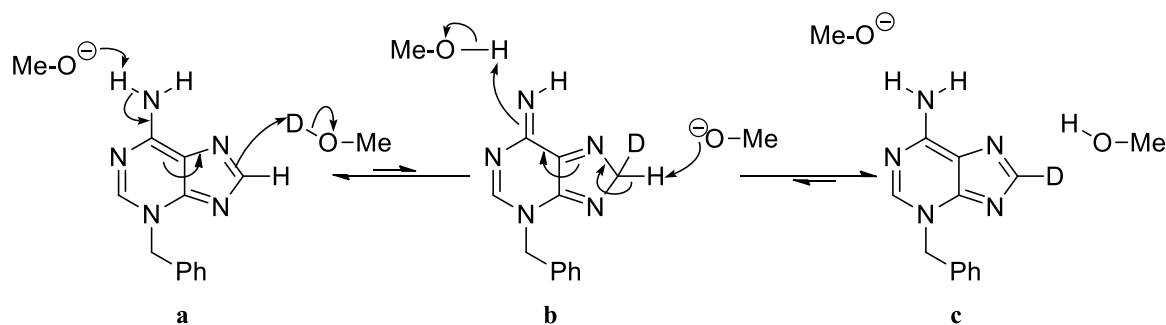


Figure 4.13: The sp^3 mediated mechanism for the deuteration at C8 of N3-benzyladenine.

A similar failure in the electron movement for the deprotonation of the C2 proton of N9-benzyladenine occurs for that of N3-benzyladenine, having the electron movement flow into the imidazole ring, thus not allowing for the sp^3 formation at the C2 position (Figure 4.14).

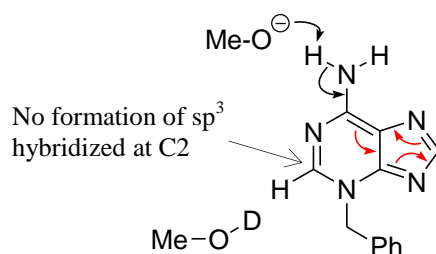


Figure 4.14: Failure of the sp^3 mediated mechanism for the deuteration at C2 of N3-benzyladenine.

Therefore, from the predicted results from the sp^3 mediated mechanism, the N3- and N9-benzyladenine should both only deuterate at the C8 position and not at the C2-position.

4.2.3 The carbene mediated mechanism for deuteration

The base catalysed carbene mechanism mimics the “pull” mechanism for the proton transfer in the shikimate kinase⁷ in that it generates an intermediate with a carbene at the C8 position.

The use of the methoxide ion follows that of the carbene-mediated deuteration of the imidazole ring¹¹¹ discussed earlier in this chapter. This mechanism is not dependent on the presence of the exo-amino group or any other functionality of the pyrimidine ring.

The deuteration of N9-benzyladenine through the carbene mechanism is demonstrated in Figure 4.15, **a–c**. A methoxide ion, the base which catalysis the reaction, removes the proton at C8, placing a lone pair of electrons in its sp^2 hybridized orbital, triggering an electron cascade movement to the N7, which in turn, removes a deuterium from a free MeOD- d_4 (part **a**). This forms a stabilised carbene (part **b**). The lone pair of electrons from both neighbouring nitrogens are in the p-orbital, hence allowing the electrons to be donated into the vacant p-orbital of the C8 carbene. The stabilised carbene intermediate picks up a deuterium through an electron cascade due to the removal of the deuterium at N7 by a methoxide ion (part **c**).

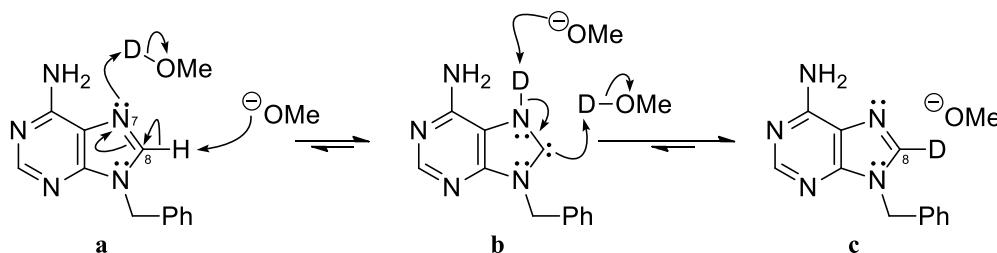


Figure 4.15: Base catalysed carbene mechanism for deuteration at C8 of N9-benzyladenine.

Considering the mechanism depicted in Figure 4.15, N9-benzyladenine should undergo hydrogen-deuterium exchange at the C8 position. If the carbene mediated mechanism is applied for the deuteration at C2 of N9-benzyladenine (Figure 4.16), the resulting carbene that is formed after a methoxide ion removes the C2-H and the N3 picks up a deuterium, cannot be stabilised due to the absence of a lone pair of electrons in the p-orbital of N1 (indicated by the red nitrogen). The N1 has a lone pair of electrons in its sp^2 hybridized orbital and has its p-orbital electrons are in conjugation with the purine ring system, which disables the donation to the

vacant p-orbital of the carbene. It can be reasoned from this that the deuteration at C2 on N9-benzyladenine will not occur.

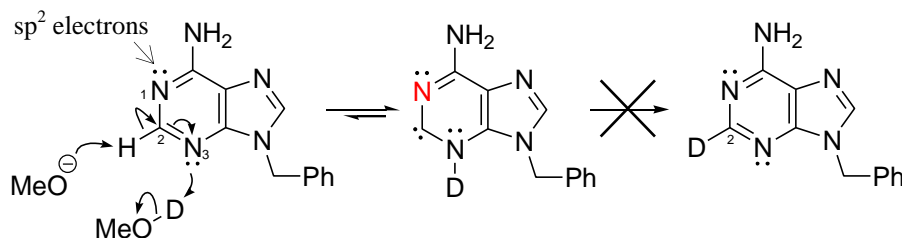


Figure 4.16: Failure of the base catalysed carbene mechanism for deuteration at C2 of N9-benzyladenine.

The base catalysed carbene mechanism for the deuteration of the C8 proton of N3-benzyladenine (Figure 4.17) yields the same problem concerning the C2 hydrogen-deuterium exchange of N9-benzyladenine through the carbene mediated mechanism. The carbene formed at C8 in N3-benzyladenine is not stabilised due to the inability of the N9 (indicated in red) to donate a lone pair of electrons into p-orbital of the C8 carbene as it is used in the aromatic conjugation of the purine ring, thus leading to the failure of deuteration at C8 when this mechanism is considered.

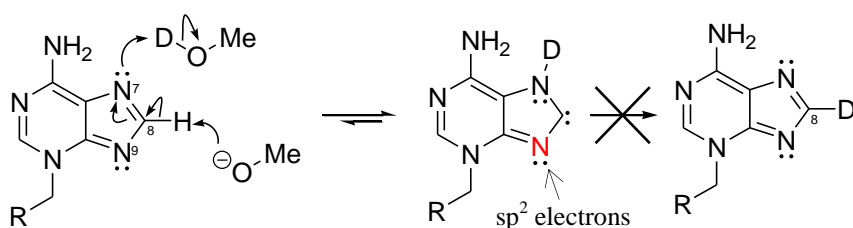


Figure 4.17: Failure of the base catalysed carbene mechanism for deuteration at C8 on N3-benzyladenine.

It is however, the only mechanism which allows for the deuteration of C2 of N3-benzyladenine (Figure 4.18), having the carbene at the C2 position stabilised by the lone pairs of electrons in the p-orbitals of N1 and N3, which donate the electrons into the vacant p-orbital of the carbene.

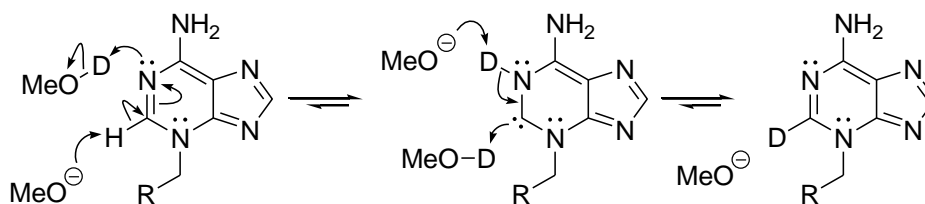


Figure 4.18: The base catalysed carbene mechanism for deuteration at C2 of N3-benzyladenine.

The two mechanisms, the sp^3 mediated mechanism and the base catalysed carbene mechanism, therefore yield different results. The former mechanism allows for the deuteration of the C8 proton in both the N3- and N9-benzyladenine and no resulting deuteration at the C2 position. The latter mechanism allows for the deuteration at C8 of N9-benzyladenine excluding deuteration at C2, whereas for the N3-benzyladenine, it only allows deuteration at the C2 position, having no supporting mechanism for the hydrogen-deuterium exchange at C8. With this at hand, the mechanisms were tested by subjecting N3- and N9-benzyladenine to deuteration to determine whether the C2-H and/or C8-H undergo hydrogen-deuterium exchange.

4.2.3.1 Refinement of the “pull” mechanism proposed for Group 4 kinases

Taking another look at the “pull” mechanism postulated by Kenyon *et al.*,⁷ reported in Chapter 1 section 1.3, in which the above carbene mediated mechanism of deuteration is based, the “pull” mechanism can be viewed in terms of the electron movement in order to form a carbene in the initial step (Figure 4.19, A). In this aspect, there will be an inflow of electrons (part A, blue arrows) into the adenylyl moiety of ATP as C8 is deprotonated by a neighbouring Ser/Thr residue. This would be simultaneously followed by protonation of the N7, which will enable the carbene at the C8 position to be stabilised by the donation of the p-orbital electrons from the neighbouring N7 and N9. The proton transfer cascade would be allowed to take place by the carbene mediated mechanism.

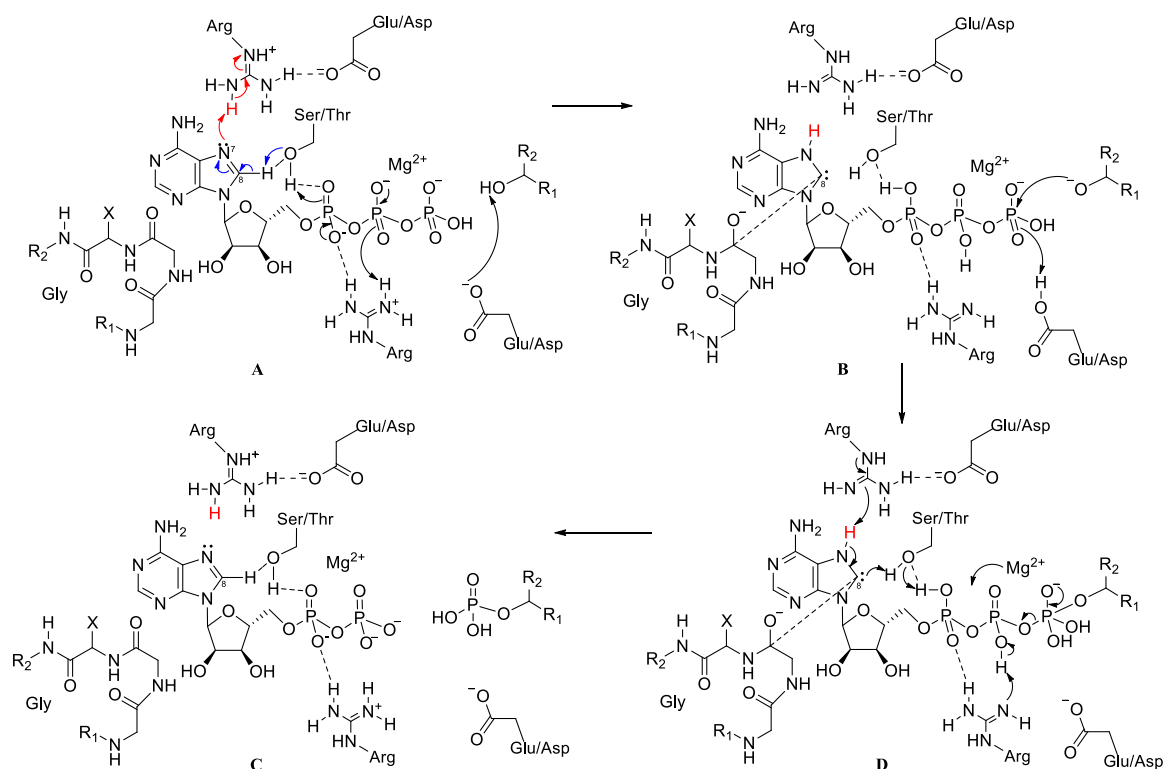
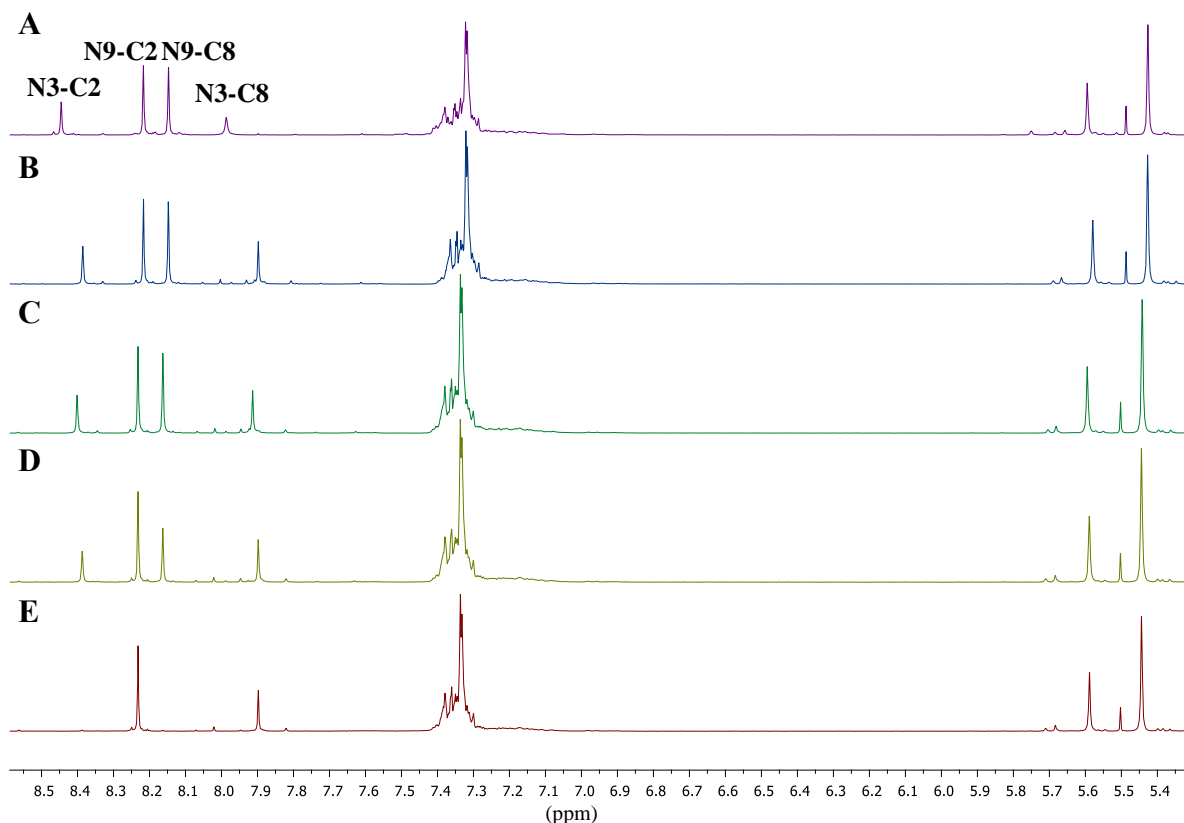


Figure 4.19: Refined “pull” mechanism for proton transfer based on the movement of electrons for formation of a carbene.

4.2.4 Deuterating N3- and N9-benzyladenine

N3- and N9-benzyladenine were deuterated using the imidazole deuteration technique, employing MeOD- d_4 and Na, as it involved no transition metal catalyst, however, there was no time specification given in the literature. Therefore, the reaction was analysed by ^1H NMR spectroscopy to study the deuteration procedure and the time required for completed deuteration. As discussed in Chapter 2, it was essential to determine the ^1H NMR spectral chemical shifts of the protons in the purine ring in different solvents as the solvents played a major role in peak shifting. N3-benzyladenine in MeOD- d_4 had the C2-H and the C8-H at 8.60 ppm and 8.21 ppm, respectively, and N9-benzyladenine had the C2-H and C8-H at 8.22 ppm and 8.15 ppm, respectively. The two compounds together in MeOD- d_4 caused shifting in the C2-H and C8-H peaks of N3-benzyladenine to 8.45 ppm (Figure 4.20 A, N3-C2) and 7.99 ppm (part A, N3-C8),

respectively, whereas the C2-H and C8-H peaks for N9-benzyladenine remained the same (part **A**, **N9-C2** and **N9-C8**).



*Figure 4.20: Deuteration of N3- and N9-benzyladenine. N3-benzyladenine C2-H and C8-H ^1H NMR spectrum (ppm) in MeOD- d_4 (400 MHz): **N3-C2** and **N3-C8**, respectively. N9-benzyladenine C2-H and C8-H ^1H NMR spectrum chemical shifts (ppm): **N9-C2** and **N9-C8**, respectively. **A**: initial ^1H NMR spectrum of N3-/N9-benzyladenine, **B**: ^1H NMR spectrum after addition of Na (0.5 eq) and heating at 60 °C, **C**: ^1H NMR spectrum of reaction 24 hours after addition of Na, **D**: ^1H NMR spectrum 48 hours after addition of Na, **E**: ^1H NMR spectrum after heating at 60 °C for 20 minutes.*

Na was added to the solution of N3- and N9-benzyladenine in MeOD- d_4 (Figure 4.20 part **A**), which was then analysed by ^1H NMR spectroscopy (part **B**). This revealed that the C2-H and C8-H peaks of N3-benzyladenine shifted to 8.39 ppm and 7.90 ppm, respectively whereas the purine ring protons of N9-benzyladenine remained the same. The reaction was analysed further by ^1H NMR spectroscopy every 24 hours for 2 days (part **C** and **D**) which reveal little to no deuteration. The solution was heated at 60 °C for 20 minutes and analysed by ^1H NMR spectroscopy immediately (part **E**), to reveal deuteration.

The integration of the proton peaks (Table 4.2) from the ^1H NMR spectra **A** to **E** were calculated relative to the phenyl multiplet proton peaks of the N3- and N9-benzyladenine as the phenyl protons do not undergo hydrogen-deuterium exchange. From this the integration ratio, $\int_{x/i}$, was calculated where the integration of a certain peak in the ^1H NMR spectrum x (where $x = \mathbf{A, B, C, D, E}$ in Figure 4.20) is compared to its initial integration, i , in the initial ^1H NMR spectrum **A**. The $\int_{x/i}$ for each proton peak is shown in Table 4.2.

*Table 4.2: Integral ratio $\int_{x/i}$ of the proton peaks in the ^1H NMR spectra **A** to **E**.*

x/i	N9-benzyladenine			$\int_{x/i}$			N9/N3 Ph ^a
	C8-H	C2-H	CH ₂	C8-H	C2-H	CH ₂	
A/A	1.00	1.00	1.00	1.00	1.00	1.00	1.00
B/A	1.00	0.90	1.00	1.00	1.00	1.00	1.00
C/A	0.90	0.90	1.00	1.00	1.00	1.00	1.00
D/A	0.60	1.00	1.00	0.83	0.80	1.00	1.00
E/A ^b	0.00	1.00	1.00	0.83	0.00	1.00	1.00

^a Overlap multiplet of phenyl protons of N3- and N9-benzyladenine.

^b $\int_{x/i}$ after heating at 60 °C.

It is evident that the CH₂ and phenyl protons of both N3- and N9-benzyladenine do not undergo hydrogen-deuterium exchange having the integration ratios remain at 1.00 as the reaction proceeds. The C2-H of N9-benzyladenine does not undergo deuteration even with additional heating at 60 °C (Figure 4.20 part **E**), however deuteration does occur at C8 over the 2 days, going from an initial $\int_{x/i}$ of 1.00 to 0.60 over 48 hours (part **D**), and is fully deuterated, $\int_{x/i} = 0.00$, within 20 minutes when heated at 60 °C. The C2-H of N3-benzyladenine was fully deuterated upon heating for 20 minutes but deuterated at a slower rate than the C8-H of N9-benzyladenine over the 2 days without heating, having the initial $\int_{x/i}$ at 1.00 which decreases to 0.80 after 48 hours. The C8-H of N3-benzyladenine did deuterate slowly having the $\int_{x/i}$ drop to 0.83 after 48 hours, in which the deuteration did not depend on the heating of the reaction as the $\int_{x/i}$ remained at 0.83 after heating at 60 °C, whereas the C2 proton deuterated fully.

It could be reasoned that the faster deuteration at C8 of N9-benzyladenine is due to two mechanisms, the sp^3 mediated mechanism and the base catalysed carbene mechanism, playing a role, whereas for N3-benzyladenine, the sp^3 mediated mechanism supports the deuteration at C8 and the carbene mediated mechanism supports the deuteration at C2. Therefore, if both mechanisms occur with equal probability, the deuteration at C8 of N9-benzyladenine should be twice as fast than that of the individual C2 and C8 of N3-benzyladenine. If this were true, then since only the C2-H of N3-benzyladenine undergoes full hydrogen-deuterium exchange upon heating at 60 °C, whereas the C8-H does not, the rate of the carbene mechanism increases with increasing temperature whereas the rate of the sp^3 mediated mechanism does not. This assumption would then lead to suggest that the reason for full deuteration of C8 of N9-benzyladenine upon heating is related to the contribution of the carbene mechanism and not the sp^3 mediated mechanism, even though it deuterates in parallel with the carbene mechanism.

4.3.4 Deuteration of N7- and N9-allyl-2,6-dichloropurine

The key point of the sp^3 mediated mechanism is that it involves deprotonation of the exo-amino group (Figure 4.21), allowing a cascade of electron movement to pick up a deuterium at the C8 position. Therefore without the exo-amino group, the mechanism will not occur.

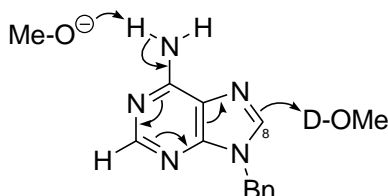


Figure 4.21: Importance of amino group in the sp^3 mediated mechanism.

N9-substituted 2,6-dichloropurine derivatives (Figure 4.22) have the exo-amino group at C6 position of adenine replaced with a chlorine and have only one site for deuteration (C8-H) as the proton at the C2 position of adenine is replaced by a chlorine. Therefore, the presence of the

chlorine at the C6 position should eliminate the opportunity for the sp^3 mediated mechanism of deuteration.

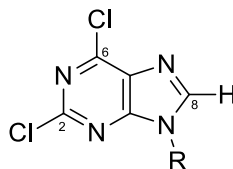


Figure 4.22: *N9*-substituted 2,6-dichloropurine.

If deuteration occurs in these compounds under the same conditions as for the deuteration of the adenine derivatives, it indicates that a mechanism of deuteration which does not involve the exo-amino group is responsible for the deuteration of the 2,6-dichloropurine derivatives, such as the carbene mediated mechanism of deuteration. This could provide evidence of the carbene mediated mechanism being involved for the deuteration of the adenine derivatives. Using *N9*-allyl-2,6-dichloropurine as a model of a 2,6-dichloropurine derivative (Figure 4.23, **23**), deuteration via the carbene mediated mechanism should allow for deuteration at the C8 position (**23-D**), having the same supporting arguments as those proposed for *N9*-benzyladenine in which the carbene is stabilised by the two available lone pairs of electrons from the neighbouring sp^3 hybridized nitrogens.

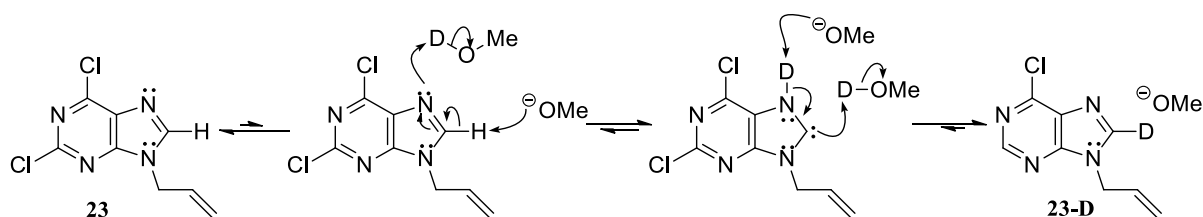


Figure 4.23: *Carbene mediated mechanism of deuteration at the C8 position of N9-allyl-2,6-dichloropurine 23.*

The carbene mediated mechanism is also applicable for the deuteration of the C8-H of *N7*-allyl-2,6-dichloropurine (Figure 4.24, **26-D**), having the mechanism identical to that of the *N9*-derivative.

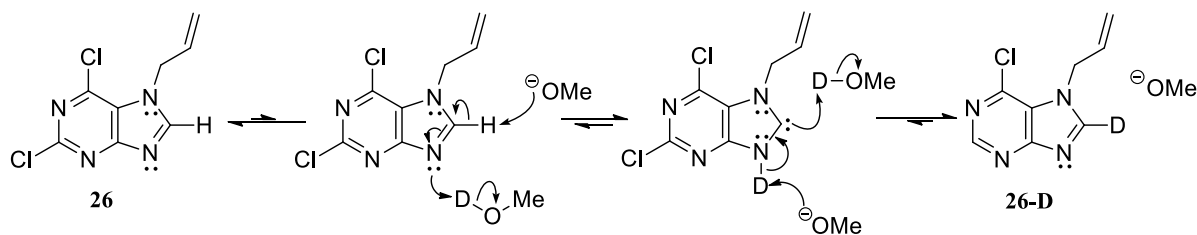


Figure 4.24: Carbene mediated mechanism of deuteration at the C8 position of N7-allyl-2,6-dichloropurine **26**.

The deuteration of N7- and N9-allyl-2,6-dichloropurine was performed under the same conditions as that of the deuteration of N3- and N9-benzyladenine, in which Na was added to a solution of the 2,6-dichloropurine derivative in MeOD- d_4 and heated at 60 °C. A series of ^1H NMR spectrum were run to monitor the reaction as the deuteration proceeded for both the N7- and N9-allyl-2,6-dichloropurine.

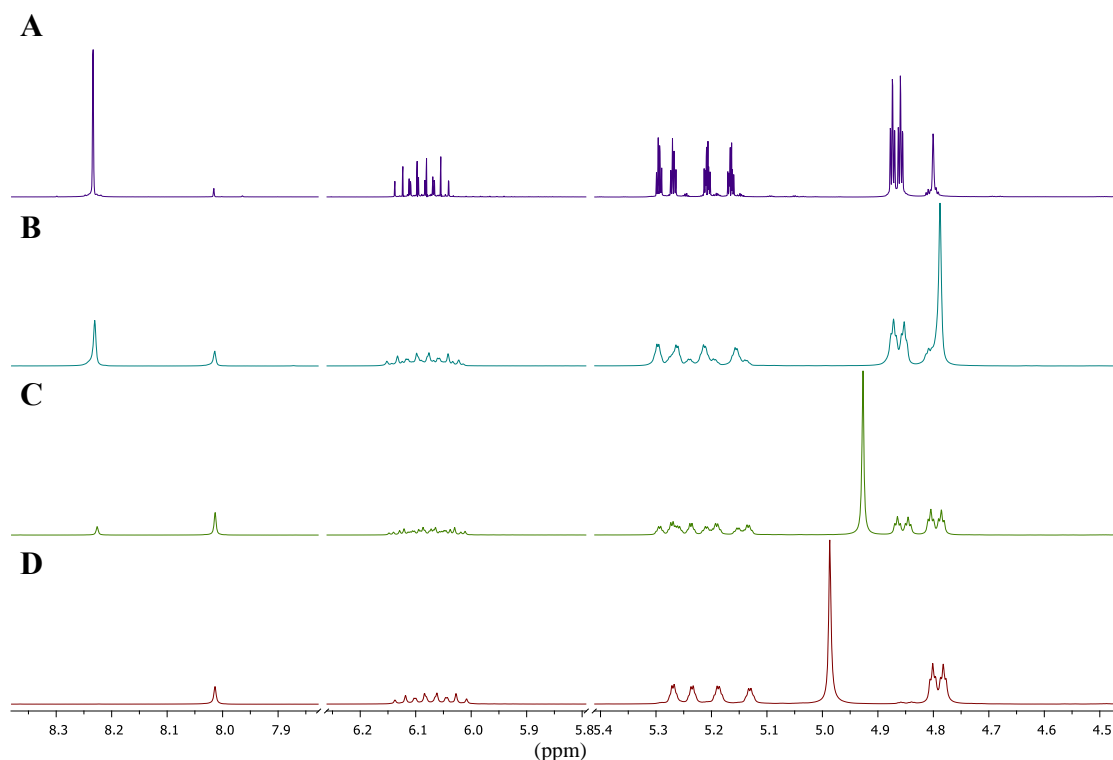
The series of ^1H NMR spectra for the deuteration of N9-allyl-2,6-dichloropurine (Figure 4.25, **A** to **D**) revealed that after the addition of Na to the solution of the N9-derivative in MeOD- d_4 and heating at 60 °C for 20 minutes (part **A**), a minor product formed, having a proton peak which resonated higher upfield than the C8-H of N9-allyl-2,6-dichloropurine (8.23 ppm), at 8.02 ppm. New proton peaks at 4.79 ppm occurred as the N9-allyl proton peaks decreased in intensity at 4.87 ppm (part **C**). These new proton peaks which appeared at 8.02 ppm and 4.79 ppm corresponded to N7-2,6-dichloropurine derivative (Table 4.3).

Table 4.3: ^1H NMR spectrum chemical shifts (ppm) of N7 and N9-allyl-2,6-dichloropurine in MeOD- d_4 with Na.

2,6-dichloropurine derivative	C8-H	CH	N-CH ₂	CH ₂
N9-allyl-2,6-dichloropurine	8.23	6.08	5.22	4.87
N7-allyl-2,6-dichloropurine	8.02	6.09	5.20	4.81

The conversion of N9- to N7-2,6-dichloropurine was seen as the deuteration proceeded (Figure 4.25 **A** to **D**), in which the final ^1H NMR spectral run (part **D**) revealed almost full conversion of the N9-derivative to the N7-derivative; minor N9-allyl proton peaks occurred at 4.87 ppm. Migration of the H₂O/MeOH alcohol peak from 4.80 ppm to 4.99 ppm occurred upon addition

of Na and grew in intensity; this could possibly be due to the formation of alkoxides (sodium methoxide) and/or the influence of hydrogen bonding.



*Figure 4.25: ^1H NMR spectra (ppm) of the deuteration of N9-allyl-2,6-dichloropurine in MeOD- d_4 (400 MHz). **A**: immediately after addition of Na (0.5 eq) and heating at 60°C for 20 minutes, **B**: 1 hour after heating at 60°C, **C**: 3 hours after heating at 60°C with added Na (0.1 eq), **D**: 5 hours after heating at 60°C with added Na (0.1 eq).*

The intensity of the C8-H of the converted N7-allyl-2,6-dichloropurine is not as intense as it should have been if no deuteration took place, therefore indicating that deuteration does indeed occur at the C8 position of the N7 derivative. The presence of the N9-derivative allyl proton peaks at 4.87 ppm, trace amounts, in the last ^1H NMR spectrum (part **D**) but the absence of the C8-H peak at 8.23 indicated that the N9-allyl-2,6-dichloropurine underwent deuteration while converting to the N7-derivative.

The deuteration of the C8-H of N7-allyl-2,6-dichloropurine under the same conditions as N9-allyl-2,6-dichloropurine was also monitored by ^1H NMR spectroscopy (Figure 4.26, **A** and **B**) to

study how the deuteration occurs as well as if there is a difference in deuteration mechanisms when compared to the N9-derivative.

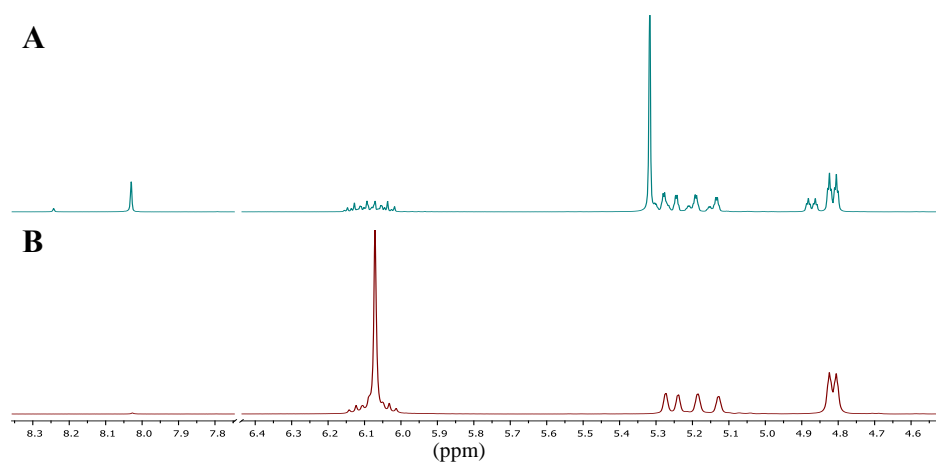


Figure 4.26: ^1H NMR spectra (ppm) of the deuteration of N7-allyl-2,6-dichloropurine in MeOD-d_4 (400 MHz). **A**: immediately after addition of Na (0.5 eq) and heating at $60\text{ }^\circ\text{C}$ for 20 minutes, **B**: 40 minutes after heating at $60\text{ }^\circ\text{C}$ with added Na (0.1 eq).

The ^1H NMR spectrum performed after the addition of Na to a solution of N7-allyl-2,6-dichloropurine and heated at $60\text{ }^\circ\text{C}$ for 20 minutes (**A**), revealed the development of the C8-H corresponding to the N9-derivative at 8.23 ppm as well as the distinctive N9-allyl protons at 4.87 ppm. However, after further heating of 20 minutes with an addition of Na (0.1 eq), the ^1H NMR spectrum (**B**) showed that the C8-H of N7-allyl-2,6-dichloropurine was fully deuterated as the proton peak at 8.02 was absent. In addition, there was no presence of the C8-H peak at 8.23 ppm and the allyl peaks at 4.87 ppm corresponding to N9-allyl-2,6-dichloropurine. Only the N7-derivative allyl peaks were present at 4.81 ppm. Again, migration of the $\text{H}_2\text{O}/\text{MeOH}$ alcohol peak was seen, moving from 5.31 ppm to 6.08 ppm and grew in intensity upon addition of Na.

Comparing the deuteration of the N9- and the N7-allyl-2,6-dichloropurine indicated two distinct differences.

- i. The first difference is the time required to deuterate the two derivatives. N9-allyl-2,6-dichloropurine required five hours for deuteration at the C8 position in which an additional 0.2 equivalents of Na was added to aid the deuteration. Deuteration of the C8-

H of N7-allyl-2,6-dichloropurine only required 40 minutes of heating at 60 °C with an additional 0.1 eq of Na added. This indicated that the N7-derivative deuterated much faster than the N9-derivative.

- ii. The second difference is based on the inter-conversion between the two products during their deuteration. The N9-allyl-2,6-dichloropurine (Figure 4.27, **A**) converted to N7-allyl-2,6-dichloropurine (90% conversion) while deuteration of the C8-H of the N9-derivative was taking place, leaving trace amounts of the N9-derivative fully deuterated (**B**) and a significant amount of the N7-derivative which was undergoing deuteration.

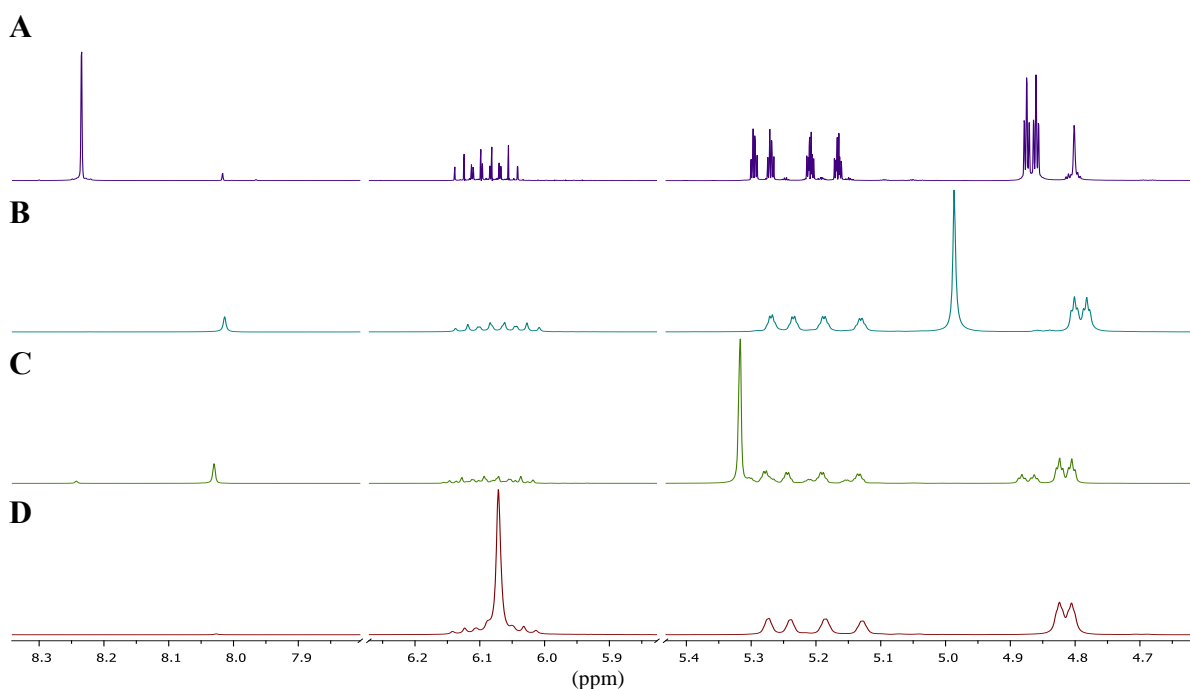


Figure 4.27: Initial and final ^1H NMR spectra of the allyl-2,6-dichloropurine derivatives during deuteration in MeOD-d_4 (400 MHz). **A**: initial ^1H NMR spectrum of N9-allyl-2,6-dichloropurine after addition of Na (0.5 eq) and heating at 60 °C, **B**: final ^1H NMR spectrum of deuterated N9-allyl-2,6-dichloropurine, **C**: initial ^1H NMR spectrum of N7-allyl-2,6-dichloropurine after addition of Na (0.5 eq) and heating at 60 °C, **D**: final ^1H NMR spectrum of deuterated N7-allyl-2,6-dichloropurine.

The N7-allyl-2,6-dichloropurine initially underwent minor conversion to the N9-derivative under deuteration conditions (**C**), however the minor amount of the N9-derivative converted back to the N7-allyl-2,6-dichloropurine (**D**) as the allyl proton peaks at 4.87 ppm disappeared.

Therefore, under the deuteration conditions used, there is an inter-conversion from N9-allyl-2,6-dichloropurine to N7-allyl-2,6-dichloropurine (Figure 4.28, **23** and **26**, respectively), having the equilibrium favour the N7-derivative. The deuteration of the C8-H of the N7-derivative is faster than that of the N9-derivative. At the end of the deuteration of N7-allyl-2,6-dichloropurine, the final deuterated N9-allyl-2,6-dichloropurine was not present with the N7-derivative, hence the equilibrium can be ruled out between the deuterated forms.

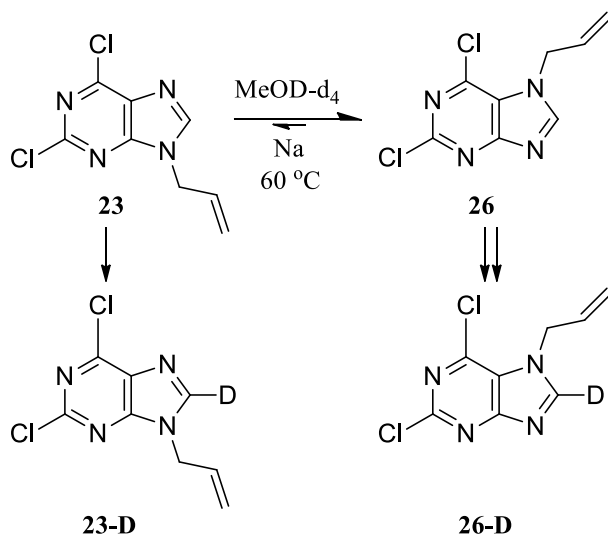


Figure 4.28: Inter-conversion between the N9-allyl-2,6-dichloropurine **23** and N7-allyl-2,6-dichloropurine **26** under deuteration conditions.

4.3 Conclusions from the deuteration study

To conclude this section, the N3-benzyladenine undergoes deuteration at the C2 and C8 positions via the sp^3 mediated mechanism and the carbene mediated mechanism, respectively. The N9-benzyladenine derivative undergoes deuteration at the C8 position. The carbene mediated mechanism displayed a higher deuteration rate than the sp^3 mediated mechanism when exposed to heat, allowing the N3-benzyladenine to undergo faster deuteration at C8 compared to C2. It was shown before that the N9-benzyladenine deuterated at a faster rate than the N3-derivative, which could be attributed to the additional sp^3 mediated mechanism of deuteration

playing an additional role. The N7- and N9-allyl-2,6-dichloropurine derivatives undergoing deuteration at the C8 position. A common mechanism of deuteration between these derivatives is the carbene mediated mechanism, which supplied convincing mechanistic schemes for each derivative. The reason for the faster deuteration of the N7-allyl-2,6-dichloropurine, as compared to the N9-allyl-2,6-dichloropurine derivative, is unclear. The steric and electronic effects of the chlorine atoms could play a role on the rate of deuteration at the C8 position of the N9 derivative, but have not been investigated.

The above deuteration of the four purine derivatives supplies strong evidence for the carbene mediated mechanism, which in turn supports the “pull” mechanism postulated by Kenyon *et al.* for the proton exchange at the C8 position of the adenyly moiety of ATP in the regulation of ATP binding and phosphoryl transfer.^{7,8}

Chapter 5

5.1 Conclusion

It is without question that, from the synthetic study performed in this research, the most reactive sites of adenine under basic conditions are the N9 and N3 positions on the purine ring, the N9 being the most favoured site. Extensive NMR spectroscopic analysis has shown how theoretically predicting the 2D ^1H - ^{13}C NMR spectroscopy correlations is an essential tool to assign the ^1H and ^{13}C NMR spectrum chemical shifts of alkylated adenine derivatives. Characteristic C2-H and C8-H peak separation is present in N9- and N3-alkylated adenine, the former being 0.1 ppm and the latter being > 0.5 ppm. The influence of NMR solvents plays a critical role in the shifting of ^1H NMR spectrum peaks, which could be misleading as it was shown that the chemical shifts of the purine protons of N3- and N9-benzyladenine in DMSO-d_6 are reversed in CDCl_3 . Using MeOD-d_4 as a NMR solvent reverses the assignment of the C2-H and C8-H chemical shifts of N9-benzyladenine in DMSO-d_6 . These results have solved many contradicting reports, which have not only miss-assigned ^1H NMR spectrum chemical shifts but also assigned the minor structural isomer, N3-alkyladenine, as N7-alkyladenine.

Using *N*-benzyladenine as the system to study the influence of solvent, we have shown that the ratio of N9-:N3-benzyladenine is controlled by solvent, having N9-benzyladenine favoured in polar aprotic solvents and N3-benzyladenine favoured in polar protic solvents. The presence of water increases the amount of N3-benzyladenine and it is almost unavoidable to have trace amounts of water present in the polar aprotic solvents used, such as DMSO and DMF. Monitoring the benzylation of adenine under basic conditions by ^1H NMR spectroscopy pointed out that there is immediate formation of N9-benzyladenine when subjecting the adenine anion to benzyl bromide. However, the appearance of unidentified migrating peaks occurred, followed

by the formation of N3-benzyladenine, indicating by-product or intermediates. Hence, three possible reasons for the formation of N3-benzyladenine arose:

- i. The N3-benzyladenine could be S_N1 controlled, being favoured in polar protic solvents, such as water, ethanol and *tert*-butanol.
- ii. The structural isomer could be a result of competitive S_N2 reactions between the N9 and N3 positions, having water and other polar protic solvents promote the N3 position.
- iii. And finally, the possibility of water-catalysed Dimroth rearrangement, which could potentially explain the unidentified peaks in the 1H NMR spectrum.

To study the most reactive sites of adenine under basic conditions, the S_N2 mechanism for the N1-, N3-, N7- and N9-pathways was simulated computationally. Analysing the reaction paths using classical and topological properties highly supported the N9-pathway followed by the N3-pathway. The site of alkylation on the purine ring of adenine follows the stability trend observed from adenine tautomers, $N9 > N7 > N3 \gg N1$, whereby the N9 and N7 sites of substitution are the most favoured. However, it is not the end product (alkylated adenine) of the competing reaction paths that determines which pathway is preferred, but rather how the interactions between atoms and fragments are changing along the reaction paths.

Simple comparison of changes (relative to the relevant *ref* state) in the electronic energies along the reaction paths indicated very little difference between the reaction paths and still showed preference for the N9- and N7-pathways at the product formation stage, N9-being the most favoured. However, a novel approach was developed using IQA-defined energy terms. These were implemented in monitoring contributions made by atoms and well-defined molecular fragments along a reaction path, which gave significant differentiation between the pathways.

Each competing pathway had equal chance of reaching the transition state, it was only after the transition state, at $d(\text{N},\text{C15}) = 2.0 \text{ \AA}$, that elimination of the N1-/N7-pathways took place, whereas at $d(\text{N},\text{C15}) \sim 1.5(\text{eq}) \text{ \AA}$ the N9-pathway dominated the N3-pathway:

- i. Changes in the IQA defined energy terms, $\Delta E_{\text{add}}^{\text{X}}$, $\Delta E_{\text{self}}^{\text{X}}$, and $\Delta E_{\text{int}}^{\text{XY}}$ for the reacting nitrogen of each pathway, N1, N3, N7, and N9 in the N1-, N3-, N7- and N9-pathways, respectively, showed that at the $d(\text{N},\text{C15})$ of 2.0 \AA , the changes in $\Delta E_{\text{add}}^{\text{A}}$ and $\Delta E_{\text{int}}^{\text{AX}}$ suggested that the reaction was largely in favour of the N3-/N9-pathways having significantly higher stabilising terms, and in least favour of the N1-/N7-pathways. At $d(\text{N},\text{C15})$ of $\sim 1.5 \text{ \AA}$ (eq) the N9-pathway was far more favourable than the N3-pathway, eliminating the competition.
- ii. The N—C15 bond formation was monitored by the inter-fragment interaction energy between the two atom fragment $\mathcal{F} = \{\text{N},\text{C15}\}$ and polyatomic fragment \mathcal{H} (the remainder of the atoms in the molecular system). When the $d(\text{N},\text{C15})$ decreased from 3.0 \AA , through the TS, to 2.0 \AA , where strengthening of the N-C15 bond took place, a large difference in repulsive $\Delta E_{\text{int}}^{\mathcal{F}\mathcal{H}}$ values was observed between N1-/N7-pathways and N3-/N9-pathways. Substitution on the N1 or N7 is disfavoured whereas the substitution on the N3 or N9 is highly favoured. The product formation, $d(\text{N},\text{C15}) \sim 1.5 \text{ \AA}$, highly favoured the N9-pathway over the N3-pathway.
- iii. The inter-fragment interaction between polyatomic fragments $\mathcal{M} = \{\text{AD}^{-}\}$ and $\mathcal{N} = \{\text{Bn}\}$, $\Delta E_{\text{int}}^{\mathcal{M}\mathcal{N}}$, at $d(\text{N},\text{C15}) = 2 \text{ \AA}$ promoted the N3-/N9-pathways, eliminating the N1-pathway. The N3-/N7-pathways were eliminated at the product formation step, where the N9-pathway dominated.
- iv. The inter-fragment interaction energy between mono-atomic fragment $\mathcal{O} = \{\text{Br}\}$ and poly-atomic fragments $\mathcal{M} = \{\text{AD}^{-}\}$ and $\mathcal{N} = \{\text{Bn}\}$, $\Delta E_{\text{int}}^{\mathcal{M}\mathcal{O}}$ and $\Delta E_{\text{int}}^{\mathcal{N}\mathcal{O}}$,

respectively, showed less repulsive interactions, $\Delta E_{\text{int}}^{\mathcal{M}^{\ominus}}$ being attractive, for the N1-/N7-pathways which indicated that the bromine atom does not leave the immediate reactive site, reducing its ability as a good leaving group. This was supported by the two pathways having highly stabilising diatomic interaction energies which involved the Br^- atom. The $\Delta E_{\text{int}}^{\mathcal{M}^{\ominus}}$ and $\Delta E_{\text{int}}^{\mathcal{N}^{\ominus}}$ of the N3-/N9- pathways were strongly repulsive, supported by the lack of stabilising diatomic interactions with the bromine atom, allowing it to leave the reaction site.

v. The change in intra-fragment interaction energy of fragment $\mathcal{M} = \{\text{AD}^-\}$, $\Delta E_{\text{int}}^{\mathcal{M}}$, at $d(\text{N}, \text{C15})$ of 2.0 Å, largely supported the N3- and N9-pathway over the N1-/N7-pathways, eliminating the latter as a possibility. At the product formation, $d(\text{N}, \text{C15}) \sim 1.5(\text{eq})$ Å, the N9-pathway dominates the N3-pathway.

vi. The interaction energy between the reacting nitrogen N and the atoms of fragment

$\mathcal{M} = \{\text{AD}^-\}$, $\Delta \sum_{\substack{X \neq \text{N} \\ X \in \mathcal{M}}} E_{\text{int}}^{\text{NX}}$, and the interaction energy between the reacting nitrogen and

the atoms of fragment $\mathcal{N} = \{\text{Bn}\}$, $\Delta \sum_{\substack{N \in \mathcal{M} \\ X \in \mathcal{N}}} E_{\text{int}}^{\text{NX}}$, show that simple analysis of individual

energy terms, such as $\Delta \sum_{\substack{N \in \mathcal{M} \\ X \in \mathcal{N}}} E_{\text{int}}^{\text{NX}}$, can be misleading, as it supports the N1-pathway

at the transition state. However, the combined effect on the molecular system,

$\Delta \sum_{\substack{X \neq \text{N} \\ X \in \mathcal{M}}} E_{\text{int}}^{\text{NX}} + \Delta \sum_{\substack{N \in \mathcal{M} \\ X \in \mathcal{N}}} E_{\text{int}}^{\text{NX}}$, showed that all pathways except the N7, had equal chance of

reaching the transition state. At $d(\text{N}, \text{C15})$ of 2.0 Å the combined energy term highly supported the N3-/N9-pathways over the N1-/N7-pathways, removing the latter for further consideration. The N9-pathway is the preferential pathway at the product equilibrium point, overruling the N3-pathway.

The experimental results were reproduced perfectly using computational methods, which gave insight into what determines the preferential sites of adenine under basic conditions as well as at what stage along the reaction path elimination of various isomers begins. This sets a new basis as to how these systems and other systems can be studied to develop conceptual understanding.

The deuteration studies performed in this research indicated that the deuteration of the C8 proton of N9-benzyladenine can occur through two possible mechanisms, the carbene mediated mechanism and the sp^3 mediated mechanism. Both mechanisms support the lack of deuteration at the C2-proton. The deuteration of N3-benzyladenine occurs at the C2 and the C8 positions, having the former take place at a significantly faster rate at higher temperatures. The carbene mediated mechanism accounts for the deuteration at the C2 position where as the sp^3 mediated mechanism supports deuteration at the C8 position of N3-benzyladenine. The two postulated mechanisms for deuteration can be applied to any N9- and N3-alkylated adenines. The deuteration of the C8-H of N9- and N7-allyl-2,6-dichloropurine were indicative of the carbene mechanism as they lack the *exo*-amino group which is essential for the sp^3 mediated mechanism. Hence the study demonstrated that the C8 proton of the N9-alkylated adenine is indeed reactive, supporting the theory of the C8-H of the ATP adenylyl moiety containing regulative function in ATP binding and phosphoryl transfer.

All aims were achieved during the course of this research, i.e. the most reactive site of adenine under S_N2 substitution conditions was determined, the preferential site was studied computationally using topological and classical properties in which a novel method was developed using IQA defined energy terms to study interacting fragments along a reaction path,

giving a rationale for the experimental results, and the activity and mechanisms for the deuteration of the C8 proton of adenine were investigated.

5.2 Future work

Having successfully determined the structure of the products from the benzylation of adenine under basic conditions and having explained this preference computationally, a future research challenge will be to use computational methods to explore the observed influence of solvent on the reaction pathway.

The opportunity to study the S_N2 mechanism in different solvents employing the PCM model and the explicit solvent model could provide the answers as to why solvent plays such a role in the N9:N3 ratio during the synthesis of N9-alkylated adenine under basic conditions. The method developed of using IQA defined energy terms to study the interactions of atoms and fragments during a reaction path could be applied to these systems, allowing the full analysis of how the system is influenced by the presence of different solvents. These techniques may be computationally expensive and would not be simple. However, if successful, a huge contribution could be made to the understanding of solvent effects during reactions. The possibility of the S_N1 theory proposed by many researchers can be analysed by simulating the S_N1 mechanism in the same manner that the S_N2 mechanism had been studied in this dissertation.

The suggestion of Dimroth rearrangement yielding the N3-alkylated product could be tested computationally by investigating the intermediates along the proposed mechanism, together with experimental analysis by subjecting N9-benzyladenine to reflux under basic conditions with the presence of water. The aromaticity of the adenine ring, which was stated to also play a role in the stability of *N*-alkylated adenines, could be studied during the reaction mechanism to investigate how it is being influenced during a reaction and if it itself has a determining factor for the site of alkylation. This could be achieved by using the aromaticity indices discussed in

the introduction of Chapter 3, such as HOMED and NICS, which measure the extent of aromaticity.

The library of inhibitors could be synthesised with better control of the N9:N3 ratio, and research expanded to enzymology studies to gain a better understanding of the reactivity of the C8 proton and the mechanisms which play a role for the proton transfer in kinase enzymes. Varying the alkyl group of the adenine inhibitors and studying the influence of the side chain on the rate of deuteration of the C8 position could give insight into better control of the inhibitory activity of these compounds.

The overall aim of this research was to develop a framework onto which future research can be built. By experimentally identifying the reactive sites of adenine under basic conditions in DMSO and using computational methods to investigate the reasoning behind the preference for certain sites, it has been shown how the integration of two fields complements each other and can be used to study other systems to develop conceptual understanding of the chemistry behind reacting systems.

Chapter 6

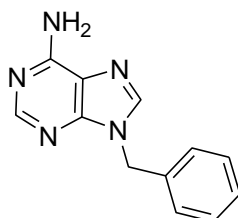
Experimental

General

The ^1H NMR spectra were recorded at 400.13 MHz with a Bruker 400 AVANCE ultrashield +, unless stated that the ^1H NMR was recorded at 300.13 MHz with a Bruker 300 AVANCE ultrashield. The decoupled ^{13}C NMR spectra were recorded at 101 MHz using the Bruker 400 AVANCE ultrashield +. ^1H NMR solvent DMSO- d_6 was referenced on the chemical shift 2.50 ppm, MeOD- d_4 was reference on the 3.31 ppm chemical shift and CDCl_3 - d was reference on the 7.24 ppm chemical shift. The ^{13}C NMR solvent DMSO- d_6 was reference on the 39.5 ppm chemical shift, MeOD- d_4 was referenced on the 49.2 ppm chemical shift and CDCl_3 - d was referenced on the 77.2 ppm chemical shift. All melting points were performed on single crystals using a Stuart melting point apparatus SMP10 and are uncorrected. All flash column chromatography was performed with silica gel 60 from Merck, Darmstadt, Germany (No. 64271). X-ray diffraction to obtain the crystal structures reported was performed on a Bruker D8 Venture (copper radiation). Compound N9-allyl-2,6-dichloropurine (22) and its N7 isomer were obtained from the synthesis by an honours student.¹¹³

Preparation of N-alkylated adenine derivative

1. N9-benzyladenine (**N9-Bn**)



KtBuO (0.436g, 3.89 mmol) and adenine (0.499g, 3.70 mmol) were added to DMF (30ml) and stirred for 30 minutes at room temperature, forming a white precipitate. Benzyl bromide (0.44ml, 5.8 mmol) was added and the solution was heated to 125 °C and stirred for 24 hours. The solvent was removed from the filtrate by a N₂(g) stream at 50 °C. The precipitate was rinsed with ethyl acetate and were isolated by flash chromatography. A gradient flash column was used, starting with an ethyl acetate: DCM: hexane (1:1:0.5); ethyl acetate: DCM: hexane (1:1:0.5), methanol (10%); ethyl acetate: DCM: hexane (1:1:0.5), methanol (12.5%). The pure compounds were recrystallized from DCM and methanol (1:1) to yield **N9-Bn** (0.251 mg, 30%) and **N3-Bn** (0.030 mg, 4%).

N9-benzyladenine (**N9-Bn**). Mp. 235–236 °C (lit.²⁶ 233–235 °C) colourless crystals. ¹H NMR (400 MHz, DMSO-d₆) δ 8.26 (s, 1H, C8-H), 8.16 (s, 1H, C2-H), 7.38–7.17 (m, 7H, NH₂, C₆H₅), 5.37 (s, 2H, CH₂). ¹³C NMR (101 MHz, DMSO-d₆) δ 156.1 (C6), 152.8 (C2), 149.6 (C4), 141.0 (C8), 137.2 (C₀, C₆H₅), 128.8 (C₆H₅), 127.9 (C₆H₅), 127.6 (C₆H₅), 118.8 (C5), 46.3 (CH₂).

¹H NMR (400 MHz, MeOD-d₄) δ 8.22 (s, 1H, C2-H), 8.15 (s, 1H, C8-H), 7.38–7.26 (m, 5H, C₆H₅), 5.43 (s, 2H, CH₂). ¹³C NMR (101 MHz, MeOD-d₄) δ 157.4 (C6), 154.1 (C2), 150.8 (C4), 142.8 (C8), 137.8 (C₀, C₆H₅), 130.1 (C₆H₅), 129.4 (C₆H₅), 128.9 (C₆H₅), 119.9 (C5), 48.2 (CH₂).

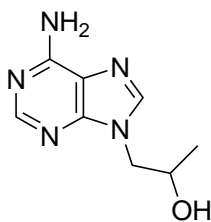
^1H NMR (400 MHz, $\text{CDCl}_3\text{-d}$) δ 8.38 (s, 1H, C2-H), 7.78 (s, 1H, C8-H), 7.38–7.25 (m, 5H, C_6H_5), 6.02 (s, 2H, NH_2), 5.36 (s, 2H, CH_2). ^{13}C NMR (101 MHz, $\text{CDCl}_3\text{-d}$) δ 154.8 (C6), 152.2 (C2), 150.1 (C4), 141.0 (C8), 135.5 (C_0 , C_6H_5), 129.4 (C_6H_5), 128.8 (C_6H_5), 128.1 (C_6H_5), 47.6 (CH_2).

N3-benzyladenine (**N3-Bn**). Mp. 279–281 °C, (lit.³³ 280–281 °C), colourless crystals. ^1H NMR (400 MHz, DMSO-d_6) δ 8.57 (s, 1H, C2-H), 7.96 (s, 2H, NH_2), 7.78 (s, 1H, C8-H), 7.50–7.40 (m, 2H, C_6H_5), 7.39–7.23 (m, 3H, C_6H_5), 5.51 (s, 2H, CH_2). ^{13}C NMR (101 MHz, DMSO-d_6) δ 154.9 (C6), 152.3 (C8), 149.6 (C4), 143.5 (C2), 136.1 (C_0 , C_6H_5), 128.6 (C_6H_5), 128.09 (C_6H_5), 128.05 (C_6H_5), 120.1 (C5), 52.1 (CH_2).

^1H NMR (400 MHz, MeOD-d_4) δ 8.60 (s, 1H, C2-H), 8.21 (s, 1H, C8-H), 7.44 (m, 2H, C_6H_5), 7.39–7.31 (m, 3H, C_6H_5), 5.63 (s, 2H, CH_2). ^{13}C NMR (101 MHz, MeOD-d_4) δ 156.2 (C6), 150.3 (C4), 150.0 (C8), 147.5 (C2), 136.2 (C_0 , C_6H_5), 130.3 (C_6H_5), 130.0 (C_6H_5), 129.3 (C_6H_5), 117.1 (C5) 54.3 (CH_2).

^1H NMR (400 MHz, $\text{CDCl}_3\text{-d}$) δ 10.34 (s, 1H, NH_2), 8.26 (s, 1H, C2-H), 8.18 (s, 1H, C8-H), 7.39 (s, 5H, C_6H_5), 6.70 (s, 1H, NH_2), 5.58 (s, 2H, CH_2). ^{13}C NMR (101 MHz, $\text{CDCl}_3\text{-d}$) δ 153.8 (C6), 148.4 (C4), 146.2 (C2), 144.5 (C8), 132.9 (C_0 , C_6H_5), 130.0 (C_6H_5), 129.8 (C_6H_5), 128.8 (C_6H_5), 53.7 (CH_2).

2. 2-(6-Amino-purin-9-yl)-propan-2-ol (**21**)

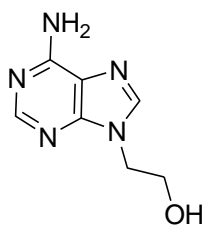


KOH (0.872g, 15.5 mmol) and adenine (1.998g, 14.80 mmol) were added to DMSO (50ml) and left to stir for 2 hrs at room temperature. Propylene carbonate (1.87ml, 22.2 mmol) in was added to this solution. This is left to stir for 48 hours at 120 °C. A solid formed, which was filtered off. The solvent was removed from the filtrate by a N₂(g) stream at 50 °C to yield a white solid. A column was used to separate two compounds: ethyl acetate: DCM (1:1), methanol (12.5%); ethyl acetate: DCM (1:1), methanol (10%) to yield (2.580 mg, 90%).

2-(6-Amino-purin-9-yl)-propan-2-ol (**21**). Mp. 192–194 °C (lit.¹¹⁴ 192–195 °C), colourless crystals. ¹H NMR (400 MHz, DMSO-d₆) δ 8.14 (s, 1H, C2-H), 8.05 (s, 1H, C8-H), 7.21 (s, 2H, NH₂), 5.06 (s, 1H, OH), 4.18–3.89 (m, 3H, N-CH₂, CH), 1.05 (d, *J* = 5.9 Hz, 3H, CH₃). ¹³C NMR (101 MHz, DMSO-d₆) δ 155.80 (C6), 152.16 (C2), 149.74 (C4), 141.71 (C8), 118.55 (C5), 64.72 (CH), 50.20 (CH₂), 20.87 (CH₃).

2-(6-Amino-purin-3-yl)-propan-2-ol. ¹H NMR (300 MHz, DMSO-d₆) δ 8.57 (s, 1H, C8-H), 7.93 (s, 2H, NH₂), 7.76 (s, 1H, C2-H), 4.19–3.89 (m, 3H, N-CH₂, CH), 1.12 (d, *J* = 5.8 Hz, 3H, CH₃).

2-(6-Amino-purin-9-yl)-ethanol (**20**)



KOH (0.872g, 15.5 mmol) was added to DMSO (70ml) and left to stir for 10 minutes. Adenine was added (2.00g, 14.8 mmol) to the solution and left to stir for 30 minutes at room temperature in which it dissolved. Ethylene carbonate (1.955g, 22.20 mmol) was added to this solution. This is left to stir for 24 hours at 120 °C. A small amount of solid formed, which was removed by filtration. The solvent was removed from the filtrate by a N₂(g) stream at 50 °C to yield a white

solid which was washed with methanol 3 times. A column was used to separate two compounds: ethyl acetate: DCM (1:1), methanol (12.5%); ethyl acetate: DCM (1:1), methanol (10%) to yield (2.230 mg, 84%).

2-(6-Amino-purin-9-yl)-ethanol (**20**). Mp. 244–245 °C. (lit.¹¹⁵ 240–243 °C), colourless crystals. ¹H NMR (400 MHz, DMSO-d₆) δ 8.13 (s, 1H, C2-H), 8.06 (s, 1H, C8-H), 7.16 (s, 2H, NH₂), 5.00 (t, *J* = 5.4 Hz, 1H, OH), 4.18 (t, *J* = 5.5 Hz, 2H, N-CH₂), 3.73 (dt, *J* = 5.5 Hz, 2H, CH₂-OH). ¹³C NMR (101 MHz, DMSO-d₆) δ 155.93 (C6), 152.26 (C2), 149.56 (C4), 141.33 (C8), 118.72 (C5), 59.26 (CH₂-OH), 45.71 (N-CH₂).

2-(6-Amino-purin-3-yl)-ethanol: ¹H NMR (300 MHz, DMSO-d₆) δ 8.23 (s, 1H, C2-H), 7.86 (s, 2H, NH₂), 7.76 (s, 1H, C8-H), 5.08 (t, 1H, OH), 4.35 (t, 2H, N-CH₂), 3.81 (m, 2H, CH₂-OH).

Deuteration experimental:

General procedure for deuteration of purine derivatives:

The purine derivative (20 mg) was dissolved in MeOD-d₄ (0.6 mL) in a standard NMR tube, in which a clean piece of Na (approximately 1 eq), free from paraffin oil, was added. A ¹H NMR spectrum was run immediately the addition after to identify the original peaks in the presence of Na. The mixture was allowed to release H₂ gas, and heated at 60 °C. The deuteration progress was monitored by ¹H NMR spectroscopy.

Deuteration of N3- and N9-benzyladenine.

N3- and N9-benzyladenine mixture: ¹H NMR (300 MHz, MeOD-d₄, Na) δ 8.39 (s, 1H, C2-H (N3)), 8.22 (s, 1H, C2-H (N9)), 8.15 (s, 1H, C8-H (N9)), 7.90 (s, 1H, C8-H (N3)), 7.42–7.24 (m, 10H, 2 × Ph (N9 and N3)), 5.58 (s, 2H, CH₂ (N3)), 5.49 (s, 1H), 5.43 (s, 2H, CH₂ (N9)).

N3-benzyladenine (0.011g, 0.044 mmol) and N9-benzyladenine (0.021g, 0.089 mmol) were added to MeOD-d₄ in a NMR tube. Na (0.021g, 0.093 mmol) was added to the solution. The mixture was allowed to stand for 2 days, in which a ¹H NMR spectra were recorded every 24 hours, which yielded very low deuteration rates. The mixture was heated at 60 °C for 20 minutes, which resulted in deuteration of the two compounds.

¹H NMR (300 MHz, MeOD-d₄) δ 8.22 (s, 1H, C2-H (N9)), 7.88 (s, 1H, C8-H (N3)), 7.40 – 7.26 (m, 10H, 2 × Ph (N9 and N3)), 5.57 (s, 2H, CH₂ (N3)), 5.49 (s, 1H), 5.43 (s, 2H, CH₂ (N9)).

Deuteration of the N7- and N9-2,6-dichloropurine derivatives.

The same general deuteration procedure above was applied to the deuteration of the N7- and N9-2,6-dichloropurine compounds. The N7- and N9-allyl-2,6-dichloropurine derivatives were deuterated separately due to the overlapping of peaks. The ¹H NMR and ¹³C NMR spectra in MeOD-d₄ for the two compounds are shown below. The ¹H and ¹³C NMR spectrum of the two compounds in MeOD-d₄ is shown below:

N9-allyl-2,6-dichloropurine: ¹H NMR (400 MHz, MeOD-d₄) δ 8.53 (s, 1H, C8-H), 6.11 (ddt, *J* = 17.1, 10.3, 5.9 Hz, 1H, CH), 5.33 (ddd, *J* = 10.3, 2.4, 1.3 Hz, 1H, CH₂), 5.26 (dtd, *J* = 17.1, 1.6, 1.0 Hz, 1H, CH₂), 4.94 (dt, *J* = 5.8, 1.5 Hz, 2H, N-CH₂). ¹³C NMR (101 MHz, MeOD-d₄) δ 162.54 (C2), 154.37 (C4), 145.22 (C8), 143.10 (C6), 133.32 (CH), 120.84 (C5), 119.46 (CH₂), 47.27 (N-CH₂).

N7-allyl-2,6-dichloropurine: ¹H NMR (400 MHz, MeOD-d₄) δ 8.53 (s, 1H, C8-H), 6.11 (ddt, *J* = 17.0, 10.3, 5.8 Hz, 1H, CH), 5.33 (ddd, *J* = 10.3, 2.4, 1.3 Hz, 1H, CH₂), 5.26 (dtd, *J* = 17.1, 1.6, 1.0 Hz, 1H, CH₂), 4.94 (dt, *J* = 5.8, 1.5 Hz, 2H, N-CH₂). ¹³C NMR (101 MHz, MeOD-d₄) δ 154.74 (C5), 153.99 (C2), 152.01 (C6), 149.02 (C8), 132.81 (CH), 131.69 (C4), 120.03 (CH₂), 47.65 (N-CH₂).

Deuteration of N9-allyl-2,6-dichloropurine

N9-allyl-2,6-dichloropurine (0.020g, 0.088 mmol) was dissolved in MeOD-d₄ (0.6 mL). To this mixture, Na was added (0.010g, 0.044 mmol) and heated at 60 °C for 80 minutes. Na (0.002g, 0.009 mmol) was added and heated at 60 °C for 40 minutes. Na (0.002g, 0.009 mmol) was added to the solution and heated at 60 °C for 2 hours. This was followed by addition of Na (0.002g, 0.009 mmol), in which the solution was heated at 60 °C for a further 2 hours

¹H NMR (300 MHz, MeOD-d₄) δ 8.01 (s, 1H, C8-H), 6.07 (ddt, *J* = 16.0, 10.4, 5.7 Hz, 1H, CH), 5.22 (m, 2H, CH₂), 4.85 (m, 1H, CH₂), 4.79 (dt, *J* = 5.7, 1.4 Hz, 2H, N-CH₂).

Deuteration of N7-allyl-2,6-dichloropurine

N7-allyl-2,6-dichloropurine (20.004 mg, 0.088 mmol) was dissolved in MeOD-d₄ (0.6 mL). To this mixture, Na was added (1.009 mg, 0.044 mmol) and heated at 60°C for 20 minutes. Na (0.202 mg, 0.009 mmol) was added and heated at 60°C for 20 minutes.

¹H NMR (300 MHz, MeOD-d₄) δ 6.08 (m, 1H, CH), 5.26 (d, *J* = 10.3 Hz, 1H, CH₂), 5.16 (dd, *J* = 17.1, 0.8 Hz, 1H, CH₂), 4.81 (dt, *J* = 5.6 Hz, 2H, N-CH₂).

N9-benzyladenine NMR scaled reaction

Adenine (0.022g, 0.17 mmol) was dissolved in DMSO-d₆ (0.6 mL) in a NMR tube. To this solution K^tBuO (0.018g, 0.17 mmol) was added and allowed to stir for 30 minutes. Benzylbromide (0.03 mL, 0.3 mmol) was added to the mixture and heat at 120 °C for 12 hours and analysed by ¹H NMR spectroscopy at 0, 1, 2, 3, 4, 5 and 12 hours (refer to Chapter 2, 2.2.1).

^1H NMR (400 MHz, DMSO- d_6) δ 10.02 (s, 1H), 9.15 (s, 1H), 8.94 (s, 1H), 8.65 (s, 1H), 8.48 (s, 1H), 8.40 (s, 1H), 8.34 (s, 1H), 8.31 (s, 1H), 8.29 (s, 1H), 8.15 (s, 1H), 7.77 (s, 1H), 7.52–7.42 (m, 4H), 7.41–7.15 (m, 34H), 5.92 (s, 2H), 5.64 (s, 2H), 5.54 (s, 1H), 5.37 (d, $J = 6.3$ Hz, 5H), 4.47 (s, 1H).

Supporting Material

Attached compact disk

NMR data: ^1H , ^{13}C NMR spectra and HSQC 2D (^1H - ^{13}C) spectrum of N3- and N9-benzyladenine

N9-Benzyladenine crystal data

N3-benzyladenine crystal data

N7-allyl-2,6-dichloropurine crystal data

2-(6-Amino-purin-9-yl)-ethanol crystal data

Computational Supporting Material: Tables S1–S46

References

- (1) Shah, N. S.; Wright, A.; Bai, G.-H.; Barrera, L.; Boulahbal, F.; Martín-Casabona, N.; Drobniowski, F.; Gilpin, C.; Havelková, M.; Lepe, R. *Emerg. Infect. Dis.* **2007**, *13*, 380.
- (2) Segura-Cabrera, A.; Rodríguez-Pérez, M. A. *Bioorg. Med. Chem. Lett.* **2008**, *18*, 3152.
- (3) Congreve, M.; Murray, C. W.; Blundell, T. L. *Drug Discov. Today.* **2005**, *10*, 895.
- (4) Hartmann, M. D.; Bourenkov, G. P.; Oberschall, A.; Strizhov, N.; Bartunik, H. D. *J. Mol. Biol.* **2006**, *364*, 411.
- (5) Gu, Y.; Reshetnikova, L.; Li, Y.; Wu, Y.; Yan, H.; Singh, S.; Ji, X. *J. Mol. Biol.* **2002**, *319*, 779.
- (6) Kenyon, C. P.; Steyn, A.; Roth, R. L.; Steenkamp, P. A.; Nkosi, T. C.; Oldfield, L. C. *BMC Biochem.* **2011**, *12*, 36.
- (7) Kenyon, C. P.; Roth, R. L.; van der Westhuyzen, C. W.; Parkinson, C. J. *BMC Research Notes* **2012**, *5*, 131.
- (8) Kenyon, C. P.; Roth, R. L. *BMC Biochem.* **2012**, *13*, 15.
- (9) Cheek, S.; Zhang, H.; Grishin, N. V. *J. Mol. Biol.* **2002**, *320*, 855.
- (10) Cheek, S.; Ginalski, K.; Zhang, H.; Grishin, N. V. *BMC Struct. Biol.* **2005**, *5*, 6.
- (11) Ortega, C.; Liao, R.; Anderson, L. N.; Rustad, T.; Ollodart, A. R.; Wright, A. T.; Sherman, D. R.; Grundner, C. *PLoS Biol.* **2014**, *12*, e1001746.
- (12) Raboisson, P.; Lugnier, C.; Muller, C.; Reimund, J.-M.; Schultz, D.; Pinna, G.; Le Bec, A.; Basaran, H.; Desaubry, L.; Gaudiot, F.; Seloum, M.; Bourguignon, J.-J. *Eur. J. Med. Chem.* **2003**, *38*, 199.
- (13) Bourguignon, J.-J.; Désaubry, L.; Raboisson, P.; Wermuth, C.-G.; Lugnier, C. *J. Med. Chem.* **1997**, *40*, 1768.
- (14) Torphy, T. J. *Am. J. Resp. Crit. Care.* **1998**, *157*, 351.

- (15) Teixeira, M. M.; Gristwood, R. W.; Cooper, N.; Hellewell, P. G. *Trends Pharmacol. Sci.* **1997**, *18*, 164.
- (16) Doherty, A. M. *Curr. Opin. Chem. Biol.* **1999**, *3*, 466.
- (17) Boichot, E.; Wallace, J. L.; Germain, N.; Corbel, M.; Lugnier, C.; Lagente, V.; Bourguignon, J.-J. *J. Pharmacol. Exp. Ther.* **2000**, *292*, 647.
- (18) Martin, R.; Bielekova, B.; Lincoln, A.; McFarland, H. *J. Immunol.* **2000**, *164*, 1117.
- (19) Hakimelahi, G. H.; Ly, T. W.; Moosavi-Movahedi, A. A.; Jain, M. L.; Zakerinia, M.; Davari, H.; Mei, H.-C.; Sambaiah, T.; Moshfegh, A. A.; Hakimelahi, S. *J. Med. Chem.* **2001**, *44*, 3710.
- (20) Phadtare, S.; Kessel, D.; Corbett, T. H.; Renis, H. E.; Court, B. E.; Zemlicka, J. *J. Med. Chem.* **1991**, *34*, 421.
- (21) Petrov, V.; Ozerov, A.; Novikov, M.; Pannecouque, C.; Balzarini, J.; De Clercq, E. *Chem. Heterocyc. Comp.* **2003**, *39*, 1218.
- (22) Johnson, F.; Pillai, K.; Grollman, A. P.; Tseng, L.; Takeshita, M. *J. Med. Chem.* **1984**, *27*, 954.
- (23) Lambertucci, C.; Antonini, I.; Buccioni, M.; Dal Ben, D.; Kachare, D. D.; Volpini, R.; Klotz, K.-N.; Cristalli, G. *Bioorg. Med. Chem.* **2009**, *17*, 2812.
- (24) Camaioni, E.; Costanzi, S.; Vittori, S.; Volpini, R.; Klotz, K.-N.; Cristalli, G. *Bioorg. Med. Chem.* **1998**, *6*, 523.
- (25) Isobe, Y.; Tobe, M.; Ogita, H.; Kurimoto, A.; Ogino, T.; Kawakami, H.; Takaku, H.; Sajiki, H.; Hirota, K.; Hayashi, H. *Bioorg. Med. Chem.* **2003**, *11*, 3641.
- (26) Siah, H.-S. M.; Gundersen, L.-L. *Synth. Commun.* **2013**, *43*, 1469.
- (27) Laxer, A.; Major, D. T.; Gottlieb, H. E.; Fischer, B. *J. Org. Chem.* **2001**, *66*, 5463.
- (28) Hanus, M.; Kabelac̃, M.; Rejnek, J.; Ryjac̃ek, F.; Hobza, P. *J. Phys. Chem. B* **2004**, *108*, 2087.

- (29) Platzer, N.; Galons, H.; Bensaïd, Y.; Miocque, M.; Bram, G. *Tetrahedron* **1987**, *43*, 2101.
- (30) Nair, V.; Chi, G.; Uchil, V. R. Diketo acids with nucleobase scaffolds: anti-HIV replication inhibitors targeted at HIV integrase. E.P. Patent 1,848,697, October 31,2007.
- (31) Sun, Z.; Hosmane, R. S. *Synth. Commun.* **2001**, *31*, 549.
- (32) Ranganathan, D.; Rathi, R. *J. Org. Chem.* **1990**, *55*, 2351.
- (33) Leonard, N. J.; Henderson, T. R. *J. Am. Chem. Soc.* **1975**, *97*, 4990.
- (34) Leonard, N. J.; Achmatowicz, S.; Loepky, R. N.; Carraway, K. L.; Grimm, W.; Szweykowska, A.; Hamzi, Q.; Skoog, F. *Proceedings of the National Academy of Sciences of the United States of America* **1966**, *56*, 709.
- (35) Neiman, Z.; Bergmann, F. *Israel J. Chem.* **1967**, *5*, 243.
- (36) Fox, J. R. Proton magnetic resonance spectral assignments and deuterium exchange reactions in substituted purines. PhD Thesis, University of illinois, Urbana, IL, April 1965.
- (37) Jardetzky, C. D. *J. Am. Chem. Soc.* **1960**, *82*, 229.
- (38) Reddy, G.; Mandell, L.; Goldstein, J. *J. Chem. Soc.* **1963**, 1414.
- (39) Leonard, N. J.; Fujii, T.; Saito, T. *Chem. Pharm. Bull.* **1986**, *34*, 2037.
- (40) Leonard, N. J.; Fujii, T. *J. Am. Chem. Soc.* **1963**, *85*, 3719.
- (41) Leonard, N. J.; Fujii, T. *Proceedings of the National Academy of Sciences of the United States of America* **1964**, *51*, 73.
- (42) Montgomery, J.; Thomas, H. *J. Heterocyclic Chem.* **1964**, *1*, 115.
- (43) Montgomery, J. A.; Thomas, H. *J. Am. Chem. Soc.* **1963**, *85*, 2672.
- (44) Montgomery, J. A.; Thomas, H. *J. Org. Chem.* **1965**, *30*, 3235.
- (45) Jones, J. W.; Robins, R. K. *J. Am. Chem. Soc.* **1962**, *84*, 1914.

- (46) Fujii, T.; Walker, G. C.; Leonard, N. J.; DeLong, D. C.; Gerzon, K. *J. Med. Chem.* **1979**, *22*, 125.
- (47) Marek, R.; Křístková, A. k.; Maliňáková, K. i.; Toušek, J. r.; Marek, J. r.; Hocek, M.; Malkina, O. L.; Malkin, V. G. *J. Phys. Chem. A.* **2010**, *114*, 6689.
- (48) Maliňáková, K.; Novosadová, L.; Pipiška, M.; Marek, R. *ChemPhysChem.* **2011**, *12*, 379.
- (49) Estep, K. G.; Josef, K. A.; Bacon, E. R.; Carabateas, P. M.; Rumney, S.; Pilling, G. M.; Krafte, D. S.; Volberg, W. A.; Dillon, K.; Dugrenier, N. *J. Med. Chem.* **1995**, *38*, 2582.
- (50) Abshire, C.; Berlinguet, L. *Can. J. Chem.* **1964**, *42*, 1599.
- (51) Thibon, J.; Latxague, L.; Déléris, G. *J. Org. Chem.* **1997**, *62*, 4635.
- (52) Enkvist, E.; Raidaru, G.; Uri, A.; Patel, R.; Redick, C.; Boyer, J. L.; Subbi, J.; Tammiste, I. *Nucleos. Nucleot. Nucl.* **2006**, *25*, 141.
- (53) Lucas, B.; Rosen, N.; Chiosis, G. *J. Comb. Chem.* **2001**, *3*, 518.
- (54) Meltzer, P. C.; Liang, A. Y.; Matsudaira, P. *J. Org. Chem.* **1995**, *60*, 4305.
- (55) Joule, J. A.; Mills, K. *Heterocyclic chemistry*; John Wiley & Sons, 2008; pp 516.
- (56) Zhong, M.; Robins, M. J. *J. Org. Chem.* **2006**, *71*, 8901.
- (57) Zhong, M.; Nowak, I.; Cannon, J. F.; Robins, M. J. *J. Org. Chem.* **2006**, *71*, 4216.
- (58) Jacobsen, M. F.; Knudsen, M. M.; Gothelf, K. V. *J. Org. Chem.* **2006**, *71*, 9183.
- (59) Joshi, R. V.; Zemlicka, J. *Tetrahedron* **1993**, *49*, 2353.
- (60) Rasmussen, M.; Hope, J. *Aust. J. Chem.* **1982**, *35*, 535.
- (61) Beasley, A.; Rasmussen, M. *Aust. J. Chem.* **1981**, *34*, 1107.
- (62) Engel, J. D. *Biochem. Biophys. Res. Commun.* **1975**, *64*, 581.
- (63) Kania, J.; Gundersen, L. L. *Eur. J. Org. Chem.* **2013**, *2013*, 2008.
- (64) Chavakula, R.; Mutyala, N.; Chennupati, S. *Org. Prep. Proced. Int.* **2013**, *45*, 336.

- (65) Rad, M. N. S.; Khalafi-Nezhad, A.; Behrouz, S.; Faghihi, M. A.; Zare, A.; Parhami, A. *Tetrahedron* **2008**, *64*, 1778.
- (66) Sečkářová, P. n.; Marek, R.; Maliňáková, K.; Kolehmainen, E.; Hocková, D.; Hocek, M.; Sklenář, V. *Tetrahedron lett.* **2004**, *45*, 6259.
- (67) Bartl, T.; Zacharová, Z.; Sečkářová, P.; Kolehmainen, E.; Marek, R. *Eur. J. Org. Chem.* **2009**, *2009*, 1377.
- (68) Chandra, A. K.; Nguyen, M. T.; Uchimar, T.; Zeegers-Huyskens, T. *J. Phys. Chem. A* **1999**, *103*, 8853.
- (69) Salter, L. M.; Chaban, G. M. *J. Phys. Chem. A* **2002**, *106*, 4251.
- (70) Cohen, B.; Hare, P. M.; Kohler, B. *J. Am. Chem. Soc.* **2003**, *125*, 13594.
- (71) Raczyńska, E. D.; Makowski, M.; Zientara-Rytter, K.; Kolczyńska, K.; Stępniewski, T. M.; Hallmann, M. *J. Phys. Chem. A* **2013**, *117*, 1548.
- (72) Raczyńska, E. D.; Makowski, M. *J. Mol. Model.* **2014**, *20*, 1.
- (73) Gonnella, N. C.; Nakanishi, H.; Holtwick, J. B.; Horowitz, D. S.; Kanamori, K.; Leonard, N. J.; Roberts, J. D. *J. Am. Chem. Soc.* **1983**, *105*, 2050.
- (74) Dreyfus, M.; Dodin, G.; Bensaude, O.; Dubois, J. *J. Am. Chem. Soc.* **1975**, *97*, 2369.
- (75) Raczyńska, E. D.; Kolczyńska, K.; Stępniewski, T. M.; Kamińska, B. *Comput. Theor. Chem.* **2013**, *1022*, 35.
- (76) Poater, J.; Fradera, X.; Duran, M.; Sola, M. *Chem. Eur. J.* **2003**, *9*, 400.
- (77) Raczyńska, E. D.; Hallman, M.; Kolczyńska, K.; Stępniewski, T. M. *Symmetry* **2010**, *2*, 1485.
- (78) Krygowski, T. M. *J. Chem. Inf. Comp. Sci.* **1993**, *33*, 70.
- (79) Schleyer, P. v. R.; Maerker, C.; Dransfeld, A.; Jiao, H.; Hommes, N. J. v. E. *J. Am. Chem. Soc.* **1996**, *118*, 6317.
- (80) Stanger, A. *J. Org. Chem.* **2006**, *71*, 883.

- (81) Chen, Z.; Wannere, C. S.; Corminboeuf, C.; Puchta, R.; Schleyer, P. v. R. *Chem. Rev.* **2005**, *105*, 3842.
- (82) Close, D. M.; Crespo-Hernández, C. E.; Gorb, L.; Leszczynski, J. *J. Phys. Chem. A* **2008**, *112*, 12702.
- (83) Kim, H.-S.; Ahn, D.-S.; Chung, S.-Y.; Kim, S. K.; Lee, S. *J. Phys. Chem. A* **2007**, *111*, 8007.
- (84) Fonseca Guerra, C.; Bickelhaupt, F.; Saha, S.; Wang, F. *J. Phys. Chem. A* **2006**, *110*, 4012.
- (85) Gu, J.; Leszczynski, J. *J. Phys. Chem. A* **1999**, *103*, 2744.
- (86) Nowak, M. J.; Lapinski, L.; Kwiatkowski, J. S.; Leszczynski, J. *J. Phys. Chem.* **1996**, *100*, 3527.
- (87) Aidas, K.; Mikkelsen, K. V.; Kongsted, J. *Phys. Chem. Chem. Phys* **2010**, *12*, 761.
- (88) Chenon, M. T.; Pugmire, R. J.; Grant, D. M.; Panzica, R. P.; Townsend, L. B. *J. Am. Chem. Soc.* **1975**, *97*, 4636.
- (89) Eastman, J. *Ber. Bunsen-Ges. Phys. Chem.* **1969**, *73*, 407.
- (90) Schumacher, M.; Guenther, H. *J. Am. Chem. Soc.* **1982**, *104*, 4167.
- (91) Bergmann, E.; Weiler-Feilchenfeld, H.; Neiman, Z. *J. Chem. Soc. B* **1970**, 1334.
- (92) Peng, C.; Ayala, P. Y.; Schlegel, H. B.; Frisch, M. J. *J. Comput. Chem.* **1996**, *17*, 49.
- (93) Peng, C.; Schlegel, H. B. *Isr. J. Chem.* **1993**, *33*, 449.
- (94) Blanco, M.; Martín Pendás, A.; Francisco, E. *J. Chem. Theory Comput.* **2005**, *1*, 1096.
- (95) Bader, R. F. *Atoms in molecules*; Oxford University Press: Oxford, U.K., 1990.
- (96) Francisco, E.; Martín Pendás, A.; Blanco, M. *J. Chem. Theory Comput.* **2006**, *2*, 90.
- (97) Toyama, A.; Miyagawa, Y.; Yoshimura, A.; Fujimoto, N.; Takeuchi, H. *J. Mol. Struct.* **2001**, *598*, 85.

- (98) Brush, C. K.; Stone, M. P.; Harris, T. M. *Biochemistry* **1988**, *27*, 115.
- (1) Shah, N. S.; Wright, A.; Bai, G.-H.; Barrera, L.; Boulahbal, F.; Martín-Casabona, N.; Drobniewski, F.; Gilpin, C.; Havelková, M.; Lepe, R. *Emerg. Infect. Dis.* **2007**, *13*, 380.
- (2) Segura-Cabrera, A.; Rodríguez-Pérez, M. A. *Bioorg. Med. Chem. Lett.* **2008**, *18*, 3152.
- (3) Congreve, M.; Murray, C. W.; Blundell, T. L. *Drug Discov. Today.* **2005**, *10*, 895.
- (4) Hartmann, M. D.; Bourenkov, G. P.; Oberschall, A.; Strizhov, N.; Bartunik, H. D. *J. Mol. Biol.* **2006**, *364*, 411.
- (5) Gu, Y.; Reshetnikova, L.; Li, Y.; Wu, Y.; Yan, H.; Singh, S.; Ji, X. *J. Mol. Biol.* **2002**, *319*, 779.
- (6) Kenyon, C. P.; Steyn, A.; Roth, R. L.; Steenkamp, P. A.; Nkosi, T. C.; Oldfield, L. C. *BMC Biochem.* **2011**, *12*, 36.
- (7) Kenyon, C. P.; Roth, R. L.; van der Westhuyzen, C. W.; Parkinson, C. J. *BMC Research Notes* **2012**, *5*, 131.
- (8) Kenyon, C. P.; Roth, R. L. *BMC Biochem.* **2012**, *13*, 15.
- (9) Cheek, S.; Zhang, H.; Grishin, N. V. *J. Mol. Biol.* **2002**, *320*, 855.
- (10) Cheek, S.; Ginalski, K.; Zhang, H.; Grishin, N. V. *BMC Struct. Biol.* **2005**, *5*, 6.
- (11) Ortega, C.; Liao, R.; Anderson, L. N.; Rustad, T.; Ollodart, A. R.; Wright, A. T.; Sherman, D. R.; Grundner, C. *PLoS Biol.* **2014**, *12*, e1001746.
- (12) Raboisson, P.; Lugnier, C.; Muller, C.; Reimund, J.-M.; Schultz, D.; Pinna, G.; Le Bec, A.; Basaran, H.; Desaubry, L.; Gaudiot, F.; Seloum, M.; Bourguignon, J.-J. *Eur. J. Med. Chem.* **2003**, *38*, 199.
- (13) Bourguignon, J.-J.; Désaubry, L.; Raboisson, P.; Wermuth, C.-G.; Lugnier, C. *J. Med. Chem.* **1997**, *40*, 1768.
- (14) Torphy, T. J. *Am. J. Resp. Crit. Care.* **1998**, *157*, 351.

- (15) Teixeira, M. M.; Gristwood, R. W.; Cooper, N.; Hellewell, P. G. *Trends Pharmacol. Sci.* **1997**, *18*, 164.
- (16) Doherty, A. M. *Curr. Opin. Chem. Biol.* **1999**, *3*, 466.
- (17) Boichot, E.; Wallace, J. L.; Germain, N.; Corbel, M.; Lugnier, C.; Lagente, V.; Bourguignon, J.-J. *J. Pharmacol. Exp. Ther.* **2000**, *292*, 647.
- (18) Martin, R.; Bielekova, B.; Lincoln, A.; McFarland, H. *J. Immunol.* **2000**, *164*, 1117.
- (19) Hakimelahi, G. H.; Ly, T. W.; Moosavi-Movahedi, A. A.; Jain, M. L.; Zakerinia, M.; Davari, H.; Mei, H.-C.; Sambaiah, T.; Moshfegh, A. A.; Hakimelahi, S. *J. Med. Chem.* **2001**, *44*, 3710.
- (20) Phadtare, S.; Kessel, D.; Corbett, T. H.; Renis, H. E.; Court, B. E.; Zemlicka, J. *J. Med. Chem.* **1991**, *34*, 421.
- (21) Petrov, V.; Ozerov, A.; Novikov, M.; Pannecouque, C.; Balzarini, J.; De Clercq, E. *Chem. Heterocyc. Comp.* **2003**, *39*, 1218.
- (22) Johnson, F.; Pillai, K.; Grollman, A. P.; Tseng, L.; Takeshita, M. *J. Med. Chem.* **1984**, *27*, 954.
- (23) Lambertucci, C.; Antonini, I.; Buccioni, M.; Dal Ben, D.; Kachare, D. D.; Volpini, R.; Klotz, K.-N.; Cristalli, G. *Bioorg. Med. Chem.* **2009**, *17*, 2812.
- (24) Camaioni, E.; Costanzi, S.; Vittori, S.; Volpini, R.; Klotz, K.-N.; Cristalli, G. *Bioorg. Med. Chem.* **1998**, *6*, 523.
- (25) Isobe, Y.; Tobe, M.; Ogita, H.; Kurimoto, A.; Ogino, T.; Kawakami, H.; Takaku, H.; Sajiki, H.; Hirota, K.; Hayashi, H. *Bioorg. Med. Chem.* **2003**, *11*, 3641.
- (26) Siah, H.-S. M.; Gundersen, L.-L. *Synth. Commun.* **2013**, *43*, 1469.
- (27) Laxer, A.; Major, D. T.; Gottlieb, H. E.; Fischer, B. *J. Org. Chem.* **2001**, *66*, 5463.
- (28) Hanus, M.; Kabelac̃, M.; Rejnek, J.; Ryjac̃ek, F.; Hobza, P. *J. Phys. Chem. B* **2004**, *108*, 2087.

- (29) Platzer, N.; Galons, H.; Bensaïd, Y.; Miocque, M.; Bram, G. *Tetrahedron* **1987**, *43*, 2101.
- (30) Nair, V.; Chi, G.; Uchil, V. R. Diketo acids with nucleobase scaffolds: anti-HIV replication inhibitors targeted at HIV integrase. E.P. Patent 1,848,697, October 31,2007.
- (31) Sun, Z.; Hosmane, R. S. *Synth. Commun.* **2001**, *31*, 549.
- (32) Ranganathan, D.; Rathi, R. *J. Org. Chem.* **1990**, *55*, 2351.
- (33) Leonard, N. J.; Henderson, T. R. *J. Am. Chem. Soc.* **1975**, *97*, 4990.
- (34) Leonard, N. J.; Achmatowicz, S.; Loepky, R. N.; Carraway, K. L.; Grimm, W.; Szweykowska, A.; Hamzi, Q.; Skoog, F. *Proceedings of the National Academy of Sciences of the United States of America* **1966**, *56*, 709.
- (35) Neiman, Z.; Bergmann, F. *Israel J. Chem.* **1967**, *5*, 243.
- (36) Fox, J. R. Proton magnetic resonance spectral assignments and deuterium exchange reactions in substituted purines. PhD Thesis, University of illinois, Urbana, IL, April 1965.
- (37) Jardetzky, C. D. *J. Am. Chem. Soc.* **1960**, *82*, 229.
- (38) Reddy, G.; Mandell, L.; Goldstein, J. *J. Chem. Soc.* **1963**, 1414.
- (39) Leonard, N. J.; Fujii, T.; Saito, T. *Chem. Pharm. Bull.* **1986**, *34*, 2037.
- (40) Leonard, N. J.; Fujii, T. *J. Am. Chem. Soc.* **1963**, *85*, 3719.
- (41) Leonard, N. J.; Fujii, T. *Proceedings of the National Academy of Sciences of the United States of America* **1964**, *51*, 73.
- (42) Montgomery, J.; Thomas, H. *J. Heterocyclic Chem.* **1964**, *1*, 115.
- (43) Montgomery, J. A.; Thomas, H. *J. Am. Chem. Soc.* **1963**, *85*, 2672.
- (44) Montgomery, J. A.; Thomas, H. *J. Org. Chem.* **1965**, *30*, 3235.
- (45) Jones, J. W.; Robins, R. K. *J. Am. Chem. Soc.* **1962**, *84*, 1914.

- (46) Fujii, T.; Walker, G. C.; Leonard, N. J.; DeLong, D. C.; Gerzon, K. *J. Med. Chem.* **1979**, *22*, 125.
- (47) Marek, R.; Křístková, A. k.; Maliňáková, K. i.; Toušek, J. r.; Marek, J. r.; Hocek, M.; Malkina, O. L.; Malkin, V. G. *J. Phys. Chem. A.* **2010**, *114*, 6689.
- (48) Maliňáková, K.; Novosadová, L.; Pipiška, M.; Marek, R. *ChemPhysChem.* **2011**, *12*, 379.
- (49) Estep, K. G.; Josef, K. A.; Bacon, E. R.; Carabateas, P. M.; Rumney, S.; Pilling, G. M.; Krafte, D. S.; Volberg, W. A.; Dillon, K.; Dugrenier, N. *J. Med. Chem.* **1995**, *38*, 2582.
- (50) Abshire, C.; Berlinguet, L. *Can. J. Chem.* **1964**, *42*, 1599.
- (51) Thibon, J.; Latxague, L.; Déléris, G. *J. Org. Chem.* **1997**, *62*, 4635.
- (52) Enkvist, E.; Raidaru, G.; Uri, A.; Patel, R.; Redick, C.; Boyer, J. L.; Subbi, J.; Tammiste, I. *Nucleos. Nucleot. Nucl.* **2006**, *25*, 141.
- (53) Lucas, B.; Rosen, N.; Chiosis, G. *J. Comb. Chem.* **2001**, *3*, 518.
- (54) Meltzer, P. C.; Liang, A. Y.; Matsudaira, P. *J. Org. Chem.* **1995**, *60*, 4305.
- (55) Joule, J. A.; Mills, K. *Heterocyclic chemistry*; John Wiley & Sons, 2008; pp 516.
- (56) Zhong, M.; Robins, M. J. *J. Org. Chem.* **2006**, *71*, 8901.
- (57) Zhong, M.; Nowak, I.; Cannon, J. F.; Robins, M. J. *J. Org. Chem.* **2006**, *71*, 4216.
- (58) Jacobsen, M. F.; Knudsen, M. M.; Gothelf, K. V. *J. Org. Chem.* **2006**, *71*, 9183.
- (59) Joshi, R. V.; Zemlicka, J. *Tetrahedron* **1993**, *49*, 2353.
- (60) Rasmussen, M.; Hope, J. *Aust. J. Chem.* **1982**, *35*, 535.
- (61) Beasley, A.; Rasmussen, M. *Aust. J. Chem.* **1981**, *34*, 1107.
- (62) Engel, J. D. *Biochem. Biophys. Res. Commun.* **1975**, *64*, 581.
- (63) Kania, J.; Gundersen, L. L. *Eur. J. Org. Chem.* **2013**, *2013*, 2008.

- (64) Chavakula, R.; Mutyala, N.; Chennupati, S. *Org. Prep. Proced. Int.* **2013**, *45*, 336.
- (65) Rad, M. N. S.; Khalafi-Nezhad, A.; Behrouz, S.; Faghihi, M. A.; Zare, A.; Parhami, A. *Tetrahedron* **2008**, *64*, 1778.
- (66) Sečkářová, P. n.; Marek, R.; Maliňáková, K.; Kolehmainen, E.; Hocková, D.; Hocek, M.; Sklenář, V. *Tetrahedron lett.* **2004**, *45*, 6259.
- (67) Bartl, T.; Zacharová, Z.; Sečkářová, P.; Kolehmainen, E.; Marek, R. *Eur. J. Org. Chem.* **2009**, *2009*, 1377.
- (68) Chandra, A. K.; Nguyen, M. T.; Uchimaru, T.; Zeegers-Huyskens, T. *J. Phys. Chem. A* **1999**, *103*, 8853.
- (69) Salter, L. M.; Chaban, G. M. *J. Phys. Chem. A* **2002**, *106*, 4251.
- (70) Cohen, B.; Hare, P. M.; Kohler, B. *J. Am. Chem. Soc.* **2003**, *125*, 13594.
- (71) Raczyńska, E. D.; Makowski, M.; Zientara-Rytter, K.; Kolczyńska, K.; Stępniewski, T. M.; Hallmann, M. *J. Phys. Chem. A* **2013**, *117*, 1548.
- (72) Raczyńska, E. D.; Makowski, M. *J. Mol. Model.* **2014**, *20*, 1.
- (73) Gonnella, N. C.; Nakanishi, H.; Holtwick, J. B.; Horowitz, D. S.; Kanamori, K.; Leonard, N. J.; Roberts, J. D. *J. Am. Chem. Soc.* **1983**, *105*, 2050.
- (74) Dreyfus, M.; Dodin, G.; Bensaude, O.; Dubois, J. *J. Am. Chem. Soc.* **1975**, *97*, 2369.
- (75) Raczyńska, E. D.; Kolczyńska, K.; Stępniewski, T. M.; Kamińska, B. *Comput. Theor. Chem.* **2013**, *1022*, 35.
- (76) Poater, J.; Fradera, X.; Duran, M.; Sola, M. *Chem. Eur. J.* **2003**, *9*, 400.
- (77) Raczyńska, E. D.; Hallman, M.; Kolczyńska, K.; Stępniewski, T. M. *Symmetry* **2010**, *2*, 1485.
- (78) Krygowski, T. M. *J. Chem. Inf. Comp. Sci.* **1993**, *33*, 70.
- (79) Schleyer, P. v. R.; Maerker, C.; Dransfeld, A.; Jiao, H.; Hommes, N. J. v. E. *J. Am. Chem. Soc.* **1996**, *118*, 6317.

- (80) Stanger, A. *J. Org. Chem.* **2006**, *71*, 883.
- (81) Chen, Z.; Wannere, C. S.; Corminboeuf, C.; Puchta, R.; Schleyer, P. v. R. *Chem. Rev.* **2005**, *105*, 3842.
- (82) Close, D. M.; Crespo-Hernández, C. E.; Gorb, L.; Leszczynski, J. *J. Phys. Chem. A* **2008**, *112*, 12702.
- (83) Kim, H.-S.; Ahn, D.-S.; Chung, S.-Y.; Kim, S. K.; Lee, S. *J. Phys. Chem. A* **2007**, *111*, 8007.
- (84) Fonseca Guerra, C.; Bickelhaupt, F.; Saha, S.; Wang, F. *J. Phys. Chem. A* **2006**, *110*, 4012.
- (85) Gu, J.; Leszczynski, J. *J. Phys. Chem. A* **1999**, *103*, 2744.
- (86) Nowak, M. J.; Lapinski, L.; Kwiatkowski, J. S.; Leszczynski, J. *J. Phys. Chem.* **1996**, *100*, 3527.
- (87) Aidas, K.; Mikkelsen, K. V.; Kongsted, J. *Phys. Chem. Chem. Phys* **2010**, *12*, 761.
- (88) Chenon, M. T.; Pugmire, R. J.; Grant, D. M.; Panzica, R. P.; Townsend, L. B. *J. Am. Chem. Soc.* **1975**, *97*, 4636.
- (89) Eastman, J. *Ber. Bunsen-Ges. Phys. Chem.* **1969**, *73*, 407.
- (90) Schumacher, M.; Guenther, H. *J. Am. Chem. Soc.* **1982**, *104*, 4167.
- (91) Bergmann, E.; Weiler-Feilchenfeld, H.; Neiman, Z. *J. Chem. Soc. B* **1970**, 1334.
- (94) Blanco, M.; Martín Pendás, A.; Francisco, E. *J. Chem. Theory Comput.* **2005**, *1*, 1096.
- (95) Bader, R. F. *Atoms in molecules*; Oxford University Press: Oxford, U.K., 1990.
- (96) Francisco, E.; Martín Pendás, A.; Blanco, M. *J. Chem. Theory Comput.* **2006**, *2*, 90.
- (97) Toyama, A.; Miyagawa, Y.; Yoshimura, A.; Fujimoto, N.; Takeuchi, H. *J. Mol. Struct.* **2001**, *598*, 85.
- (98) Brush, C. K.; Stone, M. P.; Harris, T. M. *Biochemistry* **1988**, *27*, 115.

- (99) Nowak-Wydra, B.; Szafran, M. *J. Org. Chem.* **1983**, *48*, 2327.
- (100) Coburn, R.; Landesberg, J.; Kemp, D.; Olofson, R. *Tetrahedron.* **1970**, *26*, 685.
- (101) Esaki, H.; Ito, N.; Sakai, S.; Maegawa, T.; Monguchi, Y.; Sajiki, H. *Tetrahedron.* **2006**, *62*, 10954.
- (102) Herrmann, W. A.; Koecher, C. *Angew. Chem. Int. Ed. Engl.* **1997**, *36*, 2162.
- (103) Bourissou, D.; Guerret, O.; Gabbai, F. P.; Bertrand, G. *Chem. Rev.* **2000**, *100*, 39.
- (104) Arduengo III, A. J.; Dias, H. R.; Harlow, R. L.; Kline, M. *J. Am. Chem. Soc.* **1992**, *114*, 5530.
- (105) Wanzlick, H. *Angew. Chem. Int. Ed. Engl.* **1962**, *1*, 75.
- (106) Dhaouadi, Z.; Ghomi, M.; Austin, J.; Girling, R.; Hester, R.; Mojzes, P.; Chinsky, L.; Turpin, P.; Coulombeau, C. *J. Phys. Chem.* **1993**, *97*, 1074.
- (107) Iyer, R. S.; Voehler, M. W.; Harris, T. M. *J. Am. Chem. Soc.* **1994**, *116*, 8863.
- (108) Storr, T. E.; Baumann, C. G.; Thatcher, R. J.; De Ornellas, S.; Whitwood, A. C.; Fairlamb, I. J. *J. Org. Chem.* **2009**, *74*, 5810.
- (109) Storr, T. E.; Firth, A. G.; Wilson, K.; Darley, K.; Baumann, C. G.; Fairlamb, I. J. *Tetrahedron* **2008**, *64*, 6125.
- (110) Ito, N.; Maesawa, T.; Muto, K.; Hirota, K.; Sajiki, H. Method for deuteration of a heterocyclic ring. U.S. Patent 7,517,990, April 14, 2009.
- (111) Joule, J.; Smith, G. *Heterocyclic Chemistry*; Van Nostrand Reinhold: New York, 1978; 311.
- (112) Clayden, J.; Greeves, N.; Warren, S. *Organic Chemistry*; 2nd ed.; Oxford University Press Inc.: New York, 2012; pp 1050.
- (113) Olivier, H. Alkylation of the N9-position of purines. Honours Thesis, University of Pretoria, Pretoria, SA, June 2013, pp 39.
- (114) Schaeffer, H. J.; Vince, R. *J. Med. Chem.* **1967**, *10*, 689.

(115) Thompson, R. D.; Secunda, S.; Daly, J. W.; Olsson, R. A. *J. Med. Chem.* **1991**, *34*, 2877.